
EXPLORING THE ROLE OF SULFORAPHANE IN PROSTATE METABOLISM

Omar S. Al Kadhi

Quadram Institute Bioscience

A thesis for the Degree of Doctor
of Philosophy to the University of
East Anglia

2017

This copy of the thesis has been supplied on condition that anyone who consults it is understood to recognise that its copyright rests with the author and that use of any information derived there from must be in accordance with current UK Copyright Law. In addition, any quotation or extract must include full attribution

Abstract

Prostate cancer is a worldwide health problem with a higher incidence in older men. Prostate cancer risk is lower in Asian countries compared to the west, this has largely been attributed to difference in diets between the two populations. To date evidence from case-control studies has indicated that cruciferous vegetables and regular exercise reduce the risk of prostate cancer progression; however, other similar studies have shown no association. These contrasting results may be due to study heterogeneity and the long latent period of prostate cancer.

The aim of the work presented in this thesis is to further understand the role of sulforaphane, an isothiocyanate derived from broccoli plants in preventing prostate cancer by exploring its effect on the metabolic microenvironment of the prostate.

One of the key metabolic pathways that is altered in prostate cancer is the Krebs' cycle. Citrate, a product of the Krebs' cycle accumulates in healthy prostate tissue and is reduced in prostate cancer. It was demonstrated by using a novel liquid chromatography and tandem mass spectrometry method that the levels of citrate within *in vitro* models of prostate cancer are markedly different to those of human tissue. Furthermore, citrate levels altered when prostate cells were exposed to reactive oxygen species. The addition of physiological quantities of sulforaphane to prostate cells in culture inhibited the reactive oxygen species-mediated changes on the Krebs' cycle.

A randomised, double-blinded human intervention study was undertaken to further understand the role of sulforaphane in prostate cancer by recruiting men with early prostate cancer into three different study arms delivering sulforaphane in increasing concentrations through naturally bred broccoli varieties. A subgroup analysis demonstrated significant metabolite changes in prostate tissue that were driven by the study diet with accumulation of sulfate common to all three arms. This was positively correlated with lower rates of cancer at 12 months.

The work presented here strengthens the argument that sulforaphane in physiologically achievable concentrations can alter the metabolic environment of the prostate and that this may contribute to the cancer preventing properties of cruciferous vegetables.

Acknowledgements

I would like to give a special thank you to my supervisor Professor Richard Mithen for giving me this great opportunity to undertake research in his group and for his patience and support that has enabled me to complete this work.

Thank you to Professor Colin Cooper for supervising my research and to Mr Robert Mills for supporting my academic career and for teaching me to be a better surgeon. To Dr Maria Traka for her encouragement and friendship.

I would like to express my sincere gratitude to Dr Antonietta Melchini, her untiring efforts in being a mentor and a friend have made it possible for me and many other students to succeed as research scientists. To Dr Lee Kellingray for his guidance and for proof reading the entirety of this thesis.

To Dr Shikha Saha, for teaching me all I needed to know about liquid chromatography and to Tharsini Sivapalan for the microarray data. To Dr Marianne Defernez for her help with statistical analysis.

I am grateful to the Prostate Cancer Foundation and The Biotechnology and Biological Sciences Research Council for their financial support.

Last but not least a big thank you to my family, without your love and support I would not be where I am today.

List of contents

CHAPTER 1.	1
1.1. INTRODUCTION.....	2
1.2. DIAGNOSIS OF PROSTATE CANCER	5
1.2.1 Prostate biopsy.....	6
1.3. TREATMENT OF PROSTATE CANCER.....	7
1.3.1 Active surveillance for low and intermediate-risk prostate cancer cases... 9	
1.3.2 Surgery, radiotherapy and pharmacological treatment.....	10
1.4. PROSTATE CANCER METABOLISM	11
1.5. PROSTATE CANCER AND CRUCIFEROUS VEGETABLES: EPIDEMIOLOGY, HUMAN STUDIES AND CELLULAR MODE OF ACTION	15
CHAPTER 2.	19
2.1. INTRODUCTION.....	20
2.2. AIM.....	22
2.3. MATERIALS AND METHODS	22
2.3.1 Plasma and urine samples.....	22
2.3.2 Human cell lines.....	22
2.3.3 Prostate tissue	23
2.3.4 Liquid chromatography tandem mass spectrometry.....	23
2.4. RESULTS.....	29
2.4.1 Optimization of mass spectroscopy conditions and LC parameters	29
2.4.2 Method validation	30
2.4.3 Identification and quantification of TCA cycle intermediates in human urine samples	33
2.4.4 Identification and quantification of TCA cycle intermediates from human plasma 35	
2.4.5 Quantification of TCA cycle intermediates from cell lysates.....	36
2.4.6 Identification and quantification of citric acid from prostate tissue	39
2.5. DISCUSSION	42
2.6. CONCLUSION.....	43
CHAPTER 3.	44
3.1. INTRODUCTION.....	45
3.2. HYPOTHESES	47

3.3.	MATERIALS AND METHODS	47
3.3.1	Cell culture.....	47
3.3.2	Treatment with hydrogen peroxide.....	48
3.3.3	Treatment with sulforaphane.....	48
3.3.4	Analysis of TCA cycle intermediates by LC-MS/MS.....	48
3.3.5	Aconitase enzyme activity assay	50
3.3.6	Measurement of intracellular ROS production by fluorescence	51
3.3.7	Microarray expression analysis	51
3.4.	RESULTS.....	52
3.4.1	Characterization of TCA cycle intermediates in prostate cell lysates	52
3.4.2	Effect of culture media on TCA cycle metabolites.....	59
3.4.3	Measurement of aconitase activity in PC3 and PNT1A cells.....	64
3.4.4	Gene expression profiles of enzymes of TCA cycle and associated fatty acid synthesis pathways in PC3 and PNT1A cells	65
3.4.5	The effect of oxidative stress on the TCA cycle	68
3.4.6	The in vitro effect of sulforaphane on the TCA cycle	69
3.5.	DISCUSSION	72
3.5.1	Changes to the TCA cycle in prostate cells.....	72
3.5.2	Oxidative stress and TCA cycle dysfunction	76
3.6.	CONCLUSIONS	79
CHAPTER 4.	80
4.1.	INTRODUCTION.....	81
4.2.	AIM.....	82
4.3.	MATERIALS AND METHODS	82
4.3.1	Patient selection	82
4.3.2	Tissue sampling procedure	82
4.3.3	Histological analysis	84
4.3.4	Metabolomic analysis.....	84
4.3.5	Liquid chromatography/Mass Spectrometry (LC-MS, LC-MS2)	84
4.3.6	Gas chromatography/Mass Spectrometry (GC-MS).....	84
4.3.7	Mass determination and MS/MS fragmentation (LC-MS), (LC-MS/MS)...	85
4.3.8	Data quality provided by Metabolon®	85
4.3.9	Statistical analysis	87
4.3.10	Batch variability.....	88

4.4.	RESULTS.....	89
4.4.1	<i>Analysis of benign tissue.....</i>	90
4.4.2	<i>Analysis of cancerous tissue</i>	103
4.5.	DISCUSSION	104
4.5.1	<i>The peripheral zone of the prostate has a unique metabolic signature .</i>	105
4.6.	CONCLUSION.....	109
CHAPTER 5.	110
5.1.	INTRODUCTION.....	111
5.1.1	<i>Prostate cancer and cruciferous vegetables: epidemiology, human studies and cellular mode of actions</i>	111
5.1.2	<i>Active surveillance for low- and intermediate-risk prostate cancer cases</i>	112
5.1.3	<i>Prostate biopsy.....</i>	113
5.2.	AIM.....	113
5.3.	MATERIAL AND METHODS.....	114
5.3.1	<i>Trial management</i>	114
5.3.2	<i>Individual contributions to the trial</i>	114
5.3.3	<i>Trial population</i>	115
5.3.4	<i>Recruitment policy.....</i>	115
5.3.5	<i>Trial design</i>	117
5.3.6	<i>Trial objectives.....</i>	118
5.3.7	<i>Trial procedure</i>	121
5.3.8	<i>Trial intervention</i>	121
5.3.9	<i>Phytochemical analysis of the trial intervention</i>	122
5.3.10	<i>Randomisation.....</i>	123
5.3.11	<i>Lifestyle assessment</i>	123
5.3.12	<i>Trial compliance</i>	123
5.4.	EXPERIMENTAL METHODS.....	124
5.4.1	<i>Prostate biopsies and processing</i>	124
5.4.2	<i>Histological analysis</i>	126
5.4.3	<i>Blood sampling and processing</i>	126
5.4.4	<i>HbA1c analysis.....</i>	127
5.4.5	<i>Metabolite profiling.....</i>	127
5.4.6	<i>Urinary biomarkers.....</i>	127

5.4.7	<i>Biobanking for future research</i>	128
5.4.8	<i>Statistical analysis</i>	128
5.5.	RESULTS.....	128
5.5.1	<i>Trial cohort</i>	128
5.5.2	<i>Baseline anthropometric measurements</i>	129
5.5.3	<i>Baseline blood measurements</i>	129
5.5.4	<i>Phytochemical characterization of the trial intervention</i>	132
5.5.5	<i>Follow-up blood measurements</i>	134
5.6.	DISCUSSION	137
5.7.	CONCLUSIONS	138
CHAPTER 6.	139
6.1.	INTRODUCTION.....	140
6.2.	AIM	141
6.3.	MATERIALS AND METHODS	141
6.3.1	<i>Biological samples collection</i>	141
6.3.2	<i>Metabolite profiling</i>	144
6.3.3	<i>Statistical analysis</i>	144
6.4.	RESULTS.....	145
6.4.1	<i>Tolerability and compliance to study diet</i>	145
6.4.2	<i>ESCAPE study extension</i>	148
6.4.3	<i>Calorie expenditure and habitual diet analysis</i>	148
6.4.4	<i>Histological analysis by template prostate biopsy</i>	150
6.4.5	<i>Metabolomic analysis of prostate tissue samples from ESCAPE sub-cohort</i> 155	
6.5.	DISCUSSION	166
6.5.1	<i>Changes in prostate tissue metabolites</i>	168
6.6.	CONCLUSION.....	169
CHAPTER 7.	170
7.1.	GENERAL DISCUSSION	171
7.2.	THE LIMITED TRANSLATIONAL VALUE OF EXPERIMENTAL EVIDENCES OBTAINED FROM <i>IN VITRO</i> MODELS OF PROSTATE CANCER	172
7.3.	A PROSTATECTOMY-BASED <i>EX VIVO</i> MODEL AS ALTERNATIVE TOOL FOR STUDYING PROSTATE METABOLISM	174

7.4. CHANGES OF PROSTATE METABOLISM INDUCED BY DIETARY BIOACTIVES: EVIDENCE FROM A RANDOMISED DOUBLE-BLINDED TRIAL	177
7.5. CONCLUSIONS	182

List of figures

Figure 1.1 Cancer Research UK statistics showing the 10 most common cancers in males in the UK in 2013	2
Figure 1.2 Cancer Research UK statistics data showing the five most common cancers in males aged 50-74 years (A) and those over the age of 75 (B) in the UK between 2011 and 2013	3
Figure 1.3 Age-specific incidence rates in males in the UK between 2011 and 2013	4
Figure 1.4 PCa incidence in Great Britain from 1980 to 2012	5
Figure 1.5 Diagram reported by Chen and Zhou indicating both the modern Gleason grading system and the new 'Grade Group' classification adopted by the WHO in 2016	9
Figure 1.6 Drugs approved for PCa treatment by the US Food and Drug Administration (FDA since 2004	11
Figure 1.7 Metabolic pathways that contribute to the transformation of citrate in the cytosol. Citrate is converted to different substrates that are used in cholesterol and FA syntheses through specific enzymatic reactions. The enzymes shown in red have been shown to be upregulated in many human cancers. ACLY, ATP citrate lyase; HMGCR, hydroxyl methyl glutaryl CoA reductase; ACC, acetyl-coA carboxylase.	15
Figure 2.1 A diagram representing the Tricarboxylic acid (TCA) cycle	21
Figure 2.2 Chemical structure of TCA cycle intermediates	24
Figure 2.3 Extraction of TCA cycle intermediates from cultured cells	28
Figure 2.4 LC-MS/MS chromatograms of citrate and isocitrate in human urine	34
Figure 2.5 LC-MS/MS chromatograms of citrate and isocitrate in human plasma	35
Figure 2.6 LC-MS/MS chromatogram of standards of TCA cycle intermediates	37
Figure 2.7 LC-MS/MS chromatograms of TCA cycle intermediates extracted from PC3 cell lysates	38
Figure 2.8. LC-MS/MS chromatograms of citrate in human prostate tissue. Citrate peak detected in benign (A) and cancer tissue (B). CA, citrate	39
Figure 2.9 Citrate concentration (mmol) in human tissue	40
Figure 3.1 Outline of main reactions in the TCA cycle	46
Figure 3.2 Images of epithelial prostate cell lines used in this project	49
Figure 3.3 Chemical reactions explaining the principle of the aconitase enzyme assay ...	51
Figure 3.4 Concentration of citrate in prostate cell lines normalised to 10^6 cells	52

Figure 3.5 Concentration of iso-citrate in prostate cell lines normalised to 10^6 cells	53
Figure 3.6 Concentration of α -KG in PNT1A and PC3 cells	54
Figure 3.7 Concentration of succinate in prostate cell lines normalised to 10^6 cells.....	54
Figure 3.8 Concentration of fumarate in prostate cell lines normalised to 10^6 cells	55
Figure 3.9 Concentration of malate in prostate cell lines normalised to 10^6 cells.....	56
Figure 3.10 Concentration of glutamate in prostate cell lines normalised to 10^6 cells.....	56
Figure 3.11 Concentration of lactate in prostate cell lines normalised to 10^6 cells	57
Figure 3.12 Citrate concentration in culture media measured using LC-MS/MS	61
Figure 3.13 A comparison between levels of TCA cycle intermediates in PC3 cell lysates cultured using different growth media	62
Figure 3.14 Comparison of TCA cycle intermediates in PNT1A and PC3 cells cultured using the same growth medium.....	63
Figure 3.15 Activity of aconitase enzyme measured by rate of production of NADPH ...	64
Figure 3.16 Microarray data of key TCA cycle-related genes.....	66
Figure 3.17 Microarray data of lipogenesis and anaplerosis-related genes	67
Figure 3.18 Baseline levels of ROS in prostate cell lines.....	68
Figure 3.19 Citrate levels in prostate cell lines exposed to oxidative stress.....	69
Figure 3.20 Citrate levels in PNT1A and PC3 cells exposed to SF.....	70
Figure 3.21 Citrate levels in PC3 cells exposed to SF for 24 hours prior to treatment with H_2O_2 for 30 minutes	71
Figure 3.22 Citrate levels in PNT1A cells exposed to SF for 24 hours prior to treatment with H_2O_2 for 30 minutes	71
Figure 3.23 Lipid synthesis and glycolysis in cancer	73
Figure 3.24 The effect of ROS on pyruvate metabolism and TCA cycle function	78
Figure 4.1 Transverse section of the prostate specimen showing sampling sites.....	83
Figure 4.2 Venn diagram showing the number of metabolites shared between the two separate batches of samples.....	89
Figure 4.3 Principal component (PC) scores plot of metabolite data from 72 prostate tissue cores after excluding xenobiotic metabolites	92
Figure 4.4 Principal component analysis (PCA) after calculating the average value of right and left sided samples and excluding cancer cores failed to separate the prostate zones.....	93
Figure 4.5 Scores plot between the selected principal components (PCs)	93
Figure 4.6 Important features identified by PLS-DA	94
Figure 4.7 Pathways that are overrepresented in the peripheral zone.....	98
Figure 4.8 Impact scores obtained from topology analysis in the peripheral zone.....	98

Figure 4.9 Pathways that were overrepresented in the transitional zone.....	99
Figure 4.10 Impact scores obtained from topology analysis in the transition zone.....	99
Figure 4.11 A comparison of citrate to choline-plus-creatine ratio between the two prostate zones.....	100
Figure 4.12 A comparison of TCA cycle-related metabolites between the two prostate zones.....	101
Figure 5.1 Gaining ethical and regulatory approvals for conducting the ESCAPE study.....	116
Figure 5.2 ESCAPE study outline.....	119
Figure 5.3 Trial flow chart.....	124
Figure 5.4 Outline of the setup for transperineal template biopsy procedure of the prostate.....	125
Figure 5.5 Recruitment rate in the ESCAPE study.....	129
Figure 5.6 Lipid profile at baseline.....	130
Figure 5.7 Fasting glucose levels (A) and HbA1c % (B) at baseline.....	130
Figure 5.8 PSA concentrations at baseline.....	131
Figure 5.9 Kidney function assessed in randomised participants before starting the intervention.....	131
Figure 5.10 Liver function assessed in randomised participants before starting the intervention.....	132
Figure 5.11 LC-MS chromatograms of study soups.....	133
Figure 5.12 Glucoraphanin concentrations in standard (n=10), Beneforte® (n=7) and Beneforte extra (n=11) broccoli soups.....	134
Figure 5.13 PSA levels measured at 3-month intervals during the intervention.....	135
Figure 5.14 Lipid profile measured at 3-month intervals during the intervention.....	136
Figure 5.15 Fasting glucose levels measured at several intervals during the intervention.....	136
Figure 6.1 Collection of tissue samples through transperineal template (TPB) biopsy procedure as part of the ESCAPE protocol.....	142
Figure 6.2 Metabolomic analysis and histopathological assessment of pre- and post-intervention tissue samples obtained from patients recruited into the ESCAPE trial.....	143
Figure 6.3 Liver function before and after the 12-months diet intervention.....	146
Figure 6.4 Kidney function before and after the 12-months diet intervention.....	147
Figure 6.5 Baseline and post- intervention Body Mass Index (BMI) values. Data presented as mean (SD).	147

Figure 6.6 Physical activity measures derived from baseline and 12-month CHAMPS questionnaire across the three dietary arms.....	149
Figure 6.7 Sulfur intake calculated from 7-day diet diaries repeated three times during the trial.....	150
Figure 6.8 Average (\pm SD) of prostate tissue samples collected from a cohort of ESCAPE study participants (n=15) at baseline (A) and after 12 months of dietary intervention (B)	151
Figure 6.9 Changes in percentage of cancer samples detected on prostate biopsy.....	152
Figure 6.10 Percentage of patients who had upgraded Gleason score on repeat prostate biopsy	153
Figure 6.11 Histological assessment of prostate biopsy samples collected from a subgroup of ESCAPE study patients (n=15) at baseline and after 12 months.....	154
Figure 6.12 Principal component (PC) scores plots for all prostate tissue metabolite data at baseline and after 12-months dietary intervention	156
Figure 6.13 Scores plot between the selected principal components (PCs) using Partial Least Squares-Discriminate Analysis (PLS-DA).....	156
Figure 6.14 Important features identified by PLS-DA	157
Figure 6.15 Principal component (PC) scores plots for all prostate tissue metabolite data at baseline with the three study arms	158
Figure 6.16 Principal component (PC) scores plots for all prostate tissue metabolite data at 12 months with the three study arms.....	158
Figure 6.17 Important features identified by PLS-DA carried out on prostate tissue extracts at the end of the 12-month intervention	159
Figure 6.18 Pathway analysis of prostate metabolite data at baseline and 12 months	163
Figure 6.19 Linear regression analysis of sulfate levels.....	164
Figure 6.20 Linear regression analysis of adenosine diphosphate (ADP) levels.....	164
Figure 6.21 Linear regression analysis of glutathione levels.....	165
Figure 6.22 Linear regression analysis of Uridine diphosphate (UDP).....	166
Figure 7.1 A model of citrate-enhanced metastatic cell behaviour described by Mycielska	174
Figure 7.2 Images of prostate sections.....	175
Figure 7.3 Metabolic sub-pathways found significantly higher in the PZ compared to the TZ.....	176
Figure 7.4 Physiological absorption and excretion of sulfate.....	179
Figure 7.5 Schematic diagram of the physiological system for the metabolism of xenobiotics.....	180

Figure 7.6 SMCSO is mainly metabolised to inorganic sulfate..... 181

List of Tables

Table 1.1 Prostate cancer staging system by the American Joint Committee on Cancer....	7
Table 2.1 Advantages and disadvantages of the two major technologies used for metabolite profiling (adapted from [16])	22
Table 2.2 LC-MS/MS parameters of each analyte (reproduced with permission from Al Kadhi et al (126))	26
Table 2.3 validation data for each analyte (human plasma sample).....	31
Table 2.4 Comparison between the described method and other methods of detection/quantification of Krebs's cycle acids.....	32
Table 2.5 Description of tissue samples used for the extraction of TCA cycle intermediates	41
Table 2.6 Average concentration of citrate in benign and cancerous prostate tissue expressed as nM per gram of tissue (SD).....	41
Table 3.1 Characteristics of human prostate cell lines used in this experimental design..	47
Table 3.2 Average (SD) concentration of TCA cycle metabolites in commonly used prostate cell lines obtained using LC-MS/MS analysis of cell extracts.	58
Table 3.3 A comparison between constituents of RPMI-1640 and HAM-F12 media.....	59
Table 4.1 Results of process variability.....	85
Table 4.2 Quality control and standardisation procedures performed by Metabolon®.....	86
Table 4.3 Summary of metabolite identifiers between the two batches of samples	89
Table 4.4 Demographic and prostate biopsy characteristics of study patients prior to surgery	89
Table 4.5 List of statistically significant metabolites between the two prostate zones	94
Table 4.6 Summary of statistically significant lipid metabolites identified in each of the prostate zones	102
Table 4.7 Summary of cancerous samples identified in the cohort.....	103
Table 4.8 List of metabolites significantly different between cancerous and non-cancerous samples	104
Table 5.1 Eligibility criteria for the trial.....	117
Table 5.2 Trial primary and secondary aims	120
Table 5.3 Baseline anthropometric measurements	129
Table 5.4 Sulfate, SMCSO and total sulfur concentrations expressed as (µmol/300 g fresh weight) in the ESCAPE broccoli soups.....	134
Table 6.1 Pattern of cruciferous vegetable intake of the ESCAPE study cohort (n=15).....	150
Table 6.2 List of metabolites statistically significant in prostate tissue	159

Table 6.3 Results of pathway analysis from prostate tissue metabolites at baseline vs end of study	161
--	-----

Abbreviations

5-HT 5-hydroxy tryptamine	101
ABC1 ATP binding cassette protein 1	67
ACAA1-2 Acetyl-CoA acyltransferase 1-2	67
ACACA Acetyl-CoA carboxylase alpha	67
ACC Acetyl-coA carboxylase	14
Ach Acetylcholine	101
ACLY ATP citrate lyase	14
ADP Adenosine 5'-diphosphate	164
ALP Alkaline phosphatase	131
ALT Alanine aminotransferase	131
AMACR Alpha-methylacyl-CoA racemase	67
APCI+ Positive ion atmospheric pressure chemical ionisation	122
APS Adenosine phosphosulfate	170
AR Androgen receptor	46
AS Active surveillance	7
ASA American Society of Anaesthesiologists	89
AST Aspartate aminotransferase	13
ATCC American Type Culture Collection	46
ATP Adenosine triphosphate	13
BaP Benzo (a) pyrene	77
BPE Bovine pituitary extract	47
BPH Benign prostate hyperplasia	108
BSTFA Bistrimethyl-silyl-trifluoroacetamide	84
CBS cystathionine β - synthase	180
CDO cysteine dioxygenase	181
CHAMPS Community Healthy Activities Model Program for Seniors	123
CRN Clinical Research Network	114
CS Citrate synthase	45
CTH cystathionine γ - lyase	180
DCFH-DA 2',7'-dichlorofluorescein diacetate	50
DHA Docosahexaenoic acid	109
DPA Docosapentaenoate	109
ECACC European Collection of Authenticated Cell Cultures	23
ECG electrocardiography	121
EDTA Ethylenediaminetetraacetic acid	48

EERP Endoscopic extra peritoneal radical prostatectomy	82
eGFR Estimated glomerular filtration rate	132
EPA Eicosapentaenoic acid	109
ESI Electrospray ionisation	24
FA Fatty acids	14
FADH Flavin adenine dinucleotide	44
FASN Fatty acid synthase	65
FBS Foetal bovine serum	23
FH Fumarate hydrates	65
FT-ICR Fourier transform ion cyclotron resonance	85
GCPs Glutamate carboxypeptidases	106
GDP Guanosine 5'- diphosphate	164
GLUT-1 glucose transporter-1	12
GM Genetically modified	17
GOT1 glutamic-oxaloacetic transaminase	181
GOT1 Glutamic-oxaloacetic transaminase 1	67
GPE Glycerol-3-phosphorylethanolamine	94
GPG Glycero-3-phosphoglycerol	94
GPI Glycerol-3-phosphoinositol	94
GSH γ -Glutamylcysteineglycine	118
GSH Reduced glutathione	165
GSTM1 Glutathione S-transferase Mu 1	118
GSTT1 glutathione S-transferase theta 1	118
H&E Hematoxylin and eosin	7
HbA1c Glycated haemoglobin	126
HGPIN High-grade prostatic intraepithelial neoplasia	112
HMDB Human Metabolite Data Base	88
HMGRC 3-hydroxy-3-methylglutaryl-CoA reductase	67
HMGRC Hydroxyl methyl glutaryl CoA reductase	14
HNU Human nutrition unit	115
HPV Human papilloma virus	73
ICP-MS Inductively coupled plasma-mass spectrometry	122
IDH1 Iso-citrate dehydrogenase	65
ITC isothiocyanate	16
KEGG Kyoto Encyclopaedia of Genes and Genomes	65
K-SFM Keratinocyte serum free medium	47

LA Local anaesthesia	113
LC-MS Liquid chromatography tandem mass spectrometry	21
LDH Lactate dehydrogenase	45
LDLR Low density lipoprotein receptor	67
LIMS Laboratory Information Management System	86
LIT Linear ion-trap	84
LOO Leave one out	91
LysoPC Lysophosphatidylcholines	108
mACO m-aconitase	13
MCAT Malonyl CoA:ACP acyltransferase	67
MDH Malate dehydrogenase	45
MDH Malate dehydrogenase enzyme	55
ME malic enzyme	66
MET Metabolic equivalent of task	149
MLYCD Malonyl-CoA decarboxylase	67
MRI Magnetic resonance imaging	107
MRM Multiple reaction monitoring	24
MRSA Methicillin-resistant Staphylococcus aureus	121
MRSI Magnetic resonance spectroscopy imaging	72
NAA N-acetyl-L-aspartate	106
NAAG N-acetyl-aspartyl-glutamate	101
NADH nicotinamide adenine dinucleotide	44, 104
NE Neuroendocrine cells	106
NICE National Institute for Health and Clinical Excellence	10
NIHR National Institute for Health Research Clinical Research Network	114
NMR Nuclear magnetic resonance	20
NMSC Non-melanoma skin cancer	3
NNUH Norfolk and Norwich University Hospital	10
NRES National Research Ethics Service	114
NRF2 Nuclear factor erythroid 2-related factor 2	17
OGDH Oxaloglutarate dehydrogenase	66
PAPS 3'-phosphoadenosine 5'-phosphosulfate	170
PAPSS2 PAPS synthetase	181
PBS Phosphate-buffered saline	26
PC Phosphatidylcholine	94
PCA Principal component analysis	87

PCa Prostate cancer	2
PDH Pyruvate dehydrogenase	12
PDHA1-2 Pyruvate dehydrogenase alpha 1-2	66
PDK Pyruvate dehydrogenase kinase	12
PE Phosphoethanolamine	94
PIS Participant information sheet	115
PKM2 Pyruvate kinase muscle 2	66
PLS-DA Partial least square discriminate analysis	87
PSA Prostate specific antigen	4
PSMA Prostate specific membrane antigen	106
PUFA Polyunsaturated fatty acids	102
PZ peripheral zone	81
REC Research Ethics Committee	114
ROS Reactive oxygen species	13
RPMI Roswell Park Memorial Institute	47
SCD-1 Stearoyl Co-A desaturase-1	14
SDH Succinate dehydrogenase	45
SDHA-C Succinate dehydrogenase subunit A-C	66
SDHAF2 Succinate dehydrogenase complex assembly factor 2	66
SF sulforaphane	16
SFAa Saturated fatty acids	14
SMSCO S-methyl-L-cysteine sulphoxide	17
SOPs Standard operating procedures	142
SULT Sulfotransferases	181
SUOX sulphide oxidase	181
TCA Tricarboxylic acid	11
TPB Transperineal biopsy	6
TRUS trans-rectal ultrasound biopsy	6
TURP Trans-urethral resection of the prostate	38
TZ transitional zone	82
UCSF University of California San Francisco	169
UDP Uridine diphosphate	166
UEA University of East Anglia	82
VIP Variable importance in the projection	91
WHO World Health Organization	7
ZIP1 Zinc transporter member 1	45

α -KG Alpha ketoglutarate	53
α -KGDH α -ketoglutarate dehydrogenase	69

Chapter 1.

General Introduction

Summary

Prostate cancer represents a global health problem. The lifetime risk for men to develop prostate cancer in the UK is estimated to be 1 in 8. Several studies have examined the effect of diet on cancer prevention in the last two decades. Most of these studies have examined the risk of prostate cancer in relation to certain dietary bioactives such as selenium and lycopene, in addition to total intake of fruit and vegetables. However, many of these dietary studies have been criticised for heterogeneity of study populations, differences in reporting habitual diets, and recall bias. As a result, the evidence to date remains conflicting.

1.1. Introduction

Prostate cancer (PCa) is the most common cancer in men in the UK and represents 26% of all male cancers as estimated by cancer registration statistics in 2013 (1). The number of new PCa cases is increasing each year with more than 47,000 new cases in 2013 (Figure 1.1) (2). The incidence is linked with age (Figure 1.2 and Figure 1.3) with the highest rate of diagnoses found in the 65-69 year age group (UK data 2011-2013) (3).

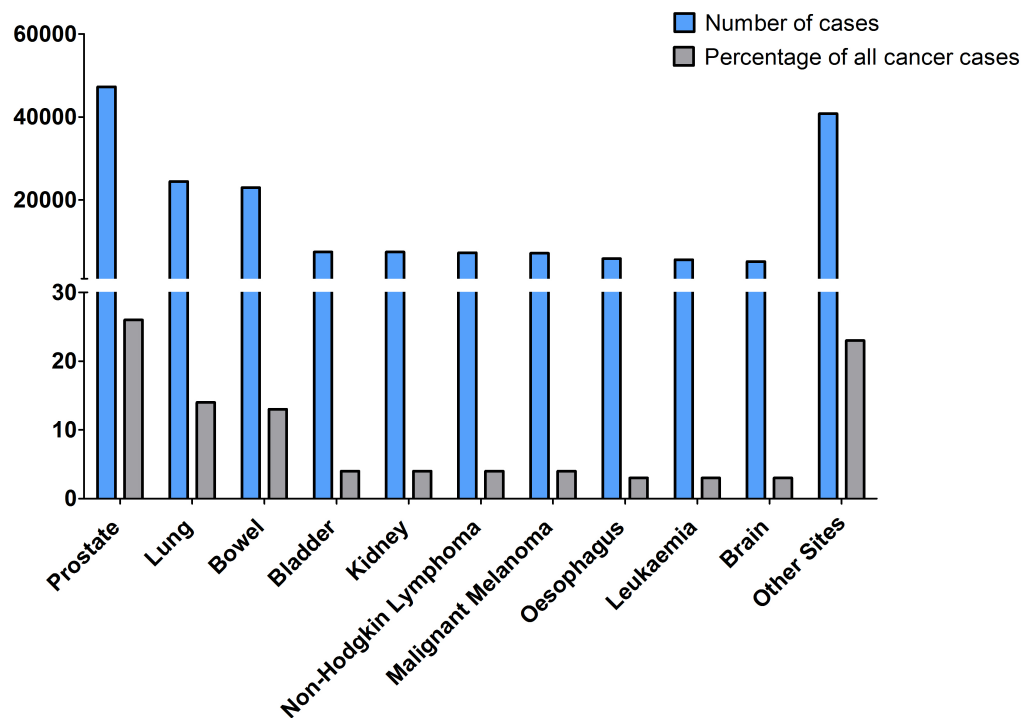
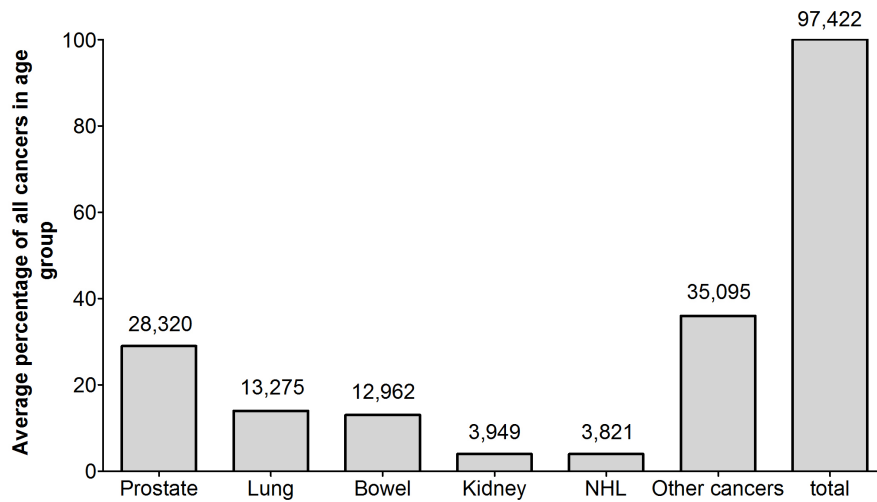


Figure 1.1 Cancer Research UK statistics showing the 10 most common cancers in males in the UK in 2013. Prostate cases were estimated around 47,300 accounting for 26% of all cancers if non-melanoma skin cancer (NMSC) were excluded. NMSC data were not taken in consideration due to under-reporting limitations. Cancer cases indicated as ‘Brain’ in this chart include brain, other central nervous system and intracranial tumours.

A)



B)

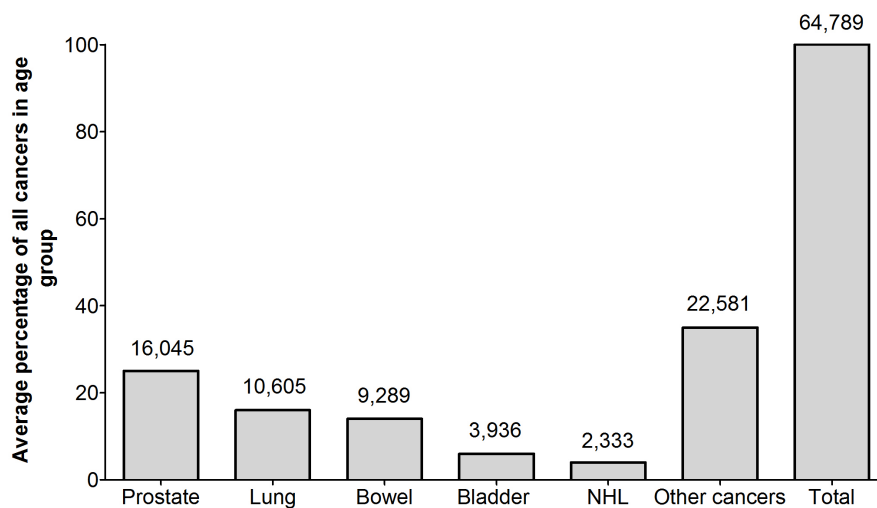


Figure 1.2 Cancer Research UK statistics data showing the five most common cancers in males aged 50-74 years (A) and those over the age of 75 (B) in the UK between 2011 and 2013. The average for PCa cases was 29% and 25% in the two age groups represented in A and B, respectively. Non-melanoma skin cancer (NMSC) were excluded due to under-reporting limitations.

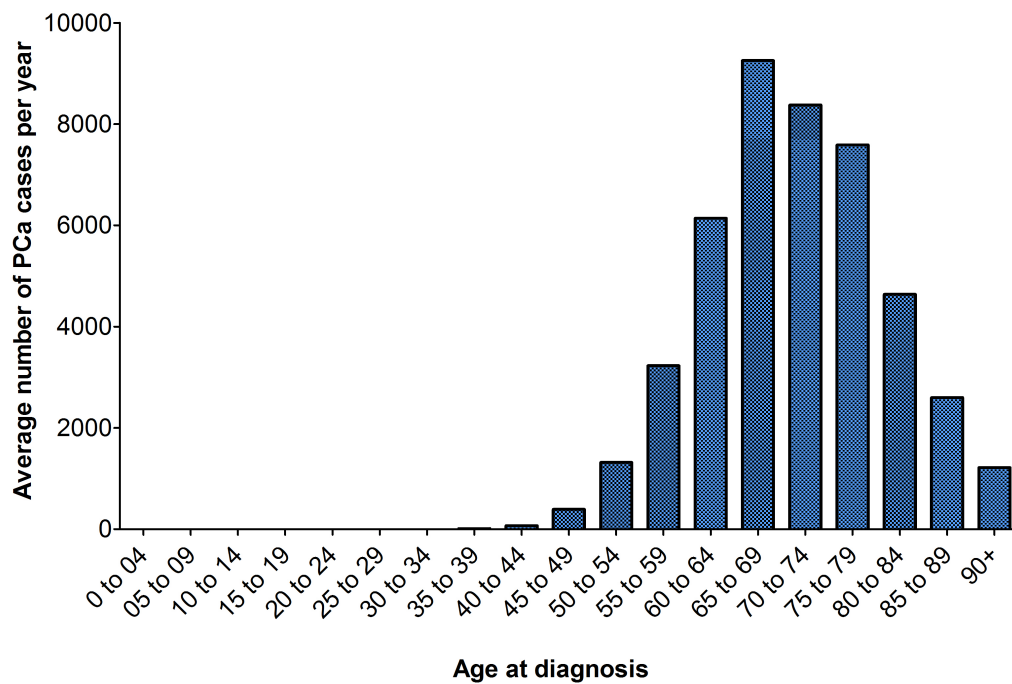


Figure 1.3 Age-specific incidence rates in males in the UK between 2011 and 2013. The average number of cases is indicated per 100,000 population per year.

The incidence of PCa is different across the world (~ 1 million new cases worldwide in 2012), and UK rate is 17th highest in Europe as indicated by cancer registration data from other European countries (~ 417,000 new cases in 2012). There is little variation between UK regions; however PCa incidence in Norfolk is higher than UK average with an age-standardised incidence rate of 116.2 new cases per 100,000 population (104.9 UK average) and an annual average number of 725 new diagnosed cases between 2008 and 2010 (4). The age-standardised rates were calculated using the European Standard Population which is a standard population structure introduced in 1976 to allow the comparison of incidence data across Europe (5).

Since 1970, a dramatic increase in PCa incidence has been registered in Great Britain with a particular increase during the early 1990s and 2000s (Figure 1.4). This observation has been mainly explained with the introduction of the prostate specific antigen (PSA) test in general practice (6-8); however the recruitment into two trials known as Prostate testing for cancer and Treatment (ProtecT; NCT02044172) and Comparison Arm for ProtecT (CAP; ISRCTN92187251) which randomised men in the 50-69 age group to PSA testing in primary care has been also considered responsible of the increase reported in the early 2000s (9).

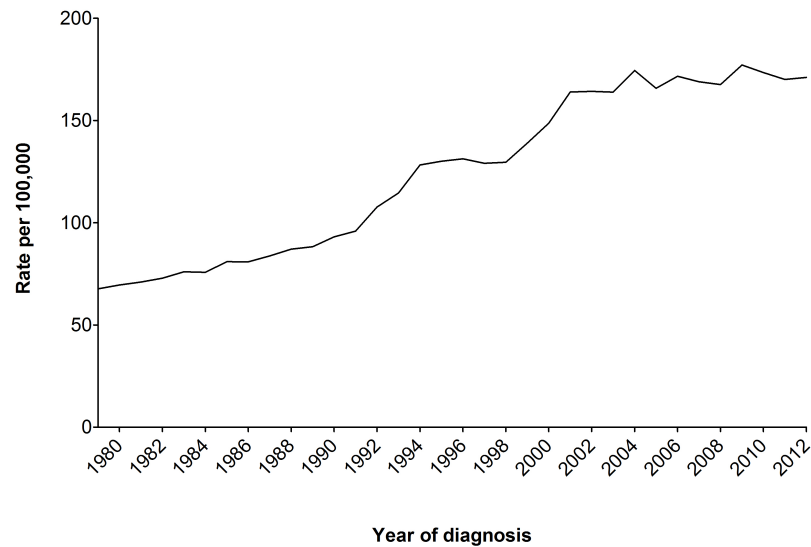


Figure 1.4 PCa incidence in Great Britain from 1980 to 2012. Cancer Research UK data.

1.2. Diagnosis of prostate cancer

Several methods are clinically used to diagnose PCa and their application varies from the initial screening to the final diagnosis. A biochemical test to measure serum PSA levels and physical examination of the prostate (digital rectal examination, DRE) are currently widely used for screening. MRI scanning of the prostate is not recommended routinely in the UK however many centres are utilising MRI together with PSA and biopsy to increase the accuracy of PCa diagnosis. PSA testing was initially approved by the U.S. Food and Drug Administration (FDA) (1986) for the follow up of men already diagnosed with PCa, and subsequently its use in combination with DRE was regulated for screening purposes. Compared to other European countries and the US, PSA testing in the UK is thought to be low. One study of UK general practices examined the records of 126,000 men and showed that overall only 6.2% of those aged 45-89, were tested (10). In this cross-sectional study it was estimated that PSA testing rate was even lower at 1.4 % in men aged 45-49 and 11.3% in men aged 75-79. In the UK, it is advised that men considering a PSA test should be counselled appropriately by their clinician regarding the limitations of PSA testing and that a full assessment is carried out taking into account the patients age, family history and DRE findings. PSA alone is not diagnostic of prostate cancer as it can be elevated in other benign conditions, in addition there is little agreement on what constitutes a normal PSA level as PCa can be found in almost all levels (although less frequently when $< 1.5 \mu\text{g/l}$). The controversies regarding PSA cut off levels and prostate cancer detection are beyond the scope of this thesis however most laboratories now use a cut off level of $4.0 \mu\text{g/l}$ above which it is regarded as abnormal.

Novel clinical biomarkers with high specificity and accuracy are currently needed in order to reduce the number of biopsy procedures that are found to be unnecessary and the overtreatment of low-grade non-aggressive cases. Several reports were recently published describing new diagnostic approaches based on the use of messenger RNA (mRNA) or microRNAs (miRNAs) that are found to be associated with PCa and measurable in urine samples (11, 12). Target genes overexpressed in urinary exosomes have been also suggested as potentially useful PCa biomarkers (13-15). Despite the large body of evidence supporting the potential diagnostic power of DNA-, RNA- and protein- based biomarkers found in a wide range of bio fluids (15), further studies are needed to translate these findings to clinical practice.

1.2.1 Prostate biopsy

Needle core biopsies of the prostate provide histological diagnosis of PCa in addition to assessment of volume of disease within the gland. Accurate assessment of disease burden is paramount in determining the most suitable treatment option for patients especially when surveillance is recommended.

Traditionally, trans-rectal biopsies using TRUS guidance (TRUS biopsy) involve the use of an ultrasound probe to visualise the prostate and direct the needle through the rectum to obtain the samples. This method is operator dependent and due to the lack of a systematic sampling technique, localising the area of tumour in relation to various zones of the prostate is difficult. Cancer detection rates have improved since the description of this technique in 1989 (16) by increasing the number of cores taken and taking more samples from the peripheral parts of the gland, however; the anterior and transitional zones of the prostate are often under-sampled (17).

Transperineal biopsies (TPB) are obtained through the skin of the perineum. The technique uses TRUS to visualise the prostate, the needle samples are then passed through a grid template placed over the perineum that has perforations 5 mm apart in a pre-defined systematic pattern offering the advantage of sampling more prostate tissue within a wider area of the prostate leading to more accurate assessment of tumour distribution. This has been shown to diagnose more cancerous lesions in the anterior and transitional zones of the gland that might have been missed by the trans-rectal route (17). A recent study suggested that men who had PCa on one side of the prostate that was diagnosed using TRUS biopsy were later found to have cancer on both sides in up to 55% of cases when they had a TPB biopsy (46 median core samples). In addition, the same study indicated that up to 23% of

tumours were upgraded when repeat biopsies using a transperineal template were carried out. Infection rates are lower with TPB whilst other complications are comparable (18). One criticism of TPB is that unlike the TRUS biopsy that can be performed under local anaesthesia, template biopsies require general or regional anaesthesia. In this thesis, the use of TPB procedures as part of the protocol of a human dietary intervention study will be explained in further detail. This will provide an opportunity to discuss how this clinical procedure can provide more accurate assessment of the disease, which has previously been diagnosed as low to intermediate-risk following TRUS Biopsy, and ensure the safety of continued active surveillance.

1.3. Treatment of prostate cancer

Several treatment options can be offered at the time of diagnosis according to the grade and stage of the disease ranging from surveillance to radical surgery or radiotherapy as well as hormonal manipulation and in some cases chemotherapy. PCa staging is based on the TNM system: (T) primary tumour, (N) regional lymph node, and (M) metastases (Table 1.1). This system has been updated by the American Joint Committee on Cancer in 2010 (19). The histological grading was established by Gleason in in the 1960s–1970s, and is based on architectural patterns of the cancer stained on hematoxylin and eosin (H&E) sections (20). Normal cells are given a Grade 1 and 2, whereas cancer cells can vary between Grades 3 and 5 with Grade 5 being correlated with poor prognosis. The presence of different cancer grades within the same gland led to the establishment of an overall Gleason score which results by the sum of the primary and secondary grades. For example, if the primary and secondary grades are 3 and 4, respectively, the overall Gleason score is equal to 7 (Gleason $7=3+4$). When only one grade is observed, primary and secondary grades are equally considered (e.g. Gleason $6=3+3$ is given when Gleason 3 is present as primary and secondary grade). However, the original Gleason grading system has been significantly changed over the years (21, 22). Figure 1.5 describes the most recent Gleason grading, and the new “Grade Group” system adopted by the World Health Organization (WHO) in 2016 (23, 24). The new Grade Group system was introduced by the International Society of Urologic Pathology (ISUP) in 2014, and is based on five Grade Groups (1-5) with the lowest grade 1 equivalent to the Gleason score 6 (25).

Table 1.1 Prostate cancer staging system by the American Joint Committee on Cancer

Primary Tumor (T)	Regional Lymph Nodes (N)	Distant Metastasis (M)
TX Primary tumor cannot be assessed	NX Regional lymph nodes were not assessed	M0 No distant metastasis
T0 No evidence of primary tumor	N0 No regional lymph node metastasis	M1 Distant metastasis
T1 Clinically inapparent tumor neither palpable nor visible by imaging	N1 Metastasis in regional lymph node(s)	M1a Nonregional lymph node(s)
T1a Tumor incidental histologic finding in 5% or less of tissue resected		M1b Bone(s)
T1b Tumor incidental histologic finding in more than 5% of tissue resected		M1c Other site(s) with or without bone disease
T1c Tumor identified by needle biopsy (for example, because of elevated PSA)		
T2 Tumor confined within prostate		
T2a Tumor involves one-half of one lobe or less		
T2b Tumor involves more than one-half of one lobe but not both lobes		
T2c Tumor involves both lobes		
T3 Tumor extends through the prostate capsule		
T3a Extracapsular extension (unilateral or bilateral)		
T3b Tumor invades seminal vesicle(s)		
T4 Tumor is fixed or invades adjacent structures other than seminal vesicles, such as external sphincter, rectum, bladder, levator muscles, and/or pelvic wall		

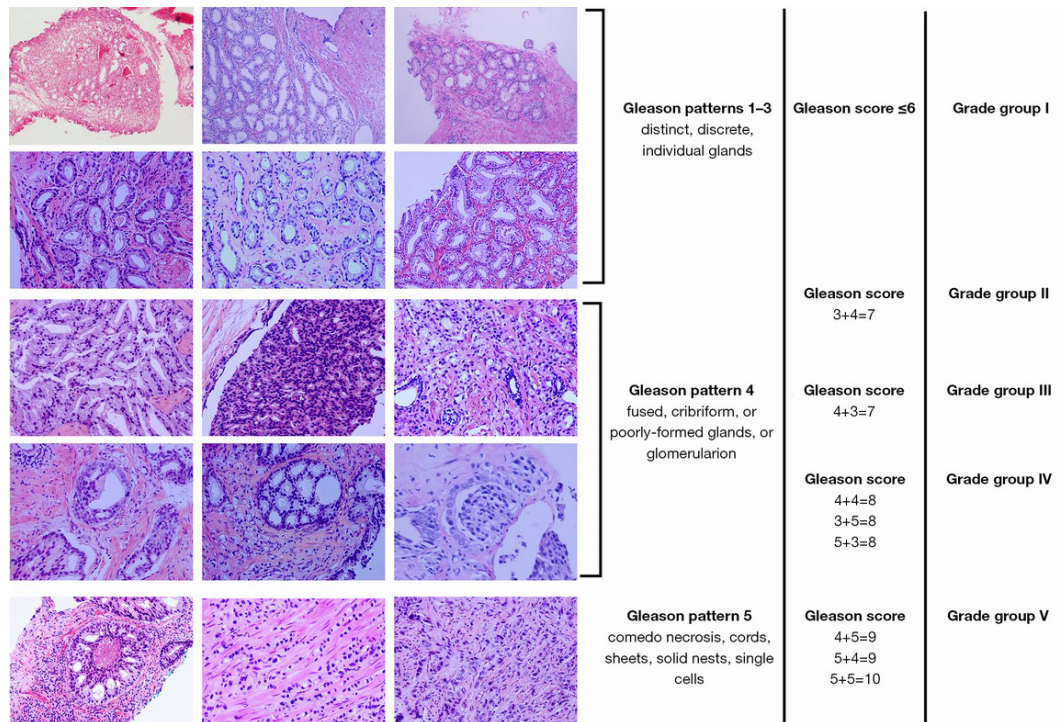


Figure 1.5 Diagram reported by Chen and Zhou indicating both the modern Gleason grading system and the new 'Grade Group' classification adopted by the WHO in 2016

1.3.1 Active surveillance for low and intermediate-risk prostate cancer cases

Studies have shown that men with low-grade organ-confined PCa are at low risk of progression (26, 27). This category of men can often avoid or delay radical treatment which can be associated with significant morbidity (28). AS is the process by which patients with organ-confined PCa are managed expectantly with regular monitoring. Treatment is only initiated when signs of progression are observed. Identifying patients suitable for AS can be done through the use of a number of variables like PSA, Gleason score sum (29), and clinical stage. A variety of tools that stratify patients according to risk of treatment failure have emerged over the last decade incorporating these variables. These tools have undergone extensive testing and validation (30).

The protocol for AS can vary between hospitals and there is a strong need for standardising the criteria of AS inclusion and follow up not only on a national basis but also worldwide. One of the most common stratification tools was described by D'Amico. This defines low-risk PCa as those men with Gleason score ≤ 6 , PSA $< 10 \mu\text{g/l}$ and stage T1c or T2a (tumour-node-metastasis staging system 2002), intermediate-risk as those with Gleason score 7, PSA of $10\text{--}20 \mu\text{g/l}$ and stage T2b-T2c and high-risk patients as those with PSA $> 20 \mu\text{g/l}$

and stage \geq T3 (31). These stratification criteria are widely used and are adopted by the National Institute for Health and Clinical Excellence (NICE). National cancer data suggest that in 2010, more than 160 patients with PCa opted for AS in Norwich (UK); some of those would have gone onto other treatments but were likely to have been on AS for at least a year. The local database for PCa at the Norfolk and Norwich University Hospital (NNUH) indicates that just over 300 patients with low to intermediate-risk disease are currently on AS (32).

1.3.2 Surgery, radiotherapy and pharmacological treatment

Radical surgery on the prostate is usually offered with a curative intent depending on the stage, Gleason score, PSA and the patient's general health. Radical prostatectomy is the most common surgical treatment for localized PCa (33), and is mainly performed as a robot-assisted procedure (RARP) (34). There is increasing evidence that RARP represents a safe and effective procedure also in patients with clinically high-risk PCa (35). Despite the advantages of cancer cure, surgery carries significant morbidity with most men undergoing radical prostatectomy experiencing urinary incontinence and/or erectile dysfunction with varying degrees of severity and duration (33, 36). Radiotherapy is used as a form of radical treatment as an alternative to surgical prostatectomy usually in conjunction with hormonal manipulation or as a palliative treatment option to control symptoms. The outcomes from radiotherapy are comparable to surgery but carry additional side effects such as bladder and bowel symptoms and may not be suitable for patients with underlying inflammatory bowel disease or those who have received pelvic radiation in the past for other conditions. In terms of pharmacological treatments, they are mostly reserved for late stages of the disease. There have been some significant advances in the use of pharmacotherapy in the last two decades, Figure 1.6 describes the most important drugs introduced for the treatment of PCa to date.

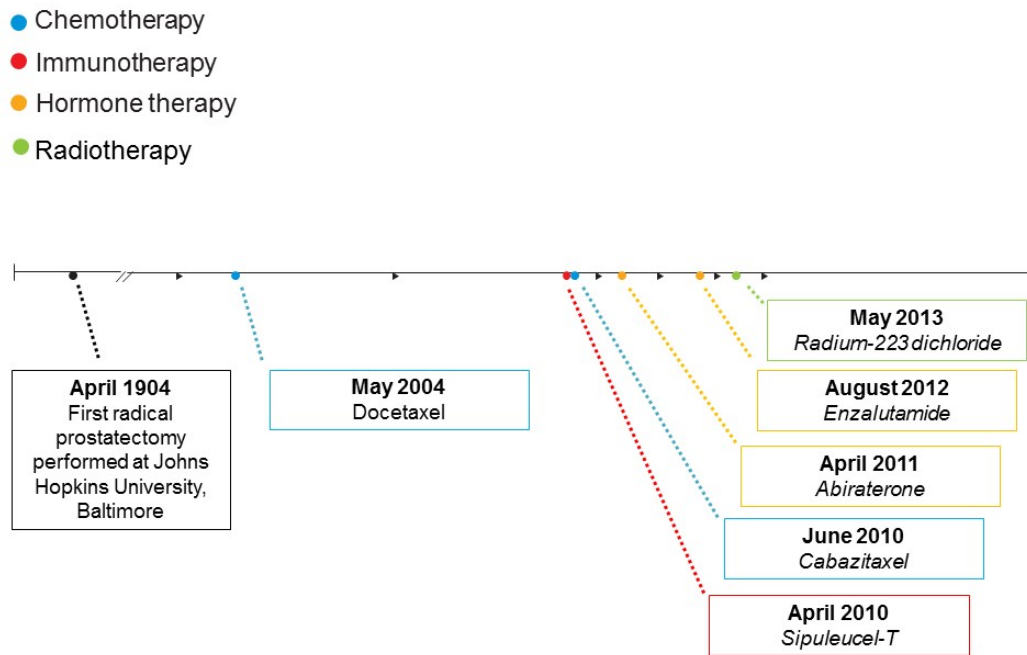


Figure 1.6 Drugs approved for PCa treatment by the US Food and Drug Administration (FDA) since 2004. This figure was adapted from an article published in *Nature* by Richard Hodson (37).

1.4. Prostate cancer metabolism

The key metabolic pathways that cells adopt to produce energy for growth and replication are altered in cancer, diverting energy and precursor production to glycolysis and using less oxidative respiration even in the presence of adequate amounts of oxygen (38, 39).

In normal prostate cells, the metabolic pathway known as the tricarboxylic acid (TCA) cycle or Krebs's cycle is modified to allow the export of citrate from the mitochondrion into prostatic secretions; this process provides abundance of citrate, the main source of energy for sperm (40). It is thought that this alteration to cellular metabolism might put prostate cells at a higher risk for cancerous transformations as these changes also create an environment that facilitates tumour growth (41). It is therefore not surprising that prostate cell metabolism has been of interest to researchers exploring an association between metabolic change and tumorigenesis (42). Costello and colleagues have undertaken numerous studies investigating the association of citrate levels and PCa as discussed in section 1.4.1.2 (41-46).

1.4.1.1. *Glucose metabolism and cancer*

Glucose is converted to pyruvate that enters the mitochondria where it is converted to acetyl CoA by the action of pyruvate dehydrogenase (PDH) enzyme, a process that releases energy. Acetyl CoA can then enter the TCA cycle and is converted to citrate (47). Cancer cells have been shown to express high levels of pyruvate dehydrogenase kinase (PDK) that inhibits PDH allowing more pyruvate to be converted to lactate and as a result alternative precursors for TCA cycle intermediates are sought in a process termed anaplerosis (48).

Tumour cells have also been shown to over-express glucose transporters (49) such as glucose transporter-1 (GluT1), one of 12 glucose transporters that have been shown to be tissue specific (50). Overexpression of GluT1 has been linked to cancers of the lung and colon which could explain the ability of these cells to import larger amounts of glucose necessary to fuel the higher energy demands (51-53). While some research groups have found similar evidence in PCa others have failed to do so (54). For example, Stewart and colleagues observed that GluT1 expression was proportional to the histological pattern (Gleason score) of the disease. More aggressive cancers with poor differentiation (high Gleason score) showed greater expression of GluT1 (55). In contrast, there is evidence to suggest that glucose is not over-utilised as an energy source in in the TCA cycle in PCa cell lines despite its availability; instead, cells appear to rely more on fatty acid β -oxidation. One possible explanation for this is the channelling of glucose to lactate that further enhances the acidic tumour environment (56). In clinical practice, the lack of high glucose uptake in prostate cancer tissue limits the use of glucose-based radio-labelled isotope scans such as fluoro-deoxy-glucose (FDG) positron emission tomography (PET). In other cancers, the high uptake of glucose results in greater uptake of FDG and cancer tissue appear as hot spots on PET enabling the use of such scans in the diagnosis and follow up of cancer patients.

1.4.1.2. *Citrate uptake and metabolism in prostate cancer*

Citrate is normally metabolised in the mitochondria by means of the TCA cycle to produce energy (47). This process in prostate epithelial cells is altered to allow the export of citrate into prostatic secretions where it plays an important role in supplying energy to sperm (41). The reduction in citrate oxidation leads to its accumulation in prostate tissue and produces an energy deficit. It was found that a drop in the activity of a key mitochondrial enzyme named m-aconitase (mACO), is responsible for this change (46). mACO catalyses the conversion of citrate to iso-citrate in the TCA cycle. Free cellular zinc, which forms a small proportion of the body's total zinc content, competes with mACO; thus, high levels of zinc appear to inhibit the enzymatic action of mACO. Costello and colleagues have studied this

metabolic phenomenon which is unique to the prostate gland and found that benign epithelial prostate cells accumulate abnormally high levels of zinc which might explain the truncation of the TCA cycle and the high levels of citrate compared to cancerous tissue (42). When prostate epithelial cells undergo cancerous transformation, they lose the ability to accumulate zinc and therefore more mACO is available to oxidise citrate and restore the TCA cycle. This enables more citrate to be used to generate adenosine triphosphate (ATP) to sustain the high cellular turnover (57).

However, TCA cycle enzymes such as mACO appear to be sensitive to the cellular redox status and their activities can be strongly affected by high levels of reactive oxygen species (ROS)(58). Several reports have shown inhibition of mACO and other TCA cycle enzyme with exposure to oxidative stress resulting in perturbations to the TCA cycle function (58, 59). Whether ROS cause TCA cycle changes in human prostate cells is not well characterised.

1.4.1.3. Anaplerosis

In the absence of glucose, other sources of intermediates are sought to replenish the oxaloacetate used to generate citrate molecules in the TCA cycle (60). There are two main sources for this; the first is aspartate; an amino acid that is taken up from the plasma and converted to oxaloacetate by the enzyme aspartate aminotransferase (AST)(61, 62). The second source of intermediates comes from the amino acid glutamine(63). The TCA cycle balance is maintained by converting glutamate to alpha-ketoglutarate (a key TCA cycle intermediate) which is in turn converted to citrate by reversal of the TCA cycle through a series of reductive carboxylation reactions (64).

1.4.1.4. The role of lipid metabolism in prostate cancer

Cell replication not only requires energy but also, building blocks in the form of structural proteins and lipids for the generation of new cells. This process is upregulated in cancer (65). Lipids also provide an additional energy source in the form of fatty acids (FA), they form complex lipids used in cell signalling, and play a role in protein modification (66). A study carried out using *in vitro* models has shown increased expression of choline kinase an important enzyme in the formation of key cellular phospholipids in lung, colorectal and PCa cell lines (67).

Citrate is converted to acetyl CoA in the cytosol by the action of ATP citrate lyase (ACLY) enzyme. ACLY was found to be up regulated in many human cancers including PCa (68). Acetyl CoA is converted to mevalonate by the enzymatic action of hydroxyl methyl

glutaryl CoA reductase (HMGRC), which regulates cholesterol synthesis (Figure 1.7) It is now becoming increasingly evident that enhanced cholesterol synthesis is strongly associated with PCa pathogenesis (69). Interestingly, statins, which are cholesterol-lowering drugs, act as HMGRC inhibitors, and their anti-proliferative action in human cancer cells has been well-documented (70-72). However, there is still conflicting evidence regarding their role *in vivo*.(73, 74).

Acetyl-CoA is also used as substrate for the production of malonyl CoA by acetyl-coA carboxylase (ACC) that is channelled into a series of reactions ending in the formation of saturated fatty acids (SFAs) (47). An anabolic enzyme known as fatty-acid synthase (FASN) plays a key role in the regulation of the condensation reactions of acetyl groups that lead to the *de novo* biosynthesis of SFAs (75, 76); the most abundant of which is palmitate, a 16-carbon FA. These SFAs are then elongated or desaturated by enzymatic action to form long chain FAs that play a role in cellular membrane structure (77). An increased expression of FASN has been observed in many human cancers, and this could explain the strong link between FA synthesis and cancer development (78, 79). Swinnen and colleagues have suggested a selective activation of FA synthesis in PCa (80). They reported an increased expression of both FASN and ACC in PCa cases compared to normal controls, but no significant changes in the expression of two genes involved in the synthesis of cholesterol. Stearoyl Co-A desaturase-1 (SCD-1) belongs to a family of enzymes involved in fatty acid synthesis that has been found to be upregulated in PCa. Fritz and colleagues demonstrated that the inhibition of SCD-1 slowed prostate cancer progression in a xenograft model (81). The alteration of citrate and FA synthesis in the prostate demonstrates that the metabolic changes that develop in PCa occur in multiple pathways(82).

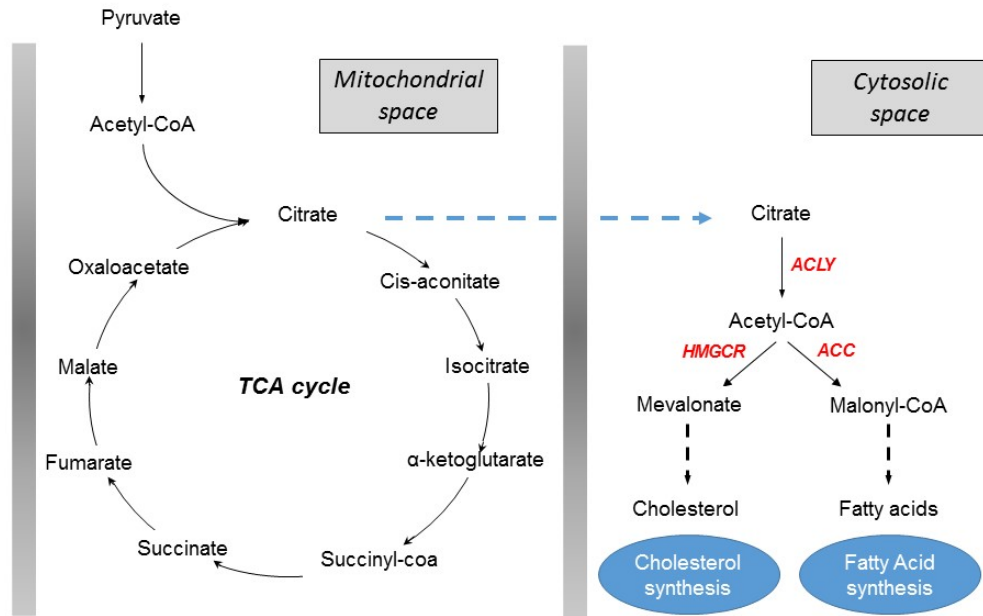


Figure 1.7 Metabolic pathways that contribute to the transformation of citrate in the cytosol. Citrate is converted to different substrates that are used in cholesterol and FA syntheses through specific enzymatic reactions. The enzymes shown in red have been shown to be upregulated in many human cancers. ACLY, ATP citrate lyase; HMGCR, hydroxyl methyl glutaryl CoA reductase; ACC, acetyl-coA carboxylase.

1.5. Prostate cancer and cruciferous vegetables: epidemiology, human studies and cellular mode of action

Many studies have shown that the development of PCa is associated with multiple genetic and metabolic changes within prostate tissue (83, 84). Dietary intake of bioactive compounds could represent a promising chemo preventive strategy. Diet may be able to prevent the proliferation of existing cancer clones by altering gene expression and metabolism within the cancerous clones themselves or the tumour micro- and macro-environment (85, 86). Several studies have examined the effect of diet on cancer prevention in the last two decades (87-89). A number of these studies have examined the risk of PCa in relation to certain dietary substances such as selenium and lycopene (90, 91), in addition to total intake of fruit and vegetables (92). However, many of these dietary studies have been criticised for different reasons including heterogeneity of study populations, differences in food diaries and recall bias. As a result, the evidence remains conflicting. The European Prospective Investigation into Cancer and nutrition study (EPIC) has several strengths compared to other dietary studies, such as the prospective nature of the study and a robust 7-day food diary that has been validated in a number of publications (93). Despite the high quality of the dietary data in EPIC cohorts, PCa risk in relation to diet remains unclear as some studies show no reduction in the risk of developing the disease, whereas others have found clear protective properties of various plant foods.

Data obtained from epidemiological studies suggest that diets rich in cruciferous vegetables, such as broccoli, may reduce the incidence and progression of PCa (94). Richman and colleagues reported a reduced risk of approximately 60% when more than 8 portions of cruciferous vegetables are consumed per week (86). The same research group has found a similar protective effect induced by exercise (brisk walking) that could suggest a common molecular mechanism between cruciferous vegetables and physical activity (95). However, Key and colleagues reported that there was no association between total fruit and vegetable intake and PCa risk for 1104 men diagnosed with the disease who were part of the EPIC cohort; this was also true for cruciferous vegetable intake when examined separately (92). These results, however, were obtained after a relatively short follow up of 4.8 years and with a median age of 52 at recruitment. Given the fact that PCa incidence increases with age, and has a protracted course it is possible that with longer follow up a clearer correlation is seen. This is what a later study by Steinberger and colleagues showed when they reported on a larger number of men with PCa amongst the EPIC-Heidelberg cohort (96). In this study, they found an inverse relationship between cruciferous vegetables intake and PCa risk. The men in the latter study were followed up for a longer period with an average of 9.4 years. The authors examined the food diaries in more detail and were able to give a clearer estimate on the total consumption of cruciferous-derived phytochemicals when compared to the study previously published by Key and colleagues. It may become apparent therefore that with longer follow up clearer associations are recognised.

These vegetables are unique in their ability to accumulate sulphur-containing glycosides known as glucosinolates, including glucoraphanin. Following consumption, these compounds produce bioactive isothiocyanates (ITCs). *In vitro*, animal and human studies provide robust evidence of the ability of ITCs to target multiple signalling pathways that are associated with prostate carcinogenesis (97). Broccoli accumulates the glucosinolate glucoraphanin. When consumed, glucoraphanin is converted to the isothiocyanate sulforaphane (SF), either by the action of the plant enzyme myrosinase or by the gut microbiota, if the myrosinase has been denatured by cooking. The research group led by Prof Richard Mithen at the Quadram Institute Bioscience (QIB) has developed over the last twenty years a cultivar of broccoli (Beneforte®) delivering a threefold higher concentration of SF than standard broccoli (98). Plant breeders at Seminis seeds developed the Beneforte® broccoli cultivar, which is subject to very stringent quality control and is now widely commercialised in US and several European countries, including the UK. The breeders have developed another broccoli cultivar which has been termed Beneforte extra, which

has almost double the amount of glucoraphanin compared to Beneforte® broccoli. These broccoli varieties represent the result of a special crossbreeding programme and are not genetically modified (GM) plant foods. However, broccoli is not only a rich source of glucoraphanin but other several sulphur-containing compounds such as sulphate and S-methyl-L-cysteine sulphoxide (SMCSO) (99).

The scientific evidence supporting the health-promoting effects of bioactive compounds from broccoli is largely provided by studies carried out using *in vitro* and animal models. One of the most studied phytochemicals from broccoli is SF (100). Numerous publications indicate the diversity of SFs targets with many mechanisms of action that are observed in a variety of cell types including the prostate (97, 101). The main molecular target of SF appears to be nuclear factor erythroid 2-related factor 2 (NRF2) with consequent improvement of antioxidant defence mechanisms (102-104). However, the limitations of translating the experimental findings obtained in cells and animals are now becoming clearer to the science community, and the number of randomised controlled trials to test the preventive properties of broccoli and other cruciferous vegetables is increasing. To date there are more than 30 trials looking at the effect of SF on human health which are registered on clinicaltrials.gov. High-glucoraphanin broccoli varieties (Beneforte® and Beneforte extra) are currently tested in several randomised trials undertaken at the Norwich Research Park in order to obtain high quality data that aim to further define the biological mechanism of action as well as the bioavailability of SF and other ITCs derived from consumption of broccoli vegetables (105-109). There are only a few reports in the literature on the bioavailability of high-glucosinolate broccoli varieties (110, 111) and perhaps more importantly on the bioavailability of other sulphur containing compounds such as SMCSO that could potentially share a similar biological profile to ITCs.

The work presented in this thesis is a multimodal approach to examine the effect of SF on the human prostate. The primary hypothesis is that SF derived from broccoli can change the metabolic environment of the prostate to one that is less favourable for cancer propagation. This is addressed in several ways:

- a. By developing a novel sensitive method using LC-MS/MS to detect TCA cycle intermediates in prostate cells to gain a broader understanding of the TCA cycle function *in vitro*.
- b. Testing the effect of SF extract in physiological concentrations on the TCA cycle of benign and cancerous prostate cell lines and test whether the antioxidant properties of SF have a role in maintaining TCA cycle function in a high ROS environment.

- c. Obtaining a global non-targeted map of the prostate metabolome from two distinct prostate tissue zones extracted from patients undergoing surgery for prostate cancer.
- d. A randomised double blinded human intervention study to examine the effect of three different concentrations of SF from three broccoli varieties on prostate metabolism.

Chapter 2.

Optimising a
chromatography method to
examine the TCA cycle in
human biological samples

Summary

Perturbations from metabolic homeostasis are critically involved in the emergence of cancerous clones, resulting in otherwise localised tumours becoming more aggressive and requiring clinical intervention. A better understanding of changes in metabolism associated with malignant transformation may help researchers to identify lifestyle (diet, exercise) or therapeutic interventions that could restore metabolic homeostasis, thereby reducing the risk of tumour progression. It is now well-established that the TCA cycle plays an important role on the metabolic transformation occurring in PCa. This Chapter describes the development of a chromatography-based method to study the TCA cycle in body fluids and tissues of human origin. This method has been established taking into consideration problems and limitations of existing techniques, and its application to different biological matrices will not only allow capture of metabolic changes in tissue but also in cell extracts, urine and blood samples.

2.1. Introduction

The TCA or Krebs' cycle represents a crucial metabolic pathway in almost all living organisms (Figure 2.1). It encompasses a series of reactions that include oxidization and decarboxylation, resulting in the release of energy and a number of different intermediates that can be used for amino acid and lipid synthesis (112).

Unlike most mammalian cells, prostate epithelial cells favour citrate export to oxidation, and although this incurs an energy disadvantage to the cell, it serves a role in providing energy to sperm by supplying seminal fluid with citrate (113). Cancerous prostate cells lose the ability to export citrate, and it is thought that they revert to using citrate to generate energy (114). The different metabolic fate of citrate in PCa cells has been the focus of attention of several research groups; it has been studied as a possible adjunct to diagnosis and explored as a possible target for PCa therapy (42, 115, 116).

Many of the published reports on the role of citrate in prostate cell metabolism have used enzymatic or Nuclear Magnetic Resonance (NMR) methods to quantify or detect this six-carbon metabolite (117-120). Studies that used enzymatic methods often relied on spectrophotometric methods, and thus provide indirect measurement of citrate and related TCA intermediates (121-123). NMR offers the advantage of requiring minimal sample preparation, but lacks sensitivity in comparison to liquid chromatography (LC). Analysis of small molecules using targeted liquid chromatography tandem mass spectrometry (LC-

MS/MS) is thought to provide higher sensitivity, especially from matrices where compounds or molecules are at low concentrations (124). A list of the advantages and disadvantages of using NMR and LC-MS techniques for metabolites profiling is presented in Table 2.1 **Error! Reference source not found.**

It was envisaged that measuring TCA cycle intermediates with LC-MS/MS could be a useful research tool, and may provide a more holistic picture of the changes that occur in the TCA cycle in PCa. This Chapter describes the development of a LC-MS/MS method that would allow the identification and quantification of TCA intermediates in different biological matrices with a relatively easy sample preparation process and high sensitivity.

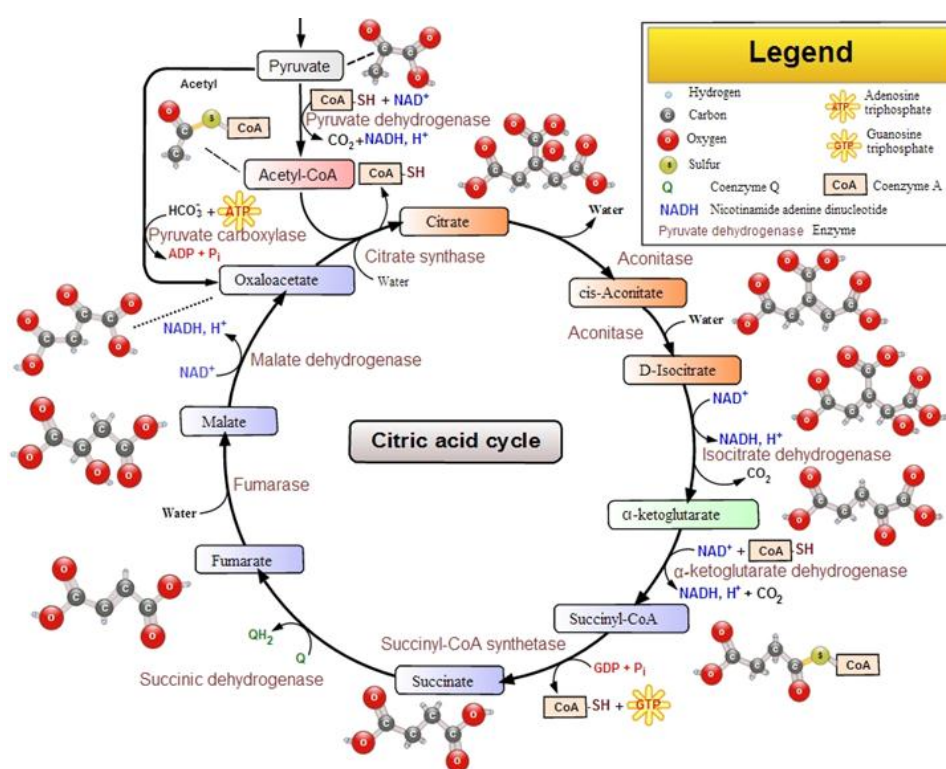


Figure 2.1 A diagram representing the Tricarboxylic acid (TCA) cycle (adapted from(125))

Table 2.1 Advantages and disadvantages of the two major technologies used for metabolite profiling (adapted from [16])

Technology	Advantages	Disadvantages
NMR spectroscopy	Fast Quantitative Separation and derivatization steps are not required Detects all organic classes Possible identification of new compounds Great availability of software and databases	Low sensitivity (~ 5 μ M) Large sample volume (~500 μ l) Expensive instrumentation Large instrument footprint
LC-MS	High sensitivity Flexible technology Detects most organic and some inorganic molecules Separation can be avoided (direct injection) Low sample volume (10 μ l)	Limited availability of software and databases Samples not recoverable Expensive instrumentation Slow Not easy to use for the identification of new compounds

2.2. Aim

- ❖ To develop a reliable method to simultaneously analyse the TCA cycle intermediates using LC-MS/MS
- ❖ To apply this LC-MS/MS method to examine the TCA cycle in different biological matrices of human origin

2.3. Materials and Methods

2.3.1 Plasma and urine samples

For purposes of method development and with local ethical approval, urine and plasma samples were obtained from historic aliquots collected from completed human intervention studies. These studies recruited healthy volunteers who gave consent for further research use of their samples after study completion. Synthetic urine control samples and fatty acid-free human serum albumin (HSA) were purchased from Sigma® (Sigma-Aldrich).

2.3.2 Human cell lines

Human cancerous prostate adenocarcinoma (PC3) cells were purchased from European Collection of Authenticated Cell Cultures (ECACC) (No 90112714). Cells were routinely

cultured as monolayers in HAM F-12 medium supplemented with 10% foetal bovine serum (FBS) in a humidified atmosphere containing 5% CO₂ at 37 °C. Complete medium was changed every 48 hours. Cells were grown to 80% confluency on 10 cm dishes before performing the extraction of the TCA cycle as described on page 27.

2.3.3 Prostate tissue

Frozen samples of histologically proven benign (n=5) and cancerous (n=5) prostate tissue were obtained from the Norwich Biorepository (NNUH). The protocol was approved by the Faculty of Medicine and Health Science Research Ethics Committee (reference: 20122013-37) in January 2013. Informed written consents were obtained from all patients using the current version of the Human Tissue Bank– Information Sheet for Patients and Consent Form, Version 11, Adult (23 March 2011). All samples were histologically examined by NNUH pathologists, and anonymised clinical information was provided by NNUH tissue bank.

2.3.4 Liquid chromatography tandem mass spectrometry

2.3.4.1. *Reagents and acid standards*

All reagents used for LC-MS/MS were prepared from stock solutions following manufacture's advice. A mobile phase was made with 0.2% formic acid. TCA cycle standards were purchased from Sigma® (Sigma-Aldrich) as powder and reconstituted in mobile phase at the concentration of 1 mg/ml that has been used for subsequent serial dilutions. Water was obtained from a Milli-Q® Integral Water Purification System (Millipore Ltd). Deuterated D4-citric acid (2, 2, 4, 4-D4, 98%) was purchased from Cambridge Isotope Laboratories, Inc. A standard curve of a number of TCA intermediates was produced from stock solutions at the concentration of 1 mg/ml; glutamic acid (≥99%), citric acid (≥99%), iso-citric acid (≥93%), α-ketoglutaric acid (≥99%), malic acid (≥99%), oxaloacetic acid (≥97%), succinic acid (≥99%), fumaric acid (≥99%), pyruvic acid (≥98%) and lactic acid (≥85%) were all solubilised in the relevant matrix (synthetic urine, 5% fatty-acid free HSA, water and cell culture medium both acidified with 10% 0.3 mM perchloric acid). 100 µl of each standard were mixed together in a total volume of 1,000 µl to obtain a solution of 100 µg/ml of each standard. A five point standard curve was produced with a 10-fold serial dilution over the range of 10,000 ng/ml to 10 ng/ml. 10 µl of deuterated D4-citric acid was added to all samples as internal standard (final concentration of 10 µg/ml) to allow quantification based on the ratio of the internal standard to each intermediate peak. Figure 2.2 shows the chemical structure of measured compounds of the TCA cycle.

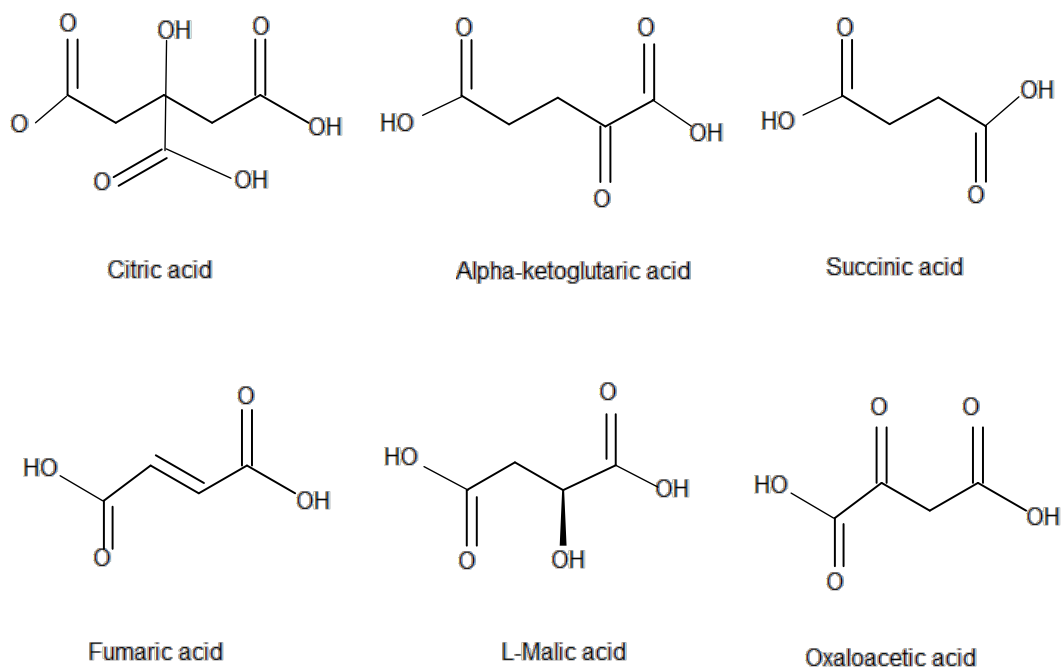


Figure 2.2 Chemical structure of TCA cycle intermediates.

2.3.4.2. LC-MS/MS setup

For LC-MS/MS analysis, the Agilent 1200 Series LC 6490 Triple Quad LC-MS mass spectrometer was used (Agilent Technologies). The HPLC column was a Kinetex C18 1.7 μm (100 x 2.1 mm) from Phenomenex. The Agilent system used for this study comprised of a degasser, binary pump, cooled autosampler, column oven, diode array detector and 6490 mass spectrometer. The gas temperature was 200 $^{\circ}\text{C}$ with a gas flow of 16 l/min, a sheath gas temperature of 300 $^{\circ}\text{C}$ with a sheath gas flow of 11 l/min, a nebuliser pressure of 50 psi and capillary voltage were 3500 $^{\circ}\text{C}$ for positive polarity and 3000 $^{\circ}\text{C}$ for negative polarity. The LC eluent flow was sprayed into the mass spectrometer interface without splitting. TCA cycle intermediates were monitored by tandem MS using multiple reaction monitoring (MRM) mode. Identification was achieved on the basis of retention time and product ions. Electrospray ionisation (ESI) was used in the positive mode for glutamic acid and in the negative mode for the other TCA cycle intermediates. 2 μl was used for the injection volume and the auto sampler was maintained at 4 $^{\circ}\text{C}$.

Table 2.2 summarises the monitored ions and the optimised MS operating parameters of the analytes.

Agilent 6490 Mass spectroscopy includes i-Funnel Technology (Agilent Jet Stream, Hexabore capillary, high pressure and low pressure i-Funnels) and high throughput quadrupole driver electronics improve ion transmission and allow virtually instantaneous

polarity switching. The polarity switching from positive ion mode to negative ion mode is only 20 ms.

The 6490 mass spectroscopy design uses printed circuit board technology with only a small conductive rim in the i-Funnel resulting in a reduced capacitance load. This makes +/- ion switching fast.

Therefore, Agilent 6490 Mass spectroscopy allows switching polarity between positive and negative in a single method without time segmenting.

Table 2.2 LC-MS/MS parameters of each analyte (reproduced with permission from Al Kadhi et al (126))

Analyte	Retention time (min)	Precursor Ion (m/z)	Product Ion (m/z)	Collision energy	Cell Accelerator Voltage	Polarity
D4-citric acid	1.13	195	114	12	4	Negative
D4-citric acid	1.13	195	177	10	4	Negative
Iso-citric acid	0.85	191	155	10	5	Negative
Citric acid	1.13	191	111	10	5	Negative
Citric acid	1.13	191	87	18	5	Negative
Glutamic acid	0.6	148	130	8	4	Positive
Glutamic acid	0.6	148	84	12	4	Positive
Malic acid	0.7	133	115	10	5	Negative
Malic acid	0.7	133	71	14	5	Negative
Succinic acid	1.6	117	99	10	5	Negative
Succinic acid	1.6	117	73	10	5	Negative
Fumaric acid	1.3	115	71	10	5	Negative
Fumaric acid	1.3	115	41	18	5	Negative
Lactic acid	1.05	89	43	10	4	Negative
α -ketoglutaric acid	1.03	145	101	10	5	Negative
α -ketoglutaric acid	1.03	145	57	10	5	Negative
Oxaloacetic acid	0.58	131	87	10	5	Negative
Oxaloacetic acid	0.58	131	41	54	5	Negative

2.3.4.3. *Urine and plasma sample preparation*

Urine samples were filtered by using a minisart Sterile-ED 0.20 µm filter. After filtration, an aliquot (10 µl) was mixed with 0.2% formic acid (80 µl) and 0.1 mg/ml internal standard (deuterated D4-citric acid, 10 µl). The mixture was vortexed for 30 seconds and kept on ice for 5 minutes (vortex twice/2 minutes). Samples were then centrifuged at 13,000 \times g for 5 minutes (4 °C). Supernatants were transferred to HPLC vials and analysed by the LC-MS/MS method in the same day. Plasma samples (10 µl) were added to 5% trichloroacetic acid (80 µl) and 0.1 mg/ml internal standard (deuterated D4-citric acid, 10 µl). The mixture was processed as described above for urine samples. After centrifugation, supernatants were transferred to HPLC vials for analysis by LC-MS/MS.

2.3.4.4. *Cell lysate preparation*

Cell medium was removed once the cells reached 80% confluence, and cells were washed twice with 10 ml cold 0.9% sodium chloride (Sigma Aldrich). Cells were harvested using 0.025% (w/v) trypsin (GibcoBRL) in a phosphate-buffered saline solution (D-PBS w/o Calcium Magnesium, Life Technologies Ltd). After cell count with a haemocytometer, cell suspensions were centrifuged at 1,200 \times g for 10 minutes at room temperature. After decanting the supernatant, 10 ml of 0.9% sodium chloride was added and cells were gently suspended with a pipette before centrifugation at 1,200 \times g for 10 minutes. Subsequent removal of supernatant was followed by addition of 0.5 ml of 0.3 mM perchloric acid, the reaction mixture was kept on ice for 10 minutes followed by further centrifugation at higher speed of 12,000 \times g for 10 minutes. Supernatant was then collected and frozen at -20 °C until required for analysis. LC-MS/MS analysis was carried out within 24-72 hours from sample collection. All reagents were kept on ice (below 6 °C) at all times. TCA intermediate concentrations were normalised per 10⁶ cells. A schematic description of sample preparation from cultured cells is described in Figure 2.3.

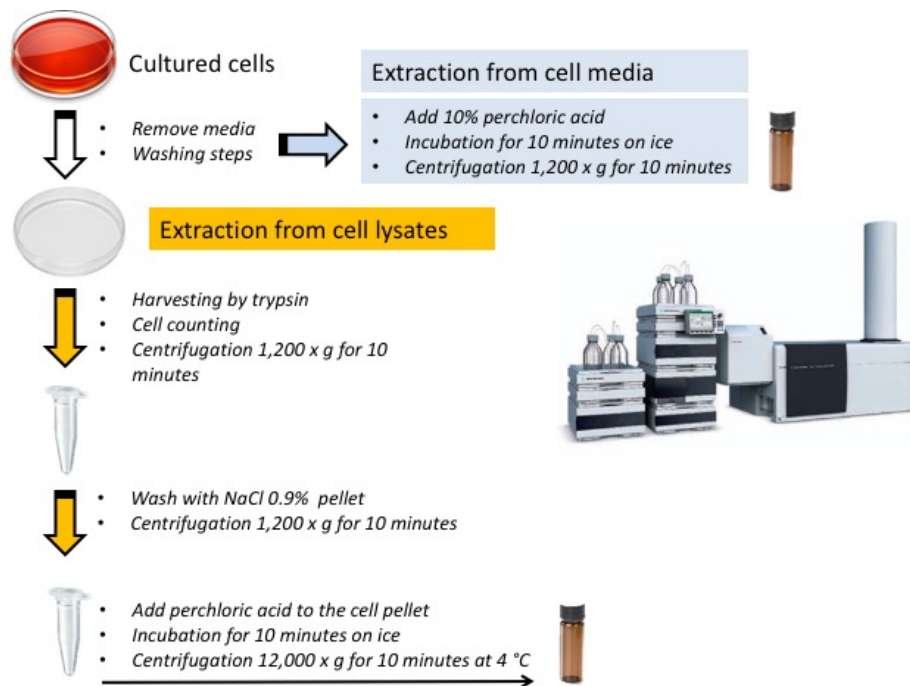


Figure 2.3 Extraction of TCA cycle intermediates from cultured cells.

2.3.4.5. Tissue preparation

Each vial of tissue representing an independent sample was received frozen from The Norwich Biorepository and kept at -80 °C until processed. Tissue was pulverized with liquid nitrogen using a tissue grinder (BioPulverizer, Stratech Scientific Limited). 500 µl of 3 M perchloric acid was added to each 20 mg of tissue powder and homogenised using an automated tissue homogeniser (IKA Ultra-Turrax T8 Disperser, Fisher Scientific Ltd) for 1 minute on medium speed. The homogenate was left on ice for 10 minutes then centrifuged at 12,000 \times g for 10 minutes at 4 °C. The supernatant was collected and transferred to a HPLC vial and analysed by the LC-MS/MS method on the same day. Results were obtained as mmol per kg of tissue. These values were converted to nM per g to facilitate comparison with available reference ranges.

2.3.4.6. Data analysis

Data files were explored and analysed using MassHunter Workstation software (Agilent Technologies). The peak areas of the analytes were determined, and the concentration of the analyte was calculated using the peak area ratio (peak area of analyte/peak area of the internal standard). In the present study, the treatment consisted of a number of doses thus requiring one-way ANOVA followed by Bonferroni multiple comparison tests.

2.4. Results

2.4.1 Optimization of mass spectroscopy conditions and LC parameters

The automated Agilent MassHunter Optimizer software was used to obtain precursor and products ions in each analyte. The most intense fragmentation patterns for organic acids are known to be decarboxylation and/or water elimination (127). In the current study, the precursor and product ions produced by the Agilent 6490 mass spectrometer were comparable with these patterns. However, selective fragments were also observed, and they can be useful if further identification is needed. An important example is represented by the fragmentation patterns observed for citric and isocitric acids. Both citric and isocitric acids show a main product ion with m/z 111 corresponding to $[M-H-CO_2-2 H_2O]^-$; however, isocitric acid also gives rise to a relatively stable product ion with m/z 155 corresponding to the neutral loss of two water molecules. The fragment m/z 155 produced by isocitric acid is hardly seen in the fragmentation pattern of citric acid. The same fragment 155 from isocitric acid was also observed by Bylund and colleagues (128). In terms of chromatographic separation, the use of Kinetex- C18 columns allowed good

separation and peak shapes for all TCA intermediates by using isocratic mobile phase 0.2% formic acid in water.

2.4.2 Method validation

This novel LC-MC/MS method was validated against published acceptance criteria for linearity, accuracy, precision, recovery, sample stability and matrix effect (129).

Briefly, calibration curves were obtained by using authentic standards spiked in a matrix containing deuterated D4-citric acid as internal standard. Ratio of analyte and internal standard peak area was plotted against the corresponding concentration to obtain the calibration curve. For all TCA analytes, the calibration curves showed linearity with correlation coefficients $r^2 > 0.9998$. In terms of sensitivity, limit of detection (LOD) and limit of quantification (LOQ) were calculated by injecting diluted solutions of TCA analytes in each matrix. LOD was estimated as the concentration of TCA intermediates that generated a peak with an area at least 3 times higher than the baseline noise. LOQ was calculated at a signal to-noise ratio 10 times higher than the baseline noise of these compounds. Furthermore, intraday precision was assessed by repeating the analysis of a single human plasma sample (number of repeat analysis= 10); CV (%) value was less than 10% for all TCA intermediates. The same samples were analysed on 5 days to determine interday precision, and CV (%) was < 15% for most of the analytes except for succinic acid (18.8%); an explanation for the higher CV (%) could be its low concentration in human plasma (Table 2.3). The results obtained from this method were compared to similar published work and outlined in Table 2.4.

Recovery was determined by spiking TCA intermediates at known concentrations in different matrices (0.2% formic acid in water; acidified synthetic urine and fatty acid-free HAS) with internal standard (deuterated D4-citric acid), and recoveries > 95% were found for all analytes.

Finally, the use of Agilent 12000 series high performance auto sampler with an injection program was used to minimise carry-over effects which have been assessed by the injection of acidified water after running the highest concentration of each TCA standard. No carry-over effect has been reported except for glutamic acid (< 1%).

Table 2.3 validation data for each analyte (human plasma sample).ⁱ

Analyte	Linearity	R ²	Precision		LOD*	LOQ*
	Range (µM)		Intraday (%) (n=10)	Interday (%) (n=5)		
Citric acid	0-520	0.9998	4.9	6.3	0.06	0.18
Iso-citric acid	0-520	0.9997	4.6	10.5	0.06	0.18
Malic acid	0-372	0.9999	8.9	13.5	0.06	0.18
Lactic acid	0-1100	0.9987	4.4	9.9	1	3
Succinic acid	0-840	0.9998	8.1	18.9	0.06	0.18
Fumaric acid	0-430	0.9998	8.8	12.2	1	3
Glutamic acid	0-340	0.9998	7.4	12.6	0.05	0.15

*values in µM for 1:10 sample dilution

Reproduced from Al Kadhi et al 2017 (126)

Table 2.4 Comparison between the described method and other methods of detection/quantification of Kreb's cycle acids

Author	Year published	Method	Matrix analysed	Number of detected TCA cycle metabolites	Run time	LOD of citric acid (μM)	LOQ of citric acid (μM)
Al Kadhi et al (current method)	2017	LC-MS/MS	Cell lysates (PC3 human prostate cancer), human plasma and urine samples	7	3 min	0.06	0.18
Luo et al(127)	2007	LC-MS/MS	Bacterial cell extracts (<i>E. coli</i>)	7	N/A	0.04	179.8
Bylund et al(128)	2007	LC-MS/MS	Soil solution and stream water	10	30 min	0.002	N/A
Tan et al(130)	2014	LC-MS/MS with derivatization	Cell lysate (human ovarian carcinoma) and mouse tumour tissue	8	8 min	N/A	N/A

2.4.3 Identification and quantification of TCA cycle intermediates in human urine samples

A synthetic urine sample was used with the addition of deuterated D4-citric acid standard to enable quantification. Following de-proteinisation with perchloric acid, TCA cycle intermediates were successfully detected in human urine samples (n=5). The calibration curve of each compound was linear and the correlation coefficient ranged from 0.95 to 0.99 in the linear range of concentrations of 0-10,000 ng/ml. An example of detected citrate (acquisition time=1.1 min) and isocitrate (acquisition time=0.8 min) is shown in Figure 2.4. The average citrate level measured in urine collected from healthy subjects (n=5) was 369.3 ± 37.1 $\mu\text{g/ml}$. Previous reports have indicated that urinary citrate excretion ranged between 350 and 1,200 mg/ day in healthy subjects (131, 132). Data obtained were comparable to the reported range of urinary citrate excretion taking into account that the normal range for 24-hour urine volume is 800 to 2,000 ml per day.

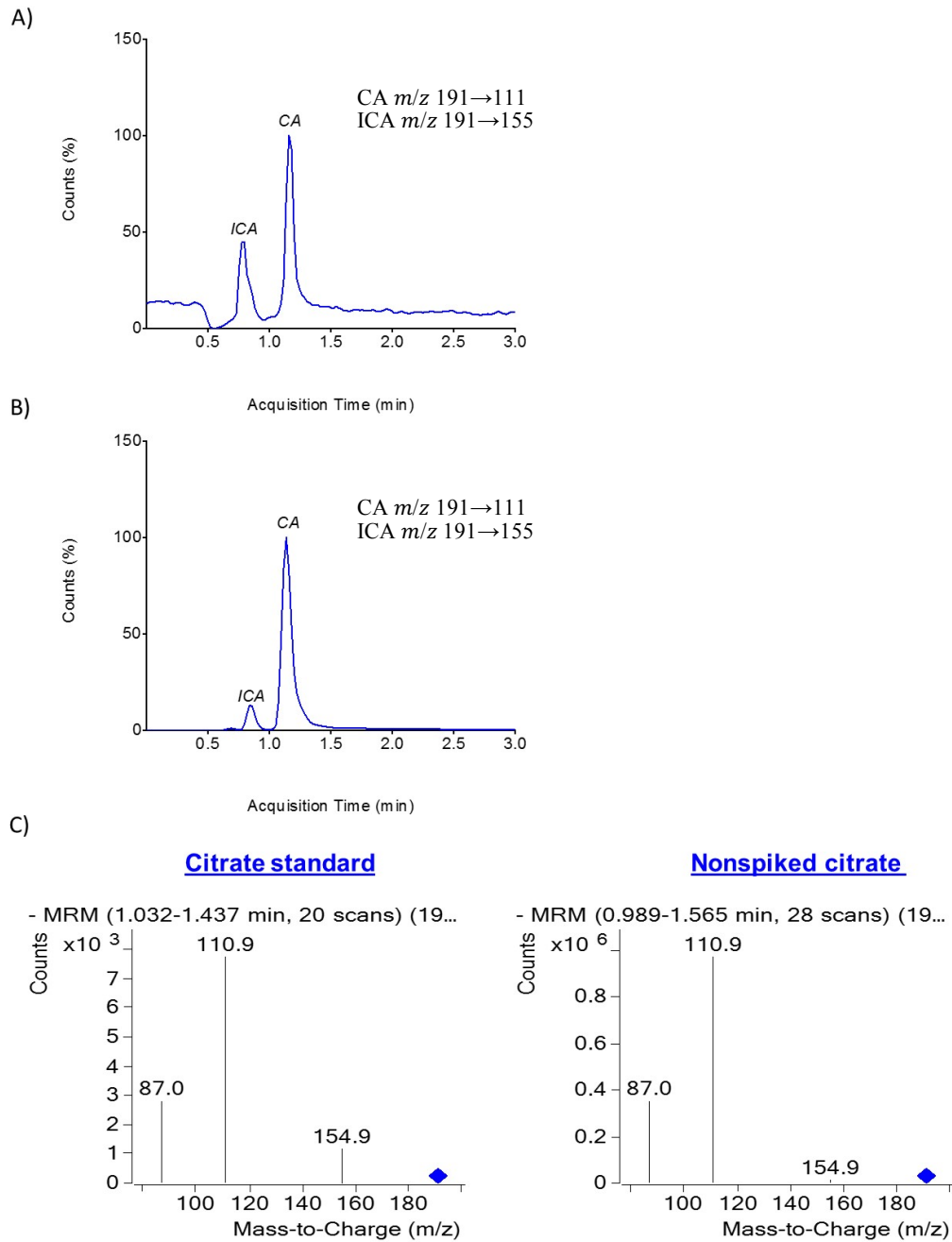


Figure 2.4 LC-MS/MS chromatograms of citrate and isocitrate in human urine. (A) Citrate and isocitrate standards spiked into a synthetic urine sample; (B) Citrate and isocitrate peaks in a nonspiked urine sample. (C) MS/MS spectra of citrate in both nonspiked and spiked urine samples. CA, citrate; ICA, isocitrate

2.4.4 Identification and quantification of TCA cycle intermediates from human plasma

TCA cycle intermediates were isolated and measured from human plasma (n=10). Figure 2.5 shows the detection of citrate and isocitrate standards in a bovine albumin construct and actual citrate/isocitrate detection peaks in human plasma. The calibration curve of each compound was linear and the correlation coefficient ranged from 0.96 to 1.0 in the linear range of concentrations of 0-10,000 ng/ml. The average concentrations obtained from human samples (143 ± 39.1 nM) were comparable to known reference range of citrate (100-300 nM) (133, 134). Previous studies confirmed that citrate with an average concentration of 135 μ M represents the most abundant intermediate of the TCA cycle in human blood (135).

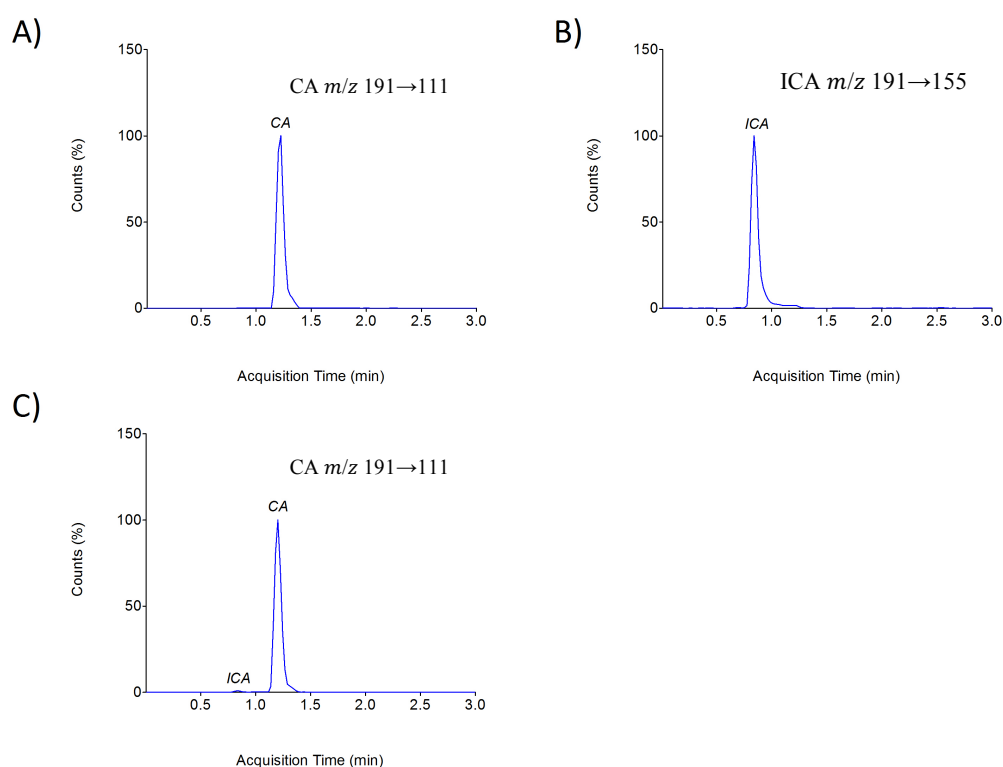


Figure 2.5 LC-MS/MS chromatograms of citrate and isocitrate in human plasma. A) Citrate standard spiked into a bovine albumin construct. B) Isocitrate standard spiked into a bovine albumin construct. C) Citrate and isocitrate peaks detected in human plasma sample. CA, citrate; ICA: isocitrate.

2.4.5 Quantification of TCA cycle intermediates from cell lysates

For the purpose of method development PC3, malignant androgen-independent prostate cells were cultured as previously described. Most of the TCA cycle intermediates were successfully detected and quantified using standard solutions. The calibration curve of each compound was linear and the correlation coefficient ranged from 0.96 to 1.0 in the linear range of concentrations of 0-10,000 ng/ml. Some of the TCA cycle intermediates were more pH sensitive and very unstable such as oxaloacetate and α -ketoglutarate; both of these organic acids were difficult to detect and quantify. Figure 2.6 and

Figure 2.7 show chromatograms of synthetic standards of TCA cycle intermediates and the TCA cycle intermediates detected from PC3 cell lysates, respectively.

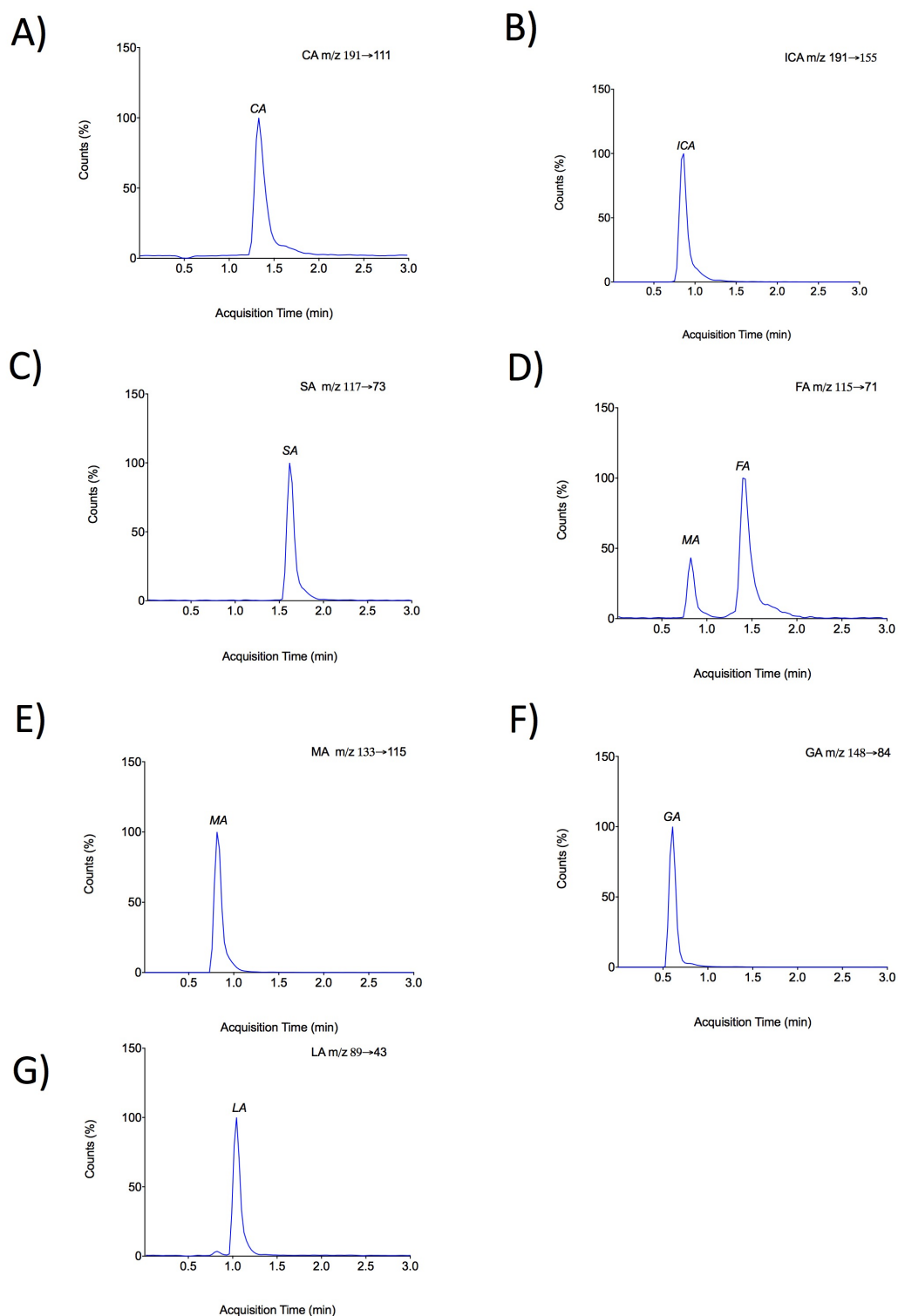


Figure 2.6 LC-MS/MS chromatogram of standards of TCA cycle intermediates. Standards were spiked into mobile phase (0.2% formic acid) and run as a mixture of all compounds. CA, citrate (A); ICA, isocitrate (B); SA, succinate (C); FA, fumarate. A second peak is observed here which is malic acid; MA, malate (E); GA, glutamate (F); LA, lactate (G).

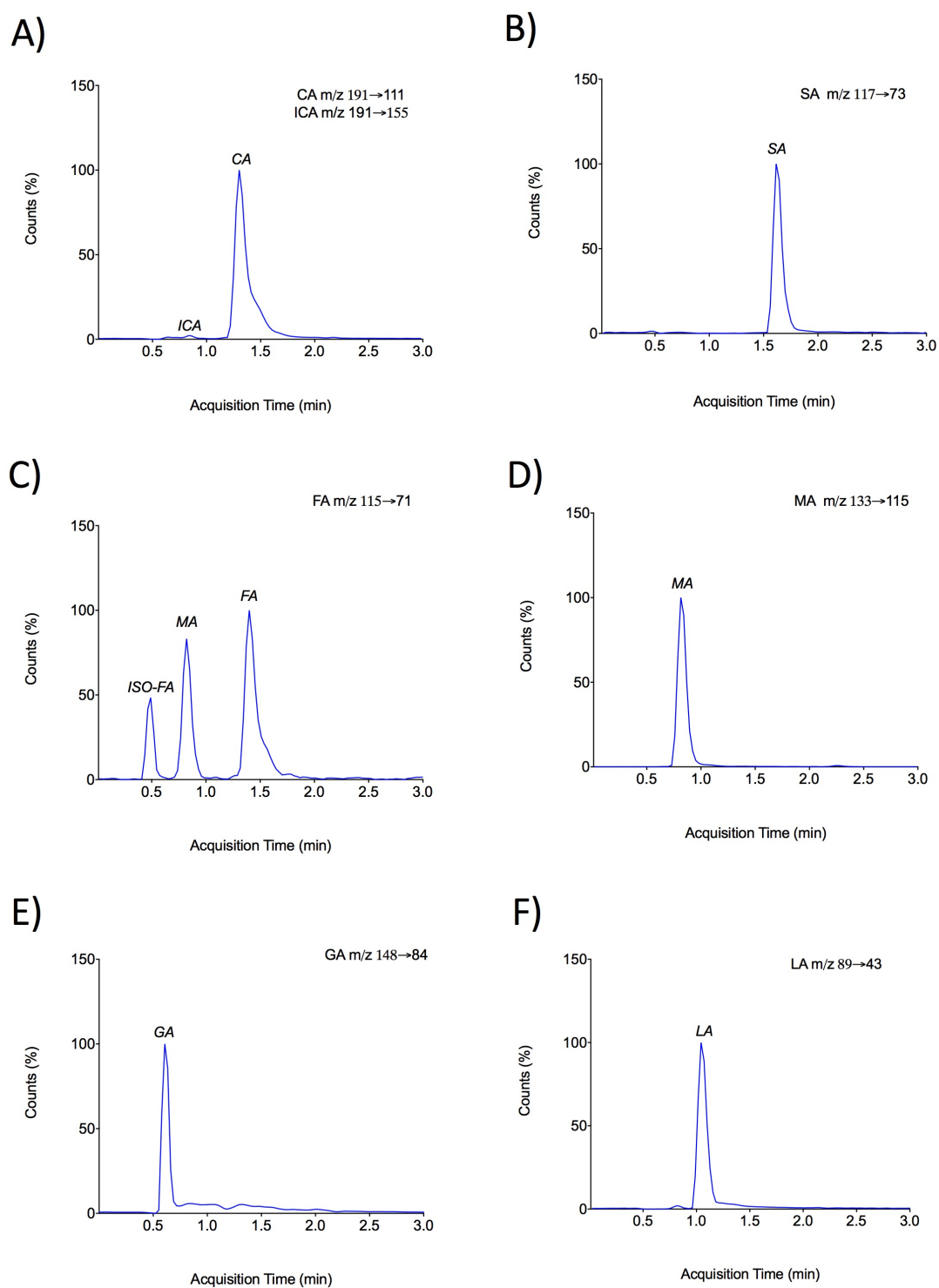


Figure 2.7 LC-MS/MS chromatograms of TCA cycle intermediates extracted from PC3 cell lysates. CA, citrate and ICA, isocitrate (A), SA, succinate (B), FA, fumarate. Two other acids are detected here; first is the likely isomer of fumarate (ISO-FA) and the second peak is malic acid (MA) (C); MA, malate (D); glutamate (E); LA, lactate acid (F).

2.4.6 Identification and quantification of citric acid from prostate tissue

Five histologically proven cancerous and five benign prostate tissue samples were obtained from the Norwich Biorepository (NNUH) in accordance with local regulatory approvals. Tissue originated from either radical prostatectomy/cysto-prostatectomy specimens or trans-urethral resection of the prostate (TURP). Table 2.5 outlines the origin of prostate tissue used in this experiment. Details of grade/stage were not included as the purpose of this experiment was for method development.

Citrate was successfully detected and quantified by LC-MS/MS in both benign and cancer tissue (Figure 2.9). The relative concentration of citrate was comparable with that of published data (Table 2.6) (136).

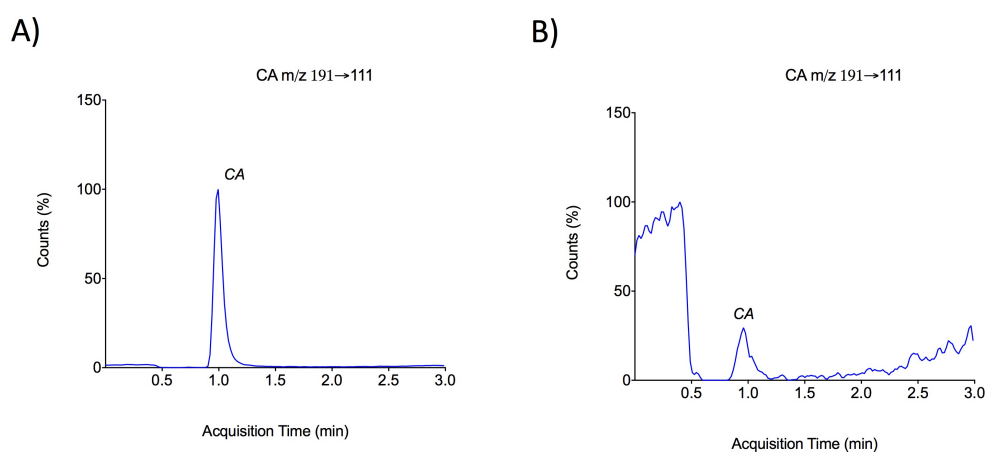


Figure 2.8. LC-MS/MS chromatograms of citrate in human prostate tissue. Citrate peak detected in benign (A) and cancer tissue (B). CA, citrate.

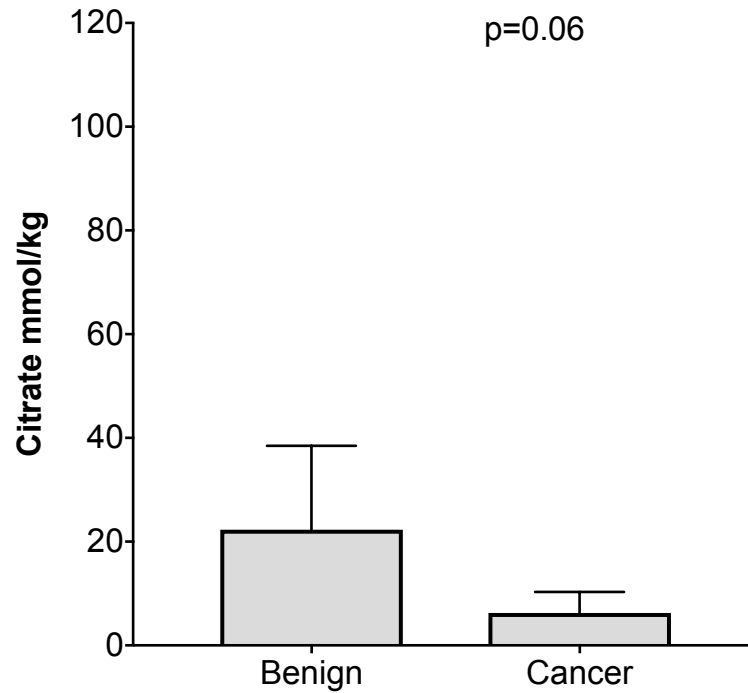


Figure 2.9 Citrate concentration (mmol) in human tissue. Frozen tissue samples were ground to powder before subsequent extraction. Citrate (mmol) was quantified from benign (n=5) and cancer (n=5) prostate tissue samples using LC-MS/MS. The results are corrected for tissue weight (kg). Bars represent the mean (SD) Statistical value obtained from student t-test.

Table 2.5 Description of tissue samples used for the extraction of TCA cycle intermediates

ID	Type of tissue	Specimen origin	Histological diagnosis
C1	Prostate (anterior left lobe)	Radical prostatectomy	Adenocarcinoma
C2	Prostate	TURP	Adenocarcinoma
C3	Prostate (left lobe)	Radical prostatectomy	Adenocarcinoma
C4	Prostate (right lobe)	Radical prostatectomy	Adenocarcinoma
C5	Prostate (left lobe)	Radical prostatectomy	Adenocarcinoma
B1	Prostate (left lobe)	Cysto-prostatectomy	Benign
B2	Prostate (right lobe)	Radical prostatectomy	Benign
B3	Prostate (left lobe)	Radical prostatectomy	Benign
B4	Prostate (left lobe)	Radical prostatectomy	Benign
B5	Prostate (right lobe)	Cysto-prostatectomy	Benign

Table 2.6 Average concentration of citrate in benign and cancerous prostate tissue expressed as nM per gram of tissue (SD)

Tissue	Citrate nM/g tissue	Reference citrate nM/g wt (136)
Benign	22,311 (16,160)	12,000-14,000
Cancer	6,220 (4,034)	200-2,000

2.5. Discussion

The metabolite profiling of tissue and body fluids has become increasingly important to study fundamental physiological aspects of human health and disease, as well as understanding the influence of different factors, such as diet and lifestyle changes (137).

Using LC-MS/MS methods for quantification of metabolites from biological matrices enables accurate detection of target compounds in relatively low concentrations, reducing interference (124, 138). When examining the TCA cycle intermediates, LC-MS/MS is arguably superior to enzymatic assays that invariably rely on fluorescence techniques to measure concentrations of substrates indirectly, and only allow measurement of one compound at a time (139). The LC-MS/MS method described in this Chapter allows simultaneous measurement of most TCA cycle intermediates with relatively easy sample preparation. In addition, it allows measurement of lactate and glutamate which provide key information regarding the processes of glycolysis and glutaminolysis, both of which influence the concentration of metabolites that are used as substrates in the TCA cycle reactions.

In a previous report describing LC-MS/MS quantification of TCA cycle intermediates from soil samples, Bylund *et al* outlined the retention times and ion mass/charge ratio (m/z) for each of the TCA cycle intermediates (128). These data were used in the current study to develop a method to quantify the same intermediates but using a different biological matrix (human prostate, plasma and urine). The extraction technique and mobile phase were modified to optimise the number of intermediates that could be measured in one batch. This significantly improved detection and run time resulting in high sensitivity and relatively short run-times compared to published data (Table 2.4). Despite this, both α -ketoglutarate and oxalate were difficult to detect. This is likely due to their instability and pH sensitivity, which has been previously reported (127, 140).

The method described in this Chapter showed successful detection of TCA cycle intermediates from a variety of biological sources. Measurement of citrate in particular, is shown to be reproducible and comparable to the ranges already reported in published literature (136). Citrate has been the most studied of the TCA cycle intermediates in relation to prostate metabolism, and has often been used as a surrogate for the function of the TCA cycle (135). It has also been reported that citrate plasma levels are the highest among TCA cycle intermediates in humans, and for this reason citrate metabolism is often studied to

better understand the role of the TCA cycle on the development of human metabolic diseases (134, 141).

The key metabolic pathways that cells adopt to produce energy for growth and replication appear to be altered in cancer, diverting energy and precursor production to glycolysis and using less oxidative respiration, even in the presence of adequate amounts of oxygen (142). In normal prostate cells, the TCA cycle is modified to allow the export of citrate from the mitochondrion into prostatic secretions; this process provides abundance of citrate, the main source of energy for sperm (135). It is therefore thought that this alteration to the normal metabolism might put prostate cells at a higher risk for cancerous transformations, as these changes also create an environment that facilitates tumour growth (42). In the next Chapter of this thesis, the method described here is applied to study the TCA cycle function in a number of prostate cell lines that are frequently used in *in vitro* studies. Furthermore, the effect of oxidative stress on the TCA cycle in cancerous and benign prostate cell lines is explored, and the potential effect of SF, a bioactive derived from broccoli plants against TCA disruption is investigated.

2.6. Conclusion

Measuring TCA cycle intermediates using LC-MS/MS is feasible and allows accurate quantification of multiple compounds simultaneously. The described method offers several advantages compared to methods previously reported, mainly in terms of easy sample preparation without derivatization steps and high sensitivity. The potential application of this method for analysing the TCA cycle in different biological matrices could be important in translational studies looking at metabolic changes in response to therapeutic or dietary agents. The method outlined here is used in the subsequent chapter to assess the role of SF *in vitro* on TCA cycle function in human prostate cell lines.

Chapter 3.

The *in vitro* effect of
sulforaphane on the TCA
cycle

Summary

The TCA cycle represents a crucial metabolic pathway in almost all living organisms. Several pathological conditions are characterised by an altered TCA cycle that is thought to be in part due to the disruption of ROS homeostasis and redox regulation. This chapter describes the use of the developed LC-MS/MS method for quantifying TCA cycle intermediates to further understand the complex role of cellular metabolism in normal and malignant prostate cell lines. Furthermore, it investigates whether the bioactive SF can alter the relationship between the TCA cycle and ROS production through its protective effects against oxidative stress.

3.1. Introduction

The TCA cycle is an important modulator of intracellular ROS through the production of nicotinamide adenine dinucleotide (NADH) and flavin adenine dinucleotide (FADH₂) from decarboxylation/oxidation reactions, and from having a direct link to the electron transport chain (143). It has been shown that human prostate epithelial cells, unlike most other eukaryotic cells, have modified the function of the TCA cycle to support the export of citrate out of the cytoplasm (114). Despite the energy deficit that incurs from not oxidizing citrate in the TCA cycle, this appears to be favoured by normal prostate epithelial cells to allow citrate to be used as both an energy source and to regulate the pH of seminal fluid. In contrast, cancerous prostate cells are thought to revert to utilizing citrate as a source of energy (144).

The different metabolic fate of citrate in prostate cells has been attributed to a major difference in the activity of a key TCA cycle enzyme named aconitase. This enzyme regulates the amount of citrate converted to iso-citrate, and therefore acts as a rate-limiting step in the cycle (Figure 3.1). Early research had suggested that the higher levels of zinc found in healthy compared to malignant prostate cells, inhibited the function of aconitase resulting in truncation of the TCA cycle and accumulation of citrate (Figure 3.1) (43, 145). However, more recent studies have challenged this view suggesting that zinc may not be responsible for the observed differences between benign and malignant cell types (121). Moreover, other factors have been found to influence the activity of TCA cycle enzymes such as the cellular oxidative status (146).

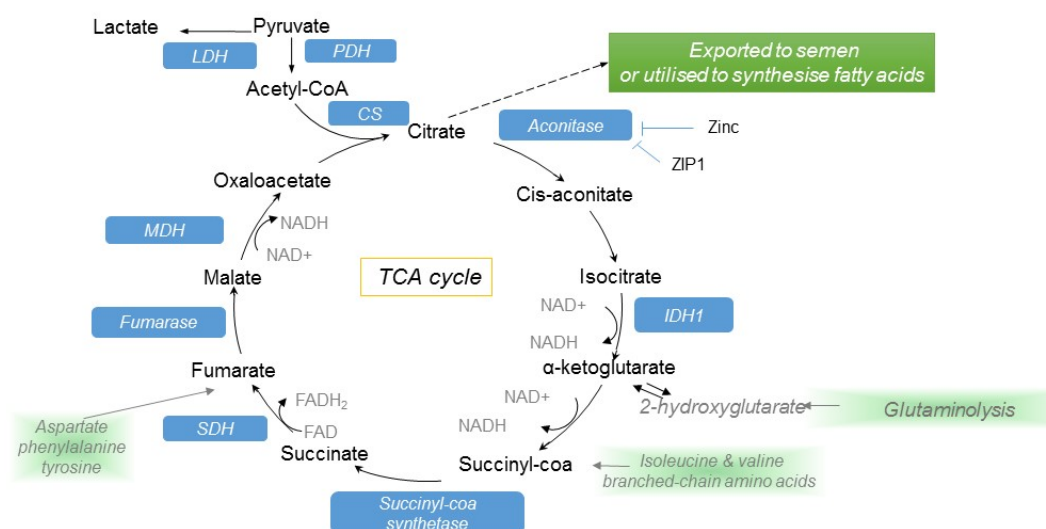


Figure 3.1 Outline of main reactions in the TCA cycle (solid black arrows). In prostate epithelial cells, citrate is exported out of mitochondria (dotted line) due to the inhibition of aconitase enzyme by zinc. PDH, pyruvate dehydrogenase. LDH, lactate dehydrogenase. CS, citrate synthase. IDH1, iso-citrate dehydrogenase 1. SDH, succinate dehydrogenase. MDH, malate dehydrogenase. ZIP1, Solute Carrier Family 39 (Zinc transporter), Member 1

SF is a naturally occurring phytochemical derived from cruciferous vegetables that has been found to have potential anti-cancer properties in a number of animal and cell models (147-149). Studies on the mechanism of action of SF in prostate cells have shown that it enhances the antioxidant capacity of the cell, largely via induction of phase II enzymatic pathways including glutathione and Nrf2 (102, 104, 150). The antioxidant potential of SF could therefore result in changes to redox-sensitive processes, which are known to regulate cellular metabolism, including the TCA cycle. SF has been shown to affect a number of mitochondrial functions in non-prostate cells through its antioxidant role (151). As a result, it would be reasonable to hypothesise that SF could alter the function of TCA cycle in the prostate.

This chapter describes the TCA cycle intermediates in a variety of prostate cells including benign, malignant, and metastatic phenotypes. The effect of dietary SF on these compounds in a cell culture environment was also investigated (Table 3.1). Because the reactions in the TCA cycle happen in a stepwise fashion, measuring changes in levels of the TCA cycle compounds would help understand if the cycle is perturbed by SF as a whole, and potentially identify which steps in the process are altered.

Table 3.1 Characteristics of human prostate cell lines used in this experimental design

Cell line	Description	Morphology	AR	Reference
PNT1A	Human Caucasian normal prostate, immortalised with SV40. Established from a histologically normal prostate of a 35 year old male at post mortem	Epithelial	Absent	(152)
RWPE-1	Human Caucasian normal prostate, immortalised with HPV-18. Established from a histologically normal prostate (peripheral zone) of a 54 year old male	Epithelial	Present	(153)
DU145	Human Caucasian prostate adenocarcinoma. Established from brain metastasis of a 69 year old male	Epithelial	Absent	(154)
LNCAP	Human Caucasian prostate carcinoma. Established from a lymph node metastasis of a 50 year old male	Epithelial	Present	(155)
PC3	Human Caucasian prostate adenocarcinoma. Established from bone metastasis of a 62 year old male	Epithelial	Absent	(156)

AR, androgen receptor

3.2. Hypotheses

- ❖ The TCA cycle intermediates in benign and malignant prostate cell lines commonly used in research experiments are different.

- ❖ SF *in vitro* can alter the TCA cycle of prostate cells exposed to ROS.

3.3. Materials and Methods

3.3.1 Cell culture

Human normal prostatic epithelial PNT1A (EAACC No 95012614) and RWPE (ATCC No CRL-11609) cell lines were purchased from ECACC and American Type Culture Collection (ATCC), respectively. PNT1A and RWPE are benign epithelial androgen insensitive immortalised cell lines. PNT1A cells were cultured in Roswell Park Memorial Institute (RPMI-1640) medium supplemented with 10% FBS, and RWPE1 cells were cultured in keratinocyte serum free medium (K-SFM). K-SFM medium was supplemented

with bovine pituitary extract (BPE, 0.05 mg/ml) and human recombinant epidermal growth factor (EGF, 5 ng/ml). Human cancerous Caucasian prostate adenocarcinoma DU145 (ATCC No HTB-81) and LNCaP (ATCC CRL-1740) were purchased from ATCC and cultured in EMEM and RPMI, respectively, both supplemented with 10% FBS. Human cancerous prostate adenocarcinoma PC3 cells were purchased from ECACC (No 90112714) and were routinely cultured in Ham's medium supplemented with 10% FBS. The three cancerous cell lines (PC3, DU145, and LNCaP) are immortalised cells derived from metastatic PCa samples, and only LNCaP is androgen sensitive.

All cells were routinely cultured as monolayers in a humidified atmosphere containing 5% CO₂ at 37 °C and were grown to 80% confluency on 10 cm dishes before performing the extraction of the TCA cycle intermediates as described in Chapter 2.

3.3.2 Treatment with hydrogen peroxide

Hydrogen peroxide (H₂O₂) was purchased from Sigma-Aldrich (Cat. No. 216763) and diluted in sterile MilliQ water and subsequently in culture medium to achieve a final concentration of 500 µM. All media were replaced for 24 hours before extraction. In the treatment group, media were changed to that containing H₂O₂ for 30 minutes before extraction of TCA cycle intermediates. DMSO was used as vehicle control.

3.3.3 Treatment with sulforaphane

4-(methylsulfinyl) butyl isothiocyanate (SF) (CAS 4478-93-7) (purity > 98%) was purchased from LKT Laboratories (St. Paul, USA). In each experiment, SF was added to culture media for 24 hours before treatment with H₂O₂ or extraction. The final concentration of SF in the media was 2 µM. Our research group has previously demonstrated that this concentration is representative of physiological levels of SF that are achieved in human plasma from consumption of cruciferous vegetables, such as broccoli (157).

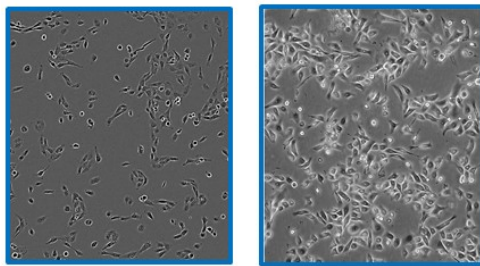
3.3.4 Analysis of TCA cycle intermediates by LC-MS/MS

To compare the level of citrate and other compounds of intermediary metabolism in benign and cancerous prostate models, LC-MS/MS analysis was performed after extracting the intermediates from cultured PNT1A, RWPE, DU145, LNCaP, and PC3 cells (Figure 3.2). Cells were counted using a haemocytometer after being harvested with 0.05% trypsin 0.53 mM ethylenediaminetetraacetic acid (EDTA). Cell lysate preparation and LC-MS/MS setup have been fully described in Chapter 2 (page 23-27).

The concentration of TCA cycle intermediates was normalised by dividing the total concentration by the cell count. Results are presented as nmol per 1 x 10⁶ cells in each

experiment. Data were expressed as mean \pm SD of two or more technical replicates from a minimum of three independent biological replicates. Statistical comparisons were carried out using analysis of variance (ANOVA) followed by Bonferroni multiple comparisons tests.

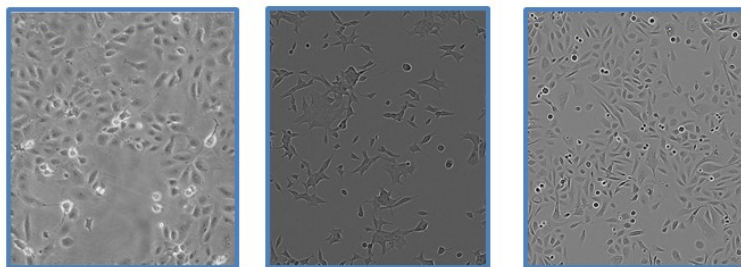
A) Human normal prostate cell lines



PNT1A

RWPE-1

B) Human cancerous prostate cell lines



DU145

LNCaP

PC3

Figure 3.2 Images of epithelial prostate cell lines used in this project. **A)** Benign epithelial androgen insensitive immortalised cells (PNT1A and RWPE1). **B)** Cancerous cell lines (PC3, DU145, and LNCaP) derived from metastatic PCa samples. Images were sourced from ATCC and ECACC websites.

3.3.5 Aconitase enzyme activity assay

Aconitase is an iron-sulfur protein that catalyses the isomerisation of citrate to iso-citrate via cis-aconitate. The enzymatic activity of aconitase of PNT1A and PC3 cells was measured by using a highly sensitive colorimetric assay (Cayman, Cat. No. 705502) following manufacturer's guidelines. The colorimetric assay is based on the conversion of citrate into iso-citrate by the aconitase enzyme present in the cell samples. Iso-citrate is then converted to α -ketoglutarate in a reaction catalysed by isocitric dehydrogenase. These reactions are monitored by measuring the increase in absorbance at 340 nm due to the production of NADPH. The rate of NADPH production is proportional to aconitase activity (Figure 3.3). PNT1A and PC3 cells were routinely cultured as previously described, and were grown to 80% confluency on 10 cm dishes before being processed following the protocol recommended by the manufacturer's instructions. After consecutive washing steps with cold PBS, cells were detached using a scraper and transferred to centrifuge tubes. After centrifugation at 800 x g for 10 minutes at 4 °C, the supernatant was discarded and the pellet was re-suspended in cold assay buffer. Cell suspensions were then sonicated with 20 one-second bursts. After centrifugation at 20,000 x g for 10 minutes at 4 °C, the resulting pellet was re-suspended in cold assay buffer and stored at -80 °C until assayed. 50 μ l of the sample was added in each well of a clear 96-well plate with 5 μ l of assay buffer, 50 μ l of NADP⁺ reagent, and 50 μ l of isocitric dehydrogenase assay buffer. The reaction was initiated by adding 50 μ l of substrate solution, and absorbance was measured at 340 nm for 30-60 minutes at 37 °C by using a filter-based multi-mode microplate reader (FLUOstar-Optima, BMG Labtech). Activated aconitase provided by the manufacturer was used as positive control.

The enzyme activity was determined as the rate of the reaction by calculating the change of absorbance of NADPH at 340 nm (ΔA_{340}) per minute. Absorbance values at each time point were used to produce a linear curve. The change in absorbance can be calculated from the following equation by choosing any two time points:

$$\Delta A_{340} = \left[\frac{A_{340}(\text{Time } 2) - A_{340}(\text{Time } 1)}{\text{Time } 2(\text{min.}) - \text{Time } 1(\text{min.})} \right]$$

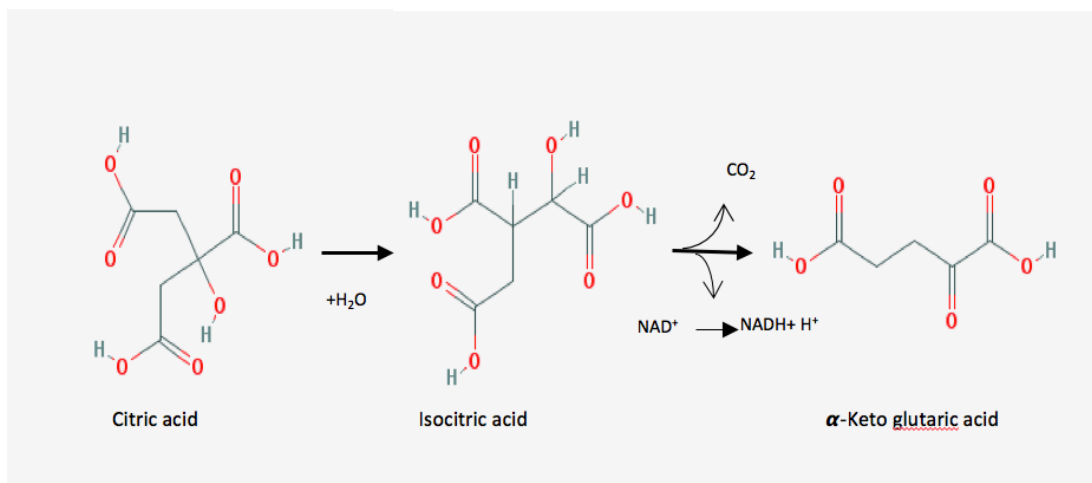


Figure 3.3 Chemical reactions explaining the principle of the aconitase enzyme assay.

3.3.6 Measurement of intracellular ROS production by fluorescence

Intracellular ROS levels were measured using the oxidant-sensitive probe 2',7'-dichlorofluorescein diacetate (DCFH-DA). PNT1A and PC3 cells were routinely cultured as previously described, and were grown to 80% confluency in a black bottom-clear 96 well plate. Cells were washed twice with PBS and incubated with DCFH-DA (20 μM) at 37 $^\circ\text{C}$ for 45 minutes in the dark. The dye, penetrating into viable cells, is metabolised in its free form, which can react with ROS and thereby develop fluorescence. Fluorescence was measured using a FLUOstar-Optima plate reader using 485 nm as λ_{exc} and 530 nm as λ_{em} . All data were analysed and expressed as means \pm SD of three independent experiments.

3.3.7 Microarray expression analysis

Whole genome extraction analysis using Affymetrix GeneChip[®] Human Exon 1.0ST microarrays was performed on extracted RNA from cultured prostate cells. RNA extraction was carried out by a PhD student of the Food and Health Programme (Ms T. Sivapalan) as part of her research project. Total RNA was extracted from treated cells using the QIAGEN[®] RNeasy Mini Kit according to manufacturer's instructions. RNA quantification was carried out using NanoDrop ND-1000 spectrophotometer using an average of three readings. The ratio of 260/280 absorbance (nucleic acid absorbance wavelength/protein absorbance wavelength) provided by the NanoDrop machine indicates RNA integrity. The RNA samples were sent to Nottingham Arabidopsis Stock centre and the Affymetrix GeneChip[®] Human Exon 1.0ST array was carried out according to manufacturer's protocols.

The data analysis was carried out using R/Bioconductor package (r-project.org). The raw signal intensity data was provided in .CEL files. The data was RMA (robust multi-array analysis)-background corrected and quantile normalised to determine if any outliers were present. Once complete, linear probe level models were fit to the data to analyse gene level summaries. Subsequent statistical data analysis was performed to identify differentially expressed genes using R/limma software. Identification of genes that were differentially expressed were analysed for the level of statistical significance at different Benjamini and Hochberg adjusted p-values, to account for the potential false discovery rate.

3.4. Results

3.4.1 Characterization of TCA cycle intermediates in prostate cell lysates

A summary reporting the concentrations of all TCA cycle intermediates in prostate cell lines measured by using LC-MS/MS can be found in Table 3.2.

3.4.1.1. Citrate

The concentration of citrate, which is often used as a measure of the TCA cycle function, was shown to be repeatedly higher in cancerous PC3 cells compared to all other cell lines tested (Figure 3.4). When compared to PNT1A, PC3 cells had significantly higher levels of citrate ($p < 0.01$).

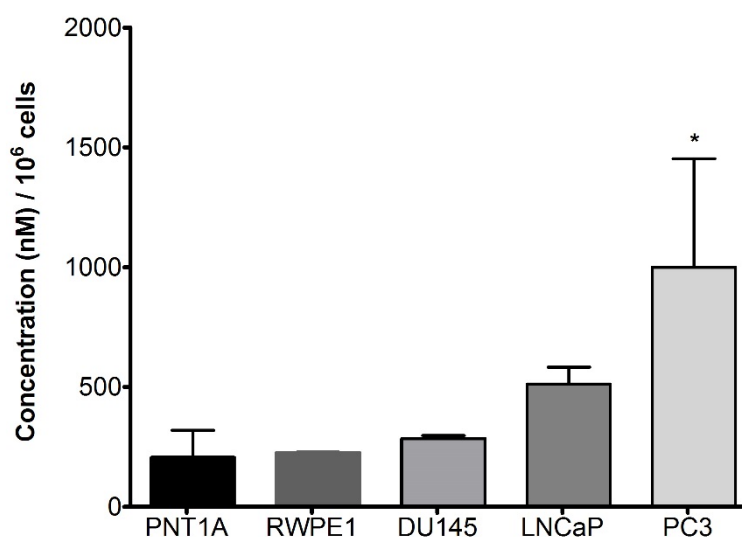


Figure 3.4 Concentration of citrate in prostate cell lines normalised to 10^6 cells. Each column represents an average of a minimum of three biological replicates. Error bars indicate standard deviation (SD). * $p < 0.01$ one-way ANOVA PC3 vs PNT1A.

3.4.1.2. *Iso-citrate*

Iso-citrate is generated from the conversion of citrate by the action of mitochondrial aconitase enzyme. Using LC-MS/MS it was possible to quantify iso-citrate despite its low concentration (Figure 3.5). Levels of iso-citrate were not statistically different between cell lines.

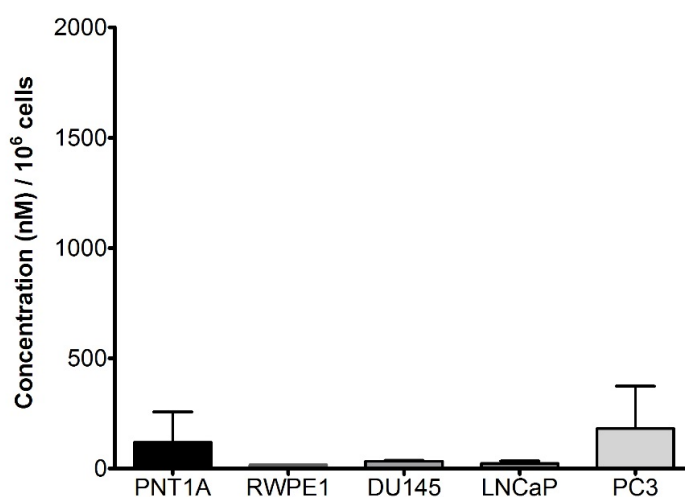


Figure 3.5 Concentration of iso-citrate in prostate cell lines normalised to 10⁶ cells. Each column represents an average of a minimum of least three biological replicates. Error bars indicate SD. Levels of iso-citrate were not statistically different between cell lines.

3.4.1.3. *Alpha- Ketoglutarate (α -KG)*

Measurement of α -KG was difficult due to pH sensitivity. Detection problems were solved by increasing the pH of the cell lysate to 7.0-7.5 with potassium hydroxide at the concentration of 0.6 mM. This enabled the successful quantification of α -KG, but the pH change resulted in the loss of the spectral signal of the other metabolites. α -KG levels in both PNT1A and PC3 cell lysates were almost identical (Figure 3.6).

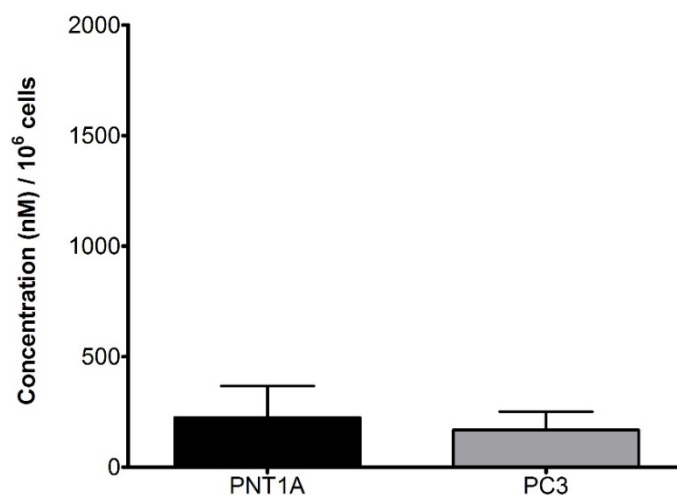


Figure 3.6 Concentration of α -KG in PNT1A and PC3 cells. Levels of α -KG were not statistically different between the two cell lines. Error bars indicate SD. Measurement of α -KG in the other cell lines was not possible, either due to low concentration or instability of the acid rendering it undetectable.

3.4.1.4. Succinate

Quantification of succinate from cell lysates was successful in all cultured cell lines. LNCaP cells had the highest concentration of succinate that was statistically significant when compared to PNT1A and PC3 cells ($p \leq 0.01$, one-way ANOVA) (Figure 3.7).

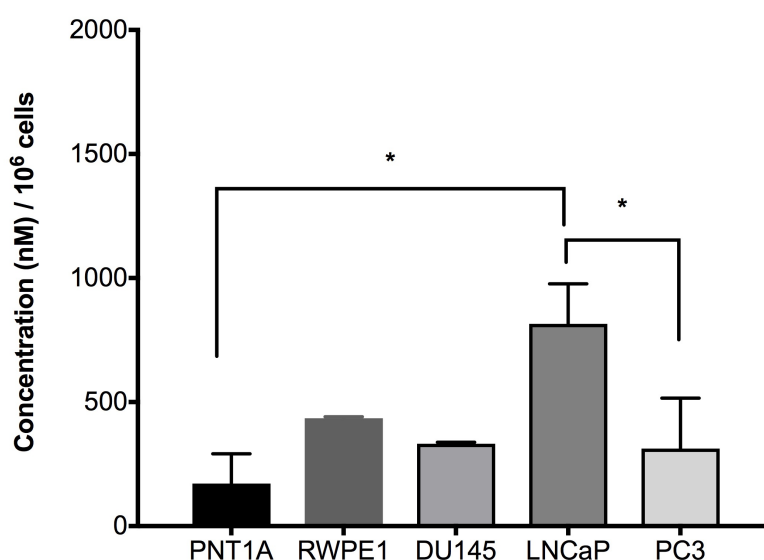


Figure 3.7 Concentration of succinate in prostate cell lines normalised to 10^6 cells. Each column represents an average of a minimum of three biological replicates. Error bars indicate SD. Statistically higher levels of succinate were observed in LNCaP cells compared to PNT1A and PC3 cells (* $p \leq 0.01$, one-way ANOVA).

3.4.1.5. *Fumarate*

PC3 cells showed the highest concentration of fumarate compared to both benign cell lines (PNT1A and RWPE1). Fumarate was not detectable in either LNCaP or DU145 cell lines with a LOD of 1 μ M (Figure 3.8).

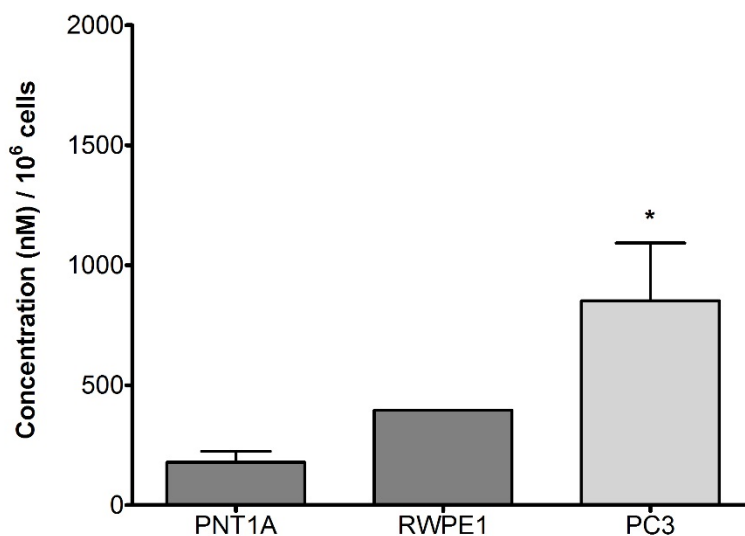


Figure 3.8 Concentration of fumarate in prostate cell lines normalised to 10⁶ cells. Each column represents an average of a minimum of three biological replicates. Error bars indicate SD. Measurement of fumarate was not feasible in all cell lines. PC3 cells showed the highest concentration of fumarate (* $p < 0.05$ PC3 vs PNT1A, one-way ANOVA).

3.4.1.6. *Malate*

Malate results from the conversion of fumarate in the mitochondria through the enzymatic conversion by malate dehydrogenase enzyme (MDH). It is also formed from the inter-conversion of cytosolic citrate via the action of malic enzyme (ME). Both LNCaP and PC3 cells showed high levels of malate, which were statistically significant when compared to PNT1A (Figure 3.9).

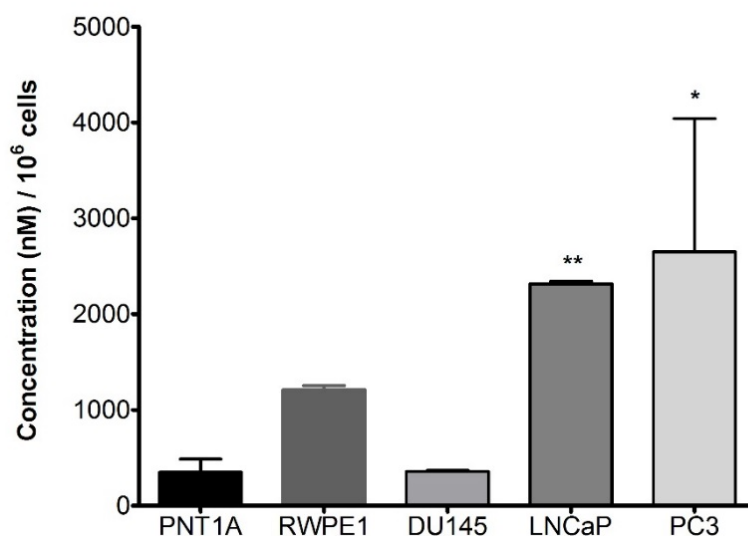


Figure 3.9 Concentration of malate in prostate cell lines normalised to 10^6 cells. Each column represents an average of a minimum of three biological replicates. Error bars indicate SD. PC3 and LNCaP cells had statistically higher levels of malate when compared to PNT1A and DU145 cells (* $p < 0.05$, ** $p < 0.001$; one-way ANOVA).

3.4.1.7. *Glutamate*

Glutamate is derived from the amino acid glutamine. In the absence of adequate glycolysis, glutamate can contribute to the TCA cycle. Therefore, its quantification can be informative when looking at the TCA cycle function. Results of glutamate analysis showed highest levels in LNCaP cell lysates (Figure 3.10).

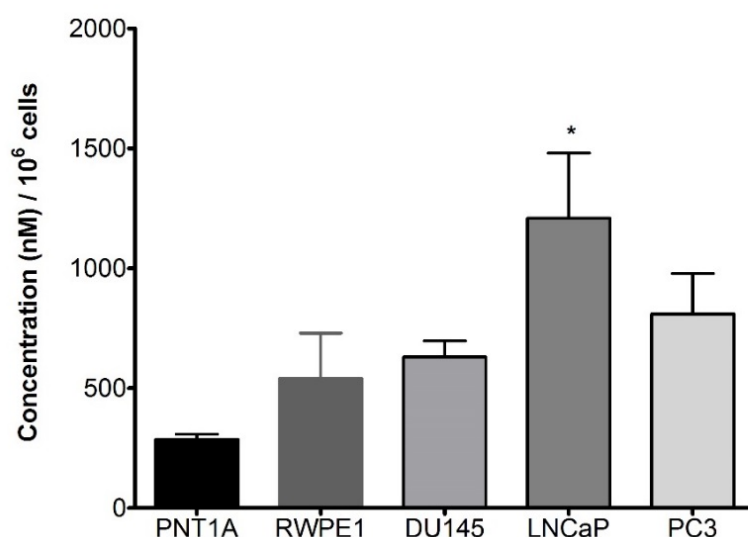


Figure 3.10 Concentration of glutamate in prostate cell lines normalised to 10^6 cells. Each column represents an average of a minimum of three biological replicates. Although glutamate is not directly part of the TCA cycle, it replenishes the intermediate α -KG through the conversion of glutamine to glutamate via the action of glutamase enzyme. (* $p < 0.01$; one-way ANOVA LNCaP vs PNT1A).

3.4.1.8. Lactate

Lactate is mainly the result of conversion of pyruvate from glucose breakdown. Tumours generally display high levels of lactate that are thought to contribute to the acidic environment which is favoured by cancer cells (158). In this analysis, lactate was almost three times higher in LNCaP cells compared to PC3 and PNT1A cells (Figure 3.11).

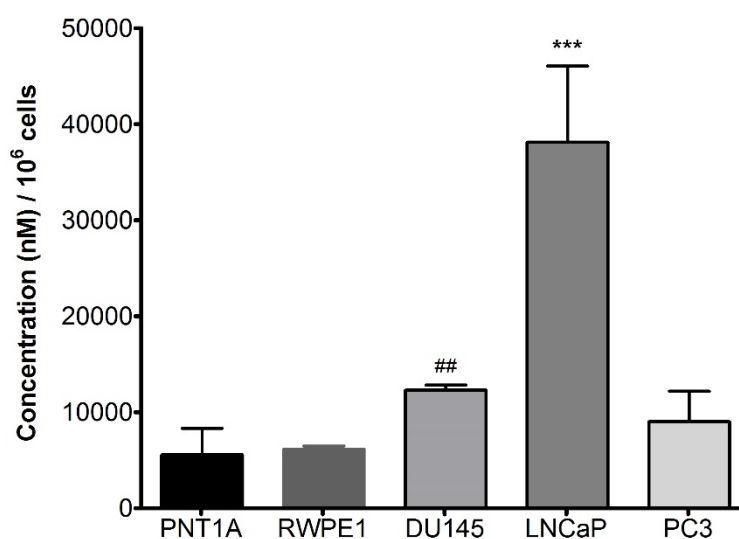


Figure 3.11 Concentration of lactate in prostate cell lines normalised to 10⁶ cells. Each column represents an average of a minimum of three biological replicates. Error bars indicate SD. LNCaP cells showed the highest concentration of lactate amongst the tested cell lines (**p<0.001 LNCaP vs PNT1A, RWPE1, PC3; ## DU145 vs LNCaP; one-way ANOVA).

Table 3.2 Average (SD) concentration of TCA cycle metabolites in commonly used prostate cell lines obtained using LC-MS/MS analysis of cell extracts.

	BR	Citrate	Iso-citrate	αKG	Succinate	Fumarate	Malate	Oxalate	Glutamate	Lactate
PC3-Hams F12	6	826 (175)	70 (4.7)	169 (81)	312 (203)	854 (514)	2,650 (1,388)	ND	154 (32)	10,551 (2,446)
PC3-RPMI	6	449 (47)	134 (10)	ND	219 (13)	ND	4,200 (370)	ND	935 (130)	6,376 (2,012)
PNT1A	6	198 (102)	18.6 (3.4)	225 (142)	182 (106)	179 (45)	306 (133)	ND	207 (111)	8,221 (5,700)
RWPE1	3	227 (2)	17 (0.4)	ND	435 (6)	395 (12)	1,210 (44)	ND	540 (189)	6,153 (326)
DU145	3	285 (13)	34 (3)	ND	332 (6)	ND	356 (13)	ND	630 (67)	12,295 (450)
LNCaP	3	511 (71)	23 (11)	ND	815 (161)	ND	2,316 (27)	ND	1,208 (272)	38,119 (7,947)
Concentration shown as (nM/10⁶ cells).										
BR; biological replicates, ND; not detected.										

3.4.2 Effect of culture media on TCA cycle metabolites

In this study, the higher levels of citrate found in the malignant PC3 cell line were contradictory to what has been described in studies of prostate tissue, which have repeatedly shown lower levels of citrate in cancerous prostates compared to benign glands (42, 115, 159, 160). One possible explanation for this result would be a different composition of the culture medium and the effect of FBS used to support the growth of cells in culture, both these possibilities were explored.

3.4.2.1. *The potential effect of foetal bovine serum on the results*

FBS was added in equal amounts to the media in each cell line. In addition, it was heat inactivated thereby eliminating any potential enzymatic effect. Therefore, the hypothesis that FBS could affect the levels of TCA cycle intermediates in the cultured prostate cell lines can be excluded.

3.4.2.2. *The effect of growth media*

To explore the influence of the culture medium on the concentration of citrate, first; the differences between the culture media of PNT1A and PC3 cells (HAM-F12 and RPMI-1640 respectively) were examined (Table 3.3). Second, an LC MS/MS analysis of TCA cycle intermediates was carried out on the cell-free growth media to quantify the levels of citrate. Finally, the levels of TCA cycle intermediates were measured in a repeat experiment where both cell lines (PNT1A and PC3) were cultured using RPMI-1640, supplemented with 10% FBS. RPMI-1640 does not contain zinc or pyruvate compared to HAM-F12 medium (Table 3.3).

Table 3.3 A comparison between constituents of RPMI-1640 and HAM-F12 media

Constituent	RPMI-1640 medium (concentration g/l)	HAM-F12 medium (concentration g/l)
Amino Acids		
Glycine	0.01	0.0075100
L-Arginine hydrochloride	0.24	0.211
L-Asparagine	0.05	0.01501
L-Aspartic acid	0.02	0.0133
L-Cystine	0.05	0.035
L-Glutamic Acid	0.02	0.0147
L-Glutamine	0.3	0.146
L-Histidine	0.015	0.02096

Constituent	RPMI-1640 medium (concentration g/l)	HAM-F12 medium (concentration g/l)
L-Hydroxyproline	0.02	NA
L-Isoleucine	0.05	0.00394
L-Leucine	0.05	0.0131
L-Lysine hydrochloride	0.04	0.0365
L-Methionine	0.015	0.00448
L-Phenylalanine	0.015	0.00496
L-Proline	0.02	0.0345
L-Serine	0.03	0.0105
L-Threonine	0.02	0.0119
L-Tryptophan	0.005	0.00204
L-Tyrosine	0.02	0.00778
L-Valine	0.02	0.0117
L-Alanine	NA	0.009
Vitamins		
Biotin	0.0002	0.0000073
Choline chloride	0.003	0.01396
D-Calcium pantothenate	0.00025	0.00048
Folic Acid	0.001	0.00132
Niacinamide	0.001	0.000037
Para-Aminobenz.oic Acid	0.001	NA
Pyridoxine hydrochloride	0.001	0.000062
Riboflavin	0.0002	0.000038
Thiamine hydrochloride	0.001	0.00034
Vitamin B12	0.000005	0.00136
i-Inositol	0.035	0.018
Others		
CuSO₄•5H₂O	NA	0.0000025
ZnSO₄•7H₂O		0.0008630
FeSO₄•7H₂O	NA	0.0008340
D-GJucose (Dextrose)	2	1.8020000
Glutathione (reduced)	0.001	
Phenol red	0.005	0.0013000
Putrescine•HCl	NA	0.0002
Pyruvic Acid•Na	NA	0.110000
Thioctic Acid	NA	0.00
Thymidine	NA	0.00073

3.4.2.3. *Quantification of citrate from growth media*

PNT1A and PC3 cells were cultured in RPMI-1640 and HAM-F12, respectively, supplemented with 10% FBS. Growth media were changed in all culture plates 24 hours prior to extraction of TCA cycle intermediates, and results were normalised per cell count. At the time of extraction, fresh aliquots of both growth media that had no contact with cells were also collected. Proteins were precipitated using equal added volumes (100 μ l) of 3 M perchloric acid. The remainder of the extraction methods were carried out as described in Chapter 2 section 2.2.4. The levels of citrate were very similar in “cell-free” RPMI-1640 and HAM-F12 media samples. Recovered media from PNT1A and PC3 cells after 24 hours of cell culture had higher levels of citrate compared to cell-free media, reflecting the cellular activity; however, there was no significant difference between the media of the two cell types (Figure 3.12).

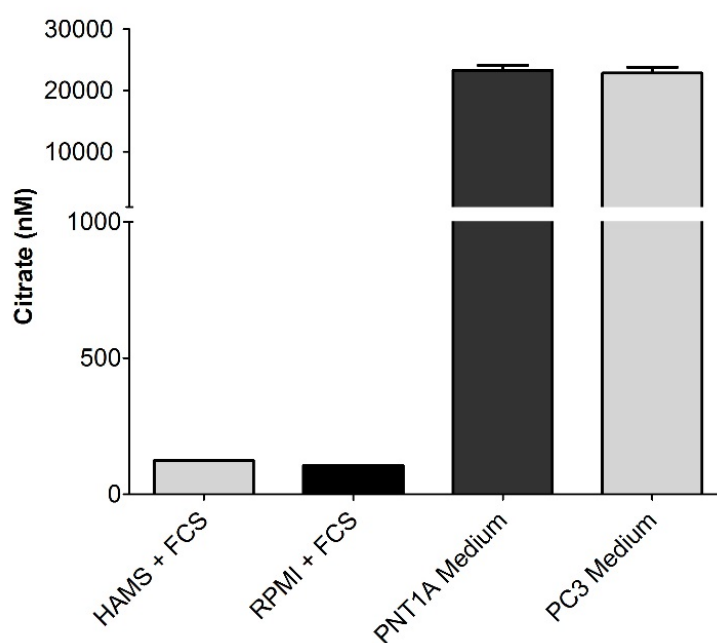


Figure 3.12 Citrate concentration in culture media measured using LC-MS/MS. The growth media was supplemented with 10% FBS. Citrate from PNT1A and PC3 culture media was measured after 24 hours of culture.

3.4.2.4. *The effect of change of culture medium on PC3 cells*

PC3 cells were grown in both RPMI-1640 and HAM-F12 media, following which TCA cycle intermediates were extracted as described in materials and methods. PC3 cells that were cultured in RPMI-1640 had lower levels of TCA cycle intermediates compared to those cultured in HAM-F12 medium, with the exception of glutamate which was significantly higher in the RPMI grown cells ($p < 0.05$) (Figure 3.13).

The concentration of the amino acid glutamine in commercial RPMI media is almost double that of HAM-F12, which could be responsible for the relatively high glutamate observed (Table 3.3).

3.4.2.5. TCA cycle intermediates in PNT1A and PC3 cells using RPMI-1640 as culture medium

When compared to PNT1A, the change of media did not affect the results significantly and there were still higher levels of intermediates in PC3 cell lysates except for lactate, which was significantly lower in PC3 cells when grown in RPMI-1640 medium (**Error! Reference source not found.**).

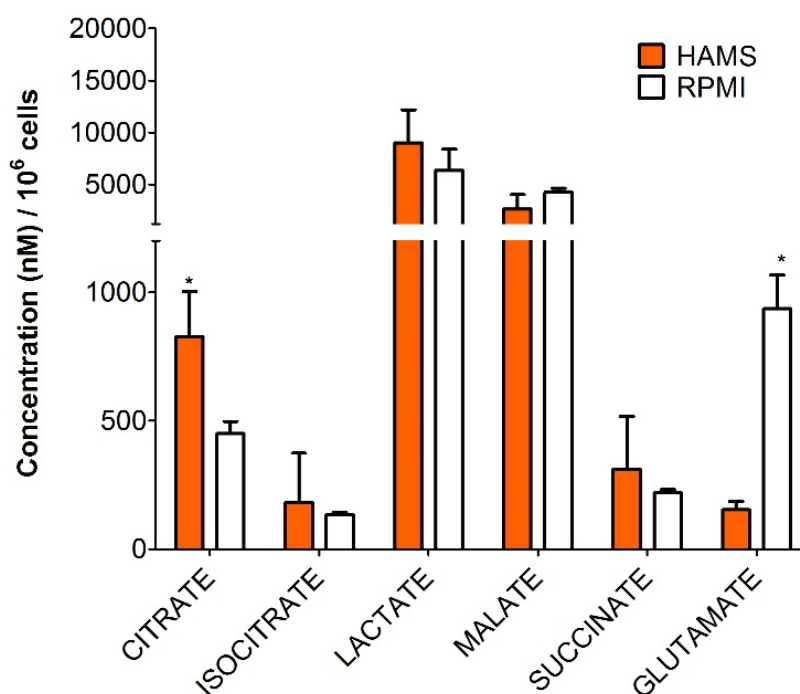


Figure 3.13 A comparison between levels of TCA cycle intermediates in PC3 cell lysates cultured using different growth media. Citrate and glutamate levels were significantly affected by change of growth medium; HAM-F12 medium (orange bars), RPMI-1640 medium (white bars). Each bar is an average of a minimum of three biological replicates. Error bars represent SD. (* $p < 0.05$, one-way ANOVA)

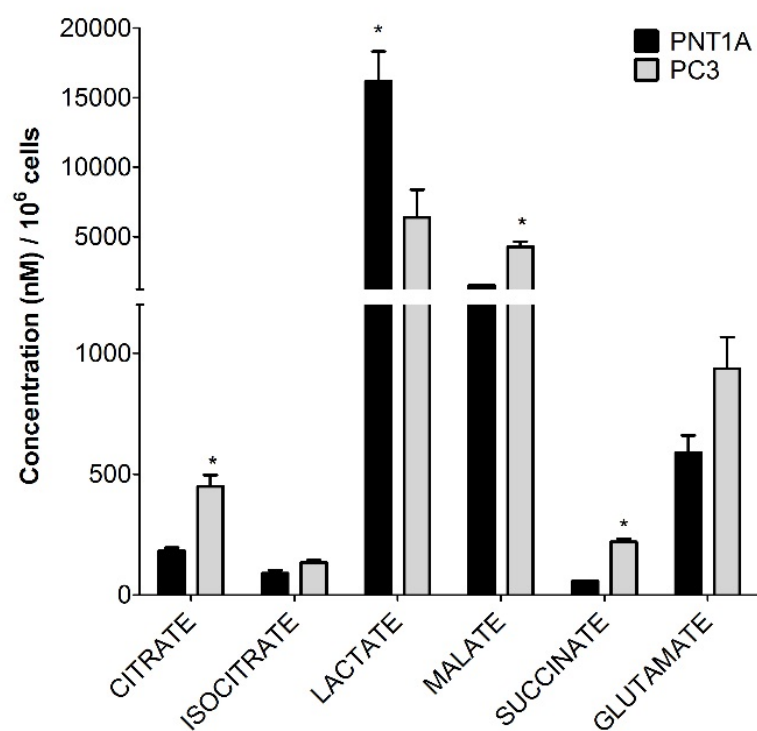


Figure 3.14 Comparison of TCA cycle intermediates in PNT1A and PC3 cells cultured using the same growth medium. PNT1A (black bars) and PC3 (grey bars) cells were cultured in RPMI-1640 medium with 10% FBS following the same experimental conditions. Each column represents an average of three biological replicates. Error bars indicate SD. (* $p < 0.05$, t-test)

3.4.3 Measurement of aconitase activity in PC3 and PNT1A cells

In order to measure the activity of aconitase in both cell lines, PNT1A and PC3 cells were cultured in the same growth medium (RPMI-1640). An enzyme extraction and activity quantification assay was performed as described in Materials and Methods (page 50). PC3 cells showed almost double the aconitase enzyme activity of PNT1A cells (4.7 vs 2.1 nmol/ml/minute, $p < 0.05$, t-test) (Figure 3.15). It is important to note that this enzymatic assay does not separate cytosolic from mitochondrial fractions of aconitase, and thus reflects the total aconitase activity of these cells lines.

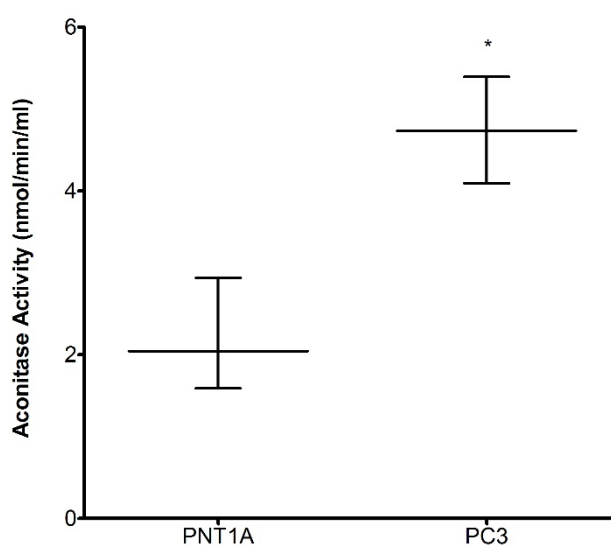


Figure 3.15 Activity of aconitase enzyme measured by rate of production of NADPH. The conversion of citrate to iso-citrate and subsequently to α -ketoglutarate releases NADPH which is measured by monitoring absorbance changes at 340 nm. The rate of reaction was calculated using the average of absorbance values between 1 and 29 minutes in three replicates. Data presented as average values and error bars indicate standard deviation from biological replicates. Data were normalised to protein content. p value < 0.05 , (unpaired t-test).

3.4.4 Gene expression profiles of enzymes of TCA cycle and associated fatty acid synthesis pathways in PC3 and PNT1A cells

The results of LC-MS/MS analysis showed that citrate was higher in the malignant cell line PC3, compared to benign PNT1A cells. These findings are in contradiction with previous studies on citrate concentration in cell models, as well as prostate tissue (119, 135, 159, 161). To investigate this further, microarray data obtained from Affymetrix analysis of RNA from both PNT1A and PC3 cells were examined. Following global analysis of gene expression, data were extracted for genes linked to the TCA cycle and lipid synthesis. Gene selection was based on reviewing metabolic pathways in Kyoto Encyclopaedia of Genes and Genomes (KEGG).

Figure 3.16 shows the fold difference in expression of key genes linked to the TCA cycle. Pyruvate dehydrogenase kinase subunits 1 & 3 (PDK 1 & 3) were strongly overrepresented in PC3 cells ($p < 0.0001$), whereas cytosolic aconitase 1 (ACO1 or cACO) was overexpressed in PNT1A cells ($p < 0.0001$). PC3 cells showed higher expression of isocitrate dehydrogenase (IDH1) and fumarate hydratase (FH), both of which could enhance the oxidization of citrate in the TCA cycle. The gene expression of the key rate-limiting mitochondrial enzyme in the TCA cycle, aconitase 2 (ACO2 or mACO), was not statistically different between the two prostate cell lines. Interestingly, several genes that control the synthesis of fatty acids and cholesterol, that have been linked with PCa, were overrepresented in the benign PNT1A cell line (Figure 3.17). HMGRC, an enzyme involved in cholesterol synthesis, and ACLY that controls citrate conversion to acetyl-CoA in the cytoplasm, were both overexpressed in PNT1A cells. PC3 cells showed higher levels of fatty acid synthase (FASN) expression, but did not reach statistical significance.

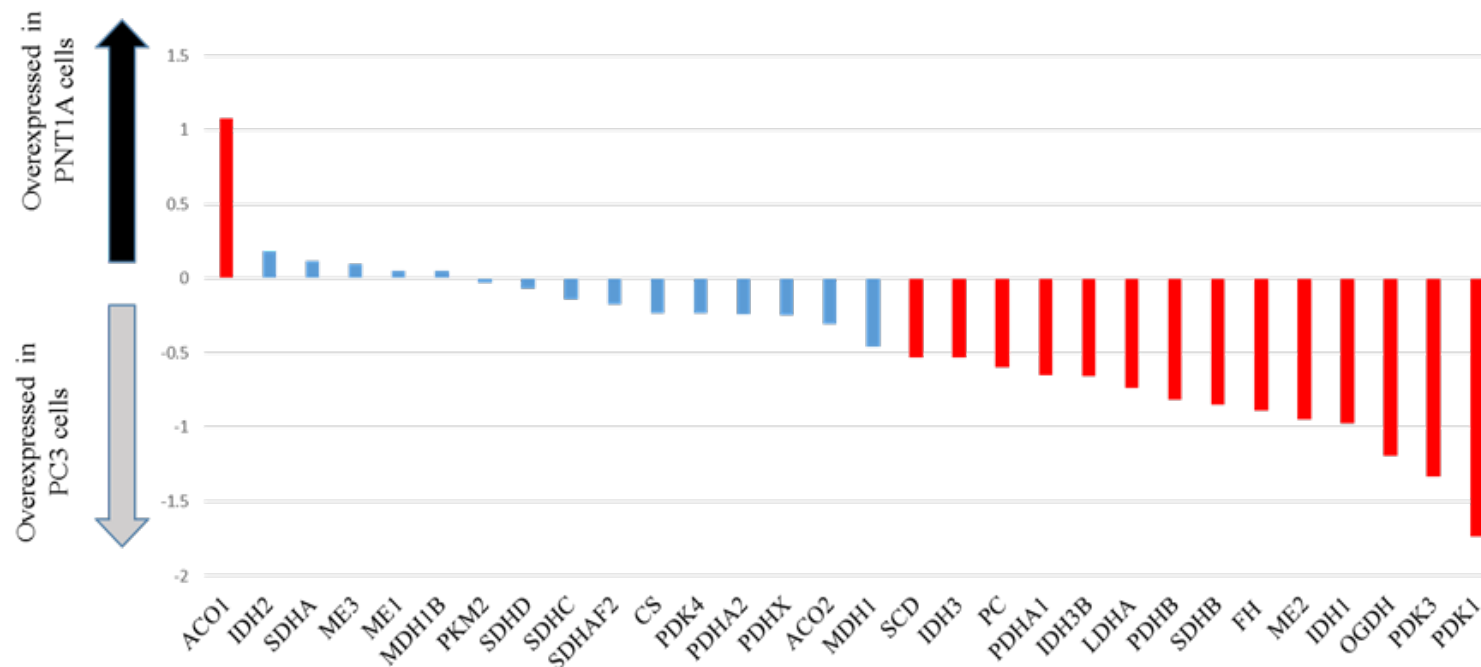


Figure 3.16 Microarray data of key TCA cycle-related genes. Data are shown as fold difference of \log_2 expression values. Statistically significant results are highlighted in red ($p < 0.05$, ANOVA). ACO1-2; aconitase 1-2, CS; citrate synthase, FH; fumarate hydratase, IDH1-3; isocitrate dehydrogenase 1-3, LDHA; lactate dehydrogenase A, MDH1; malate dehydrogenase 1 and 1B, ME1-3; malic enzyme 1-3, OGDH; oxaloglutarate dehydrogenase, SDHA-C; succinate dehydrogenase subunit A-C, SDHAF2; succinate dehydrogenase complex assembly factor 2, PDHA1-2; pyruvate dehydrogenase alpha 1-2, PDK 1-4; pyruvate dehydrogenase kinase 1-4, PKM2; pyruvate kinase muscle 2.

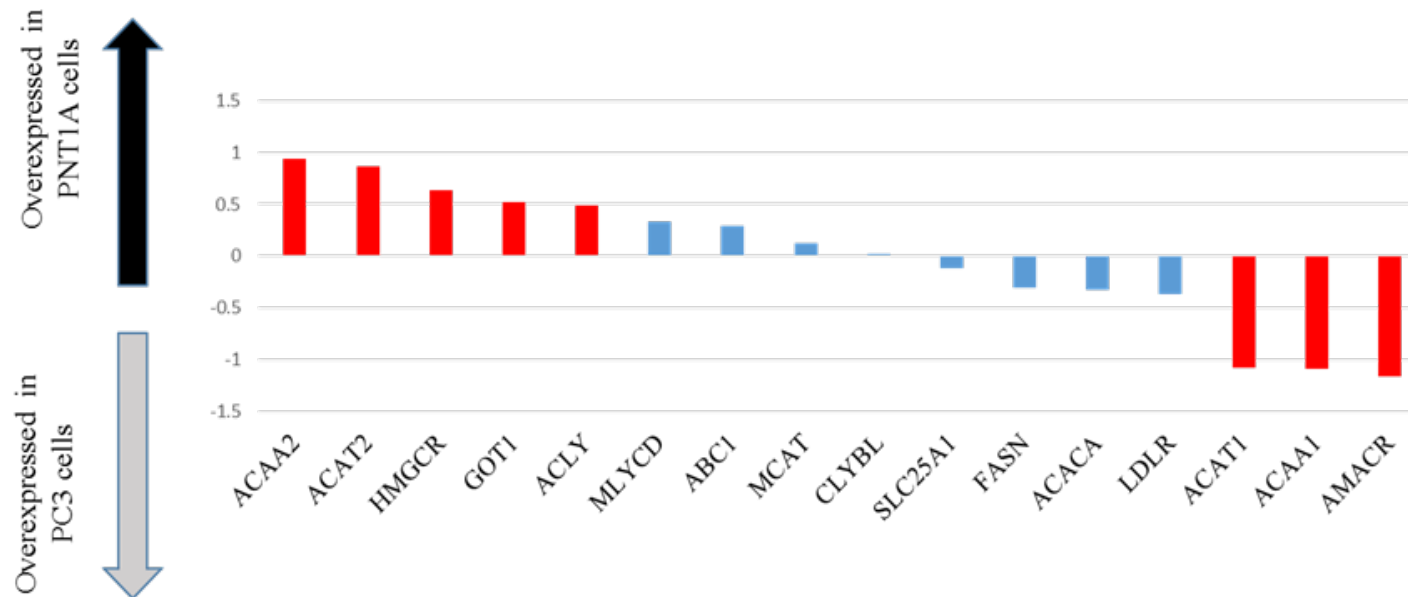


Figure 3.17 Microarray data of lipogenesis and anaplerosis-related genes. Data are shown as fold difference of log₂ expression values. Statistically significant results are highlighted in red (p<0.05, ANOVA). ABC1; ATP binding cassette protein 1, ACAA1-2; acetyl-CoA acyltransferase 1-2, ACACA; acetyl-CoA carboxylase alpha, ACAT1-2; acetyl-CoA acetyltransferase 1-2, ACLY; ATP citrate lyase, AMACR; alpha-methylacetyl-CoA racemase, CLYBL; citrate lyase beta like, FASN; fatty acid synthase, GOT1; glutamic-oxaloacetic transaminase 1, HMGCR; 3-hydroxy-3-methylglutaryl-CoA reductase, LDLR; low density lipoprotein receptor, MCAT; malonyl CoA:ACP acyltransferase, MLYCD; malonyl-CoA decarboxylase, SLC25A1; solute carrier family 25 (mitochondrial carrier; citrate transporter), member 1.

3.4.5 The effect of oxidative stress on the TCA cycle

3.4.5.1. *Baseline levels of ROS in PC3 and PNT1A cells*

In order to investigate the effect of ROS on the TCA cycle in prostate cells, benign PNT1A and malignant PC3 cells were cultured as described in Materials and Methods (page 51). Baseline levels of H₂O₂ were measured in both cell lines (Figure 3.18). PC3 cells showed almost double the amount of H₂O₂ measured in PNT1A cells, which is in accordance with published data.

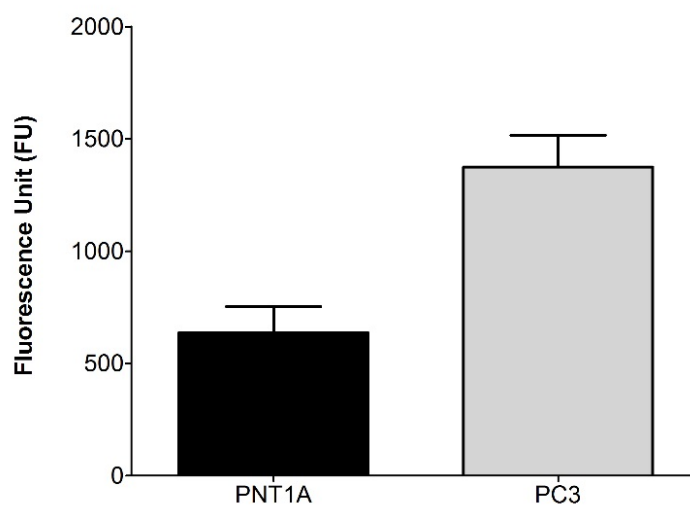


Figure 3.18 Baseline levels of ROS in prostate cell lines. PC3 cells (grey bar) display higher levels of ROS compared to PNT1A (black bar). Data are expressed as fluorescence unit from three independent experiments (average \pm SD) seeding cells at the same recommended density of 25×10^3 /well.

3.4.5.2. *The effect of exogenous hydrogen peroxide on the TCA cycle in PC3 and PNT1A cells*

A further experiment was conducted to examine the effect of oxidative stress on levels of citrate and other TCA cycle intermediates. The addition of H₂O₂, at the concentration of 500 μ M, to both cell lines for 30 minutes resulted in an increase in citrate levels compared to controls (Figure 3.19).

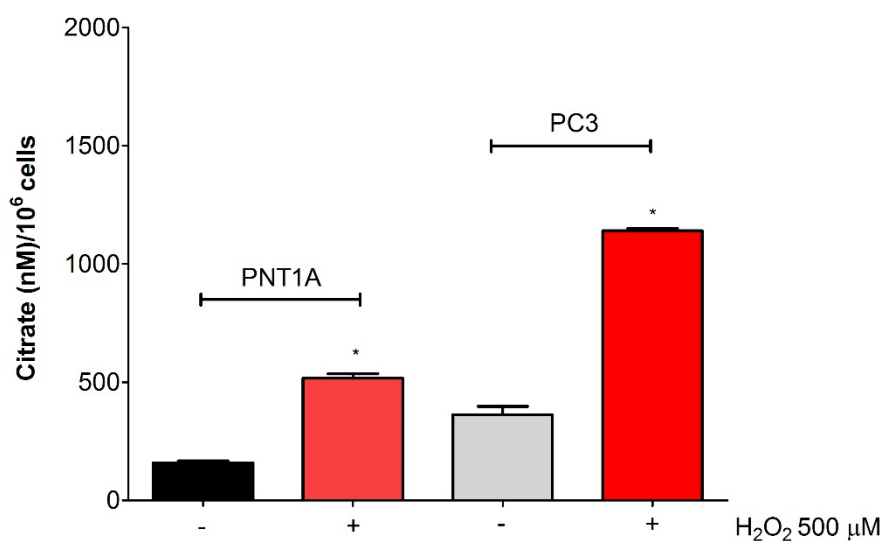


Figure 3.19 Citrate levels in prostate cell lines exposed to oxidative stress. Treatment with 500 μM of H₂O₂ results in a significant increase in citrate levels compared to controls in normal PNT1A and cancerous PC3 prostate cells; untreated PNT1A (black bars) and PC3 (grey bars). *p<0.05, unpaired t-test.

3.4.6 The *in vitro* effect of sulforaphane on the TCA cycle

Studies on the beneficial properties of dietary ITCs have reported their indirect antioxidant action through the induction of antioxidant defence mechanisms (phase II enzymes) (150). Previous work carried out in our research group has demonstrated that SF can protect prostate cells against oxidative stress and restore the activity of key enzymes involved in the TCA cycle, such as the α -ketoglutarate dehydrogenase (α -KGDH) (unpublished data). To investigate whether SF could alter the function of the TCA cycle in an oxidative stress environment, PNT1A and PC3 cells were exposed to physiologically relevant concentrations of SF before being challenged with a pro-oxidant agent (H₂O₂).

3.4.6.1. Does sulforaphane alter TCA cycle function at physiological concentrations?

Both PNT1A and PC3 cells were exposed to 2 μM SF or vehicle control (DMSO) for 24 hours before extraction of TCA cycle intermediates. SF alone did not have an effect on citrate in either of the cell lines (Figure 3.20).

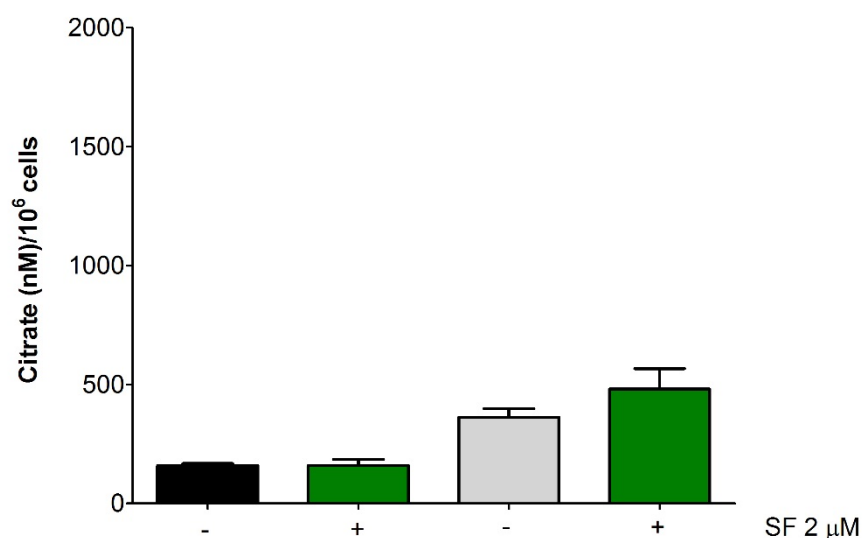


Figure 3.20 Citrate levels in PNT1A and PC3 cells exposed to SF. Treatment with SF (green bars) for 24 hours did not alter the levels of citrate compared to untreated PNT1A (black bars) and PC3 (grey bars). Each column represents an average (SD) of biological replicates.

3.4.6.2. Does sulforaphane alter TCA cycle function in the presence of oxidative stress?

3.4.6.2.1. Citrate levels in PC3 cells exposed to a pro-oxidant agent

The addition of H₂O₂ to culture media for 30 minutes markedly increases citrate levels in PC3 cell extracts ($p < 0.05$). This effect was significantly reduced when cells were exposed to SF (2 μ M) for 24 hours before being exposed to H₂O₂ challenge ($p < 0.05$, one-way ANOVA) (Figure 3.21).

3.4.6.2.2. Citrate levels in PNT1A cells exposed to a pro-oxidant agent

The exposure of PNT1A cells to H₂O₂ for 30 minutes resulted in a similar increase in citrate levels as seen in the malignant PC3 cell line; however SF did not have the same effect and no reduction was seen in levels of citrate when cells were incubated with SF before exposure to H₂O₂ (Figure 3.22).

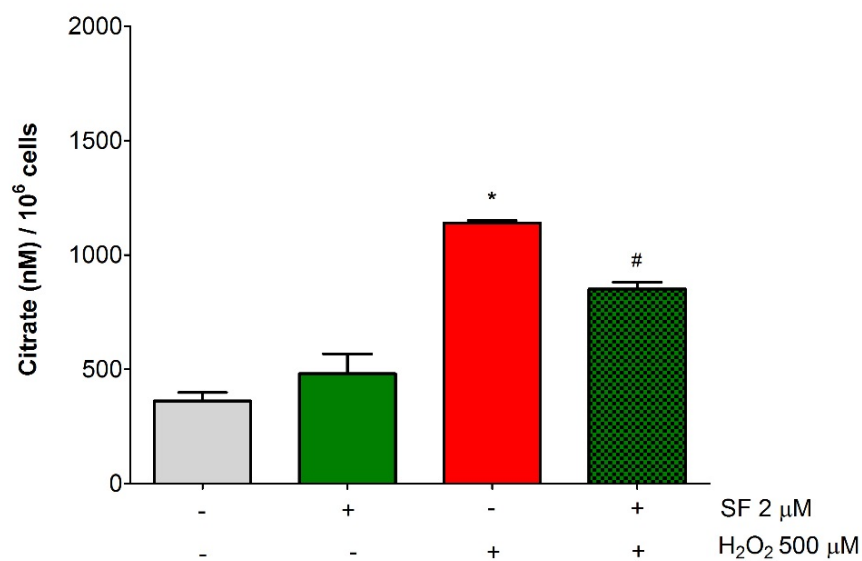


Figure 3.21 Citrate levels in PC3 cells exposed to SF for 24 hours prior to treatment with H₂O₂ for 30 minutes. Each column represents the average (SD) of biological replicates. (*p<0.001 vs untreated cells, #p<0.05 vs H₂O₂, one-way ANOVA).

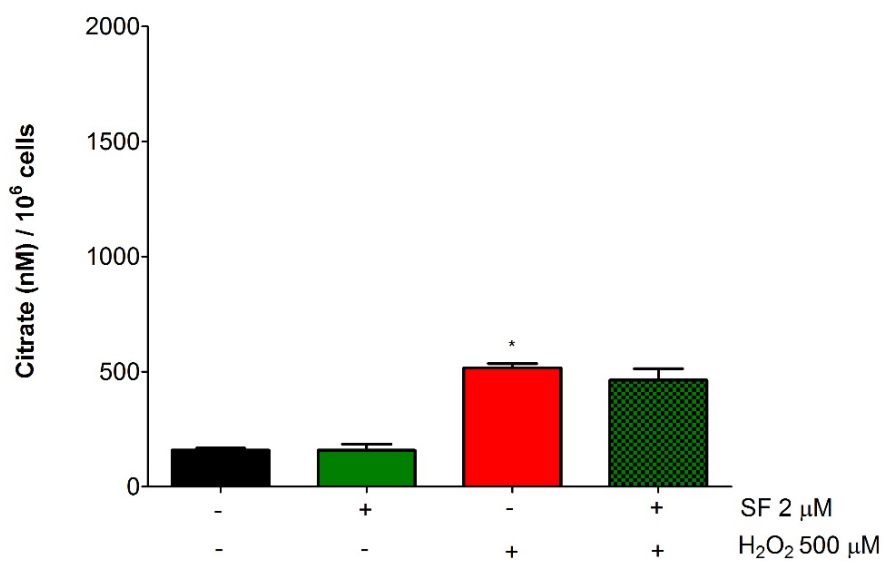


Figure 3.22 Citrate levels in PNT1A cells exposed to SF for 24 hours prior to treatment with H₂O₂ for 30 minutes. Each column represents the average (SD) of biological replicates. (*p<0.001 vs untreated cells, one-way ANOVA).

3.5. Discussion

3.5.1 Changes to the TCA cycle in prostate cells

The TCA cycle is a key metabolic process in mammalian cells (143). Acetyl-CoA from glycolysis and other nutrient breakdown enters the TCA cycle to produce citrate. Sufficient evidence now exists to support the theory of altered metabolism in prostate cells. Where most healthy mammalian cells oxidise citrate in the mitochondria to primarily produce energy; prostate cells have the ability to accumulate and subsequently excrete citrate (145). It is important to note that this property is seen in epithelial secretory prostate cells. The prostate epithelium is made up of different cellular components including epithelial secretory cells, basal, neuroendocrine, and stem cells (162). The outer portion of the prostate gland (the peripheral zone) forms the majority of the bulk of the gland, and is also the zone where most glandular tissue is found. Therefore, higher numbers of epithelial cells are seen in the peripheral zone, and similarly higher rates of adenocarcinoma are observed in this zone of tissue (162-164).

PCa cells are able to switch back to citrate oxidation. This shift to citrate oxidation provides cancer cells with energy. Studies of citrate content from prostate tissue using magnetic resonance spectroscopy imaging (MRSI) and NMR techniques, in both rodents and in humans, have repeatedly shown a drop in citrate concentration in malignant compared to healthy tissue (136, 160). This is different to what is observed in other mammalian tumours, where aerobic glycolysis is up-regulated by the action of ACLY enzyme (165). Many tumours therefore rely on a truncated TCA cycle in order to increase lipid and FA synthesis, which are used to increase tumour biomass (166). In contrast, it would appear that PCa cells have to achieve a fine balance of increasing energy supply through citrate oxidation as well as increased fatty acid β -oxidation. This would provide a constant supply of acetyl-CoA for macromolecular synthesis, especially given the fact that most PCa cells have lower capabilities of using glucose for this purpose (Figure 3.23) (56).

The ability of PCa cells to enhance lipid synthesis has been demonstrated by several groups that collectively show up-regulation in the expression of key genes that regulate crucial enzymatic steps, such as FASN, ACLY and alpha-methylacyl-CoA racemase (AMACR). AMACR is a peroxisomal enzyme that regulates the entry of branched chain fatty acids to mitochondrial β -oxidation (167-170).

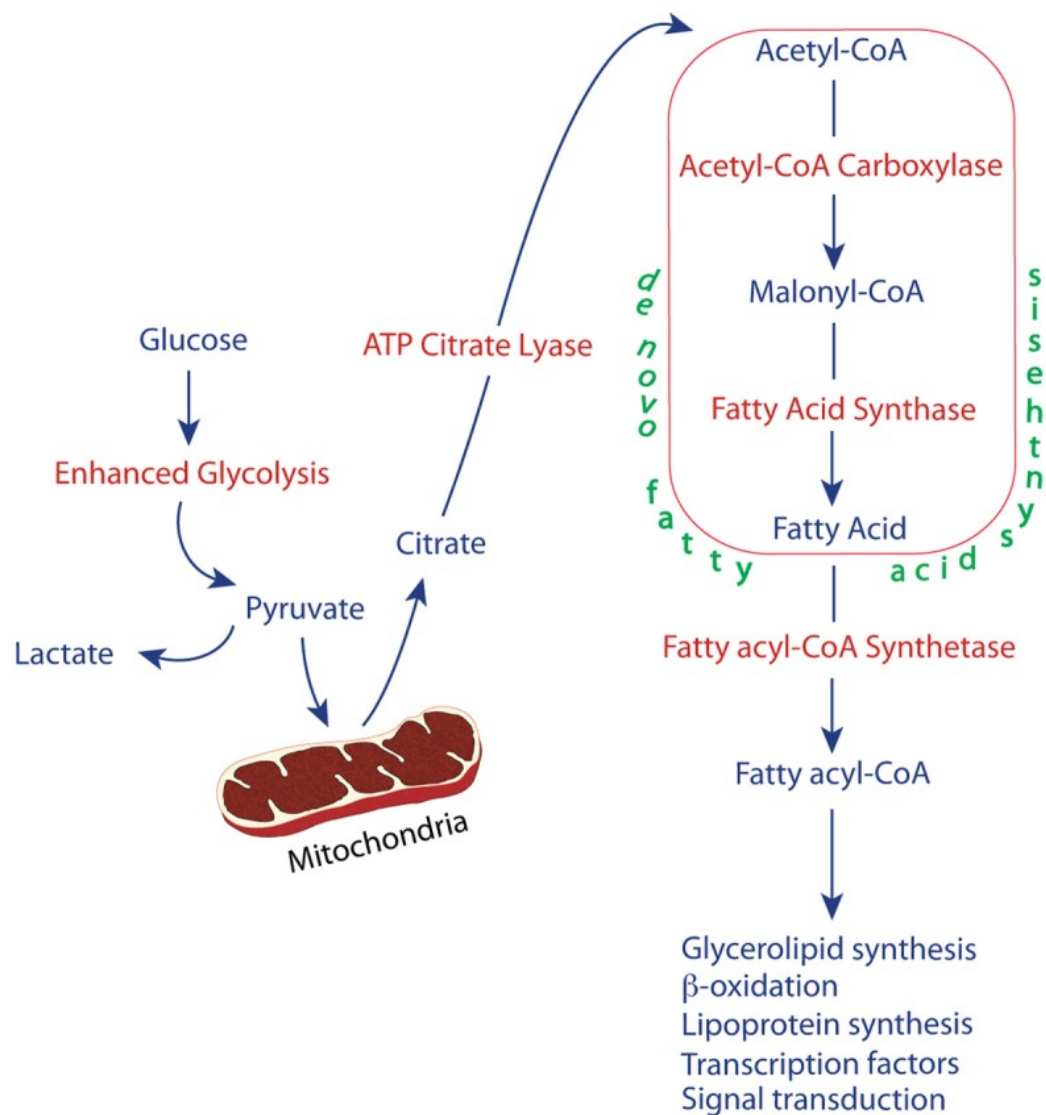


Figure 3.23 Lipid synthesis and glycolysis in cancer. Sourced from a review by Wu et al. [102].

The analysis of intermediary metabolites presented in this Chapter has demonstrated an unexpected pattern of elevated citrate concentration in cancerous PC3 cells, compared to both benign PNT1A and RWPE1 cell lines.

There are several possible causes that may explain these unexpected findings:

- *The immortalisation of the cell line may alter metabolic pathways.*

Primary epithelial cells of the prostate usually senesce after five passages, and therefore many commercial suppliers of human cells use viruses such as human papilloma virus (HPV) to immortalise cells (171). Although there is no direct evidence linking this process with altered TCA cycle function specifically, a similar observation of unexpected citrate levels was noted on an NMR study of RWPE1 cells in culture by Teahan and colleagues.

The authors were also suggesting a potential role of the immortalisation in explaining their unexpected findings (172).

- *Cell culture environment*

There is no doubt that the culture conditions differ to normal body physiology. Many of the commonly used prostate cell lines are routinely cultured in recommended growth media from their respective suppliers. Although some of these culture media differ slightly, most share common ingredients as well as the similarity in general culture conditions, in terms of temperature and CO₂ levels.

- *Role of culture medium*

PC3 cells are normally grown in HAM-F12 medium and PNT1A in RPMI-1640 medium. Therefore, the differences in media composition were explored and summarised in Table 3.3. The growth media are a mixture of amino acids, minerals, vitamins and sugars. Glucose concentrations were very similar in both growth media. Glucose would have a direct impact on the levels of pyruvate that enters the TCA cycle, and subsequently the amount of citrate produced. There were small amounts of pyruvate sodium and zinc sulphate in HAM-F12 medium that were lacking in RPMI-1640. In order to overcome the possible effect of the medium on the observed level of TCA cycle intermediates, both cells were cultured in RPMI-1640 media following identical experimental conditions. FBS was added in equal concentrations to all culture media. FBS was also heat-inactivated, therefore the enzymatic action, such as that of LDH would have been inactivated equally in all media.

Overall, the results of LC-MS/MS analysis of TCA cycle intermediates, with the exception of lactate, showed higher concentrations in PC3 cells compared to PNT1A, despite the change in the culture media. Lysates from PC3 cells still contained significantly higher levels of citrate compared to benign PNT1A cells, suggesting that the differences in the media were not enough to explain the results. A study by Toghrol and colleagues, examining the levels of citrate in rat ventral prostate samples, also showed that exogenous pyruvate did not affect the measured citrate levels (173). Although zinc may have an important role on the TCA cycle in general, it is unlikely to be responsible for the observations seen in this Chapter, as the concentration of zinc in HAM-F12 medium was very small (0.0008 g/l). A study by Matheson and colleagues demonstrated that adding zinc even at a slightly higher concentration of 0.001 g/l to PC3 cells in culture did not change the citrate concentration, nor did it alter the total ATP produced (121).

- *The role of aconitase enzyme*

The function of aconitase from cell extracts was higher in the PC3 cell line compared to PNT1A, which would be in line with published evidence on the re-activation of aconitase in PCa (46, 145, 161). However, it is important to note that the assay used in this study did not distinguish between the mitochondrial (M) and cytosolic (C) fractions of the enzyme. Similar findings were seen when comparing aconitase activity between PC3-M and PNT2-C2 cells, which share many similarities with PC3 and PNT1A cell lines (174). In that study, the mitochondrial fraction of the enzyme was functionally identical, whereas the cytosolic enzyme was much more active in PC3-M cells.

- *Role of gene expression in TCA cycle function and lipid metabolism*

In the absence of zinc and pyruvate sodium in the culture media, there was less citrate in PC3 cell extracts but citrate concentrations were still higher compared to PNT1A. To exclude a genetic cause for the observed results, gene expression profiles obtained from microarray data were interrogated. PC3 and PNT1A cells showed similar levels of ACO2 expression that encodes for the key rate-limiting enzyme mitochondrial aconitase (Figure 3.16). Interestingly, the expression of ACO1 was higher in PNT1A cells. ACO1 encodes for the cytosolic aconitase that also functions as an iron regulatory binding protein. In its metabolic function it is responsible for the interconversion of citrate to iso-citrate in the cytoplasm (175). However, data from LC-MS/MS analysis presented in this Chapter showed equal amounts of iso-citrate in both PC3 and PNT1A cells, which would suggest a negligible effect of ACO1 expression on the observed results.

Gene expression analysis also showed higher levels of PDK1 in PC3 cells. This gene is one of four that encode for PDK, which normally inhibits the action of PDH, facilitating the shunting of pyruvate away from the TCA cycle and increasing the production of lactate (Figure 3.24). This would be compatible with the results obtained when PC3 cells were cultured in HAM-F12 medium, where significantly higher amounts of lactate were produced compared to benign cells.

The expression of ACAT1 and AMACR were higher in PC3 cells. Both of these genes encode for mitochondrial enzymes that are linked to FA metabolism. There is evidence that increased ACAT1 expression correlates with the grade of PCa on tissue microarray of over 250 samples (176). AMACR overexpression was found to be associated with PCa risk on a meta-analysis of 22 studies including 4385 patients (177).

3.5.2 Oxidative stress and TCA cycle dysfunction

Tumours of different origin often share features of hypoxia and increased free radicals (178). PCa is no exception to this, with evidence suggesting increasing levels of ROS are associated with worsening degree of differentiation and increased metastatic phenotype (179).

Analysis of TCA cycle intermediates in prostate cell lines has demonstrated an unusual pattern of high citrate in malignant PC3 cells, compared to the two benign PNT1A and RWPE1 cell lines. ROS have an effect on the function of TCA cycle enzymes through direct inhibition, and this has been shown in several cell and animal models (146). Subsequently, the levels of citrate and other TCA cycle metabolites may be affected by different levels of ROS within a cell culture model. Measurement of baseline ROS demonstrated a much higher level of H₂O₂ in PC3 cells compared to PNT1A. Furthermore, inducing oxidative stress in the benign cell line PNT1A almost doubled the amount of the citrate produced. A similar increase was also noted when PC3 cells were exposed to ROS. It is clear that ROS have a direct effect on the levels of citrate and indeed the other TCA cycle intermediate compounds. This may explain the unusual pattern of high citrate in PC3 cells. In prostate tissue, little doubt exists that citrate concentration, or at least its ratio to creatine or choline, is reduced in PCa (119, 136, 160). It could be hypothesised that tumours of the prostate *in vivo* are able to achieve a better balance towards citrate oxidation through better control of ROS compared to cultured cells, or it might be that citrate produced *in vivo* in cancer tissue is utilised rapidly to form lipids and FAs.

The dietary bioactive SF from broccoli is known to have anti-oxidant properties, but its effect on citrate or other TCA cycle compounds in the prostate has not been previously examined. SF is an ITC derived from enzymatic hydrolysis of the parent group of compounds termed glucosinolates. Several epidemiological studies suggest a lower rate of PCa progression with increased consumption of glucosinolate-containing vegetables (86, 94). The data presented in this Chapter show that SF alone did not alter the level of citrate in either of the cell lines. However, SF was able to prevent the increase in citrate levels induced by oxidative stress, as demonstrated by significantly lower levels of citrate found when PC3 were exposed to physiologically relevant concentration of SF before an H₂O₂ challenge. The protective effect of SF against H₂O₂-dependent citrate increase could be explained through its indirect antioxidant potential (151). Previous findings indicate that SF at physiologically relevant concentrations did not significantly alter ROS levels in PC3 cells; however it was able to suppress H₂O₂-induced ROS production of approximately 80% (unpublished data). Most of the TCA cycle enzymes, including aconitase and α -

KGDH, are known to be sensitive to oxidation, and in the presence of elevated levels of ROS, their activity is compromised resulting in an alteration of the TCA cycle function (58, 180). Several pathological conditions considered as oxidative stress diseases are characterised by the loss of α -KGDH enzymatic activity (181-184). Therefore, the ability of SF to maintain ROS homeostasis could be crucial for restoring the activity of key TCA enzymes, and thus preventing an inefficiency of the TCA cycle. In a study where albino mice were exposed to the lung carcinogen benzo (a) pyrene (BaP), which is known to induce ROS levels; BaP caused a significant reduction in activity levels of all TCA cycle enzymes including aconitase and α -KGDH. Moreover, dietary SF fed to these mice had a protective effect against the action of BaP by increasing the activity of these enzymes (aconitase, α -KGDH; $p < 0.05$) only in BaP-treated mice but not in control animals (185). In the experimental conditions described in this Chapter, PCa cells may use the higher levels of citrate induced by ROS to initiate cholesterol synthesis and steroidogenesis, which are known to drive proliferation. By counteracting this ROS-dependent increase of citrate, SF could reduce *de novo* lipogenesis and thus may significantly delay cancer cell growth.

The inactivation of enzymes by free radicals such as H_2O_2 is not limited to the TCA cycle. Several other key metabolic processes that precede mitochondrial oxidation may also be affected. The conversion of pyruvate to acetyl-CoA is one such process that relies on the function of PDH. The phosphorylation of PDH renders it inactive and this is controlled by four kinases belonging to the PDK family. PDK2 is crucial to PDH function and has been shown to be susceptible to oxidative stress (59).

The loss of PDK inhibition would substantiate the conversion of pyruvate to acetyl-CoA, and therefore more citrate would be available. In the absence of aconitase, which is also sensitive to ROS, the citrate produced is not oxidised. Collectively this might explain the rise in citrate when prostate cells are exposed to ROS (Figure 3.24).

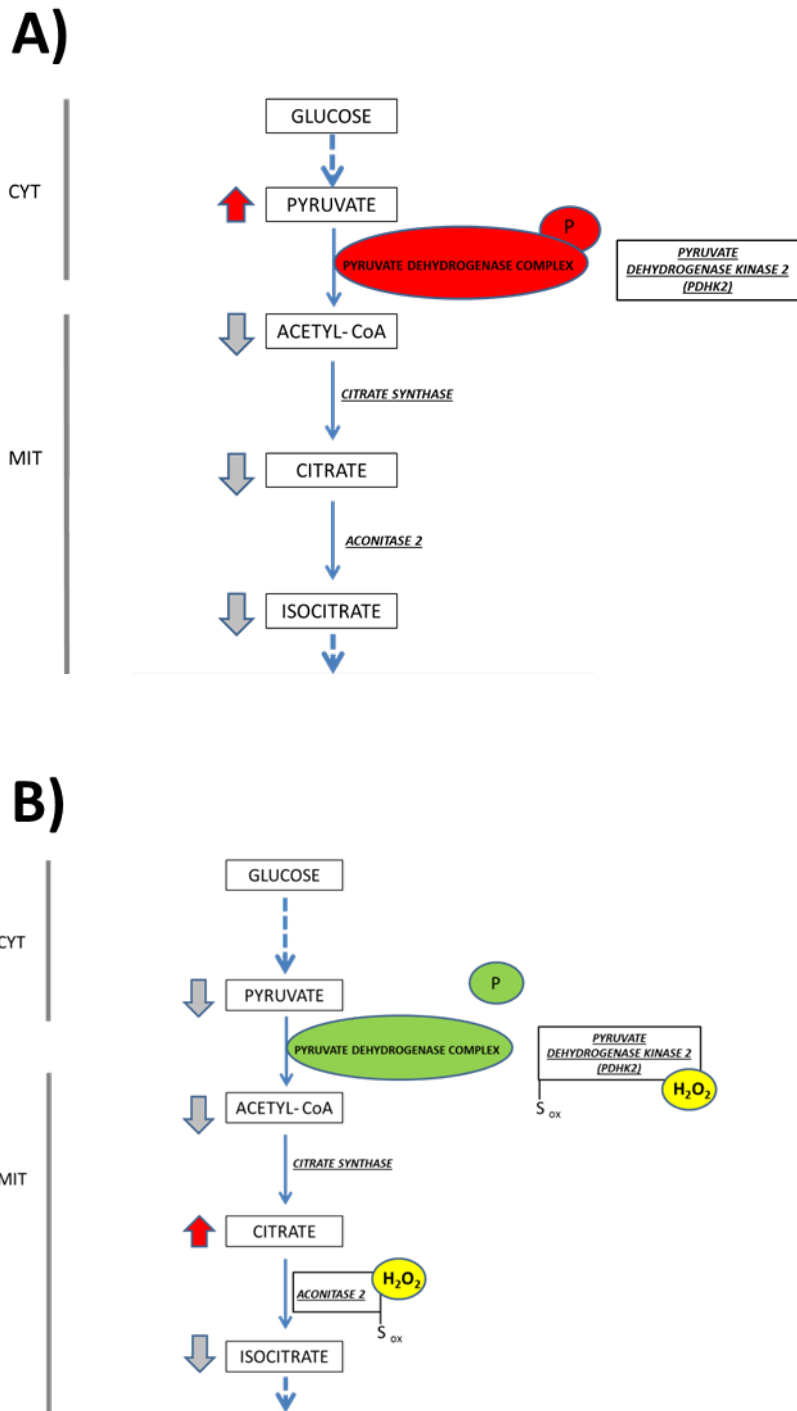


Figure 3.24 The effect of ROS on pyruvate metabolism and TCA cycle function. **A)** In normal redox balance, pyruvate dehydrogenase kinase 2 (PDHK2 or PDK2) inhibits pyruvate dehydrogenase (PDH) limiting the supply of acetyl-CoA to the TCA cycle. Exposure to excess ROS disinhibits PDH and enhances the conversion of pyruvate to acetyl-CoA.

3.6. Conclusions

In summary, PC3 cells display an abnormally high level of citrate compared to benign PNT1A cells. This is contrary to what is seen in cancerous and benign prostate tissue. The factors that influence the TCA cycle function in tissue, such as zinc concentration, do not explain the observations in cell culture. When cells were cultured in the same medium without exposure to zinc, PC3 cells still had double the amount of citrate compared to their benign counterparts.

In addition, gene expression data supported enhanced citrate oxidation and higher conversion of glucose to lactate in PC3 cells, but the opposite was observed in metabolite concentrations. Furthermore, exposure to oxidative stress led to citrate accumulation in both cell lines, suggesting inhibition of TCA cycle enzymes by ROS. SF at low physiological concentrations prevented the H₂O₂-induced increase in citrate.

Overall, the data presented in this Chapter suggest that PC3 cells, which are a model for aggressive PCa, do not share the same metabolic phenotype of cancer *in vivo*, and thus a better understanding of their usefulness and limitations to study prostate metabolism is needed. The data also suggest a mechanism by which SF could influence the redox status in the prostate and subsequently alter the metabolic environment through changes in the TCA cycle. How this translates in tissue, and indeed *in vivo*, is examined in the next two Chapters.

Chapter 4.

An *ex vivo* approach to
studying prostate
metabolism

Summary

In the previous two Chapters, a new LC-MS/MS method was found to accurately detect and quantify TCA cycle compounds even at low concentrations. Applying this method to prostate cells in culture revealed that benign and cancerous cells do not share the metabolic fate of citrate previously described in the literature. In addition, dietary SF was found to reduce the effect of ROS on the TCA cycle in both benign and malignant prostate cells. However, these findings were limited by the *in vitro* nature of the experiments. In order to further understand the exact changes in the TCA cycle as well as other metabolic pathways in the human prostate, non-targeted chromatography analyses were undertaken using an *ex vivo* model. Improving our knowledge of the metabolic profile of two distinct zones of the healthy prostate would help to identify potential metabolic pathways that could be modified by diet. In addition, it would help to understand the volume and quality of data that can be obtained from prostate biopsy specimens using chromatography platforms. Ultimately, this knowledge could help design better intervention studies looking at the role of diet in prevention or treatment of prostate diseases, such as cancer.

4.1. Introduction

In the field of PCa, metabolomic approaches have been applied in the search for new biomarkers and prognostic tools (119, 186, 187). The unique metabolism of the prostate is not a new concept and has been explored by several research groups in the last three decades (42, 145, 173, 188, 189). One of the important discoveries regarding prostate metabolism is the ability of healthy prostate epithelial cells to secrete high amounts of citrate, this process is reversed in PCa (186, 190). Other metabolic adaptations include the ability of prostate cells to accumulate high amounts of cholesterol, which have been attributed to enhanced uptake and synthesis of cholesterol (191). FA metabolism has also been found to be upregulated in PCa, with several changes to key gene regulators that control FA synthesis and oxidation, such as FASN and α -AMACR (80, 167, 168). The findings described in Chapter 3 clearly indicate the limitation of using prostate cell models *in vitro* to investigate the central carbon metabolism of the prostate, or indeed the effect of exogenous compounds like SF on this pathway, highlighting the need for further translational studies.

The outer part of the prostate at the base is called the peripheral zone (PZ), and it is known that >75% of PCa is found in this area. In contrast, most benign enlargement that commonly afflicts older men and causes restriction to the outflow of urine is seen in the transitional

zone (TZ) that surrounds the urethra (Figure 4.1) (162, 164). Despite the numerous molecular studies on PCa to date, it is still unclear why cancer is more prevalent in the PZ and less in the TZ. Studies so far have identified genetic differences between these two zones (192, 193), but whether these changes translate into unique metabolic characteristics, such as those aforementioned, is still unknown.

This Chapter describes the metabolic properties of non-cancerous tissue derived from the PZ and TZ of the prostate using a highly sensitive platform based on the combination of liquid and gas chromatography with tandem mass spectrometry. The information obtained from this *ex vivo* model will contribute to the effects of a dietary intervention with SF on prostate metabolism which is described in Chapter 5 by providing a broad picture of metabolites found non-cancerous prostate tissue through a non-targeted metabolite analysis by alcohol extraction and downstream high throughput chromatography.

4.2. Aim

- ❖ To explore differences in metabolites between the peripheral and transitional zones of the prostate.

- ❖ To test the metabolite extraction and analytical methods used on prostate tissue in the dietary study (ESCAPE).

4.3. Materials and Methods

4.3.1 Patient selection

Eighteen patients undergoing radical prostatectomy for organ-confined PCa were consented to allow the use of prostate tissue for research via the tissue bank at the NNUH, with ethical approval granted from the Faculty of Medicine and Health Sciences Research Ethics of the University of East Anglia (UEA) (Reference number: FMHS 20122014-37).

4.3.2 Tissue sampling procedure

Patients underwent endoscopic extra peritoneal radical prostatectomy (EERP). All procedures were conducted by a single surgeon (Mr Robert Mills, NNUH Urology consultant). The prostate gland was removed from the abdominal cavity immediately after resection, and rapidly biopsied after extraction to reduce ischaemic artefacts using a standard core biopsy instrument.

A total of 12 biopsy samples were collected from each prostate gland, covering both prostate zones and both sides of the prostate, as described below:

The extracted whole prostatectomy specimen was placed on a surgical table or equivalent.

- I. The apex and base of the gland were identified, the prostate was then cut transversely (axial section) halfway along the gland.
- II. Using the midline and the urethra as guides, equally sized biopsies were taken from the different zones, as shown in Figure 4.1, avoiding obvious tumour sites where feasible. The procedure was repeated in an identical manner for each side of the prostate.
- III. Four cores of tissue were collected from each prostate gland for metabolic profile assessment (TZ x2, PZx2), and were placed in 80% HPLC-grade methanol/water for 24 hours, as per manufacturers' guidelines (Metabolon®). The extracts were then frozen at -80 °C, and recovered tissue cores were sent for histological analysis.
- IV. Four tissue samples were collected from each prostate gland and kept in RNAlater for storage at -80 °C for future next generation RNA sequencing.
- V. Four tissue samples were snap frozen and stored at -80 °C for future analyses.
- VI. The remaining prostate gland was sent for histological analysis and tissue banking at the Norwich Biorepository (NNUH).

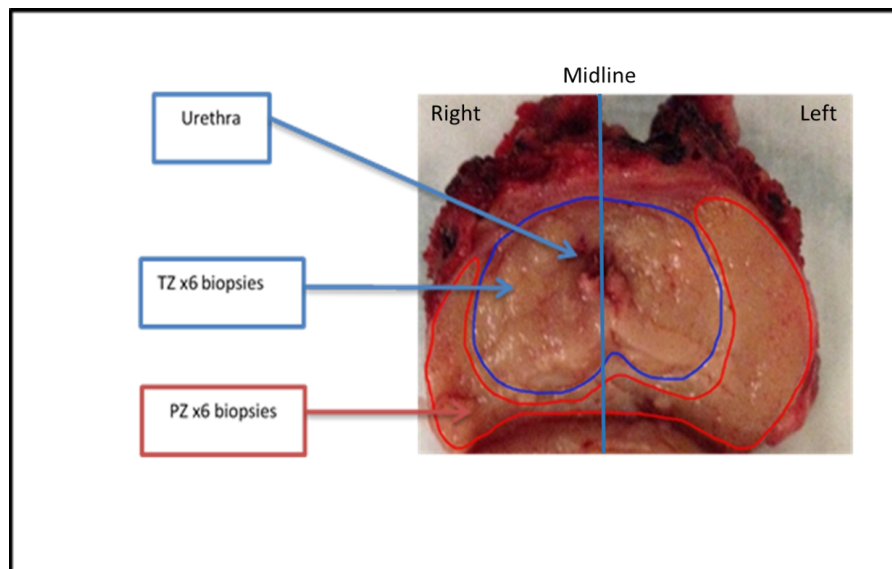


Figure 4.1 Transverse section of the prostate specimen showing sampling sites. A hypothetical midline is assumed and samples are taken in mirror fashion from both sides of the gland. PZ, peripheral zone marked in red; TZ, Transitional zone marked in blue.

4.3.3 Histological analysis

All prostatectomy specimens were examined by NNUH consultant pathologists. Tissue samples that were incubated in methanol were also examined histologically by a single pathologist with a specialist interest in urological pathology (Prof Richard Ball, NNUH histopathology consultant).

4.3.4 Metabolomic analysis

Methanol extracts were sent by a temperature-controlled courier service to Metabolon® for analysis (Metabolon, Durham, USA). Once received, samples were prepared using an automated MicroLab STAR® system from Hamilton Company. Recovery standards were added prior to the first step in the extraction process for QC purposes. A series of organic and aqueous extractions were carried out to remove the protein fraction while allowing maximum recovery of small molecules. The final extract was divided into two fractions; one for analysis by LC and one for analysis by GC. Samples were placed on a TurboVap® (Zymark) to remove the organic solvent. Each sample was then frozen and dried under vacuum. Samples were then prepared for the appropriate instrument, either LC-MS or GC-MS, as described below.

4.3.5 Liquid chromatography/Mass Spectrometry (LC-MS, LC-MS2)

The LC-MS analysis was performed using a Waters ACQUITY UPLC and a Thermo-Finnigan LTQ mass spectrometer, which was equipped with ESI source and linear ion-trap (LIT) mass analyser. The sample extract was split into two aliquots, dried, then reconstituted in acidic or basic LC-compatible solvents, each of which contained 11 or more injection standards at fixed concentrations. One aliquot was analysed using acidic positive ion optimized conditions, and the other using basic negative ion optimized conditions, in two independent injections using separate dedicated columns. Extracts reconstituted in acidic conditions were gradient eluted using water and methanol, both containing 0.1% formic acid, while the basic extracts, which also used water/methanol, contained 6.5 mM ammonium bicarbonate. The MS analysis alternated between MS and data-dependent MS2 scans using dynamic exclusion.

4.3.6 Gas chromatography/Mass Spectrometry (GC-MS)

The GC-MS analysis was carried out on dried samples that were derivatized under dried nitrogen using bistrimethyl-silyl-trifluoroacetamide (BSTFA). Samples were analysed on a Thermo-Finnigan Trace DSQ fast-scanning single-quadrupole mass spectrometer using

electron impact ionization and a 5% phenyl column. The temperature ramp was from 40 °C to 300 °C in a 16 minute period.

4.3.7 Mass determination and MS/MS fragmentation (LC-MS), (LC-MS/MS)

An aliquot was analysed by using a Waters ACQUITY UPLC and a Thermo-Finnigan LTQ-FT mass spectrometer, which had a linear ion-trap (LIT) front end and a Fourier transform ion cyclotron resonance (FT-ICR) mass spectrometer backend. For ions with counts greater than 2 million, an accurate mass measurement could be performed. Accurate mass measurements could be made on the parent ion as well as fragments. The typical mass error was less than 5 ppm. Fragmentation spectra (MS/MS) were typically generated in a data dependent manner.

4.3.8 Data quality provided by Metabolon®

4.3.8.1. *Instrument and Process Variability*

Instrument variability was determined by calculating the median relative standard deviation (RSD) for the internal standards that were added to each sample prior to injection into the mass spectrometers. Overall process variability was determined by calculating the median RSD for all endogenous metabolites (i.e., non-instrument standards) present in 100% of the pooled samples (Table 4.1).

Table 4.1 Results of process variability

QC Sample	Measurement	Median RSD
Internal standards	Instrument Variability	6 %
Endogenous biochemicals	Total Process Variability	13 %

4.3.8.2. *QA/QC*

For QA/QC purposes, a number of additional samples are included with each day's analysis. Furthermore, a selection of QC compounds were added to every sample, including those under test. These compounds were carefully chosen so as not to interfere with the measurement of the endogenous compounds. Table 4.2 describes the QC samples and compounds.

4.3.8.3. *Bioinformatics*

Metabolon's informatics system consisted of four major components: (1) Laboratory Information Management System (LIMS), (2) the data extraction and peak-identification software, (3) data processing tools for QC and compound identification, and (4) a collection of information interpretation and visualization tools.

Table 4.2 Quality control and standardisation procedures performed by Metabolon®

Type	Description	Purpose
MTRX3	Large pool of human plasma maintained by Metabolon that has been characterized extensively.	Assure that all aspects of Metabolon process are operating within specifications.
CMTRX	Pool created by taking a small aliquot from every patient sample.	Assess the effect of a non-plasma matrix on the Metabolon process and distinguish biological variability from process variability.
PRCS	Aliquot of ultra-pure water	Process Blank used to assess the contribution to compound signals from the process.
SOLV	Aliquot of solvents used in extraction.	Solvent blank used to segregate contamination sources in the extraction.
DS	Derivatization Standard	Assess variability of derivatization for GC-MS samples.
IS	Internal Standard	Assess variability and performance of instrument.

4.3.8.4. *Data extraction and Quality Assurance*

The data extraction of the raw mass spectrometry data files yielded information that was loaded into a database. Once in the database the information was examined and appropriate QC limits were imposed. Peaks were identified using Metabolon's proprietary peak integration software, and component parts were stored in a separate and specifically designed complex data structure.

4.3.8.5. *Compound identification*

Compounds were identified by comparison to library entries of purified standards or recurrent unknown entities. Identification of known chemical entities was based on comparison to metabolomic library entries of purified standards. The combination of chromatographic properties and mass spectra gave an indication of a match to the specific compound or an isobaric entity. Additional entities could be identified by virtue of their

recurrent nature (both chromatographic and mass spectral). These compounds have the potential to be identified by future acquisition of a matching purified standard or by classical structural analysis.

4.3.8.6. *Normalisation*

A data normalisation step was performed to correct variation resulting from instrument inter-day tuning differences. Each compound was corrected in run-day blocks by registering the medians to equal one (1.00) and normalizing each data point proportionately (termed the “block correction”).

4.3.9 Statistical analysis

Raw area counts for each of the metabolites identified were generated by Metabolon® platforms as previously described. The data received from Metabolon were in the form of a table that contained the raw and normalised metabolite signals from each individual tissue core. These data were used for subsequent statistical analysis carried out with Matlab (Mathworks®, USA) and Metaboanalyst software v3.0 (194, 195). The latter is a peer reviewed, open-source web-based software that was chosen mainly for its ability to perform pathway analyses (194-198). Graphpad prism® software (GraphPad Software Inc., La Jolla, USA) was also used to generate illustrations and statistical analyses where indicated.

4.3.9.1. *Multivariate analysis*

Principal component analysis (PCA) was used to visualise the variation in the data. A small number of drug metabolites had large variations in the dataset and were subsequently excluded. Despite this, PCA did not discriminate between the two prostate zones, therefore a supervised method using partial least square discriminate analysis (PLS-DA) was adopted to query the dataset. The rationale behind using a supervised method was to allow the extraction of zone-specific, meaningful data that may have been masked by the large variations in the dataset.

4.3.9.2. *Univariate analysis*

Individual metabolite differences between the two zones were examined with univariate methods. An important aspect was to account for spatial variation between samples (right and left sided biopsies) and histological status (cancerous and non-cancerous cores). The prostate gland is contiguous and has no anatomical sides, labelling right and left samples

was performed to ensure coverage of a wider part of the prostate, which would increase the likelihood of obtaining non-cancerous samples. To overcome this variation, analysis of variance accounting for both laterality and histological result was used (N-way ANOVA). The data uploaded onto Matlab were log₁₀ transformed to reduce variability. Data uploaded onto Metaboanalyst were log₂ transformed and autoscaled by dividing the metabolite values by the standard deviation.

4.3.9.3. Pathway analysis

Pathway analysis was carried out using Metaboanalyst software. The software utilises the uploaded metabolite signals from each zone to perform a pathway enrichment analysis. In addition, topology analysis with degree of centrality measurements was carried out using the software's pathway databank that is based on KEGG (196)

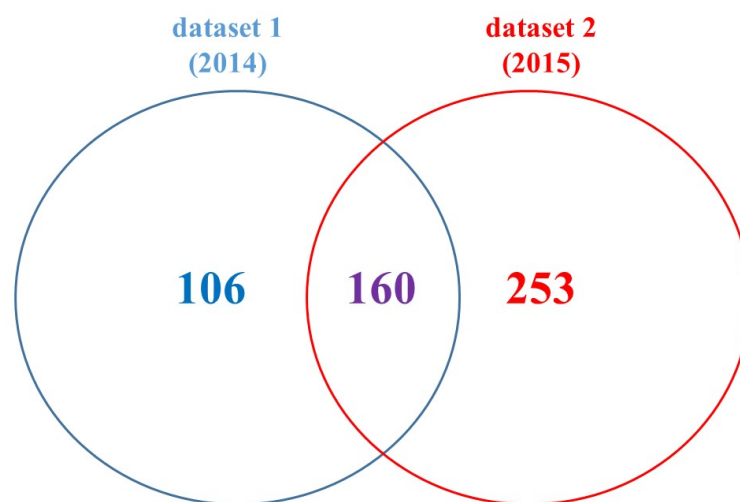
4.3.10 Batch variability

The samples were collected and sent for analysis prospectively. In order to reduce sample storage time, the methanol extracts were analysed in two batches. The first batch (n=8 patients, 32 cores of tissue, 4 from each patient) returned 266 individual metabolites from each core. The second batch (n=10 patients, 40 cores of tissue, 4 from each patient) was processed after instrument upgrade (Metabolon®, USA) using the exact techniques and standardisation procedures that were used in the first batch. The analysis of the second set of samples yielded 413 metabolites for each core of tissue. The lists of metabolites with associated Human Metabolite Data Base (HMDB) or KEGG IDs (where known) for each dataset are described in appendices 1-2. The differences in the total number of identified metabolites between batches was in part due to expansion of the metabolite detection in the second set of data due to an unanticipated change in Metabolon® platform technology. Missing values were deleted in a pair-wise fashion. Additionally, the global analytical approach resulted in a number of metabolites that did not have KEGG or HMDB identification numbers in both datasets. This led to limitations in pathway analyses, which rely on known compound identifiers for determination of metabolite interactions and topology analysis.

Table 4.3 shows a summary of the differences between the two sets of data. There were 160 common metabolites between the two datasets (appendix 3), including drug related xenobiotics that were excluded from final statistical analyses (Figure 4.2).

Table 4.3 Summary of metabolite identifiers between the two batches of samples

	Sample batch 1	Sample batch 2
Compounds with KEGG/HMDB ID	210	300
Metabolites with no KEGG ID	56	113
Total	266	413

**Figure 4.2 Venn diagram showing the number of metabolites shared between the two separate batches of samples.**

4.4. Results

A total of 72 samples from 18 men undergoing radical prostatectomy were processed (four cores per patient = one core from each zone, repeated on both sides of the gland). Table 4.4 describes the demographic and tumour stage details of the study participants. The average age was 62 ± 6.7 years, and average PSA preoperatively was 8.7 ± 4.2 $\mu\text{g/l}$. All patients had an American Society of Anaesthesiologists (ASA) co-morbidity score of 2, which reflects the average general health status of men in this age group. An ASA score of 2 implies the presence of mild diseases only without substantive functional limitations. Examples include (but not limited to): current smokers, social alcohol drinkers, well-controlled diabetes or hypertension, and mild lung disease. Thirteen of 72 cores (18%) were cancerous (10 cores from the peripheral and 3 from the transitional zone), these were analysed separately as described on page 103.

Table 4.4 Demographic and prostate biopsy characteristics of study patients prior to surgery

ID	Age	ASA	PSA (ug/l)	Gleason sum	Gleason score	Laterality	No. of +ve cores	% tissue involvement
A	54	2	5.9	7	3+4	BL	n/a	n/a
B	64	2	8.8	7	3+4	L	2	n/a
C	67	2	6	7	4+3	BL	3	12
D	59	2	6.9	6	3+3	BL	4	10
E	64	2	8.5	7	4+3	L	1	10
F	67	2	12.3	7	3+4	R	2	n/a
G	57	2	4.5	7	3+4	BL	6	25
H	64	2	8.5	7	3+4	R	1	5
J	52	2	3.4	6	3+3	R	3	5
K	73	2	8.5	6	3+3	R	1	3
L	57	2	4.3	7	3+4	R	2	2
N	66	2	10	7	3+4	R	4	60
O	47	2	3.4	7	3+4	R	4	15
P	57	2	20	7	4+3	R	3	10
Q	63	2	14	7	4+3	L	5	25
R	67	2	13.2	7	3+4	R	2	25
S	68	2	11.9	9	4+5	R	5	8
T	69	2	7.9	8	4+4	BL	n/a	n/a

ASA, American society of anaesthesiologist; PSA, Prostate specific antigen; TRUS, Transrectal ultrasound; BL, bilateral; L, Left; R, Right; No. of +ve cores, the number of samples that contained cancer (where recorded); % tissue involvement, percentage of cancer tissue found in the specimen which indirectly gives an idea of tumour burden (where recorded); n/a, data not available.

4.4.1 Analysis of benign tissue

Metabolite data from tissue samples were collated in one dataset. Thirteen cancerous tissue cores were factored in for univariate and multivariate models, details of cancerous samples are given in section 4.4.2 on page 103.

4.4.1.1. *Multivariate analysis*

A multivariate approach was used to establish whether there were obvious trends in the dataset. As the combined dataset of the two batches of metabolite extracts collected over 2 years contained 160 features for each of the 72 samples, this resulted in a large data matrix. PCA analysis demonstrated no obvious clustering of the data. A second supervised method termed PLS-DA was used to uncover potentially important metabolites that might have been otherwise overlooked. Results of both these methods are described below.

4.4.1.1.1. *Principal component analysis*

PCA provided visual information regarding outliers in the data but failed to separate the two zones. Several metabolites were significantly higher in a few samples and had a greater impact on the results. Excluding some of the extreme values and using log transformation resulted in greater homogeneity in the data (Figure 4.3). A second analysis was carried out aiming to reduce the impact of histology status and the side of the biopsy (i.e. left or right) by calculating the average of right and left side samples for each zone and excluding cancerous cores; however, there was still no obvious clustering of the two groups (Figure 4.4).

4.4.1.1.2. *Partial least square-discriminate analysis*

Component 1 of PLS-DA explained 27 % of the variance (Figure 4.5). Incorporating 5 components accounted for a total of 56.9% of the variance in the data. It is important to note that this is a supervised method of analysis that acquires the group origin of each sample during the computation. Multiple testing using Leave One Out (LOO) method did not give a statistically significant result. However, this analysis identified a number of compounds that had the biggest effect on the variation observed in the dataset. Using Variable Importance in the Projection (VIP) scores, a list of compounds was generated that was later compared with univariate analysis results (Figure 4.6).

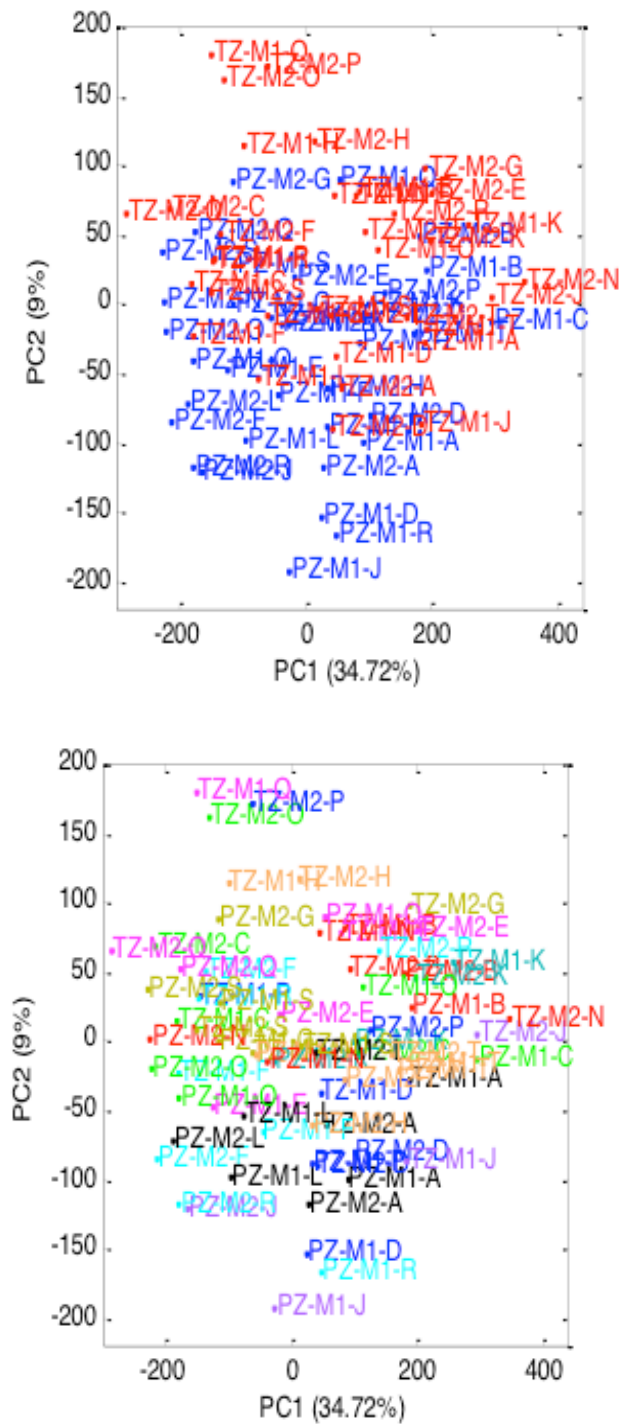


Figure 4.3 Principal component (PC) scores plot of metabolite data from 72 prostate tissue cores after excluding xenobiotic metabolites. Top plot = Zone of origin is highlighted for each core of tissue (transitional zone, TZ, red; peripheral zone, PZ, blue). Bottom plot = Samples coloured by patient.

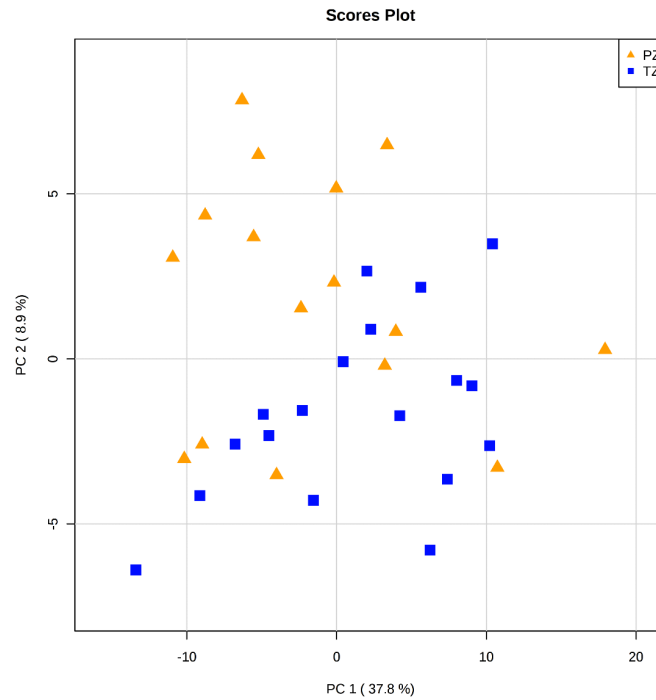


Figure 4.4 Principal component analysis (PCA) after calculating the average value of right and left sided samples and excluding cancer cores failed to separate the prostate zones. PZ, peripheral zone (orange triangles); TZ, transitional zone (blue squares).

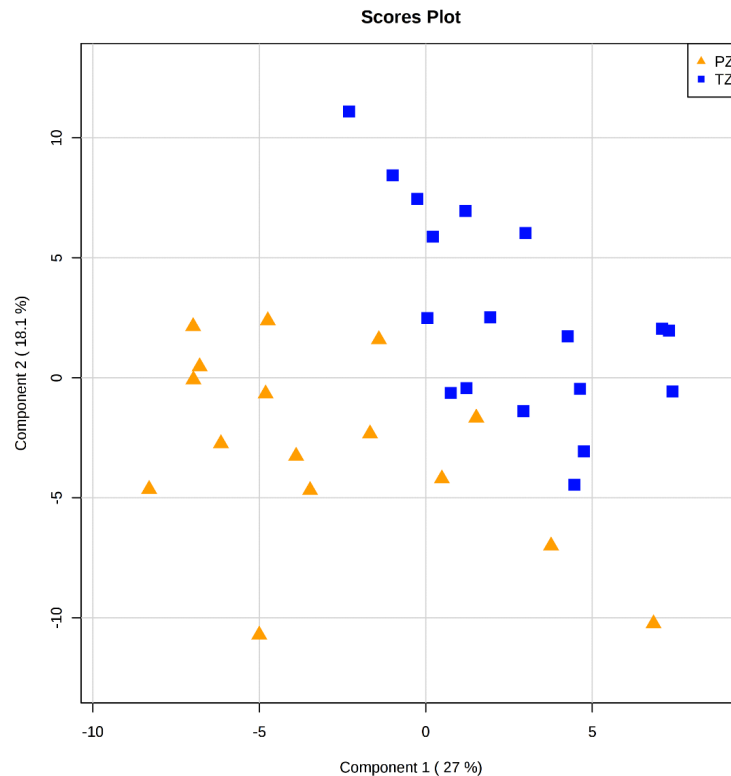


Figure 4.5 Scores plot between the selected principal components (PCs). The explained variances are shown in brackets. Multiple testing using Leave One Out method was not statistically significant. PZ, peripheral zone (orange triangles); TZ, transitional zone (blue squares).

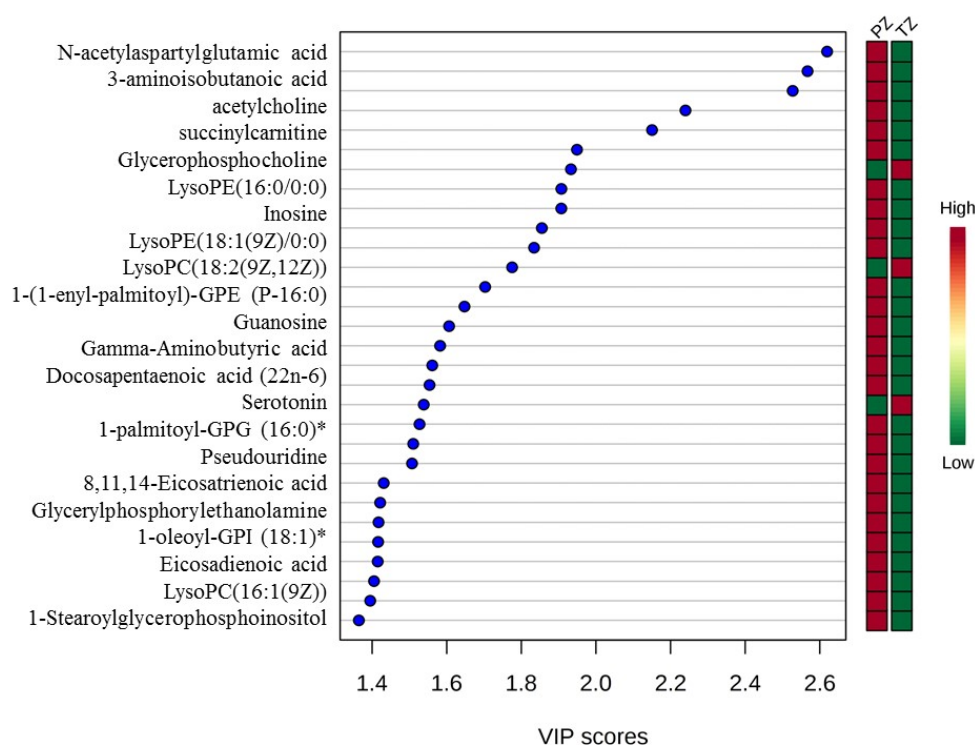


Figure 4.6 Important features identified by PLS-DA. The coloured boxes on the right indicate the relative concentrations of the corresponding metabolite in each zone of tissue. Variable Importance in Projection (VIP) is a weighted sum of squares of the PLS loading, taking into account the amount of explained Y-variation in each dimension. VIP scores ≥ 2 are considered highly significant. PE, phosphoethanolamine; PC, phosphatidylcholine; GPE, glycerol-3-phosphorylethanolamine; GPG, glycerol-3-phosphoglycerol; GPI, glycerol-3-phosphoinositol; PZ, peripheral zone; TZ, transitional zone.

4.4.1.2. Univariate analysis

Univariate methods were used to explore the differences in metabolite signals between the peripheral zone and transition zone, taking into account which side the biopsy was taken from, and the histological result. Using N-way ANOVA, a number of metabolites were found to be significantly different between the two prostate zones (Table 4.5).

Table 4.5 List of statistically significant metabolites between the two prostate zones

Compound	Super pathway	Sub pathway	Trend in prostate zone	P value
N-acetyl-aspartyl-glutamate (NAAG)	Amino Acid	Glutamate Metabolism	↑ PZ	<0.001
Serotonin	Amino Acid	Tryptophan Metabolism	↑ PZ	<0.001
Gamma-aminobutyrate (GABA)	Amino Acid	Glutamate Metabolism	↑ PZ	0.003
Ophthalmate	Amino Acid	Glutathione Metabolism	↑ PZ	0.007

Compound	Super pathway	Sub pathway	Trend in prostate zone	P value
Isobutyrylcarnitine	Amino Acid	Leucine, Isoleucine and Valine Metabolism	↑ PZ	0.008
Hypotaurine	Amino Acid	Methionine, Cysteine, SAM and Taurine Metabolism	↑ PZ	0.014
Spermidine	Amino Acid	Polyamine Metabolism	↑ PZ	0.018
Tryptophan betaine	Amino Acid	Tryptophan Metabolism	↑ PZ	0.021
Phenylacetylglutamine	Amino Acid	Phenylalanine and Tyrosine Metabolism	↑ PZ	0.024
Glutathione, reduced (GSH)	Amino Acid	Glutathione Metabolism	↑ PZ	0.029
5-oxoproline	Amino Acid	Glutathione Metabolism	↑ PZ	0.035
3-indoxyl sulfate	Amino Acid	Tryptophan Metabolism	↑ PZ	0.045
Lactate	Carbohydrate	Glycolysis, Gluconeogenesis, and Pyruvate Metabolism	↑ TZ	0.046
Succinylcarnitine	Energy	TCA Cycle	↑ PZ	<0.001
Acetylcholine	Lipid	Neurotransmitter	↑ PZ	<0.001
1-(1-enyl-palmitoyl)-GPE (P-16:0)	Lipid	Lysolipid	↑ PZ	<0.001
Glycerophosphorylcholine (GPC)	Lipid	Phospholipid Metabolism	↑ PZ	<0.001
1-palmitoyl-GPE (16:0)	Lipid	Lysolipid	↑ PZ	<0.001
1-oleoyl-GPE (18:1)	Lipid	Lysolipid	↑ PZ	0.001
1-palmitoyl-GPG (16:0)	Lipid	Lysolipid	↑ PZ	0.001
1-linoleoyl-GPE (18:2)	Lipid	Lysolipid	↑ PZ	0.001
Glycerophosphoethanolamine	Lipid	Phospholipid Metabolism	↑ PZ	0.001
Docosapentaenoate (n6 DPA; 22:5n6)	Lipid	Polyunsaturated Fatty Acid (n3 and n6)	↑ PZ	0.002
Choline phosphate	Lipid	Phospholipid Metabolism	↑ TZ	0.004
1-(1-enyl-stearoyl)-GPE (P-18:0)	Lipid	Lysolipid	↑ PZ	0.004
1-stearoyl-GPS (18:0)	Lipid	Lysolipid	↑ PZ	0.004
Octanoylcarnitine	Lipid	Fatty Acid Metabolism (Acyl Carnitine)	↑ PZ	0.008

Compound	Super pathway	Sub pathway	Trend in prostate zone	P value
1-oleoyl-GPI (18:1)	Lipid	Lysolipid	↑ PZ	0.008
Dihomo-linolenate (20:3n3 or n6)	Lipid	Polyunsaturated Fatty Acid (n3 and n6)	↑ PZ	0.01
Dihomo-linoleate (20:2n6)	Lipid	Polyunsaturated Fatty Acid (n3 and n6)	↑ PZ	0.01
1-palmitoleoyl-GPC (16:1)	Lipid	Lysolipid	↑ PZ	0.01
Eicosenoate (20:1)	Lipid	Long Chain Fatty Acid	↑ PZ	0.01
1-palmitoyl-GPI (16:0)	Lipid	Lysolipid	↑ PZ	0.014
1-stearoyl-GPI (18:0)	Lipid	Lysolipid	↑ PZ	0.015
Sphingosine	Lipid	Sphingolipid Metabolism	↑ PZ	0.025
1-stearoyl-GPC (18:0)	Lipid	Lysolipid	↑ PZ	0.026
Oleoylcarnitine	Lipid	Fatty Acid Metabolism (Acyl Carnitine)	↑ PZ	0.035
Deoxycarnitine	Lipid	Carnitine Metabolism	↑ PZ	0.039
1-linoleoyl-GPC (18:2)	Lipid	Lysolipid	↑ PZ	0.042
1-(1-enyl-oleoyl)-GPE (P-18:1)	Lipid	Lysolipid	↑ PZ	0.046
1-arachidonoyl-GPE (20:4)	Lipid	Lysolipid	↑ PZ	0.048
Stearoylcarnitine	Lipid	Fatty Acid Metabolism (Acyl Carnitine)	↑ PZ	0.050
1-palmitoyl-GPC (16:0)	Lipid	Lysolipid	↑ PZ	0.050
3-aminoisobutyrate	Nucleotide	Pyrimidine Metabolism, Thymine containing	↑ PZ	<0.001
N1-methyladenosine	Nucleotide	Purine Metabolism, Adenine containing	↑ PZ	0.001
Guanosine	Nucleotide	Purine Metabolism, Guanine containing	↑ TZ	0.002
Inosine	Nucleotide	Purine Metabolism, (Hypo)Xanthine/Inosine containing)	↑ TZ	0.003
Pseudouridine	Nucleotide	Pyrimidine Metabolism, Uracil containing	↑ TZ	0.01
Cytidine 5'-monophosphate (5''-CMP)	Nucleotide	Pyrimidine Metabolism, Cytidine containing	↑ PZ	0.02

Compound	Super pathway	Sub pathway	Trend in prostate zone	P value
Adenosine	Nucleotide	Purine Metabolism, Adenine containing	↑ TZ	0.05
4-hydroxyhippurate	Xenobiotics	Benzoate Metabolism	↑ PZ	0.005
Hippurate	Xenobiotics	Benzoate Metabolism	↑ PZ	0.043

GPE, glycerol-3-phosphorylethanolamine; GPG, glycerol-3-phosphoglycerol; GPI, glycerol-3-phosphoinositol; PZ, peripheral zone; TZ, transitional zone. p values from N-way ANOVA

4.4.1.3. Pathway analysis

Impact scores derived from pathway analysis can provide useful information as certain metabolites occupy important positions in a given pathway therefore small changes to such compounds have larger effects on the overall function of a given biochemical pathway even when their relative concentrations do not reach statistical significance. One way of quantifying this is through determining the number of connections metabolites have to other compounds and whether they occupy rate-limiting positions. This analysis can be achieved in similar fashion to gene functional analysis. Data from mass spectroscopy were uploaded onto Metaboanalyst, it was possible to perform an enrichment analysis that provided a p value with multiple testing from the comparison of the expected number of metabolites in a pathway vs the number of compounds detected. A topological value was derived from metabolites that were statistically significant on univariate analysis. Even though only a small number of pathways reached statistical significance after multiple testing, by examining the overrepresented pathways in each prostate zone it became clear that several metabolic processes are different.

Steroid hormone biosynthesis and fatty acid biosynthesis were among the most overrepresented pathways in the PZ, compared to phenylalanine biosynthesis and the pentose phosphate pathway, both of which were overrepresented in the TZ (Figure 4.7 and Figure 4.9). Alanine and glycerophospholipid metabolisms had the higher impact scores in PZ and TZ, respectively (Figure 4.8 and Figure 4.10).

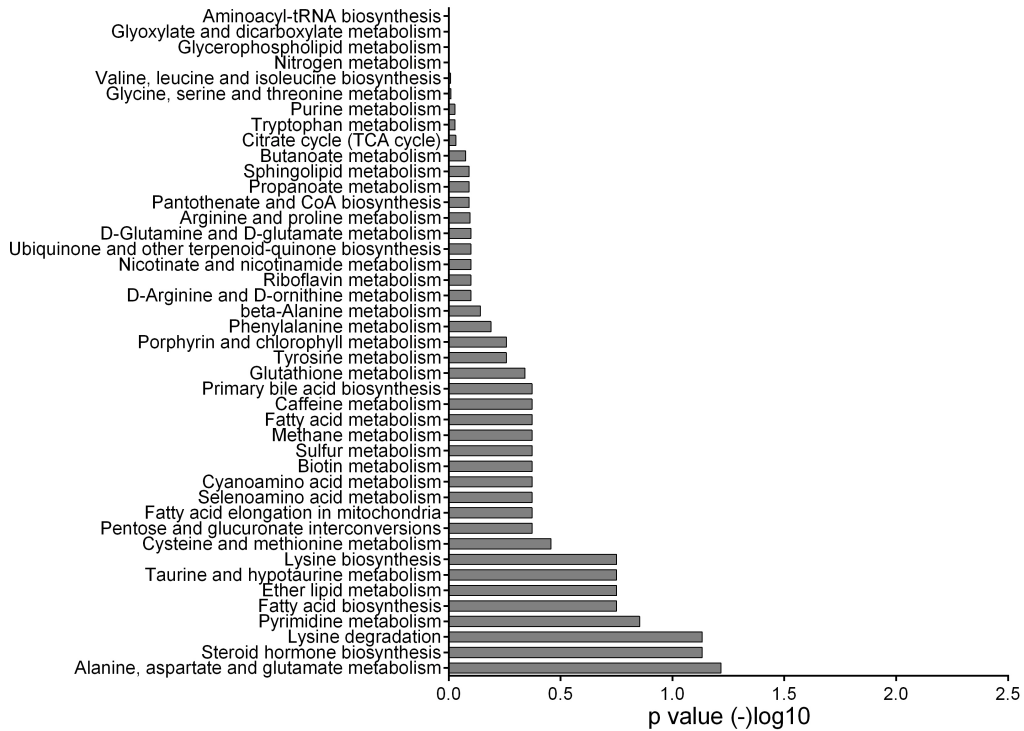


Figure 4.7 Pathways that are overrepresented in the peripheral zone. Glutamate metabolism, steroid hormone biosynthesis, and fatty acid biosynthesis were among the highly significant pathways. Each bar represents the p value of each pathway expressed as $-\log_{10}$.

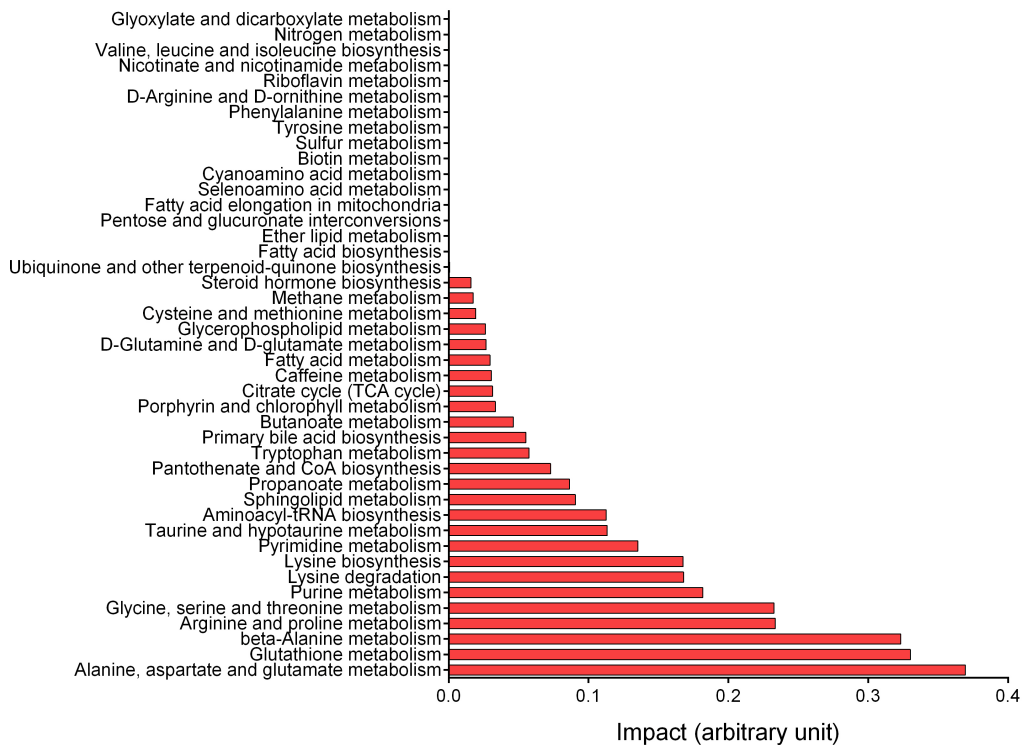


Figure 4.8 Impact scores obtained from topology analysis in the peripheral zone. Metabolites that are topologically more central within a given pathway, or have more connections to others, have a larger impact on a given pathway and will result in a higher impact score.

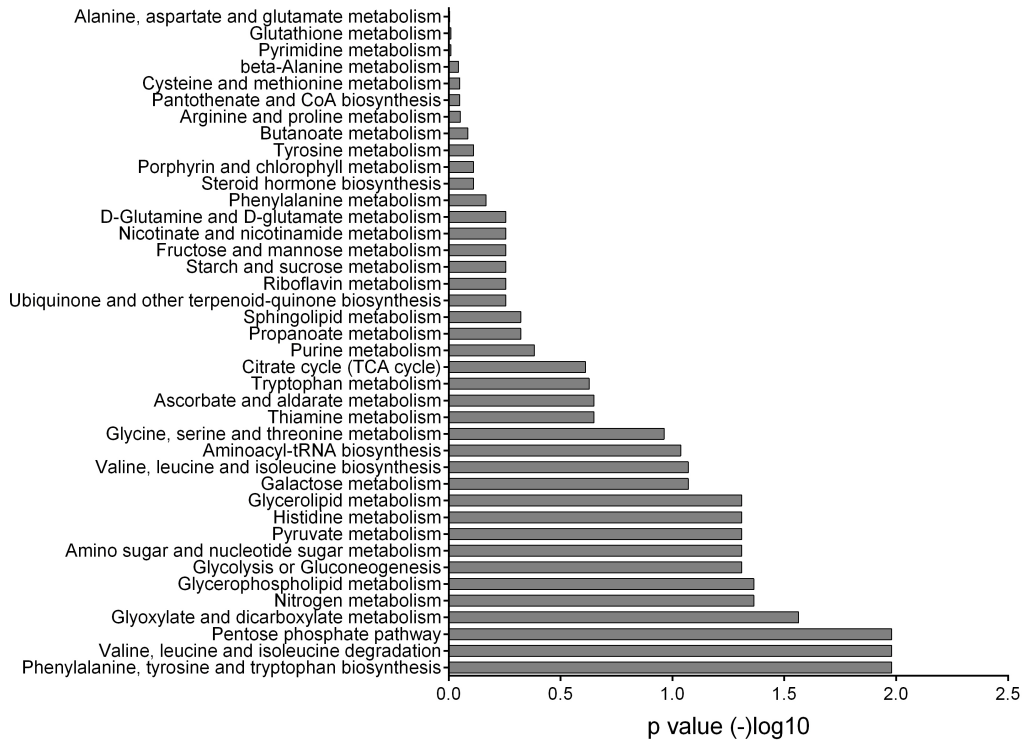


Figure 4.9 Pathways that were overrepresented in the transitional zone. Phenylalanine, pentose phosphate pathway, and pyruvate metabolism are highly significant. Each bar represents the p value of each pathway expressed as $-\log_{10}$.

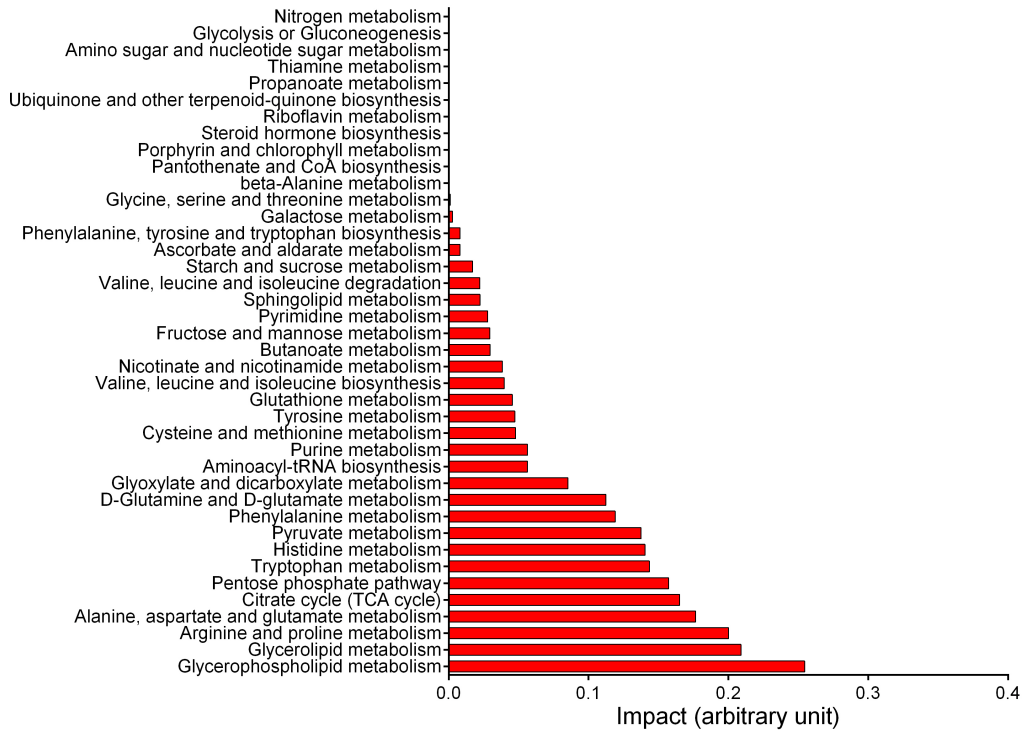


Figure 4.10 Impact scores obtained from topology analysis in the transition zone. Metabolites that are topologically more central within a given pathway, or have more connections to others, have a larger impact on a given pathway and will result in a higher impact score.

4.4.1.3.1. Tricarboxylic acid cycle metabolites

The TCA cycle is central to all mammalian metabolism. In PCa, distinct changes in levels of citrate, and the ratio of citrate to choline-plus-creatine have been previously observed. Most PCa tissues display a lower citrate level and lower citrate/choline+creatine ratio compared to non-cancerous prostate tissue (136, 160). No previous data exists on whether these ratios differ within the same gland. Comparing the ratio of citrate/choline+ -creatine between the PZ and TZ did not show a statistically significant difference ($p=0.3$) (Figure 4.11).

In the previous Chapters, the levels of TCA cycle intermediates, including citrate, measured in prostate cultured cells were surprisingly different from published *in vivo* prostate tissue studies. The TCA cycle-related metabolites from the two prostate zones were compared. Alpha-ketoglutarate and oxaloacetate were not detected in any of the samples. Levels of citrate were overall lower in the PZ but this did not reach statistical significance ($p=0.18$) (Figure 4.12).

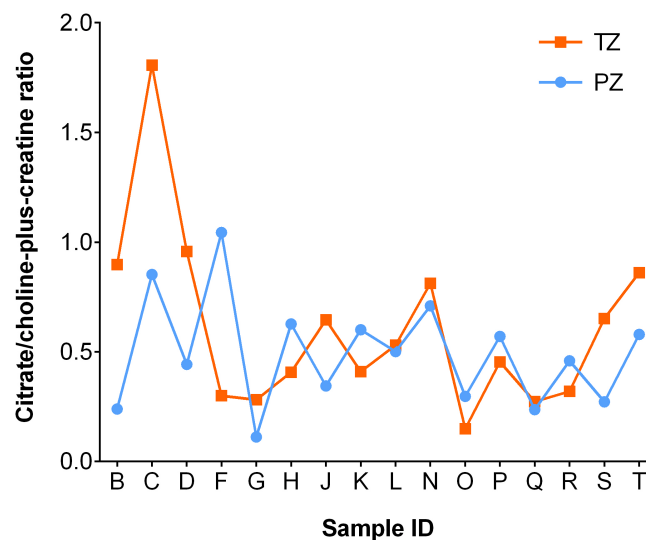


Figure 4.11 A comparison of citrate to choline-plus-creatine ratio between the two prostate zones. Data are expressed as citrate/choline-plus-creatine ratio of the peripheral zone (PZ) and transitional zone (TZ) for each patient. Cancerous samples were deleted in pairwise fashion.

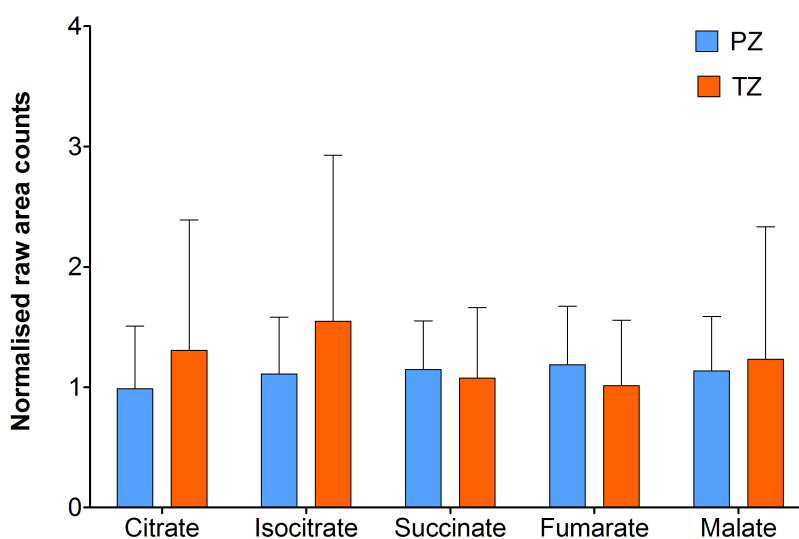


Figure 4.12 A comparison of TCA cycle-related metabolites between the two prostate zones. Cancerous samples were excluded from this analysis. PZ, peripheral zone; TZ, transitional zone.

4.4.1.3.2. *Acetylcholine, N-acetyl-aspartyl-glutamate and serotonin*

- Acetylcholine

Acetylcholine (Ach) is a neurotransmitter that stimulates muscarinic receptors. Several subtypes have been identified in the urinary tract, including the prostate (199). Levels of Ach were significantly higher in the PZ (Table 4.5).

- N-acetyl-aspartyl-glutamate

N-acetyl-aspartyl-glutamate (NAAG) is a recognised neurotransmitter, which acts as an agonist at group II metabotropic glutamate receptors, mostly described at neuron ends and glia. NAAG is degraded by NAAG-peptidases with two common classes, which have been identified in prostate tissue (200). Levels of NAAG were higher in PZ (Table 4.5).

- Serotonin

Levels of serotonin (5-hydroxy tryptamine, 5-HT) were higher in the PZ (Table 4.5). 5-HT is a biochemical messenger synthesized from the amino acid L-tryptophan, and has been linked to PCa cell growth (201).

4.4.1.3.3. *Lipid metabolites*

Analysis of the combined data from both sample batches showed a total of 56 lipid compounds. Several of these metabolites were preferentially seen in the PZ. The majority

belonged to the lysolipid sub pathway but also included polyunsaturated fatty acids (PUFA) and long-chain fatty acids (Table 4.6). Lipid metabolism plays a vital role in many human cancers, including that of the prostate (202). Lysolipids in particular have structural roles in cell membranes, as well as being degradable to free fatty acids, and have been suggested as biomarkers for PCa (203).

Table 4.6 Summary of statistically significant lipid metabolites identified in each of the prostate zones

Compound	Super pathway	Sub pathway	Trend in prostate zone	P value
Acetylcholine	Lipid	Neurotransmitter	↑ PZ	<0.001
1-(1-enyl-palmitoyl)-GPE (P-16:0)	Lipid	Lysolipid	↑ PZ	<0.001
Glycerophosphorylcholine (GPC)	Lipid	Phospholipid Metabolism	↑ PZ	<0.001
1-palmitoyl-GPE (16:0)	Lipid	Lysolipid	↑ PZ	<0.001
1-oleoyl-GPE (18:1)	Lipid	Lysolipid	↑ PZ	0.001
1-palmitoyl-GPG (16:0)	Lipid	Lysolipid	↑ PZ	0.001
1-linoleoyl-GPE (18:2)	Lipid	Lysolipid	↑ PZ	0.001
Glycerophosphoethanolamine	Lipid	Phospholipid Metabolism	↑ PZ	0.001
Docosapentaenoate (n6 DPA; 22:5n6)	Lipid	Polyunsaturated Fatty Acid (n3 and n6)	↑ PZ	0.002
Choline phosphate	Lipid	Phospholipid Metabolism	↑ TZ	0.004
1-(1-enyl-stearoyl)-GPE (P-18:0)	Lipid	Lysolipid	↑ PZ	0.004
1-stearoyl-GPS (18:0)	Lipid	Lysolipid	↑ PZ	0.004
Octanoylcarnitine	Lipid	Fatty Acid Metabolism (Acyl Carnitine)	↑ PZ	0.008
1-oleoyl-GPI (18:1)	Lipid	Lysolipid	↑ PZ	0.008
Dihomo-linolenate (20:3n3 or n6)	Lipid	Polyunsaturated Fatty Acid (n3 and n6)	↑ PZ	0.010
Dihomo-linoleate (20:2n6)	Lipid	Polyunsaturated Fatty Acid (n3 and n6)	↑ PZ	0.010
1-palmitoleoyl-GPC (16:1)	Lipid	Lysolipid	↑ PZ	0.011

Compound	Super pathway	Sub pathway	Trend in prostate zone	P value
Eicosenoate (20:1)	Lipid	Long Chain Fatty Acid	↑ PZ	0.011
1-palmitoyl-GPI (16:0)	Lipid	Lysolipid	↑ PZ	0.014
1-stearoyl-GPI (18:0)	Lipid	Lysolipid	↑ PZ	0.015
Sphingosine	Lipid	Sphingolipid Metabolism	↑ PZ	0.025
1-stearoyl-GPC (18:0)	Lipid	Lysolipid	↑ PZ	0.026
Oleoylcarnitine	Lipid	Fatty Acid Metabolism (Acyl Carnitine)	↑ PZ	0.035
Deoxycarnitine	Lipid	Carnitine Metabolism	↑ PZ	0.039
1-linoleoyl-GPC (18:2)	Lipid	Lysolipid	↑ PZ	0.042
1-(1-enyl-oleoyl)-GPE (P-18:1)	Lipid	Lysolipid	↑ PZ	0.046
1-arachidonoyl-GPE (20:4)	Lipid	Lysolipid	↑ PZ	0.048
Stearoylcarnitine	Lipid	Fatty Acid Metabolism (Acyl Carnitine)	↑ PZ	0.050
1-palmitoyl-GPC (16:0)	Lipid	Lysolipid	↑ PZ	0.050

GPC, glycerol-3-phosphocholine; GPE, glycerol-3-phosphorylethanolamine; GPG, glycerol-3-phosphoglycerol; GPI, glycerol-3-phosphoinositol; PZ, peripheral zone; TZ, transitional zone. P value derived from n-way ANOVA

4.4.2 Analysis of cancerous tissue

Thirteen tissue cores in total were malignant. Table 4.7 describes the histological details of this group of samples. As most cancers of the prostate are found in the PZ, the focus of this analysis was to compare the results of metabolite profiles between the cancerous and non-cancerous samples in PZ only. Paired samples from six individuals were included in this analysis.

Table 4.7 Summary of cancerous samples identified in the cohort

Patient	Sample ID	Zone	Gleason score	Pattern
A	PZ-M1-A	Peripheral	7	4+3
A	PZ-M2-A	Peripheral	7	4+3
C	PZ-M2-C	Peripheral	6	3+3
E	PZ-M1-E	Peripheral	7	3+4
E	PZ-M2-E	Peripheral	7	3+4
F	TZ-M1-F	Transition	7	3+4
G	PZ-M1-G	Peripheral	7	3+4
K	PZ_M2_K	Peripheral	7	3+4
L	TZ_M1_L	Transition	7	3+4
N	PZ_M2_N	Peripheral	7	3+4
O	TZ_M2_O	Transition	6	3+3
P	PZ_M2_P	Peripheral	7	4+3
Q	PZ_M1_Q	Peripheral	7	4+3

A paired sample t-test was performed on matching PZ cancer and non-cancer samples. Although limited by a small number of individuals, the data showed four metabolites that were significantly different between cancer and non-cancer tissue (Table 4.8).

Reduced nicotinamide adenine dinucleotide (NADH) was significantly lower in cancer tissue, whereas levels of the lysolipid palmitoleoyl-glycero-3-phosphocholine and the phospholipid breakdown product phosphoethanolamine were significantly higher in cancer tissue.

Table 4.8 List of metabolites significantly different between cancerous and non-cancerous samples

Compound	p-value	Trend in cancer
NADH	0.01	Down
Uridine	0.006	Down
Palmitoleoyl-glycero-3-phosphocholine	0.02	Up
Phosphoethanolamine	0.03	Up

4.5. Discussion

Delineating the so-called “prostate metabolome” has been the focus of many research studies. One notable study is that of Sreekumar and colleagues that examined over 40

prostate tissue samples with matched urine and plasma from men with benign and biopsy-proven PCa (204, 205). From a total of 518 different metabolites identified, sarcosine was one of the compounds that was highly correlated with PCa aggressiveness. Further targeted analyses of sarcosine by the same group on a different set of prostate tissue samples, showed no sarcosine in benign tissue and a proportional increase in sarcosine from localised to metastatic cancer, suggesting that sarcosine could be used as a biomarker for diagnosis. Similar studies by two independent research groups, however, either failed to associate sarcosine from urine samples with PCa or did not find a correlation as strong as that of earlier studies (206-208). This highlights some of the difficulties in reproducing metabolomic analyses, which may be the result of variation in methodology and, to a degree, heterogeneity of study populations. Interestingly, sarcosine was not detected in any of the samples presented in this Chapter.

The majority of diagnosed PCa is found in the peripheral zone compared to the transition zone (163). This zonal predilection for cancer has been explored from a gene expression standpoint by several research groups. For example, a publication by van der Heul-Nieuwenhuijsen suggested 199 genes that were preferentially expressed in the PZ, and 147 that were preferentially expressed in the TZ, based on microarray analyses of benign prostate tissue (192). The metabolic phenotype of the prostate zones remains understudied. It is not unreasonable, however, to assume that if genetic changes exist between the two zones, that these would translate into distinct metabolic alterations as many of the altered genes would directly, or indirectly, control the transcription of key proteins affecting a potentially wide range of biochemical processes.

The data presented in this Chapter describe, for the first time, metabolite profiles of non-cancerous tissue obtained from different zones of the prostate in men with localised PCa who underwent prostatectomy procedures. Using a solvent and water mixture to extract metabolites enabled the histological assessment of each individual tissue sample, in addition to the histological examination of the whole prostate gland. This collectively provided ample histopathological data to support the metabolite findings.

4.5.1 The peripheral zone of the prostate has a unique metabolic signature

After excluding metabolites that belonged to drug metabolism pathways, multivariate and univariate analyses of the combined data showed several metabolites that were significantly more abundant in the PZ compared to the TZ. Several of these metabolites belong to distinct super- or sub-pathways.

4.5.1.1. Neurotransmitters

Levels of NAAG were higher in the PZ. NAAG is a neurotransmitter that is found in abundance in the mammalian nervous system. It is catabolised to glutamate and N-acetyl-L-aspartate (NAA) by two groups of glutamate carboxypeptidases (GCP II and III). Both GCPs are membrane bound and have also been identified in the human prostate. GCPII in the prostate is called prostate specific membrane antigen (PSMA) (200). PSMA is expressed in benign and cancerous prostate tissue; however, the degree of expression is higher in cancer and increases with cancer severity (209). Radiolabelled indium coupled with an anti-PSMA antibody has shown some promise in detecting PCa recurrence after surgery (ProstaScint® scan, Cytogen Corporation, Princeton, NJ, U.S). Inhibitors of these GCPs have also shown anti-tumour properties in animal models of PCa (210). There are no studies comparing the immunohistochemical staining of PSMA in different zones of the prostate; however from the data presented here, the abundance of NAAG in benign peripheral zone tissue could indicate the low activity of GCPII. McDunn and colleagues found the breakdown product NAA to be associated with organ-confined PCa when compared to cancer that had extended beyond the capsule of the prostate, indicating more catabolism of NAAG with advanced disease (115)

A second neurotransmitter of interest is 5-HT, or serotonin. Levels of 5-HT were significantly higher in the PZ. 5-HT is a metabolite derived from tryptophan, and functions as a neurotransmitter but also has growth promoting properties. Several reports exist demonstrating the role of serotonin in inducing cell growth and proliferation in several cancer cell lines, including androgen resistant PCa (211-213). It is accepted that in hormone resistant PCa, neuroendocrine (NE)-like cells emerge and are associated with poor prognosis. NE cells typically secrete serotonin, amongst other neurotransmitters, that are thought to have an autocrine as well as a paracrine effect, promoting cell growth and migration (214). Higher levels of serotonin in the PZ therefore could favour the growth and migration of cancer.

Finally, Ach was also found to be higher in the PZ, compared to the TZ. Ach is a neurotransmitter associated with the parasympathetic nervous system. In a study looking at the change in type of innervation that prostate tissues receive in different grades of PCa, researchers found a strong correlation between the levels of Ach and high-grade/advanced disease in both animal models and in human tissue (215).

Overall, the finding of increased neurotransmitter metabolites in the PZ could represent the abundance of nerve tissue in this part of the prostate compared to the TZ; however, a significant body of evidence seems to suggest that these same metabolites are also associated with cancer and correlate to cancer severity (201, 211-215). This could indicate that the PZ tissue environment favours cancer development or tumour propagation, which could provide one possible explanation to the cancer predilection to this part of the gland. However, the neurotransmitters discussed above were not significantly different when comparing cancer to non-cancer samples within the PZ in this cohort. This might be a result of the small number of cancerous samples or a true reflection of the zone specificity of these metabolites.

4.5.1.2. *Products of intermediary metabolism*

As previously discussed, the prostate gland is characterised by high levels of zinc. This is thought to inhibit the mitochondrial enzyme aconitase, leading to citrate accumulation. PCa tissue has been repeatedly shown to have low zinc concentration and less citrate compared to benign tissue (144). Multivariate and univariate analyses of TCA cycle metabolites in both zones did not show a significant difference. Moreover, the ratio between citrate and choline plus creatine was equal when comparing the PZ and TZ in benign tissue, as well as paired cancerous and non-cancerous samples from the PZ. The citrate/choline ratio has been repeatedly shown to be low in PCa, using functional magnetic resonance imaging (MRI) techniques (119, 172)

Glucose is normally metabolised to pyruvate, which enters the mitochondria where it is converted to acetyl CoA by the action of PDH enzyme. Acetyl CoA, which can also be a product of fatty acid β -oxidation, enters the TCA cycle and is converted to citrate. Cancer cells have been shown to express high levels of PDK that inhibits PDH allowing more pyruvate to be converted to lactate. In this analysis, lactate was significantly higher in the benign TZ compared to the PZ. This could represent an ischaemic artefact, however, in the absence of a change in pyruvate and other TCA cycle intermediates that are highly influenced by tissue oxygen levels, this is less likely. Higher levels of succinylcarnitine were found in the PZ. Succinylcarnitine can be derived from the TCA cycle intermediate succinyl-CoA, which is the precursor of succinate by attaching succinyl as the acyl group with amino acid carnitine. Succinylcarnitine can be a source of both succinate and carnitine that could potentially have an impact on energy levels within the cells through the TCA cycle and mitochondrial oxidation of fatty acids (216).

4.5.1.3. *Lipid metabolites*

The metabolic analysis described in this Chapter has identified a total of 56 lipid compounds belonging to different metabolic sub-pathways. There is an accepted view of enhanced lipid synthesis in cancers in general to provide energy and membrane building blocks to rapidly growing cells (65). The PZ showed higher amounts of lipid metabolites that belong to the lysolipid metabolic sub pathway compared to the TZ, as well as other phospholipids, acylcarnitines, PUFA, and long-chain FA. Moreover, pathway analysis revealed that steroid biosynthesis, FA, and lipid metabolic pathways were overrepresented in the PZ (Figure 4.7). A previous study looking at the metabolic properties of PCa found nucleotides, lysolipids, carnitines, and free FA all to be linked to cancer and associated with increased chance of extra-capsular extension of the disease, which carries worse prognosis (115).

Lysophosphatidylcholines (LysoPC) attach to FAs of varying lengths, and not only serve as cell membrane building blocks, but also as signalling molecules and transport systems that deliver FAs to mitochondria and peroxisomes (202). One common FA incorporated into lysolipids is 16-carbon palmitate, forming several lysolipid combinations. Palmitate containing lysolipids were significantly higher in the PZ compared to the TZ. This was also the case for lysolipids containing 18-carbon fatty acids (Table 4.6).

Higher levels of four acyl carnitines were identified in the PZ of the prostate. These medium and long-chain acyl carnitines contain FAs linked to a carboxyl group via an ester bond. Acyl carnitines are sourced from diet as well as produced endogenously, and have been linked to PCa and associated with aggressive forms of the disease (216, 217). A study conducted by Giskeødegård and colleagues compared plasma metabolites from men with PCa and those with benign prostate hyperplasia (BPH). The authors found higher levels of acylcarnitines in PCa cases compared to BPH controls, including octanoylcarnitine (203). The latter was found to be significantly higher in the PZ tissue compared to the TZ in this dataset (Table 4.6). Overall, the experimental findings indicate enhanced lipid metabolism in the PZ of the prostate, which could explain the predisposition of this zone to cancer.

The finding of PUFAs in prostate tissue presented in this Chapter supports the potential role that dietary intake of these compounds could have on prostate health. Many published studies examining the association of these compounds, that are found in fish oils, with PCa, assessed plasma rather than end-organ tissue levels (218, 219). The debate about the benefit or potential harm of these diet-derived compounds has not been resolved. A recent meta-analysis examining this particular issue however, found n3 PUFAs eicosapentaenoic acid (EPA) and docosahexaenoic acid (DHA) both to be associated with high-grade PCa. Conversely, plasma levels of docosapentaenoate or DPA were associated with lower- PCa

risk (219). In the data presented here, EPA and DHA were both identified in TZ and PZ tissue but were not statistically different, whereas DPA was one of the PUFAs found to be more abundant in the benign PZ compared to the benign TZ.

4.6. Conclusion

This Chapter has demonstrated that the extraction of metabolites from prostate tissue is feasible. Several classes of compounds that are known to be associated with cancer phenotypes were found to be upregulated in the PZ of the prostate. These metabolites, such as neurotransmitters and lipids, may play a role in the development or progression of cancer by acting as substrates that promote cancer proliferation. Furthermore, the data demonstrate how compounds delivered from diet can accumulate in prostate tissue, which may have biological consequences that could be exploited in human intervention trials. In the next chapter, the effect of SF on prostate metabolism in men with prostate cancer is explored through a human dietary intervention study using broccoli.

Chapter 5.

An in vivo approach to
study the effect of
sulforaphane on the
prostate

Summary

PCa is a major public health problem for which there is a strong need for new preventive strategies based on lifestyle and drug interventions. Observational studies suggest that healthy eating patterns and increasing physical activity are associated with lower rates of PCa progression. Higher intake of cruciferous vegetables in particular has been associated with both a decreased risk of PCa progression and biochemical recurrence following radical treatment; however, the underlying biological mechanisms behind this remain poorly defined. The previous Chapters highlighted (i) the limitations of exploring the effects of SF from broccoli on prostate metabolism using *in vitro* cancer models and (ii) the feasibility of using a combined metabolomic approach in an *ex vivo* model for the profiling of tissue biopsies. Taking into consideration the experimental findings described in Chapter 4, it was envisaged that the application of this metabolomic protocol in assessing the effects of a diet intervention could yield high quality data with a translational value. This Chapter describes the design of a randomised double-blinded intervention trial that was undertaken to determine whether a diet rich in SF will result in changes in metabolites within prostate tissue *in vivo* (ESCAPE, ClinicalTrials.gov Identifier: NCT01950143). All aspects related to the design and conduct of the trial are fully outlined in the current Chapter, whereas the metabolomic data obtained from a sub-cohort of patients are presented in Chapter 6.

5.1. Introduction

5.1.1 Prostate cancer and cruciferous vegetables: epidemiology, human studies and cellular mode of actions

Data obtained from epidemiological studies suggest that diets rich in cruciferous vegetables, such as broccoli, may reduce the incidence and progression of PCa (94). These vegetables are unique in their ability to accumulate sulfur-containing glycosides known as glucosinolates, including glucoraphanin. When consumed, glucoraphanin is converted to the isothiocyanate Sulforaphane, either by the action of the plant enzyme myrosinase or by the gut microbiota. The food and health research group at QIB has developed a cultivar of broccoli (Beneforte®) over the last twenty years that delivers a threefold higher concentration of SF than standard broccoli (98). Plant breeders at Seminis seeds developed the Beneforte® broccoli cultivar, which is subject to very stringent quality control and is now widely commercialised in US and several European countries, including the UK. The breeders have developed another broccoli cultivar, which has been termed Beneforte Extra, that has almost double the amount of glucoraphanin compared to Beneforte® broccoli.

A large body of experimental evidence in model systems has shown that SF has preventive properties against cancer through multiple mechanisms of action, such as modulation of gene expression and cell signalling pathways (100, 220). This Chapter describes a randomised double-blinded intervention trial titled *Effect of Sulforaphane on prostate Cancer PrEvention* (ESCAPE) (ClinicalTrials.gov Identifier NCT01950143), which has been designed to test the hypothesis that a SF-rich diet can alter the metabolism and gene expression of prostate tissue in men with early stage PCa, in a manner that would reduce the probability of emergence and progression of aggressive cancerous clones. Traka and colleagues have shown that a broccoli-rich diet can alter prostate gene expression in men with high-grade prostatic intraepithelial neoplasia (HGPIN), a condition that is believed to be a precursor to PCa (221). However, their study was not able to distinguish between the biological effects of broccoli as a whole, which is a chemically complex food consisting of several classes of bioactive compounds, vitamins and minerals, and that of glucoraphanin and its isothiocyanate derivative, SF. The dietary intervention tested in the ESCAPE study has been designed to deliver SF through the consumption of three types of soups containing different doses of glucoraphanin (SF precursor) within a constant broccoli background, thereby enabling the effect of SF to be investigated against the background of the other compounds present in the plant.

5.1.2 Active surveillance for low- and intermediate-risk prostate cancer cases

Studies have shown that men with low-grade organ confined PCa are at low risk of progression (26, 27). This category of men can often avoid or delay radical treatment which can be associated with significant morbidity (28). AS is the process by which patients with organ-confined PCa are managed expectantly with regular monitoring. Treatment is only initiated when signs of progression are observed. Identifying patients suitable for AS can be done through risk stratification using a number of variables like PSA, Gleason score sum (29), and clinical stage to calculate the likelihood of disease progression or harbouring more aggressive disease. A number of tools exist that stratify patients with PCa into risk categories, and many have undergone extensive testing and validation (30). For the purposes of the ESCAPE study, D'Amico's risk groups were used to define low-risk PCa as those men with Gleason score ≤ 6 , PSA $< 10 \mu\text{g/l}$ and stage $\leq \text{T2a}$ (tumour-node-metastasis staging system 2002), and intermediate risk as those with Gleason score 7, PSA of $10\text{--}20 \mu\text{g/l}$, and stage T2b-T2c (31). This classification is also adopted by NICE.

The local database for PCa in NNUH indicates that just over 300 patients with low to intermediate-risk disease are currently on AS (32).

5.1.3 Prostate biopsy

AS patients require regular follow up to ensure that monitoring is still suitable. The disease progression is assessed mainly by physical examination of the prostate and PSA blood test. It is often necessary to repeat the prostate biopsies to ensure the disease has not changed histologically. At the time of writing the ESCAPE study protocol there were no national guidelines for the timing of repeat biopsies in men on AS, as a result the decision to repeat the biopsies was often made on an individual or institutional basis. Since, NICE has produced an AS protocol that recommends PSA testing every 3 to 4 months in the first year of surveillance together with 6- to 12 -monthly physical examination of the prostate and repeat prostate biopsies every 12 months (222). However, there is no consensus on the technique of obtaining needle core biopsies of the prostate, or the exact number of samples to be taken for men on AS. In general, the 1st diagnostic biopsy that men undergo is carried out with TRUS guidance under local anaesthesia (LA), although more recently several other imaging modalities replacing or augmenting ultrasound are being investigated, such as the use of MRI fusion.

One difficulty in prostate biopsy is that PCa is often not localised to one part of the gland. In addition, areas of cancer are not readily palpable on examination in early stages of the disease, and visualising these cancerous lesions during the biopsy on ultrasound is unreliable (223). The ESCAPE protocol was designed to allow tissue collection through a transperineal route (TPB biopsies). This technique enables biopsies to be taken from a wider area of the prostate, resulting in a more effective sampling of the entire gland. The trial protocol has been designed to carry out a biopsy procedure at the start of the study, and a further biopsy procedure at the end of the dietary intervention in 12 months. Although volunteers will have two additional biopsy procedures during the study, they will not need further samples for their routine follow up or care at the hospital, in addition, volunteers will be able to have TPB which offers better sampling and more accurate disease assessment ensuring safety of continued AS.

5.2. Aim

- ❖ To describe the outline of a dietary intervention trial designed to study the effect of SF on the prostate.

5.3. Material and Methods

5.3.1 Trial management

ESCAPE is a multi-institutional trial supported by the Prostate Cancer Foundation (PCF) (USA). All the institutions involved in this trial are affiliated to the Norwich Research Park (UK). Investigators at QIB designed the protocol [Dr Omar Al Kadhi (Urology Specialist Registrar & PhD student and Dr Antonietta Melchini (senior scientist)] in collaboration with clinicians at the NNUH [Dr Omar Al Kadhi and Dr Robert Mills (Consultant Urologist)] and co-investigators at the UEA. QIB is acting as sponsor and NNUH as the investigator site. The protocol was approved by the QIB Human Research Governance Committee in March 2013 and subsequently by the National Research Ethics Service (NRES) East of England – Cambridge South Research Ethics Committee (REC ref: 13/EE/0110) (Figure 5.1). ESCAPE has been adopted by the National Institute for Health Research Clinical Research Network (NIHR) Clinical Research Network (CRN) Portfolio in May 2013 (Study ID: 14482). The trial was registered on ClinicalTrials.gov (NCT01950143), International Clinical Trials Registry Platform (ISRCTN40496794), and Clinical Trials database Cancer Research UK.

5.3.2 Individual contributions to the trial

I am part of the ESCAPE study team. My roles included the following

- Trial design
- Writing the study protocol with Dr Melchini (senior scientist at QIB)
- Writing the patient information sheet (PIS)
- Completing the IRAS paperwork with Dr Melchini
- Attendance at the Research Ethics Committee meeting
- Identifying suitable participants from the Urology department at the NNUH with Dr Mills
- Conducting study talks at the QIB Human Nutrition Unit
- Collecting transporting biological samples from hospital site to QIB laboratory facilities on study days
- Conducting outpatient clinic follow up for study patients and collecting trial data
- Analysing metabolic data from prostate tissue on a subgroup of patients presented in Chapter 6

5.3.3 Trial population

The target population were men aged 18-80 years with a BMI between 19.5 and 35 kg/m², with low-risk PCa (PSA < 10 ng/ml; Gleason sum = 6; T category < T2) or intermediate-risk PCa patients (PSA 10-20ng/ml; Gleason sum = 7 (including selected Gleason 4+3 = 7 cases that will not be advised to undergo radical prostatectomy; T category T1 or T2) who have already decided to take up AS or monitoring. Eligibility criteria have been chosen to reflect the population of men on AS within the region from which patients will be recruited via NNUH. Eligibility criteria are listed in Table 5.1.

5.3.4 Recruitment policy

Eligible patients were identified and recruited by myself and Mr Robert Mills (consultant urologist) at the NNUH. Identified patients were provided with an information pack consisting of a letter of invitation, participant information sheet (PIS) and response slip to be sent to the study team using a prepaid envelope. Interested volunteers were then invited to attend an information exchange at the QIB Human Nutrition Unit (HNU) to ensure their full understanding of the study protocol prior to obtaining written informed consent. Volunteers were given at least 3 days to decide whether they would like to take part or not. After this consideration period those volunteers interested in taking part were seen in clinic at the NNUH to give written informed consent and undergo the first clinical visit.

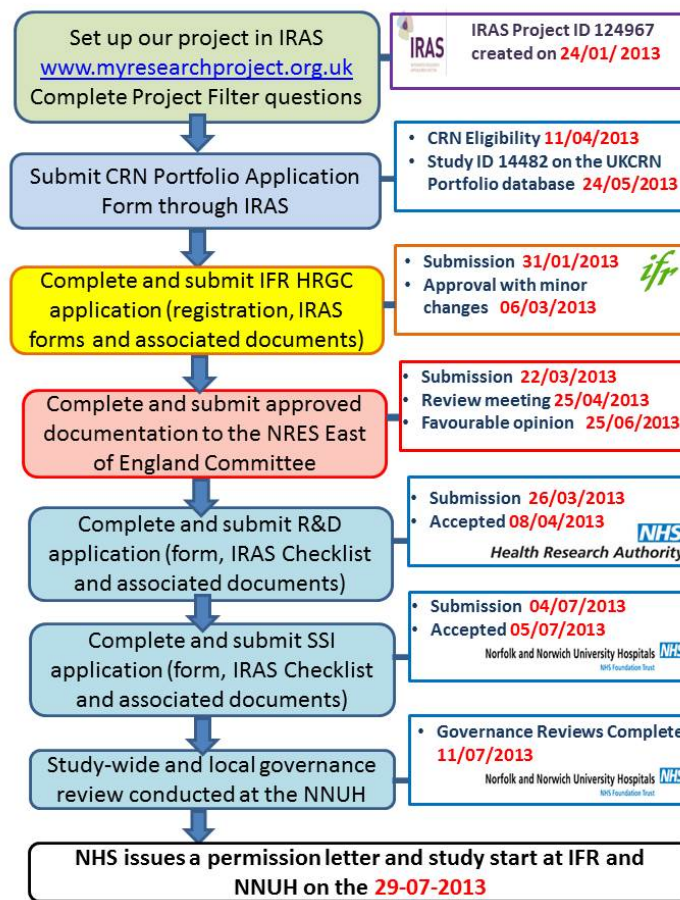


Figure 5.1 Gaining ethical and regulatory approvals for conducting the ESCAPE study.

Table 5.1 Eligibility criteria for the trial

Inclusion criteria	Exclusion criteria
Males	Those taking 5 α -reductase inhibitors or testosterone replacement supplements
On active surveillance for low- and intermediate-risk PCa (Gleason score \leq 7, PSA \leq 20 μ g/l, stage \leq T2)	Those on warfarin treatment
Aged 18-80 years	Those diagnosed with diabetes
BMI between 19.5 and 35 kg/m ²	Those diagnosed with or suspected to be at high-risk for human immunodeficiency virus (HIV) and/or hepatitis virus infection
Smokers and non-smokers	Those allergic to any of the ingredients of the broccoli soups
	Those taking dietary supplements or herbal remedies which may affect the trial outcome
	Parallel participation in another research project that involves dietary intervention
	Anybody related to or living with any member of the trial team

5.3.5 Trial design

The trial outline is presented in Figure 5.2. ESCAPE is a randomised double-blinded intervention recruiting men with low-risk or intermediate-risk PCa on AS. Patients were allocated randomly to one of three dietary arms in which they were required to consume one portion of broccoli soup per week, delivering different levels of glucoraphanin (SF precursor). This has been part of their normal diet for one year. The three types of soup contained standard broccoli (i), glucoraphanin-enriched broccoli (Beneforté®) (ii), or glucoraphanin-enriched broccoli Beneforté Extra (iii). The trial has involved lifestyle assessments and collection of prostate biopsies, blood and urine samples at baseline and after 12 months. Blood markers were monitored at regular intervals (every 3-4 months) as part of the participants' on-going clinical follow up. Prostate biopsies were obtained through TPB or standard TRUS-guided biopsy. TPB is a clinical procedure carried out under a general anaesthetic, which gives more detailed spatial information of the cancer within the prostate compared to other standard techniques. However, the patients had the possibility to choose TRUS-guided biopsy if they did not wish to undergo TPB or if they were considered unsuitable for general anaesthesia. The trial dropout rate was approximately 8% due to the clinical progression of PCa within the 12-month period. In the event of clinical progression, patients discontinued the intervention and received advice from their clinicians. If they proceeded to prostatectomy, they were asked if they would

donate part of their prostate gland for research purposes. At the end of the 12-month intervention, patients were offered the possibility to continue the broccoli diet for a further 12 months after giving a separate written consent. They were required to eat one portion of broccoli soup per week for a further 12-month period, but did not attend extra hospital visits for the purpose of the trial or give additional biological samples. Following ethical approval, the trial team created an anonymised database with clinical follow-up data for the extended intervention period.

5.3.6 Trial objectives

The primary and secondary aims of this trial are listed in Table 5.2. The trial was designed to provide information about changes in global gene expression and metabolism in response to a SF-rich diet. Recruited men on AS for PCa were randomly allocated to three dietary arms and received different levels of SF over a 12-month period. The trial design was chosen to determine whether changes in gene and metabolite levels induced by SF would occur in a dose-related fashion. The trial also incorporated analyses of blood and urine samples from the trial cohort to obtain additional information on the systemic effects of the dietary intervention.

Furthermore, it will be determined whether dietary induced changes (if any) are related to genetic polymorphisms including glutathione S-transferase Mu 1 (GSTM1). It is well-established that GST genotype influences the effects of dietary ITCs (224). When ITCs are absorbed, they are subjected to enzymatic conjugation with the tripeptide γ -glutamylcysteinylglycine (GSH) that is catalyzed by GSTs [14]. Several studies have reported that the protective effects associated with dietary consumption of ITCs were greatest in individuals who were glutathione S-transferase theta 1 (GSTT1)- and GSTM1-null, rather than those who were GSTT1- and GSTM1-positive. However, there are a few studies that showed opposite or no association [15].

Finally, the physical activity of the trial population will be assessed to determine whether metabolic changes in response to diet are correlated with their physical activity.

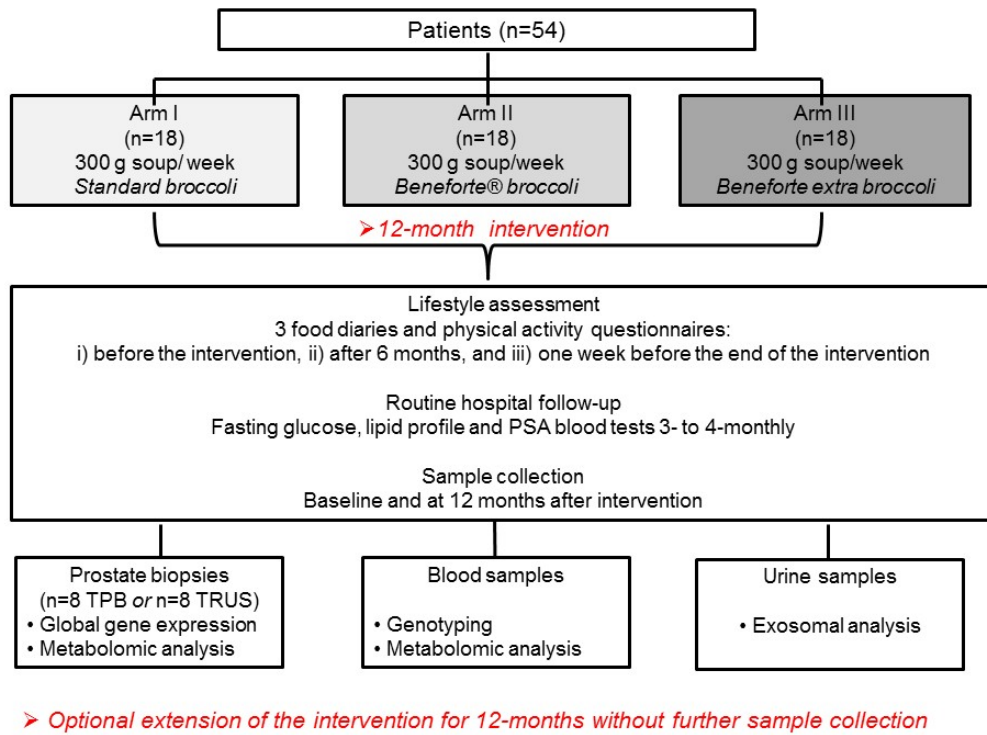


Figure 5.2 ESCAPE study outline.

Table 5.2 Trial primary and secondary aims

Primary Aim	Secondary Aims
<p>To determine whether a 12-month diet rich in broccoli results in changes in global gene expression in prostate tissue from men on AS for low- and intermediate- risk PCa. Comparisons will be made between three diets, each delivering different levels of glucoraphanin/SF, to distinguish the biological effects of glucoraphanin/SF from that of the broccoli itself.</p>	<p>To determine whether a 12-month diet rich in broccoli results in changes in levels of metabolites in prostate tissue from men on AS for low- and intermediate- risk PCa.</p>
	<p>To determine whether metabolic changes in response to diet within prostate tissue are correlated with metabolite levels in plasma.</p>
	<p>To determine whether plasma levels of PSA and other biomarkers are affected by diet.</p>
	<p>To demonstrate if the extent of modulation of gene expression and metabolite changes by diet is affected by the glutathione S-transferase Mu 1 (GSTM1) or other relevant genotypes.</p>
	<p>To determine whether the dietary intervention affects the levels and nature of RNA found within urinary exosomes.</p>

5.3.7 Trial procedure

A flow chart of the overall trial design is presented in Figure 5.3. Patients were asked to undergo 5 separate visits during their participation in the trial. Consent for the trial and clinical procedures were obtained by research nurses and urologists. In total, volunteers were asked to sign three consent forms: trial consent form (1), The Norwich Biorepository consent form (2), and NNUH standard patient agreement to investigation (3). GPs were informed by letter of their patients' participation if the volunteer gave consent. A basic health questionnaire including results from the measurement of blood pressure, heart rate, and BMI was completed at the start of the trial and repeated at 12 months. Before the biopsy procedures, patients had a pre-operative assessment carried out by telephone for patients undergoing TRUS-biopsy under local anaesthesia, or face to face with a nurse specialist at the NNUH for those undergoing TPB under GA. The pre-operative assessment at the NNUH involved electrocardiography (ECG) for patients >50 years of age or those with history of a cardiac condition, urine dipstick test to exclude infection, and pre-operative blood tests. All patients were tested for methicillin-resistant *Staphylococcus aureus* (MRSA) with skin swabs. Patients were asked not to eat cruciferous vegetables 2 days prior to the biopsy procedure where study samples (blood, urine, prostate biopsies) were collected at the same time. All biological material collected at NNUH was taken to QIB or sent to the biorepository for appropriate processing and storage.

5.3.8 Trial intervention

Three types of soup containing standard broccoli, glucoraphanin-enriched broccoli (Beneforté®), or glucoraphanin-enriched broccoli Beneforté extra broccoli, were specifically developed for this trial. These soups deliver contrasting amounts of the SF precursor, glucoraphanin, within a constant broccoli background.

Beneforté® and Beneforté extra broccoli varieties were developed by conventional breeding. Beneforté® contains a single allele of the Myb28 transcription factor from *B. villosa* that elevates the glucoraphanin content from approximately 5 to 15 $\mu\text{moles/g}$ fresh weight (fw) (225). Beneforté extra contains two Myb28 villosa alleles that elevate the glucosinolate content to approximately 30 $\mu\text{moles/g}$ fw. Standard broccoli, Beneforté®, and Beneforté extra plants have the same appearance and flavour, thus enabling a double-blinded trial to be undertaken. The three types of broccoli soups were prepared by an international food manufacturing company (Bakkavor®). In order to minimise intra-batch variability, trial soups were produced using fresh broccoli and then appropriately stored at $-20\text{ }^{\circ}\text{C}$ until delivered to participants. The volume and packaging of the study diet were specifically chosen to facilitate safe storage and delivery.

5.3.9 Phytochemical analysis of the trial intervention

LC-MS analyses to quantify glucoraphanin concentrations were performed in each batch of soups produced for the trial as described below.

5.3.9.1. *Glucosinolate analysis*

LC-MS analysis was carried out to identify the major GLSs present in the broccoli soups. GLSs were extracted from freeze-dried powder (100 mg) of soups made with (i) standard broccoli, (ii) glucoraphanin-enriched broccoli (Beneforté®), or (iii) glucoraphanin-enriched broccoli Beneforté extra broccoli using hot 70% (v/v) aqueous methanol followed by the addition of an internal standard (sinigrin, 50 µl). Briefly, samples were incubated in a water bath preheated at 70 °C for 30 minutes to inactivate the myrosinase enzymes. After centrifugation at 3,000 x g for 5 minutes at room temperature, supernatants were collected and allowed to drip slowly through a mini-column packed with DEAE- Sephadex A25, which was washed twice with 0.5 ml of de-ionized water and 0.5 mL of 0.02 M sodium acetate buffer at pH 5. GLSs were desulfated by adding 75 µl purified sulfatase to the column, which was allowed to stand at room temperature overnight. The desulfated-GLSs (DS-GLSs) were eluted with 1.25 ml of deionized water, and analysed by positive ion atmospheric pressure chemical ionisation (APCI+) LC-MS.

5.3.9.2. *Analysis of other sulfur- containing compounds*

Freeze-dried powder (~2 g) of soups made with standard broccoli, Beneforté®, and Beneforte extra broccoli was used to analyse sulfur containing compounds (total sulfur, SMSCO, sulfate). Sulfur was measured by using inductively coupled plasma-mass spectrometry (ICP-MS). ICP-MS analysis was carried out by an external company (Eurofins Scientific, UK). Sulfate and SMCSO were measured by LC-MS/MS analysis following a method developed by an QIB analytical chemist (Dr Shikha Saha). Briefly, freeze-dried powder (20-30 mg) was mixed with a water solution (1 ml) of polyvinyl polypyrrolidone (25 mg/ml) for 1 hour at 4 °C and subsequently incubated at 95 °C for 15 minutes. After centrifugation, supernatants were filtered (pore size: 0.45 µm) into HPLC vials and analysed on Agilent 6490 Mass spectroscopy in MRM mode to measure sulfate concentrations. A porous graphitic carbon column (PGC, Hypercarb) and formic acid as mobile phase (1% in water + 1% in acetonitrile) were used to carry out this analysis. A calibration curve was obtained by using a range of concentrations from 0.25 mM to 2 mM of sulfate standard purchased from Sigma®. SMCSO was measured by following the extraction method described by Bernaert and colleagues (226). Freeze-dried

powder (~50 mg) was mixed with 5 ml of O-(carboxymethyl)-hydroxylamine hemihydrochloride for 10 minutes. After centrifugation, the supernatant was diluted with 0.1% formic acid in water, and analysed by LC-MS/MS using an Agilent 6490 mass spectrometer with a photodiode array detector. The analyses of SMCSO and sulfate in the broccoli soup samples were performed by Dr Shikha Saha.

5.3.10 Randomisation

Recruited patients were randomized to one of three arms:

Arm I one portion (300 g) per week of standard broccoli soup

Arm II one portion (300 g) per week of glucoraphanin-enriched Beneforté® broccoli soup

Arm III one portion (300 g) per week of Beneforté extra broccoli soup

The randomisation was undertaken through an electronic randomisation generator (www.randomization.com). This uses a method called “Block randomisation”, whereby participants are equally distributed to the three arms.

5.3.11 Lifestyle assessment

Regular exercise and diets rich in broccoli have both been associated with the reduction in the risk of progression of PCa from localised to aggressive disease (95). The participants’ habitual diet was measured during the intervention to gain information on their broccoli intake. The QIB standard food diary was used to record food intake, beverages, and supplements consumed over a 7-day period (incorporating 7 different days, including weekends) before starting the intervention, then at 6 and 12 months. Food diaries were analysed using DietPro7 as UK food composition tables.

Considering the demographics of the trial population, Community Healthy Activities Model Program for Seniors (CHAMPS) physical activity questionnaires were used because they include the assessment of types as well as levels of physical activity that are meaningful and appropriate for older adults, including both light and more vigorous activities (227).

5.3.12 Trial compliance

Two main approaches were used to monitor compliance. Patients were asked to: (i) complete a 7-day diet diary and (ii) fill in record sheets on a weekly basis recording soup consumption. In addition, ESCAPE team members routinely delivered frozen soups to the participants’ houses and collected record sheets and pot lids.

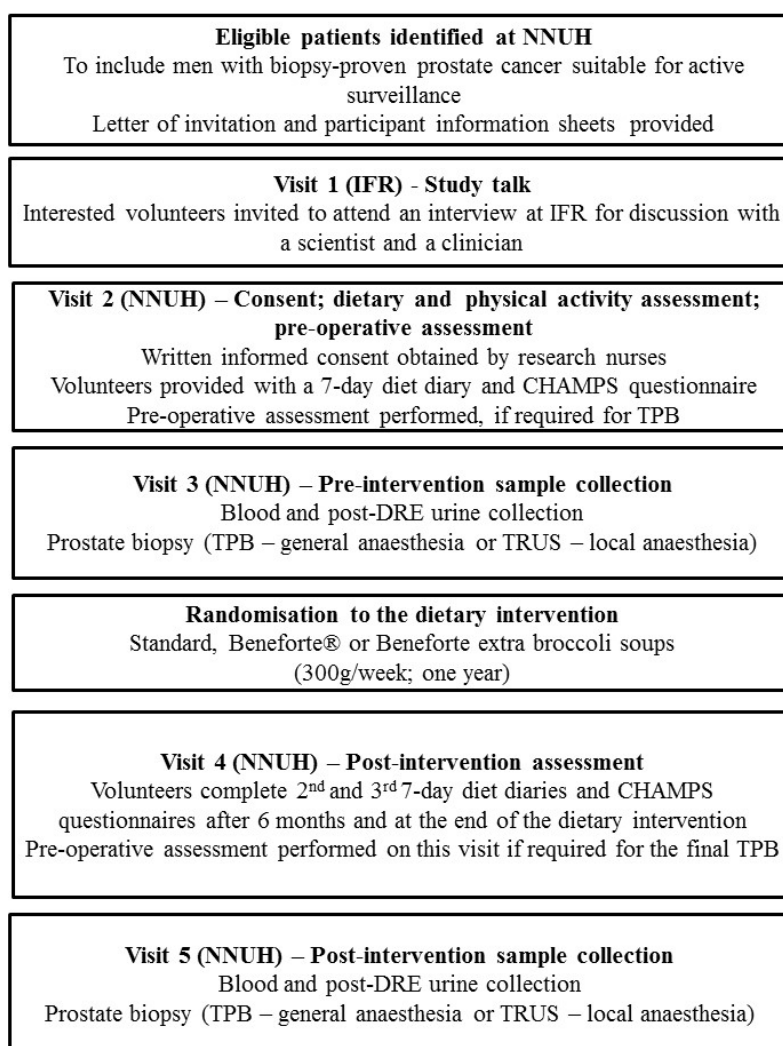


Figure 5.3 Trial flow chart.

5.4. Experimental methods

5.4.1 Prostate biopsies and processing

Prostate sampling was carried out at the NNUH. TPB procedures were performed in the operating theatre under general anaesthesia with intravenous aminoglycoside antibiotic prophylaxis, in accordance with the NNUH Trust guidelines. Patients were placed on their back for the duration of the procedure, which lasted between 45-60 minutes. In selected cases, a catheter was placed through the urethra into the bladder to allow better visualisation of the urethra and facilitate urinary drainage; these catheters were removed prior to discharge. A trans-rectal ultrasound probe was used to visualise the prostate. The skin was prepared with topical surgical antiseptic solution (povidone iodine). A pre-designed template for brachytherapy procedures (procedure whereby radioactive seeds are implanted into the prostate through the perineum) was then used to guide the biopsy needle which is

passed through the holes on the template into the prostate gland with one skin puncture per core (Figure 5.4). Each group of needle samples were labelled separately. After completion of the procedure, a dressing was applied to the perineum. Although this is a day-case procedure (i.e. patients are discharged home the same day), some patients required an overnight stay in hospital.

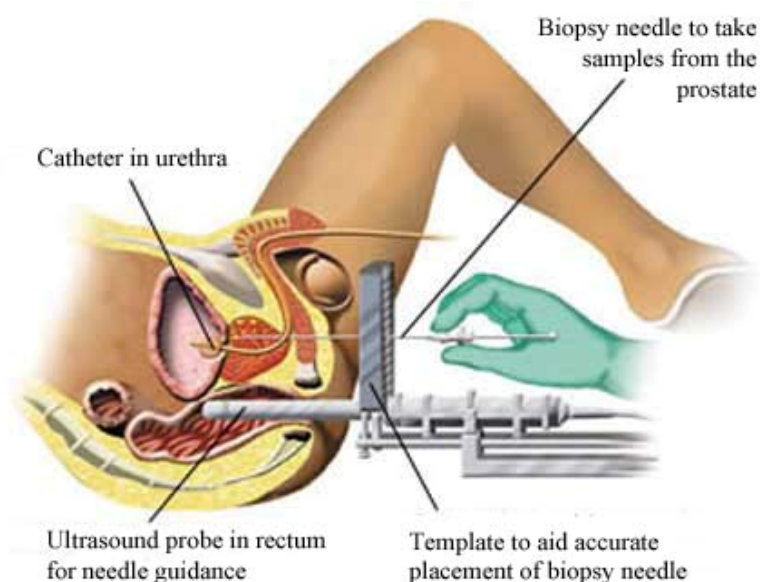


Figure 5.4 Outline of the setup for transperineal template biopsy procedure of the prostate.

If the patient was ineligible for TPB, TRUS biopsy was carried out under local anaesthesia. Patients were given oral fluoroquinolone antibiotics before the procedure and further doses supplied to reduce the risk of infection post-operatively, as per the NNUH Trust guidelines. An ultrasound probe was inserted into the rectum that guided the sampling needles into the prostate after instilling local anaesthesia (lidocaine 1%). TRUS biopsy procedures took approximately 30 minutes.

For each participant, prostate biopsies ($n=8$) were collected at baseline and after a 12-month intervention period for metabolomic and gene expression analyses. Three biopsy samples were deposited into pre-labelled vials containing room temperature extraction solvent (one biopsy per vial). Following incubation at room temperature (up to 24 hours), these biopsy samples were removed from the extraction solvent and underwent histopathological assessment, allowing detailed correlation of metabolic analysis with histopathological findings. The vials containing extracted metabolites were stored at $-80\text{ }^{\circ}\text{C}$ until required for metabolomic analysis (204). A further three prostate biopsy cores were immersed in RNA-later solution on collection and subsequently stored at

-80 °C until required for global and targeted gene expression analyses. Two prostate biopsy cores were snap frozen for future research.

5.4.2 Histological analysis

Template prostate biopsies from ESCAPE patients were fixed in 10% formal saline and processed in paraffin wax blocks using standard techniques. H&E-stained sections, 4 µm thick, were cut from each block at 3 levels for histopathological assessment. If necessary, deeper levels or other techniques (for example, immunohistochemistry) were employed to establish a definitive diagnosis for each of the biopsies. If PCa was present, it was given a Gleason sum and the proportion of tumour within the biopsy was estimated. Evidence of perineural or lymphovascular invasion was determined as well as extracapsular spread. The biopsies for metabolomic analysis were also histopathologically assessed after metabolite extraction. After 24 hours incubation with methanol, biopsy cores were processed in paraffin wax blocks and a single H&E-stained section was prepared. Each section was assessed and its various components (stroma versus glands; inflammation, etc.) were described. If cancer was present, it was given a Gleason sum and estimation of the proportion of the length of the core involved.

5.4.3 Blood sampling and processing

Blood samples were collected at baseline and after a 12-month intervention period for standard haematological and biochemical analyses (full blood count, urea and electrolytes, liver function tests, fasting glucose, glycated haemoglobin (HbA1c), lipid profile, and PSA), genotyping and metabolomic analysis. Haematological and biochemical analyses were performed by the NNUH Laboratory Medicine departments using Sysmex XE2100 analysers and Abbott Accelerator system. The same hospital platforms were used to monitor blood markers (fasting glucose, lipid profile, PSA) at regular intervals (every 3-4 months) during the intervention. Genomic DNA was extracted from each blood sample using the QIAamp DNA Mini kit protocol (Qiagen Inc.) prior to genotyping for GSTM1 using real-time PCR according to the method of Cotton and colleagues (228), and other selected genotypes considered relevant for the purposes of this study. Plasma metabolomic analysis will be performed once the collection of paired samples is completed in October 2016. Plasma samples will be analysed using the same metabolomic platforms described in Chapter 6.

5.4.4 HbA1c analysis

K²⁺EDTA-collected whole blood was used for a quantitative determination of Haemoglobin A1c concentration (HbA1c). HbA1c is an indicator of the mean daily blood glucose concentration over the preceding 6-8 weeks (229). The analysis was carried out by using a latex enhanced immunoturbidimetric assay suitable for use on RX Daytona analyser. This method allows the measurement of both HbA1c and total haemoglobin concentrations. HbA1c is reported as a percentage of the total haemoglobin concentration (% HbA1c). Briefly, whole blood samples were pre-treated with a protease enzyme to lyse red blood cells and cause hydrolysis of the haemoglobin. Total haemoglobin was measured by converting all the haemoglobin derivatives into haematin in an alkaline solution of a non-ionic detergent as previously described (230).

The production of alkaline haematin results in an increase in absorbance at 600 nm. HbA1c was measured by using a latex agglutination inhibition assay. This assay is based on the use of a synthetic polymer containing multiple copies of the immunoreactive portion of HbA1c, which causes agglutination of latex coated with HbA1c specific mouse monoclonal antibodies. When HbA1c is not present, this polymer agglutinates with the HbA1c R2 reagent, and the antibody-coated micro particles in the HbA1c R1 reagent increase the absorbance measured at 700nm. In the presence of HbA1c the rate of agglutination slows down because it competes with the HbA1c agglutinator for antibody binding sites on the latex, resulting in a decrease of absorbance. Thus, the increase in absorbance is inversely proportional to the concentration of HbA1c in the sample, which is calculated through a calibration curve. HbA1c and Total Haemoglobin values expressed in g/dl are then used to calculate % HbA1c in each sample.

5.4.5 Metabolite profiling

Metabolite profile analyses was performed on biopsy cores and plasma samples collected before and after the 12-month intervention. Metabolomic analysis was carried out by Metabolon® (Metabolon, Durham, USA). Metabolon® is a service and diagnostic products company with the ability to identify and produce a profile of up to 350 known plasma metabolites using standard metabolomics techniques, such as LC-MS and GC-MS (204). The final analyses will be performed once the sample collection is completed; however the methods were tested as part of the pilot study described in Chapter 6.

5.4.6 Urinary biomarkers

First pass urine samples were collected following DRE prior to the prostate biopsy procedure. Intact exosomal RNAs were obtained from DRE urine following the method of

Miranda et al. (231). Utilising gene-specific primers and chum RNA, cDNA was generated and multiplex analysis (up to 30 probes) of total cellular or exosomal RNA biomarkers will be performed, starting from as little as 3 ng RNA per sample, by using TaqMan® Array Microfluidic Cards (Applied Biosystems). Genes assayed will include a combination of control probes, together with diagnostic and established prognostic biomarkers.

5.4.7 Biobanking for future research

Patients were asked to sign a separate consent form agreeing to donate additional samples to the local biobank for research purposes. It is envisaged that the banking of tissue, blood and urine samples collected from this cohort of patients at the Norwich Biorepository will be invaluable for obtaining additional information for this trial and for designing further studies.

5.4.8 Statistical analysis

There are no data reporting the global effect of a diet delivering increasing concentrations of SF or other ITCs on gene expression or metabolite profiles within the prostate or at a systemic level. As the primary data analysis is based upon the use of transcriptomic and metabolite data, neither of which were used in prior diet intervention studies, it was not possible to perform conventional power calculations. Rather than define the entire experiment as a pilot study, it was decided to assess the sample size to report statistically significant changes in gene expression by two methods: i) “Sample Size for Microarray Experiments” developed by the Section of Bioinformatics of the University of Texas M. D. Anderson Cancer Centre (232), and ii) reported calculations based on previously published microarray data (233).

It has been estimated that 26 subjects in each of the three dietary groups (78 in total) are required to detect 1.5-fold differences with a significant difference ($p < 0.02$) between any two of the three dietary groups, with a power of 80% and a standard deviation of 0.66 (based on a log₂ scale of gene intensity measurements).

5.5. Results

5.5.1 Trial cohort

Fifty eligible patients were recruited from the NNUH (Figure 5.5). Since October 2013, the study response rate was 49% (84 response letters out of 170 information packs sent out) with a recruitment rate of 67% (50 recruited out of 74 study talks). Recruited patients were

randomised to the three dietary arms through an electronic randomisation generator as previously described (Diet A, n=17; Diet B, n=16; Diet C, n=17).

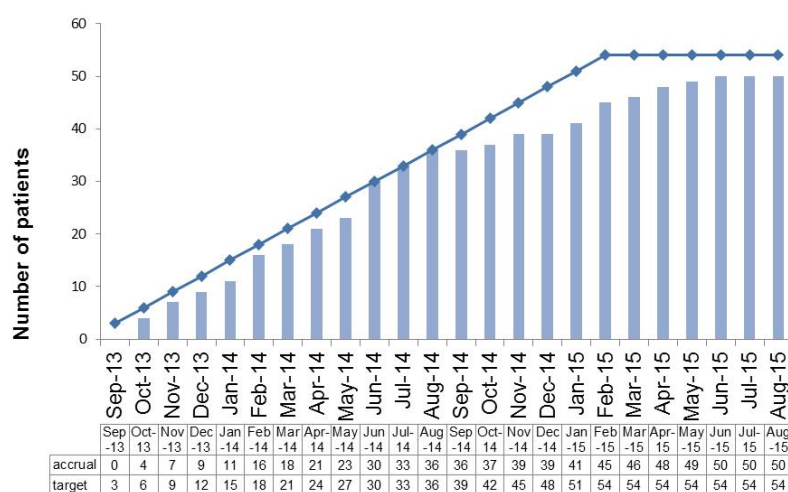


Figure 5.5 Recruitment rate in the ESCAPE study. Recruitment was terminated at 50 volunteers.

5.5.2 Baseline anthropometric measurements

Baseline anthropometric measurements of the trial population are shown in Table 5.3. Statistical analysis indicated that there were no significant differences between dietary arms for any variable except for the systolic blood pressure, which was significantly different between Diet C and the other two dietary arms ($p=0.05$ vs Diet A; $p=0.03$ vs Diet B).

Table 5.3 Baseline anthropometric measurements

	Diet A (n=17)	Diet B (n=16)	Diet C (n=17)
Age (yrs)	66±5.926	66±7.042	66±6.102
BMI (kg/m ²)	26.47±3.215	27.74±2.180	27.79±3.595
Systolic BP (mm Hg)	141.5± 15.590	141.2±16.900	150.2±14.720
Diastolic BP (mm Hg)	82.13±10.270	87.56±10.420	86.93±9.580

5.5.3 Baseline blood measurements

Levels of plasma lipids (Figure 5.6), glucose (Figure 5.7) and PSA (Figure 5.8) at baseline did not show any significant difference between the three study arms.

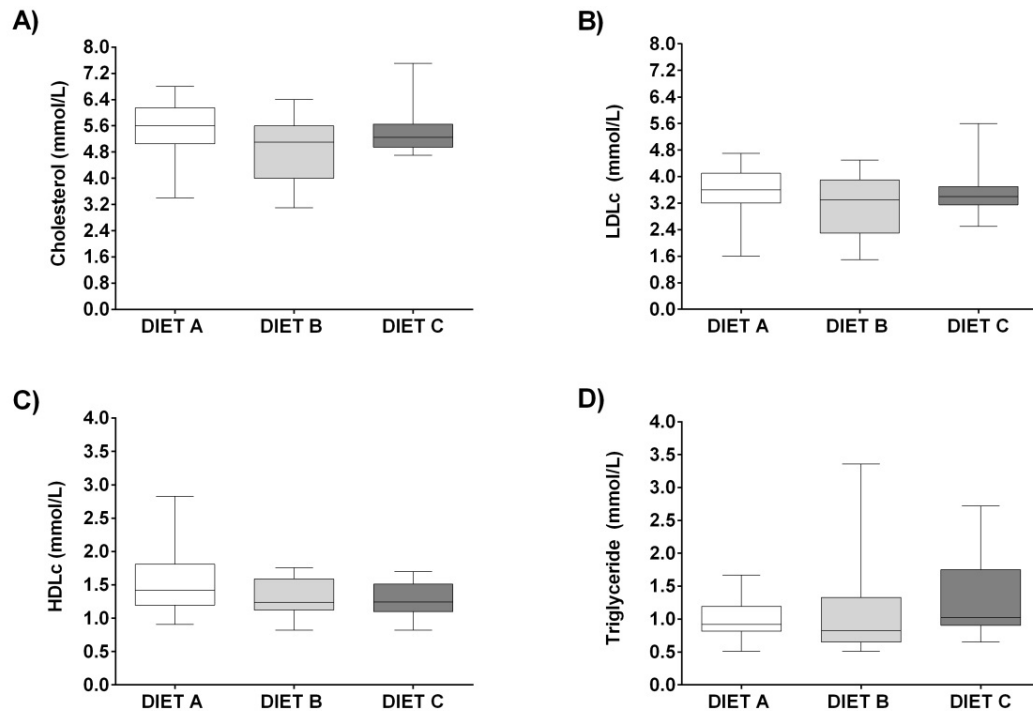


Figure 5.6 Lipid profile at baseline. A) Cholesterol, B) LDL-cholesterol, C) HDL-cholesterol, and D) triglycerides measured in patients' serum before starting the diet intervention. Box plots represent the median of each sample with 25th and 75th percentiles. Whiskers indicate the range. $p=0.10$ (A), $p=0.22$ (B), $p=0.15$ (C), $p=0.21$ (D); p values from one way ANOVA followed by Tukey's multiple comparison test.

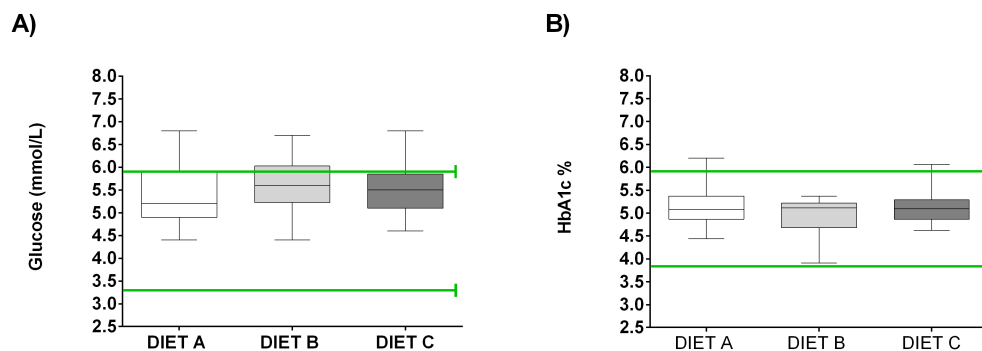


Figure 5.7 Fasting glucose levels (A) and HbA1c % (B) at baseline. Green lines indicate healthy ranges in adult males. Box plots represent the median of each sample with 25th and 75th percentiles. Whiskers indicate the range. $p=0.81$ (A), $p=0.33$ (B); p values from one way ANOVA followed by Tukey's multiple comparison test.

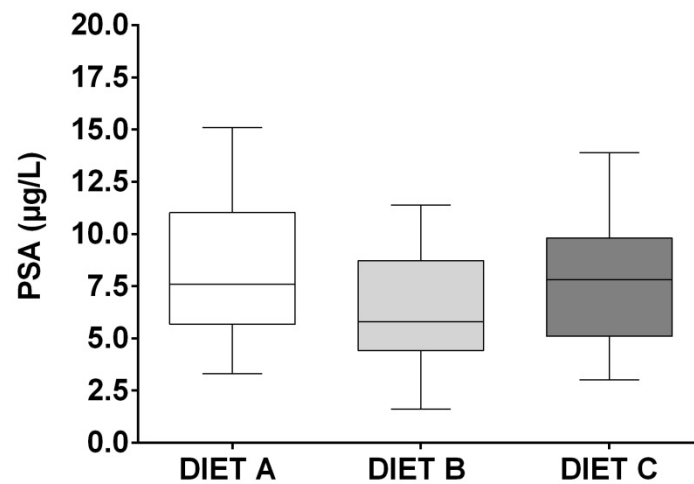


Figure 5.8 PSA concentrations at baseline. Box plots represent the median of each sample with 25th and 75th percentiles. Whiskers indicate the range. $p=0.25$; p value from one way ANOVA followed by Tukey's multiple comparison test.

The level of urea, creatinine, electrolytes (Na, K) and estimated glomerular filtration rate (eGFR) were measured in order to indirectly reflect the participants' kidney function. Liver function was also checked by measuring albumin, globulin, bilirubin, total proteins and liver enzymes, including alanine aminotransferase (ALT) and alkaline phosphatase (ALP). Figure 5.9 and Figure 5.10 indicate normal kidney and liver function for all participants randomised to the three diet interventions.

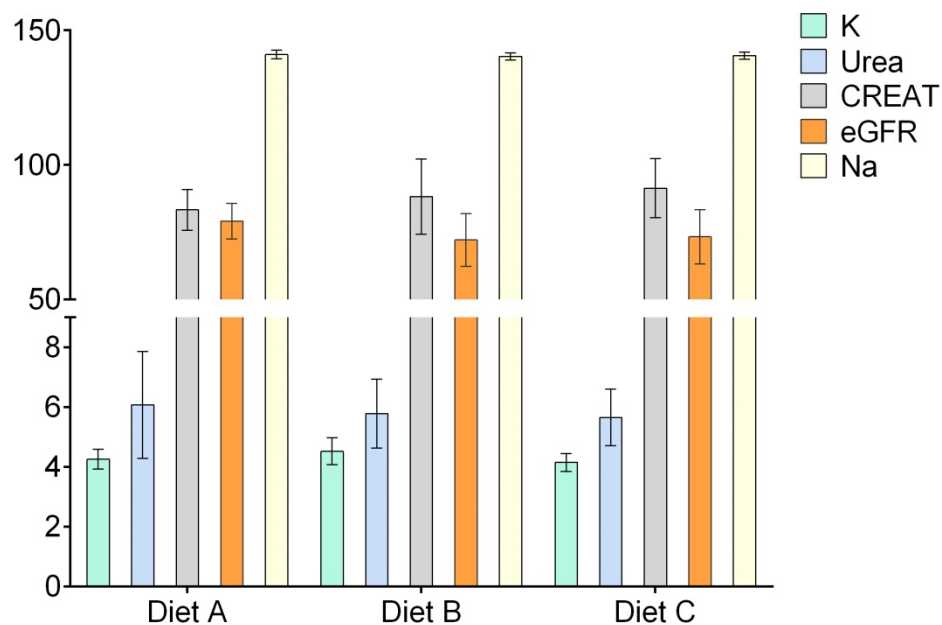


Figure 5.9 Kidney function assessed in randomised participants before starting the intervention. K; potassium (mmol/L), Urea; urea (mmol/L), CREAT; Creatinine (mmol/L), eGFR; estimated glomerular filtration rate (ml/min/1.73m²), Na; sodium (mmol/L). Data presented as mean (SD).

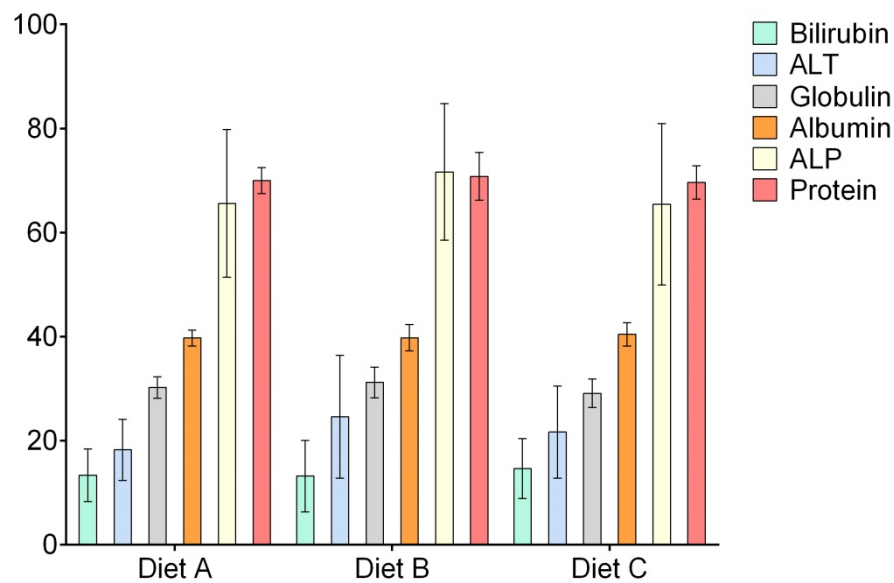


Figure 5.10 Liver function assessed in randomised participants before starting the intervention. Bilirubin; total bilirubin ($\mu\text{mol/L}$), ALT; alanine aminotransferase (U/L), Globulin; globulin (g/L), Albumin; albumin (g/L), ALP; alkaline phosphatase (U/L), Protein; total protein (g/L). Data presented as mean (SD).

5.5.4 Phytochemical characterization of the trial intervention

5.5.4.1. Glucosinolate levels

LC-MS analysis was carried out to identify the major GLSs present in standard broccoli, glucoraphanin-enriched broccoli (Beneforté®), and extra glucoraphanin-enriched broccoli (Beneforté extra) soups. This work was conducted by Dr Shikha Saha (analytical biochemist at the QIB). Two aliphatic compounds [4-Methylsulfinylbutyl glucosinolate (glucoraphanin) and 3-Methylsulfinylpropyl glucosinolate (glucoiberin)] and four indole-GLSs (hydroxyindolylmethyl-, indolylmethyl-, 1-methoxyindolylmethyl- and 4-methoxyindolylmethyl-GLSs) were identified by their target ion and further MS/MS measurements after fragmentation of $(m+H)^+$ (Figure 5.11). DS-GLSs were quantified by addition of sinigrin as internal standard. Glucoraphanin content was 42.5 ± 0.782 $\mu\text{moles}/300\text{g fw}$, 179.88 ± 4.212 $\mu\text{moles}/300\text{g fw}$ and 442.40 $\mu\text{moles}/300\text{g fw}$ in standard,

Beneforté® and Beneforte extra broccoli soups, respectively (Figure 5.12).

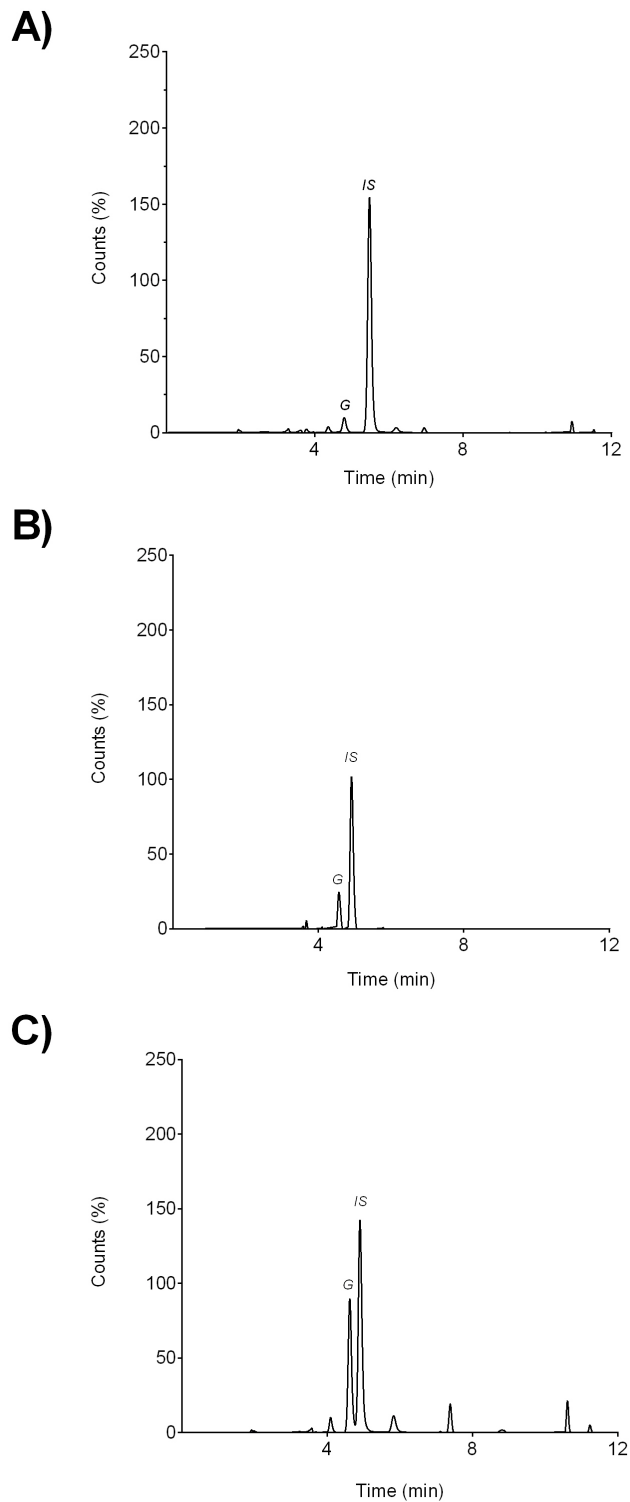


Figure 5.11 LC-MS chromatograms of study soups. A) Chromatogram of soups made with standard broccoli, B) Beneforte® broccoli, and C) Beneforte extra broccoli. IS, internal standard; G, glucoraphanin. Graph obtained with permission from Dr Shikha Saha (ESCAPE study protocol data)

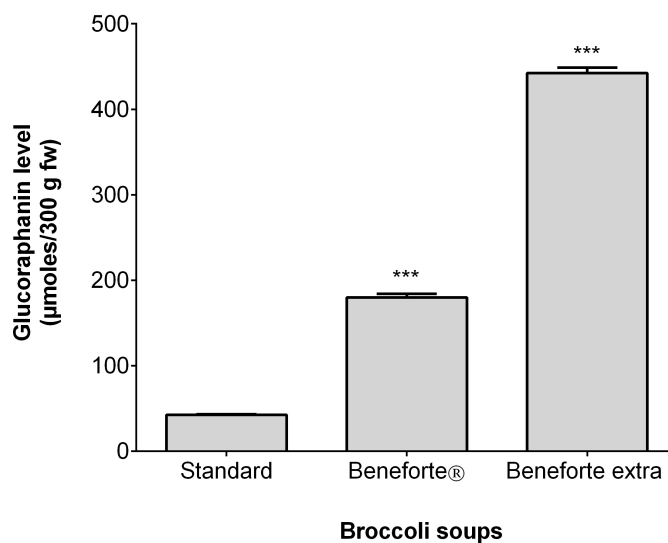


Figure 5.12 Glucoraphanin concentrations in standard (n=10), Beneforte® (n=7) and Beneforte extra (n=11) broccoli soups. Data presented as mean (SD). ***p<0.0001 vs standard broccoli soup (one-way ANOVA). Graph obtained with permission from Dr Shikha Saha (ESCAPE study protocol data).

5.5.4.2. Total sulfur, SMCSO, and sulfate levels

Sulfate, SMCSO, and total sulfur content of standard, Beneforté® and Beneforte extra broccoli soups is shown in Table 5.4. The concentration of these compounds is very similar between Beneforté® and Beneforte Extra.

Table 5.4 Sulfate, SMCSO and total sulfur concentrations expressed as (µmol/300 g fresh weight) in the ESCAPE broccoli soups

Phytochemical content	Broccoli soup		
	Standard broccoli	Beneforte® broccoli	Beneforte Extra broccoli
Sulfate	531.35 ± 24.7	444.63 ± 29.3	543.9±24.6
S-methyl-l-cysteine sulfoxide (SMCSO)	1,030.1 ±87.1	1,513.9 ±36.8	1,453.0 ±71.7
Total sulfur	4,564.8 ±162.9	6,356.4 ±102.6	6,379.2±264.3

5.5.5 Follow-up blood measurements

Blood markers were monitored at regular intervals (every 3-4 months) as part of the participants' on-going clinical follow up. PSA monitoring is part of their hospital AS programme, whereas fasting glucose and lipids were measured only for trial purposes. Data collected during the intervention were sent to participants' GPs allowing them to take action if required. Figure 5.13 shows PSA levels measured at several intervals in all three diet arms. In terms of lipid profile, no significant change was observed during the broccoli

intervention (Figure 5.14). It is important to take into consideration that 13% of the trial cohort takes cholesterol-lowering drugs (statins). Interestingly, a significant reduction in fasting glucose levels was observed with Diet B ($p < 0.001$) (Figure 5.15). A similar effect was observed in participants randomised to Diet A; however this effect was only statistically significant at 3 months ($p < 0.05$).

These findings can be interpreted once all participants have completed the intervention and the study is un-blinded.

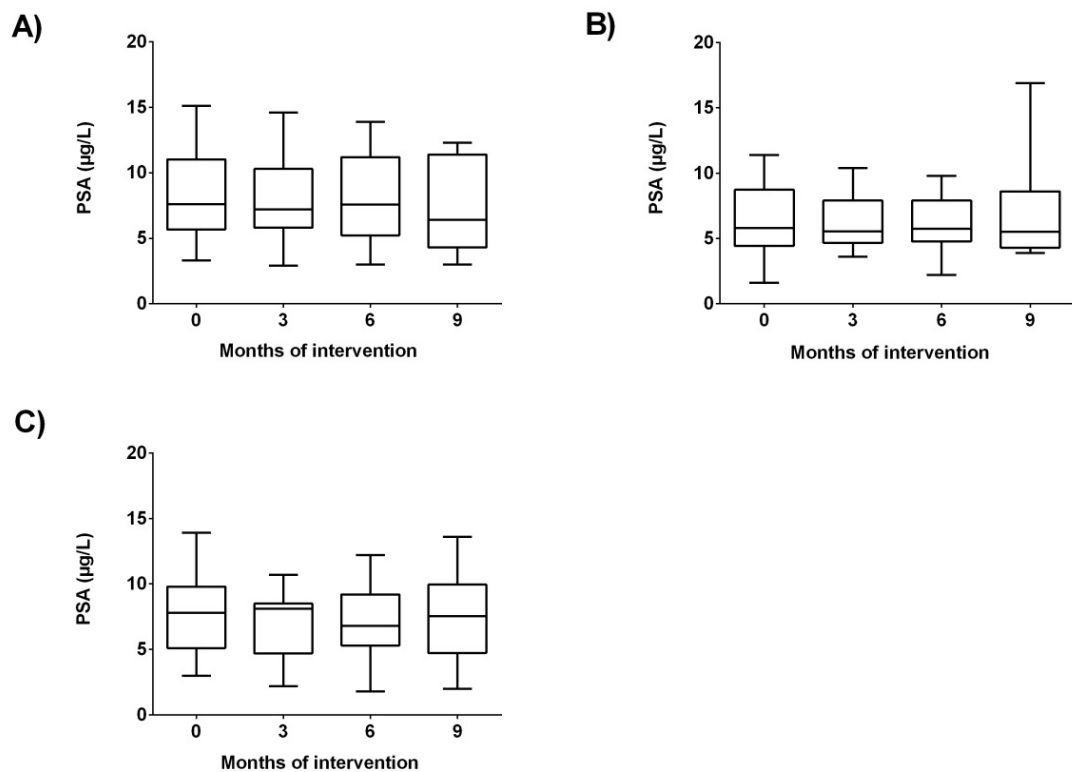


Figure 5.13 PSA levels measured at 3-month intervals during the intervention. Data obtained from participants randomised to the three study arms. Box plots represent the median of each sample with 25th and 75th percentiles. Whiskers indicate the range.: diet A (A), diet B (B) and diet C (C). p value ≥ 0.05 when comparing PSA at baseline vs 9 months in all study arms (paired t-test).

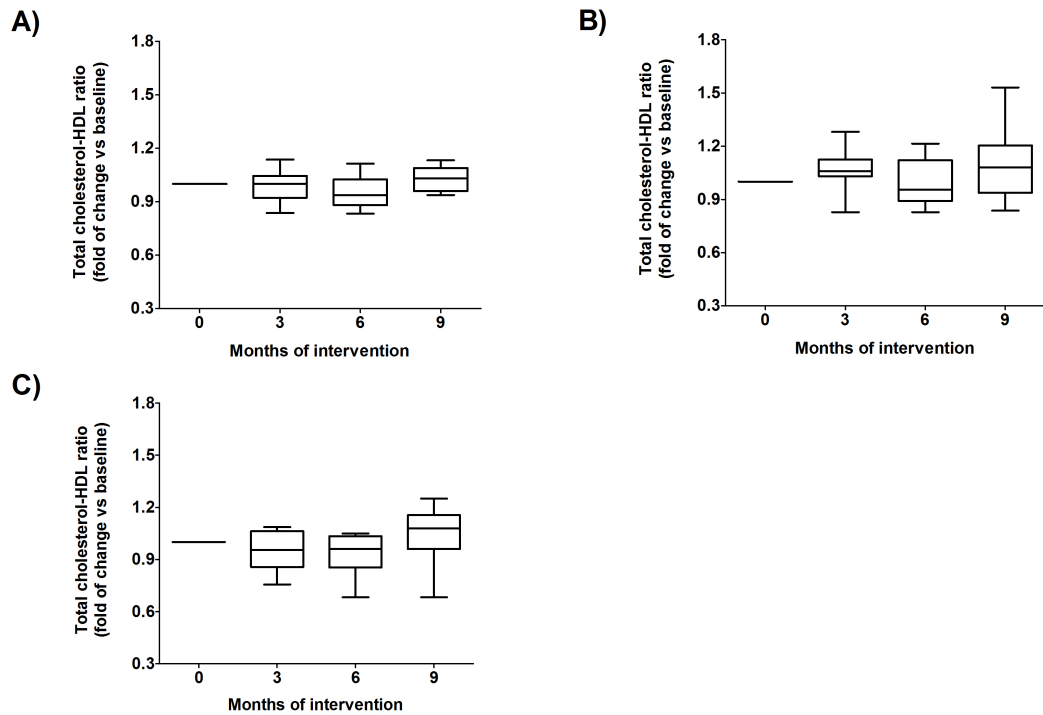


Figure 5.14 Lipid profile measured at 3-month intervals during the intervention. Box plots represent the median of each sample with 25th and 75th percentiles. Whiskers indicate the range. Data obtained from participants randomised to the three study arms: A) diet A; B) diet B; C) diet C.

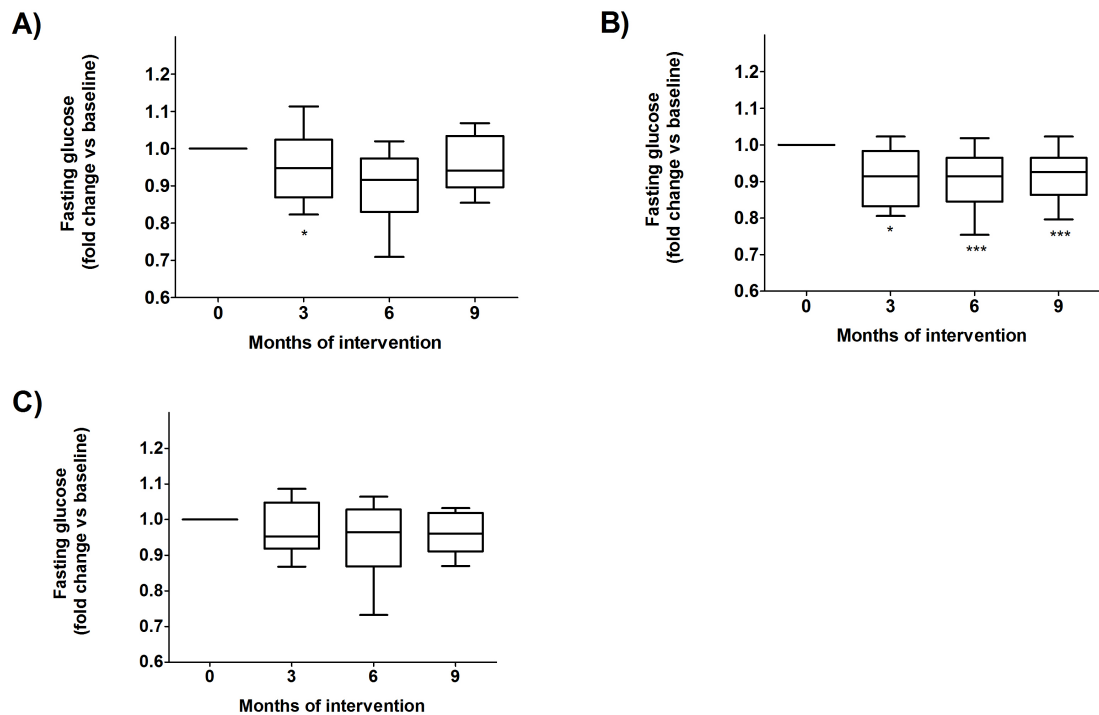


Figure 5.15 Fasting glucose levels measured at several intervals during the intervention. Box plots represent the median of each sample with 25th and 75th percentiles. Whiskers indicate the range. Data obtained from participants randomised to the three study arms. : A) diet A; B) diet B; C) diet C. * p<0.05, **p<0.01, ***p<0.001, paired *t*-test

5.6. Discussion

Increasing the consumption of fresh fruit and vegetables has been linked to a lower incidence of advanced PCa (234). Several reports from epidemiological studies indicate that cruciferous vegetables in particular might play a beneficial role in PCa prevention (94, 95, 234, 235). Currently ESCAPE is one of the few dietary trials listed on the NIHR Prostate Clinical Studies Group.

The ESCAPE study is unique because it is randomised and double-blinded, unlike many of the published reports on the role of cruciferous vegetable intake, which are largely from case-controlled studies (235-237). The use of broccoli soups as a delivery vehicle for SF has allowed for the first time, a double-blinded study to be undertaken as it is not possible to differentiate between the types of broccoli used based on colour, texture or taste. Furthermore, the comprehensive characterisation of the study soups by chromatography methods has enabled quantification of key constituents of interest such as sulfate and sulfur-containing compounds, including glucosinolates and SMSCO. The estimated intake of sulfate from a standard Western diet ranges between 0.2 to 1.5 g/day (238); cruciferous vegetables in particular have been reported to be major sources of dietary sulfate after bread (239). The results of age and anthropometric measurements as well as blood parameters at baseline demonstrate the homogeneity of the trial population. A further strength of this study is the collection of data from biological samples, as well as calorie expenditure, life style, and dietary habits, reducing the impact of these variables on the observed results.

The AS protocol which includes repeat biopsies offers great advantages for studying the effects of lifestyle interventions on PCa. Patients recruited into the ESCAPE trial undergo a biopsy procedure at the start of the trial and at the end of the intervention. The use of transperineal biopsies offers better sampling of the prostate gland by obtaining more tissue for analysis in a systematic fashion, including areas of the prostate that are difficult to access via the conventional trans-rectal route (240, 241). It will also reduce the variability of tissue sampling, improving the quality of the data. The histological data from a subgroup of men who have completed the trial is presented in Chapter 6.

When comparing PSA levels at the start of the trial and at 9 months of follow-up there was no significant change in any of the dietary arms (Figure 5.13). This may be attributed to the relatively short time of observation of 12 months to capture changes in PSA. In a study of 541 men on AS for PCa with a median follow up of 5 years, the percentage of patients experiencing any change in their PSA in the first year was 27%, compared to 95% at year

5, and only 10% had a change of $PSA \geq 1 \mu\text{g/ml}$ in the first year of follow up compared to 56% at year 5 (242). The ESCAPE study extension to > 12 months is currently capturing PSA data on men who consented to extend the study diet for a further 12 months. The longer follow up in these men may yield more informative results.

One interesting finding that emerged during follow-up was changes in fasting glucose levels. None of the participants were diabetic at the start of the study, and there was no significant difference in BMI between the study participants (Table 5.3). Additionally, all volunteers had a baseline fasting glucose, and glycated haemoglobin measurement at the start of the study (Figure 5.7). At three months, patients in study arms A and B showed significant reductions in serum fasting glucose, this persisted at 9 months in study arm B only (Figure 5.15). The exact mechanism behind this observation is not yet clear, however brassica vegetables have been previously shown to have an anti-glycaemic effect in an animal model. In a study that fed Wistar diabetic rats with an extract of *Brassica oleraceae* var *gongylodes* (Kohlrabi), the authors found a reduction in serum glucose similar to that of glibenclamide (oral hypoglycaemic drug) (243). The brassica extract fed to these rats over a course of four weeks led to a 64% reduction in fasting glucose levels that the authors attributed to a multi-factorial change in metabolism induced by the brassica diet that is likely to involve activation of AMPK pathway. More work is required to understand the exact mechanism through which the study soups in ESCAPE could have altered glucose levels, and final analysis of unblinded data will inform if a dose effect occurred.

5.7. Conclusions

The ESCAPE study is likely to offer further insights into the role of phytochemicals from diet, especially SF in PCa. The detailed analysis of the study soups together with the acquisition of extensive metabolomic, genetic, dietary and lifestyle data is the first of its kind in dietary studies on early PCa. Although, ESCAPE is not designed to assess clinical endpoints, the results from this trial may enable subsequent studies to be designed to assess whether a broccoli-rich diet could prevent the progression of PCa. In the next chapter, preliminary data from a subgroup of ESCAPE patients is presented..

Chapter 6.

Metabolomic changes
induced by a
sulforaphane- rich diet in
prostate cancer patients:
preliminary results from
the ESCAPE trial

Summary

An understanding of the molecular mechanisms by which dietary factors influence prostate carcinogenesis continues to be challenging for scientists. The combined use of techniques for studying genetic and metabolic parameters will generate a more comprehensive understanding of the role of diet in the development of PCa. The work reported in this Chapter was aimed to establish whether the experimental approach proposed in the ESCAPE protocol would be valuable to understand the effects of a SF-rich diet on prostate metabolism *in vivo*. Global biochemical profiles were determined in biopsy cores, fasting plasma and urine collected from a subset of ESCAPE patients (n=15) at baseline and at 12 months. The ESCAPE study will remain blinded until all volunteers complete the trial. Despite the limitations of the small number of participants in this subgroup analysis, the data presented here demonstrates the safety of the study diet by examining baseline and 12-month serum kidney and liver function as well as BMI and physical activity. In addition, the metabolic data have shown changes in prostate tissue metabolites that are likely to be driven by the study diet.

6.1. Introduction

Measuring the effect of a particular diet on human health is complex given the multitude of confounding factors such as individual variations in body physiology (partially linked to genetic diversity), differences in physical activity, environmental exposure and dietary habits. Furthermore it is important to take into consideration that many foods with proclaimed health benefits are a milieu of chemical compounds and minerals making it difficult to establish the role of individual constituents.

Epidemiological data stemming mostly from case-controlled studies have suggested a lower risk of PCa in men who consume cruciferous vegetables regularly (>1 portion per week) compared to less regular consumers of these vegetables (235-237, 244-246). Several studies have been conducted in order to understand the mechanism(s) behind this reported health benefit. Data obtained from *in vitro* and animal studies have related the cancer preventive efficacy of cruciferous vegetables to the ability of their degradation products ITCs to target multiple molecules or signalling pathways, and in so influencing prostate carcinogenesis (97, 220, 247-249). In particular, the ability of ITCs to ameliorate oxidative stress may represent the key factor for preventing metabolic deregulation in cancer cells (tumour development) or restoring normal metabolic function in late stages (tumour progression) (250). Despite the numerous advances achieved in our understanding of these bioactives, prospective studies in humans are still sparse.

In Chapter 5, the ESCAPE study was discussed which sets out to remove some of the ambiguity surrounding the role of glucosinolates in PCa prevention through a randomised double-blinded design. The trial involves studying the effect of SF delivered in three different concentrations through a weekly diet intervention that has been carefully selected to eliminate some of the confounding factors mentioned earlier. In addition, the study captures metabolite data from blood, prostate tissue and urine together with a wealth of genomic information. Volunteers' dietary habits and physical activity were also recorded prospectively. The ESCAPE study is still ongoing, however this Chapter deals with a subset of metabolite data from prostate tissue belonging to a cohort of volunteers (n=15) who completed 12 months of the study. The trial remains blinded therefore the three study arms are referred to as A, B and C.

6.2. Aim

- ❖ To examine preliminary data from a subgroup of ESCAPE participants focusing on changes in the metabolite profiles of prostate tissue.

6.3. Materials and Methods

6.3.1 Biological samples collection

Biological samples were collected at baseline and after the 12-month intervention from 15 patients, who have completed the ESCAPE study before April 2015. These samples were collected at the NNUH and transported to the QIB laboratory where they were appropriately processed and stored until required for analysis following study specific Standard Operating Procedures (SOPs).

6.3.1.1. Tissue samples

Prostate tissue samples were collected through a transperineal template biopsy (TPB) procedure as previously described in Chapter 5. A graphic representation of the tissue collection process is presented in Figure 6.1. TPB procedures were carried out at the NNUH by a single urological surgeon (RDM) following hospital SOPs. For metabolomic analyses, prostate needle cores (n=3) were deposited into pre-labelled vials containing room temperature extraction solvent (one biopsy per vial). Following incubation at room temperature (up to 24 hours), biopsy samples were removed from the extraction solvent and underwent histopathological assessment, allowing detailed correlation of metabolic analysis with histopathological findings. The vials containing extracted metabolites were stored at -80°C until required for metabolomic analysis (Figure 6.2).

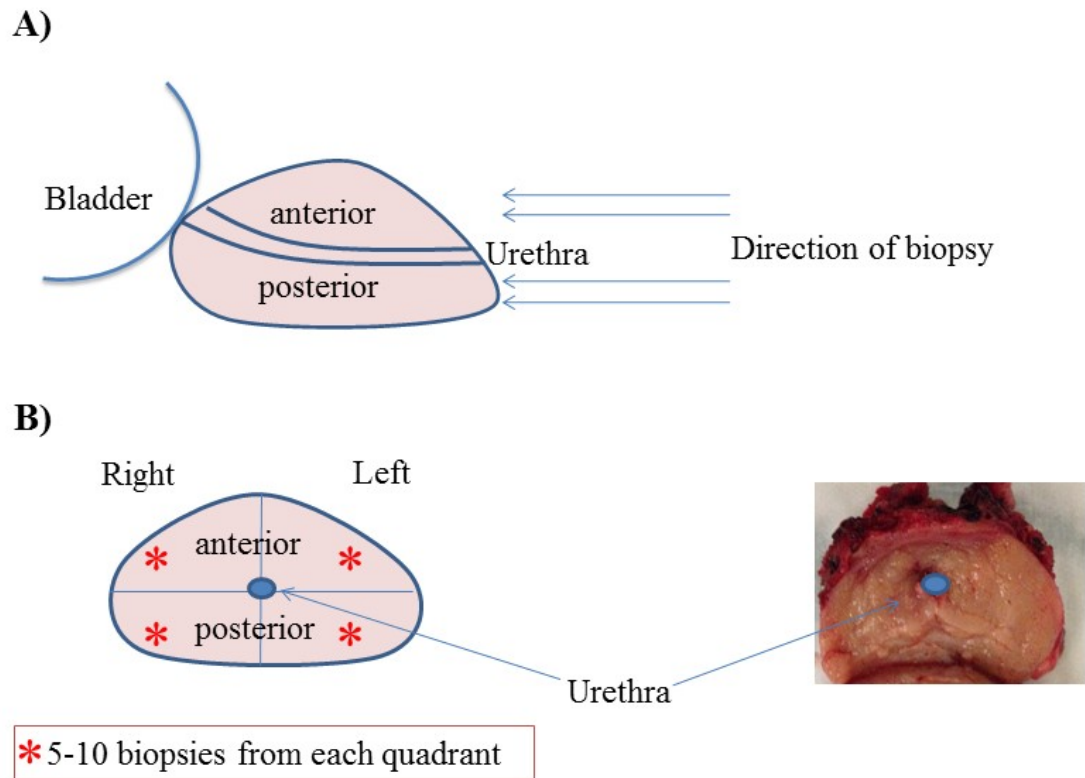


Figure 6.1 Collection of tissue samples through transperineal template (TPB) biopsy procedure as part of the ESCAPE protocol. A) Longitudinal diagram showing the anterior and posterior areas of the prostate targeted by the biopsy needle. B) Cross section diagram showing the four quadrants from which an average of 5-10 core biopsies were collected.

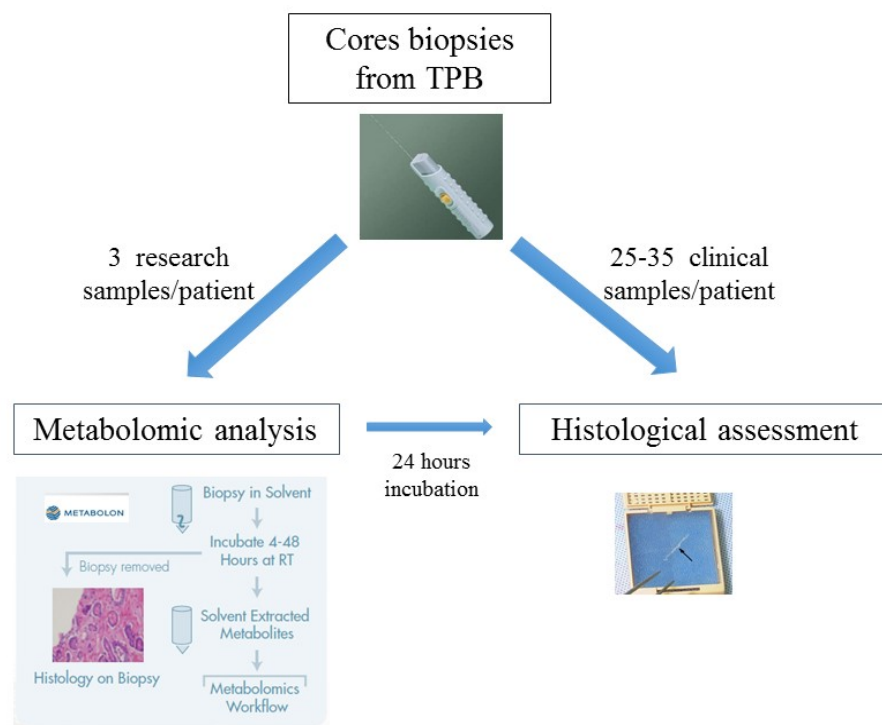


Figure 6.2 Metabolomic analysis and histopathological assessment of pre- and post-intervention tissue samples obtained from patients recruited into the ESCAPE trial.

6.3.2 Metabolite profiling

Metabolomic analysis of tissue, plasma and urine samples was carried out by an US company called Metabolon®. Briefly, the sample preparation process was performed using the automated MicroLab STAR® system from Hamilton Company. Standards were added prior to the first step in the extraction process for QC purposes. Samples were prepared using a series of organic and aqueous extractions to remove the protein fraction while allowing maximum recovery of small molecules. The resulting extract was then divided into two fractions; one for analysis by LC and one for analysis by GC. Samples were placed briefly on a TurboVap® (Zymark) to remove the organic solvent. Each sample was then frozen and dried under vacuum and thus prepared for the appropriate instrument, either LC-MS or GC-MS. Each sample was divided into five fractions: fractions 1-2 for analysis by two separate reverse phase (RP)/UPLC-MS/MS methods with positive ion mode ESI, fractions 3 for analysis by RP/UPLC-MS/MS with negative ion mode ESI, fractions 4 for analysis by HILIC/UPLC-MS/MS with negative ion mode ESI, and fractions 5 was reserved for backup. A full description of the applied metabolomic platform is presented in Chapter 4 on page 84.

6.3.3 Statistical analysis

LC and GC MS/MS data from Metabolon® were processed as described in Chapter 4 session 4.3.9 on page 87. Briefly, raw area counts from LC and GC platforms were uploaded to Metaboanalyst web platform (Metaboanalyst.ca), Minitab (version 17) and MATLAB®. Data were normalised by log transformation followed by multivariate, univariate and metabolite pathway analyses. Due to the limited sample size, two approaches to data analyses were attempted. First, the effect of being on any of the three dietary arms for 12-months was explored by grouping all participants together and comparing the metabolite profiles before and after the intervention (T0 and T12, respectively). Second, the effect of individual study diets was examined by looking at all metabolites between the three study arms at the start of the trial and at 12 months. As previously found with this type of data few values were much higher than any other and were mainly represented by xenobiotic compounds. Student's *t*-test was used for comparing means and one-way ANOVA where indicated.

Pathway analysis was undertaken using Metaboanalyst (<http://www.metaboanalyst.ca>) by comparing T0 vs T12 data obtained from all participants regardless of study arm. Biochemical names were used as identifiers on Metaboanalyst. The data were then log transformed for normalisation. Enrichment analysis was done using GlobalTest (<http://bioconductor.org/packages/release/bioc/html/globaltest.html>) which is based on

gene enrichment analysis using R (www.r-project.org) utilising Metaboanalyst's homosapien library of metabolites. Pathway topology analysis was measured using relative-betweenness centrality.

6.4. Results

6.4.1 Tolerability and compliance to study diet

A total of fifteen patients successfully completed 12 months of the study. This cohort was randomised to the three dietary arms (Diet A, n=4; Diet B, n=6; Diet C, n=5). Two main approaches were used to monitor compliance. Patients: (i) completed 7-day diet diaries and (ii) filled in record sheets on a weekly basis recording soup consumption. ESCAPE team members routinely delivered frozen soups to the participants' houses and collected record sheets and pot lids. No issues with compliance were reported.

There was no evidence of toxicity associated with any of the levels of glucoraphanin delivered by the study diet reflected in baseline and post-intervention plasma urea and electrolyte profiles as well as liver function tests (Figure 6.3 and Figure 6.4). No changes in BMI were observed in any of the three dietary arms (Figure 6.5).

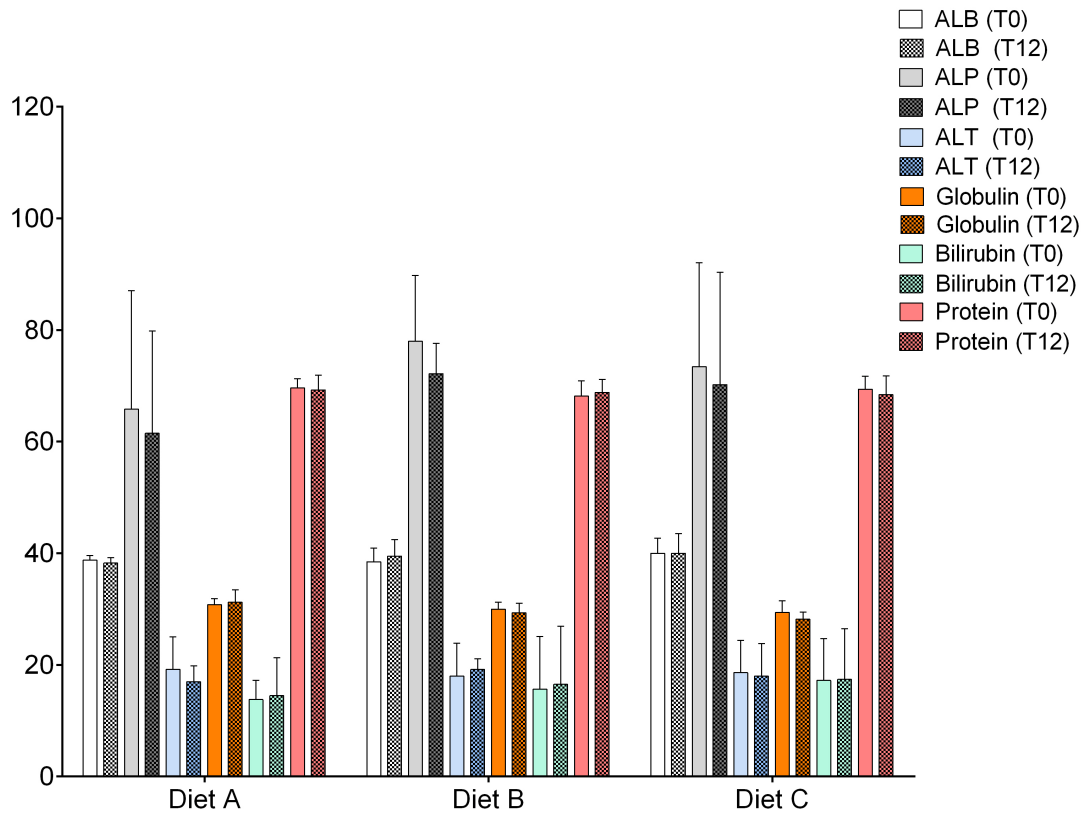


Figure 6.3 Liver function before and after the 12-months diet intervention. Albumin; albumin (g/L), ALP; alkaline phosphatase (U/L), ALT; alanine aminotransferase (U/L), Globulin; globulin (g/L), Bilirubin; total bilirubin ($\mu\text{mol/L}$), Protein; total protein (g/L). Data presented as mean (SD).

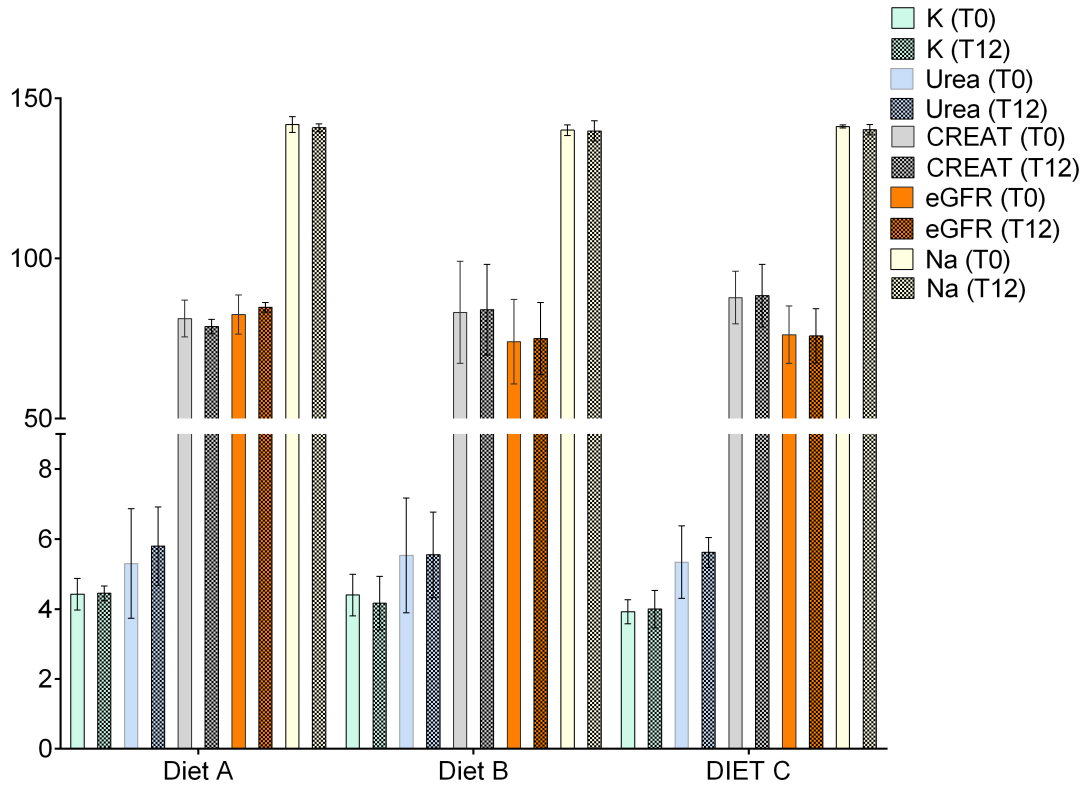


Figure 6.4 Kidney function before and after the 12-months diet intervention. K; potassium (mmol/L), Urea; urea (mmol/L), CREAT; Creatinine (mmol/L), eGFR; estimated glomerular filtration rate (ml/min/1.73m²), Na; sodium (mmol/L). Data presented as mean (SD).

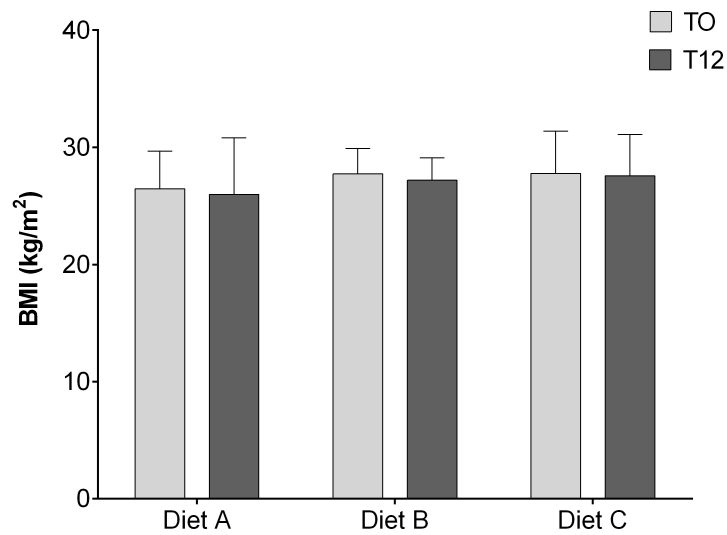


Figure 6.5 Baseline and post- intervention Body Mass Index (BMI) values. Data presented as mean (SD)..

6.4.2 ESCAPE study extension

In December 2014, a substantial amendment was approved from the NRES Research Ethics Committee (East of England- South Cambridge) to offer a further 12 months of the diet intervention once participants complete the study. At the end of the trial, patients were asked if they wish to continue the diet for a further 12 months. Those who agreed by giving written consent were asked to incorporate one pot of the study soup per week in their diet for a further 12-months. However patients were not asked to attend extra hospital visits for the purpose of the study or give additional biological samples; instead the clinical data related to their PCa follow up at the NNUH was captured.

Among the subgroup of fifteen patients discussed in this Chapter, thirteen patients gave consent for extending the diet intervention for a further 12 months. The relevant clinical information was recorded in an anonymised study database.

6.4.3 Calorie expenditure and habitual diet analysis

Participants' physical activity and habitual diet were recorded through CHAMPS questionnaires and 7-day diet diaries as described in Chapter 5. Participants' physical activity was assessed at the time of recruitment, during the intervention (6- months) and at the end of the trial. CHAMPS questionnaires were analysed as described by Stewart and colleagues taking into account anthropometric measurements at each time point (227). Due to the low sample number the average of the two time points (T6 and T12) was calculated for each of the participants. The average calorie expenditure per week, the frequency of physical activities of any intensity and specifically of moderate intensity (Metabolic Equivalent of Task, MET ≥ 3.0) were not statistically different between the study arms ($p=0.2, 0.1, 0.8$ respectively; one-way ANOVA) (Figure 6.6).

Patients completed a 7-day diet diary three times during the intervention period (baseline, 6-months and 12-months). Diet diaries were analysed by using a software package (DietPlan6) which uses UK food tables from the 7th Edition of McCance and Widdowson's The Composition of foods plus the revised Composition of Foods Integrated Data Set (251). The analysis of diet diaries has provided useful information about participants' intake of cruciferous vegetables during the intervention. Table 6.1 indicates that broccoli, cauliflower, Brussel sprouts and cabbage are the main cruciferous vegetables consumed from this cohort.

Diet analysis also revealed that the average sulfur intake was not statistically different between the three study arms (Figure 6.7).

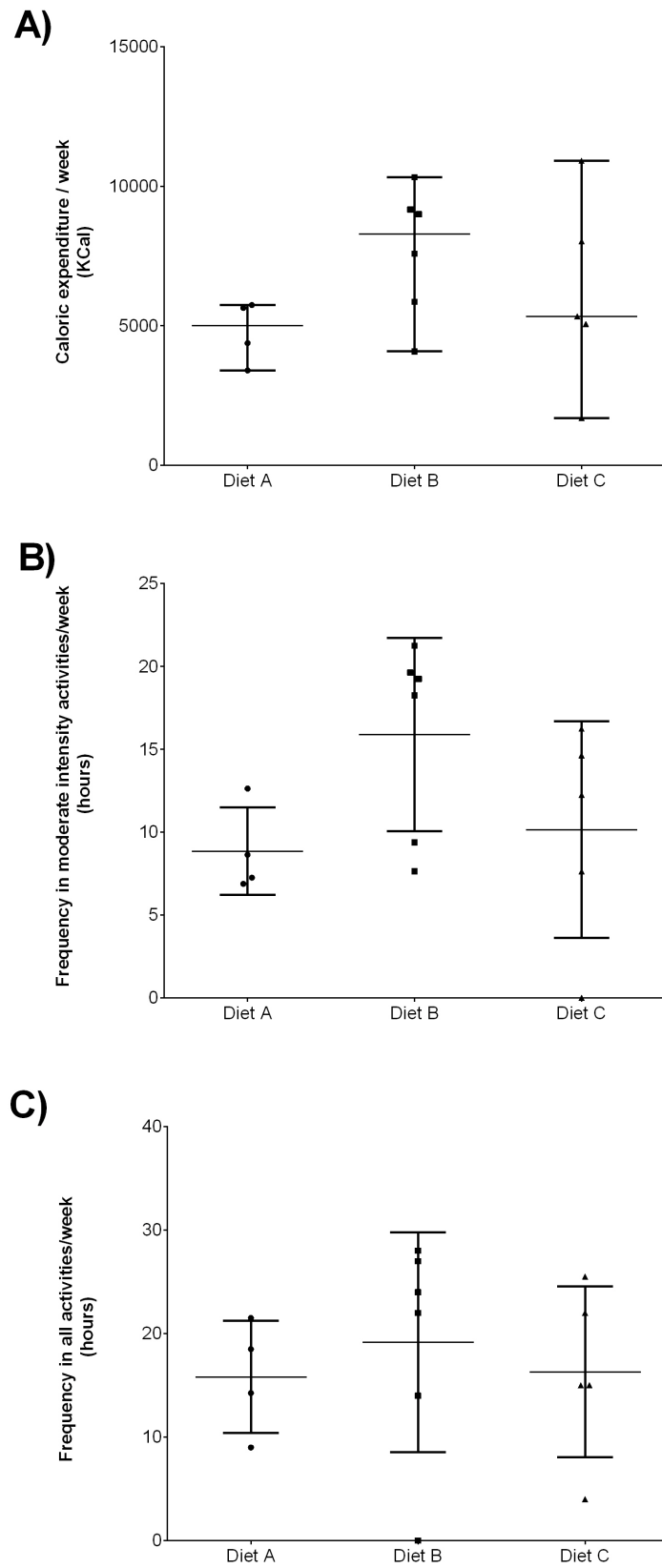


Figure 6.6 Physical activity measures derived from baseline and 12-month CHAMPS questionnaire across the three dietary arms. Data presented as mean (SD).

Table 6.1 Pattern of cruciferous vegetable intake of the ESCAPE study cohort (n=15)

Cruciferous vegetables	Total intake expressed as g/week (min-max)		
	Baseline	After 6-months	After 12-months
Broccoli	108.9 (0-527)	62.00 (0-275)	56.53 (0-220)
Cauliflower	76.64 (0-693)	73.53 (0-338)	47.33 (0-239)
Brussel sprouts	46.93 (0-260)	20.00 (0-300)	51.13 (0-361)
Cabbage	58.93 (0-240)	6.00 (0-60)	42.80 (0-355)
Mustard	0.85 (0-12)	1.833 (0-15)	2.13 (0-12)

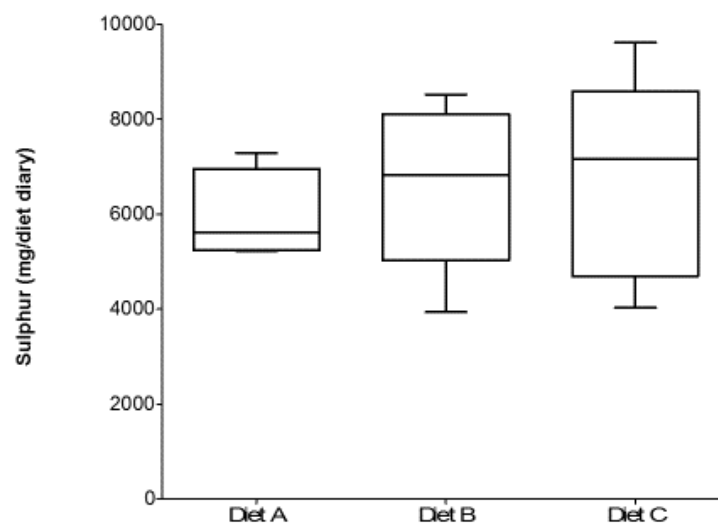


Figure 6.7 Sulfur intake calculated from 7-day diet diaries repeated three times during the trial. Box plots represent the median of each sample with 25th and 75th percentiles. Whiskers indicate the range. No statistically significant difference was observed between the three dietary arms of the study. $p=0.76$ (One-way ANOVA).

6.4.4 Histological analysis by template prostate biopsy

Recruited patients underwent TPB at the start of the study and at 12 months. The sample collection procedure was fully described in Chapter 5 at page 124. Research samples were collected separately to clinical samples and the average number of clinical biopsies taken

at the start of the study was $27 (\pm 3.6)$ and at 12 months was $26.5 (\pm 3.9)$ (p value = 0.8, paired t -test). The number of prostate cores taken at baseline and at 12 months for each dietary arm were not statistically different (one-way ANOVA with Bonferroni post-hoc test) (Figure 6.8). The number of cancer samples in each participant (percentage of cancer cores) were not affected by any of the three dietary arms (Figure 6.9). Two of four participants in study arm 'A', 2 of 6 in study arm 'B' and 1 of 5 in study arm 'C' experienced increase in Gleason score at repeat prostate biopsy at 12 months (50%, 33% and 20%, respectively) (Figure 6.10). The histological landscape of study patients at both baseline and after 12 months is shown in Figure 6.11.

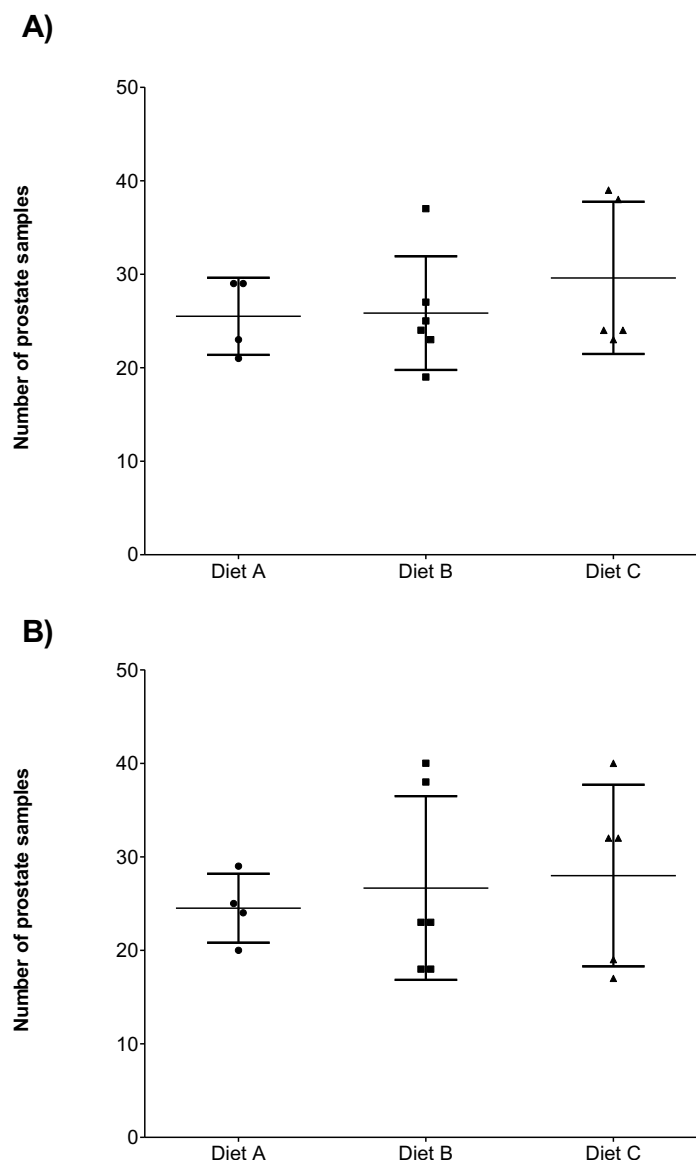


Figure 6.8 Average (\pm SD) of prostate tissue samples collected from a cohort of ESCAPE study participants ($n=15$) at baseline (A) and after 12 months of dietary intervention (B). There was no statistically significant difference in number of cores collected between study arms at both time points (One-way ANOVA).

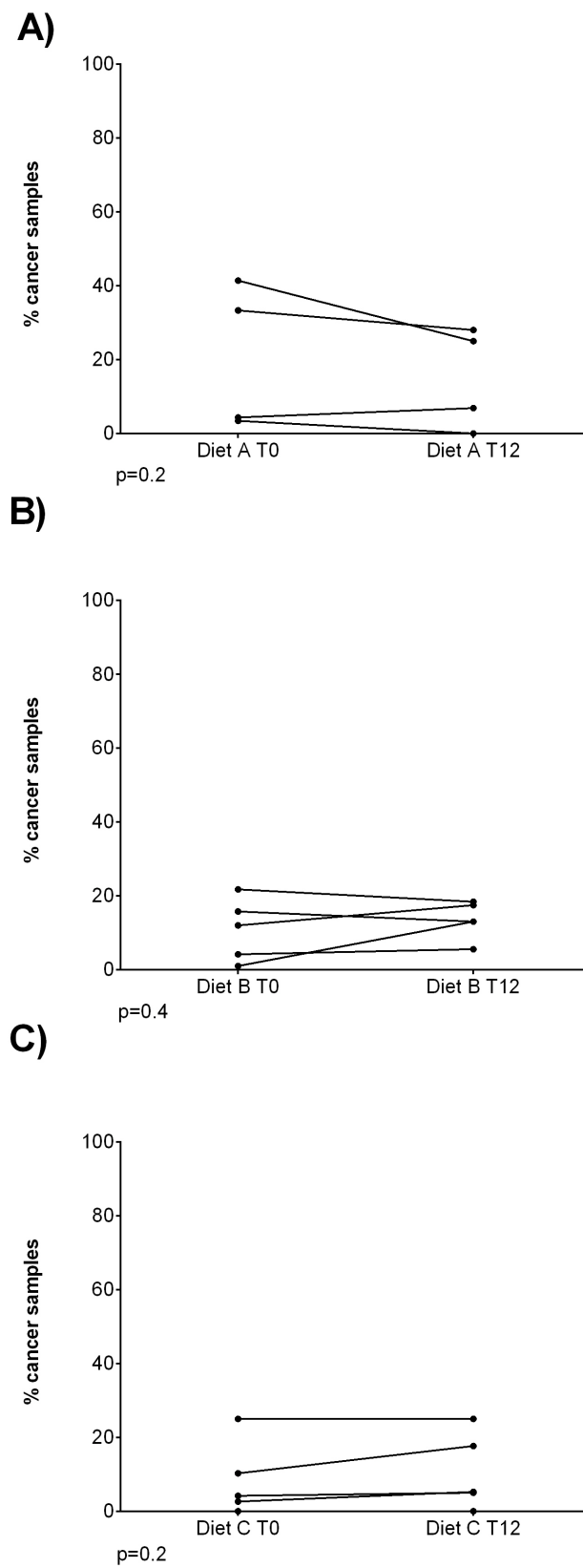


Figure 6.9 Changes in percentage of cancer samples detected on prostate biopsy. Data obtained at baseline (T0) and after 12 months of dietary intervention (T12) in each arm of the ESCAPE study (A, B and C).p value from paired student's t-test.

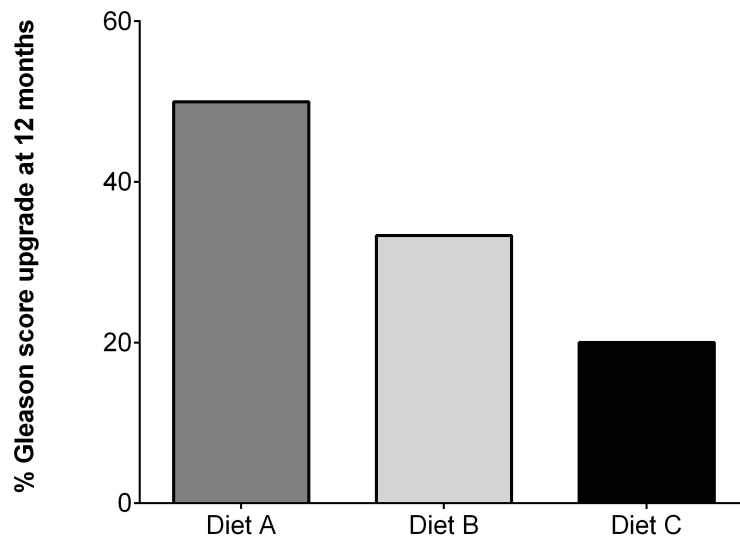


Figure 6.10 Percentage of patients who had upgraded Gleason score on repeat prostate biopsy. Data obtained from histopathological assessment of prostate core biopsies collected after 12 months of dietary intervention in each of the three study arms (Diet A, B and C).

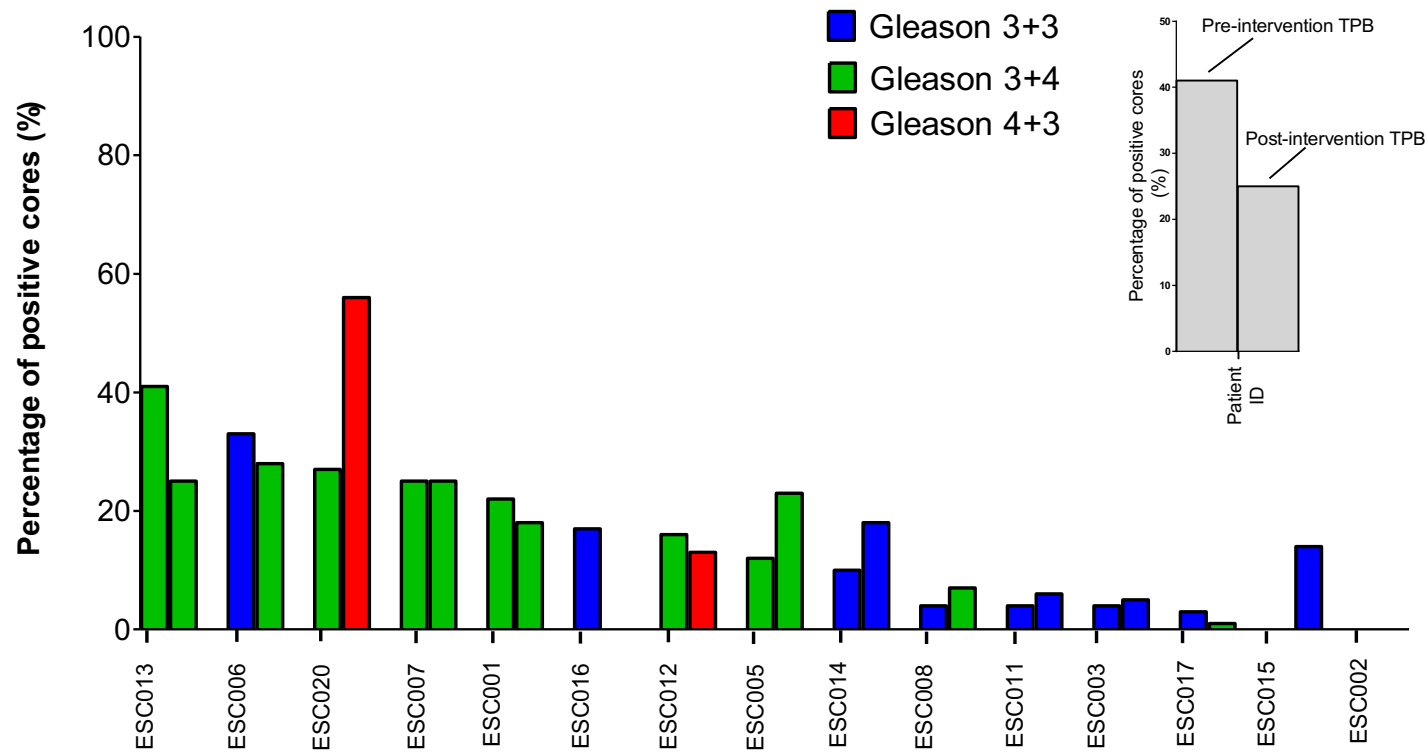


Figure 6.11 Histological assessment of prostate biopsy samples collected from a subgroup of ESCAPE study patients (n=15) at baseline and after 12 months.

6.4.5 Metabolomic analysis of prostate tissue samples from ESCAPE sub-cohort

Global biochemical profiles were determined in biopsy cores from ESCAPE patients (n=15) at baseline and at 12 months. The ESCAPE study remained blinded for the purpose of this analysis.

6.4.5.1. Multivariate analysis

6.4.5.1.1. Comparing all data between baseline and at 12 months regardless of study arm

PCA analysis was carried out on log₂ transformed data. As previously observed when analysing prostatectomy tissue in Chapter 4, drug metabolites were heterogeneous and skewed the data considerably. No separation between metabolites at T0 and T12 was observed using this method (Figure 6.12). Assigning each metabolite to a group (T0 and T12) and performing a supervised PLS-DA did not show a statistically significant difference between components on multiple testing, however it did generate a list of important compounds that were later cross-checked with univariate methods (Figure 6.12, Figure 6.13, and Figure 6.14). Multivariate testing was helpful in identifying outliers. Spermine was found to be very high in a small number of samples and subsequently excluded from the final dataset.

Levels of sulfate at 12 months feature high on VIP scores indicating that the dietary intervention had led to sulfate accumulation in all participants (Figure 6.14). An inverse trend was noted with uridine 5'-diphosphate and uridine diphosphategalactose levels of which were lower at 12 months compared to baseline (Figure 6.14).

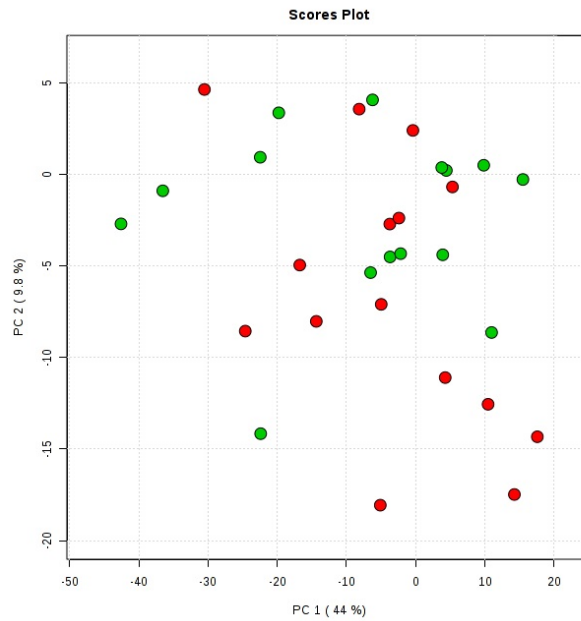


Figure 6.12 Principal component (PC) scores plots for all prostate tissue metabolite data at baseline and after 12-months dietary intervention. No clear separation between the two groups (baseline, red circles; 12-months, green circles) was demonstrated.

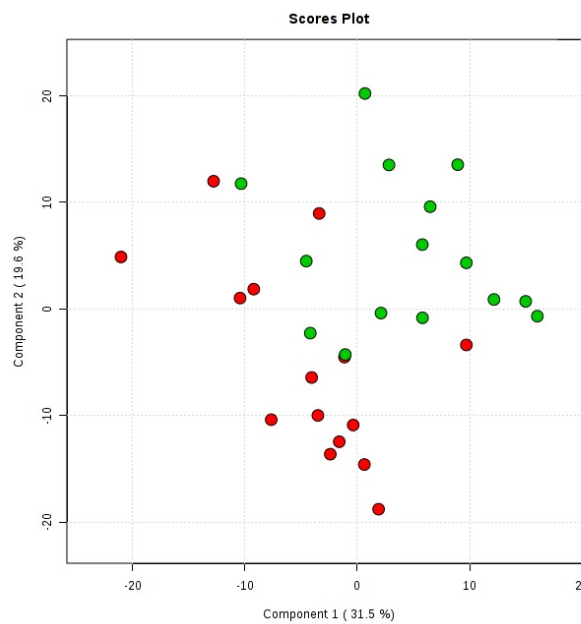


Figure 6.13 Scores plot between the selected principal components (PCs) using Partial Least Squares-Discriminate Analysis (PLS-DA). This method is supervised and assigns each feature to a pre-defined group. Baseline prostate metabolite data are shown in red circles; data at 12 months are in green circles. The explained variances are shown in brackets. Multiple testing using Leave One Out Cross Validation (LOOCV) method was not statistically significant ($p=0.8$).

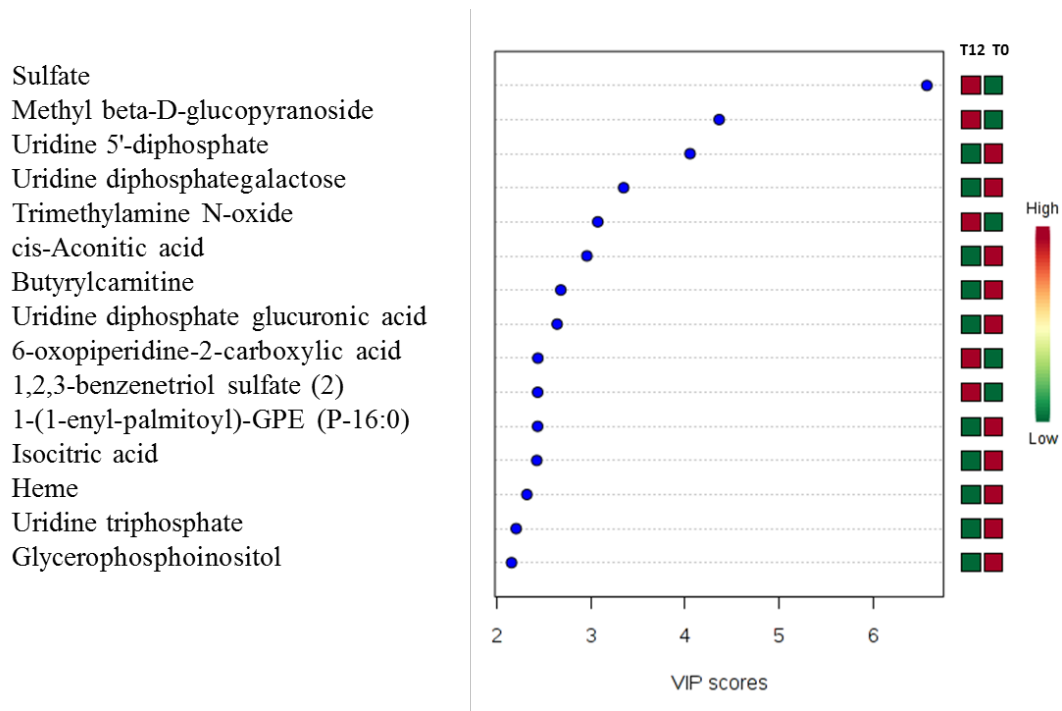


Figure 6.14 Important features identified by PLS-DA. The coloured boxes on the right indicate the relative concentrations of the corresponding metabolite in each time point. Variable Importance in Projection (VIP) is a weighted sum of squares of the PLS loadings taking into account the amount of explained Y-variation in each dimension, VIP scores ≥ 2 are considered highly significant.

6.4.5.1.2. Comparing metabolite data per study arm at baseline and at 12 months

Prostate metabolite data from each of the dietary arms were compared at baseline and then at 12 months. Using PCA, spermine was also identified as an outlier and was subsequently excluded. Once again log transformation was utilised to overcome the large variations in the data (Figure 6.15). There were notable changes in the spread of metabolites on PCA at 12 months but no clear separation between the three study arms (Figure 6.16). Further analysis with PLS-DA methods identified a list of important features, although these did not reach statistical significance on multiple testing ($p=0.1$) it highlighted contrasting levels of sulfate in the three dietary arms as well as different levels of lysolipids and unsaturated fatty acids (Figure 6.17).

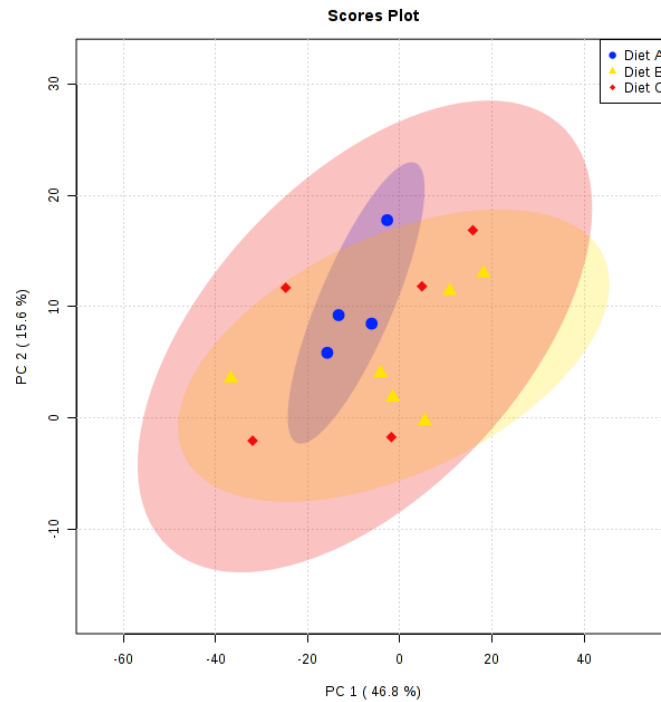


Figure 6.15 Principal component (PC) scores plots for all prostate tissue metabolite data at baseline with the three study arms. Diet A (blue), B (yellow) and C (red). Shaded areas represent 95% confidence.

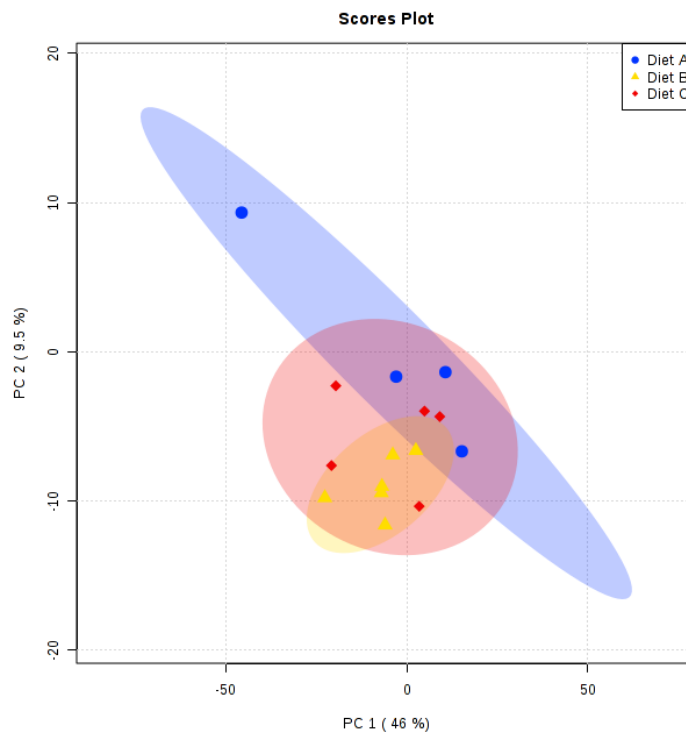


Figure 6.16 Principal component (PC) scores plots for all prostate tissue metabolite data at 12 months with the three study arms. Diet A (blue), B (yellow) and C (red). Shaded areas represent 95% confidence.

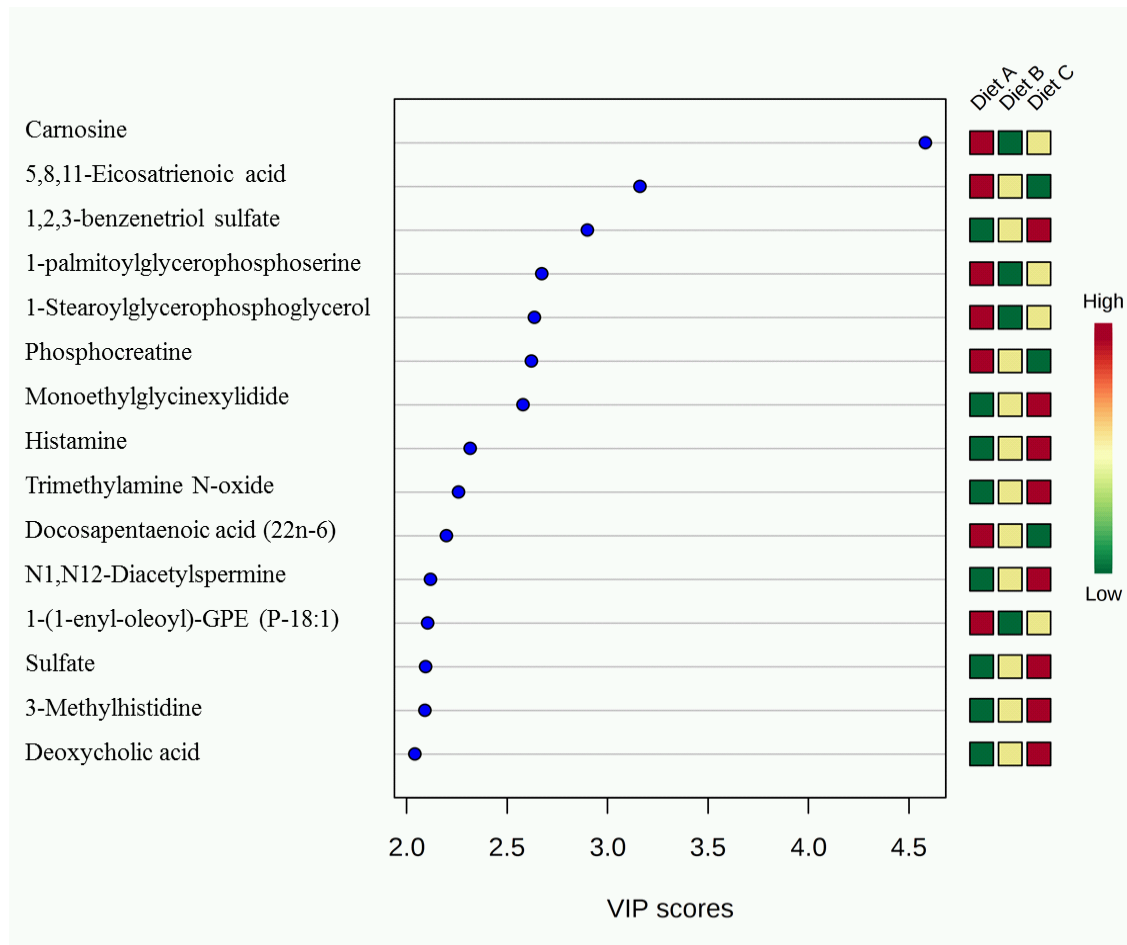


Figure 6.17 Important features identified by PLS-DA carried out on prostate tissue extracts at the end of the 12-month intervention. The coloured boxes on the right indicate the relative concentrations of the corresponding metabolite in each study arm. Variable Importance in Projection (VIP) is a weighted sum of squares of the PLS loadings taking into account the amount of explained Y-variation in each dimension. VIP scores ≥ 2 are considered highly significant.

6.4.5.2. Univariate analysis

Twenty-two metabolites were significantly different between prostate tissue at baseline and at 12-months (paired t test, $p < 0.05$) (Table 6.2). Interestingly, sulfate was significantly higher in prostate tissue at 12-months ($p = 0.0006$).

Table 6.2 List of metabolites statistically significant in prostate tissue

Biochemical	Subpathway	Trend at 12 months	p value
1-Arachidonoyl-GPE (20:4n6)	Lysolipid	Up	0.026
6-oxopiperidine-2-carboxylic acid	Lysine Metabolism	Up	0.010

Biochemical	Subpathway	Trend at 12 months	p value
Acetylcholine	Neurotransmitter	Up	0.034
Adenosine 5'-diphosphate (ADP)	Purine Metabolism, Adenine containing	Up	0.002
Adipate	Fatty Acid, Dicarboxylate	Down	0.037
Asparagine	Alanine and Aspartate Metabolism	Down	0.036
Coenzyme A	Pantothenate and CoA Metabolism	Up	0.025
Creatinine	Creatine Metabolism	Up	0.046
Cysteine-glutathione disulfide	Glutathione Metabolism	Up	0.007
Glutathione, reduced (GSH)	Glutathione Metabolism	Up	0.039
Glycerol	Glycerolipid Metabolism	Up	0.049
Guanosine 5'- diphosphate (GDP)	Purine Metabolism, Guanine containing	Down	0.038
Heme	Hemoglobin and Porphyrin Metabolism	Down	0.033
Imidazole propionate	Histidine Metabolism	Up	0.044
Methyl glucopyranoside (alpha + beta)	Food Component/Plant	Up	0.001
Phosphate	Oxidative Phosphorylation	Up	0.005
S-Adenosylmethionine (SAM)	Methionine, Cysteine, SAM and Taurine Metabolism	Up	0.021
Serotonin	Tryptophan Metabolism	Up	0.025
S-Methylglutathione	Glutathione Metabolism	Up	0.024
Spermine	Polyamine Metabolism	Up	0.024
Sulfate	Chemical	Up	0.0006
UDP-glucuronate	Nucleotide Sugar	Down	0.024
Uridine 5'-diphosphate (UDP)	Pyrimidine Metabolism, Uracil containing	Down	0.002

6.4.5.3. Pathway analysis

All data obtained from prostate tissue at baseline and 12 months regardless of study arm were uploaded to Metaboanalyst web platform. As previously experienced with *ex vivo* prostate tissue (Chapter 4), many of the biochemical compounds identified were not recognised by Metaboanalyst's library. A total of 110 compounds were not listed (28%). Despite this limitation, pathway analysis by enrichment and topology identified sulfur metabolism among the most significantly altered pathways ($p=0.0002$) which is complementary to the univariate results (Table 6.3, Figure 6.18).

Table 6.3 Results of pathway analysis from prostate tissue metabolites at baseline vs end of study

Pathway	Total	Hits	P value	FDR	Impact
Sulfur metabolism	18	3	0.000299	0.019107	0.04016
Cysteine and methionine metabolism	56	9	0.001113	0.035628	0.4023
Purine metabolism	92	16	0.008767	0.12382	0.3365
beta-Alanine metabolism	28	8	0.00895	0.12382	0.10072
Glutathione metabolism	38	10	0.009674	0.12382	0.37043
Arginine and proline metabolism	77	17	0.011724	0.12505	0.37823
Pyrimidine metabolism	60	11	0.046543	0.37347	0.27
Porphyrin and chlorophyll metabolism	104	3	0.046684	0.37347	0.05182
Fatty acid metabolism	50	4	0.060361	0.42924	0.21301
Tryptophan metabolism	79	5	0.088999	0.56959	0.20083
Methane metabolism	34	3	0.10883	0.63317	0.05444
Pantothenate and CoA biosynthesis	27	4	0.137	0.69904	0.18868
Amino sugar and nucleotide sugar metabolism	88	7	0.16254	0.69904	0.22927
Ubiquinone and other terpenoid-quinone biosynthesis	36	1	0.19302	0.69904	0.00069
Riboflavin metabolism	21	2	0.19426	0.69904	0
Pentose and glucuronate interconversions	53	6	0.20357	0.69904	0.13086
Starch and sucrose metabolism	50	4	0.2129	0.69904	0.3002
Galactose metabolism	41	6	0.22672	0.69904	0.03408
Glycerolipid metabolism	32	5	0.23748	0.69904	0.22868
Fatty acid elongation in mitochondria	27	1	0.2403	0.69904	0.26765
Valine, leucine and isoleucine degradation	40	1	0.2403	0.69904	0.04898
Terpenoid backbone biosynthesis	33	1	0.2403	0.69904	0
Glycolysis or Gluconeogenesis	31	2	0.3075	0.82735	0.04202
Valine, leucine and isoleucine biosynthesis	27	2	0.32051	0.82735	0
Glyoxylate and dicarboxylate metabolism	50	9	0.3346	0.82735	0.09086
Propanoate metabolism	35	3	0.3534	0.82735	0.05474
Citrate cycle (TCA cycle)	20	8	0.3598	0.82735	0.37232
Synthesis and degradation of ketone bodies	6	2	0.36197	0.82735	0
Inositol phosphate metabolism	39	2	0.38547	0.8507	0.13703
Glycine, serine and threonine metabolism	48	8	0.40929	0.86039	0.27259
Biotin metabolism	11	1	0.41675	0.86039	0
Thiamine metabolism	24	1	0.44432	0.8649	0
D-Arginine and D-ornithine metabolism	8	1	0.45252	0.8649	0.5
Lysine degradation	47	8	0.49665	0.8649	0.27685

Pathway	Total	Hits	P value	FDR	Impact
Taurine and hypotaurine metabolism	20	4	0.50436	0.8649	0.41188
Ascorbate and aldarate metabolism	45	8	0.51522	0.8649	0.13034
Fructose and mannose metabolism	48	2	0.51664	0.8649	0.07162
Pentose phosphate pathway	32	2	0.5263	0.8649	0.1082
Pyruvate metabolism	32	4	0.52705	0.8649	0.38933
Fatty acid biosynthesis	49	2	0.55917	0.89468	0.0218
Nicotinate and nicotinamide metabolism	44	10	0.5832	0.91036	0.08933
Phenylalanine, tyrosine and tryptophan biosynthesis	27	1	0.63808	0.96743	0
Caffeine metabolism	21	2	0.67181	0.96743	0.12066
Aminoacyl-tRNA biosynthesis	75	8	0.68089	0.96743	0.16902
Glycosylphosphatidylinositol(GPI)-anchor biosynthesis	14	1	0.72159	0.96743	0.0439
D-Glutamine and D-glutamate metabolism	11	2	0.72601	0.96743	0.02674
Lysine biosynthesis	32	6	0.75192	0.96743	0.16762
Cyanoamino acid metabolism	16	2	0.78494	0.96743	0
Glycerophospholipid metabolism	39	11	0.79012	0.96743	0.51656
Sphingolipid metabolism	25	6	0.83012	0.96743	0.53458
Primary bile acid biosynthesis	47	3	0.83204	0.96743	0.06373
Linoleic acid metabolism	15	3	0.83621	0.96743	0.65625
Phenylalanine metabolism	45	5	0.84767	0.96743	0.0315
Vitamin B6 metabolism	32	2	0.85285	0.96743	0.07958
Steroid hormone biosynthesis	99	3	0.86289	0.96743	0.01589
Ether lipid metabolism	23	2	0.86474	0.96743	0
Butanoate metabolism	40	7	0.87298	0.96743	0.14237
Nitrogen metabolism	39	5	0.87674	0.96743	0.00067
Tyrosine metabolism	76	2	0.9043	0.98094	0
Drug metabolism - cytochrome P450	86	2	0.93506	0.98956	0.02053
Histidine metabolism	44	8	0.94317	0.98956	0.12861
alpha-Linolenic acid metabolism	29	1	0.97679	0.9956	0
Alanine, aspartate and glutamate metabolism	24	8	0.99126	0.9956	0.5774
Arachidonic acid metabolism	62	2	0.9956	0.9956	0.21669
FDR, false discovery rate					

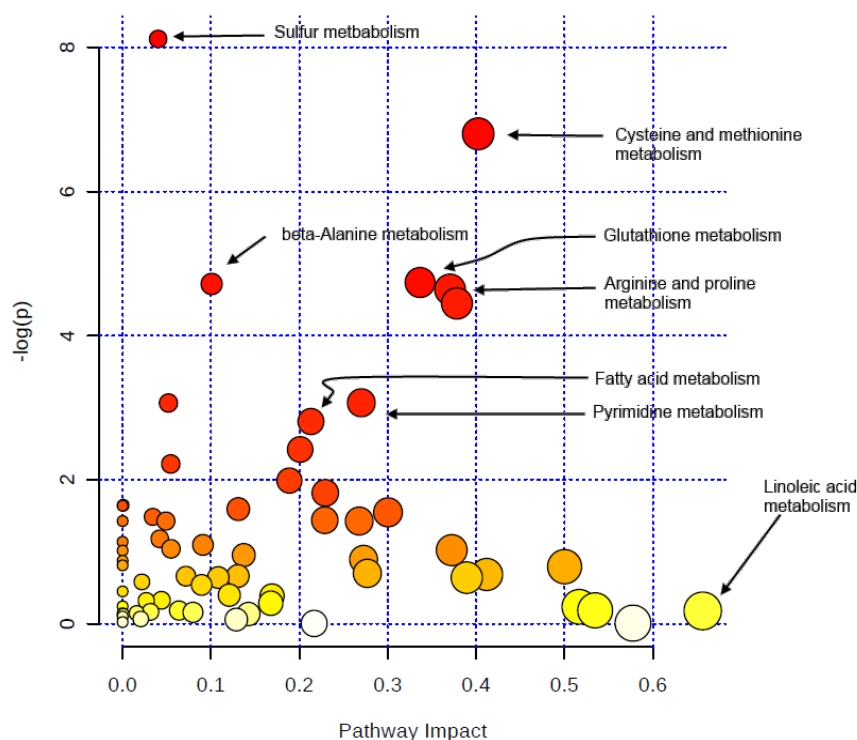


Figure 6.18 Pathway analysis of prostate metabolite data at baseline and 12 months. p value obtained from enrichment analysis is displayed as $(-)\text{natural log}$ to facilitate visualisation, therefore pathways that are most significantly altered will have higher values on the y axis. Pathway impact is shown on the x axis and is derived from metabolite topology analysis using betweenness centrality measurements therefore pathways with higher impact values indicate alterations in metabolite(s) that occupy key positions within that pathway (arbitrary units).

6.4.5.3.1. Tissue sulfate, ADP and prostate cancer

Prostate tissue sulfate was significantly higher at 12 months ($p=0.0006$) indicating accumulation in prostate tissue over the course of the trial. As previously discussed in Chapter 5, study soups were characterised in terms of sulfur containing compounds by using LC-MS analysis and a high sulfate content was reported ($8.35 \mu\text{mol/g dw}$ normal broccoli; $9.42 \mu\text{mol/g dw}$ Beneforte broccoli; $11.67 \mu\text{mol/g dw}$ Beneforte extra broccoli). Furthermore, significant diet-induced changes in nucleotides were observed with increased adenosine 5'-diphosphate (ADP) ($p=0.001$) and decreased guanosine 5'- diphosphate (GDP) ($p=0.002$) at 12-months. The pathway analysis described earlier also indicated a significant alteration in both these metabolites' pathways (sulfur and purine metabolic pathways respectively). In order to establish whether this was related to changes in PCA status in the participants, the correlation with the percentage of prostate tumour measured at 12 months was examined. Interestingly, tissue ADP and sulfate accumulation were both inversely associated with the percentage of cancerous samples found on template biopsy at 12 months (Figure 6.19 and Figure 6.20).

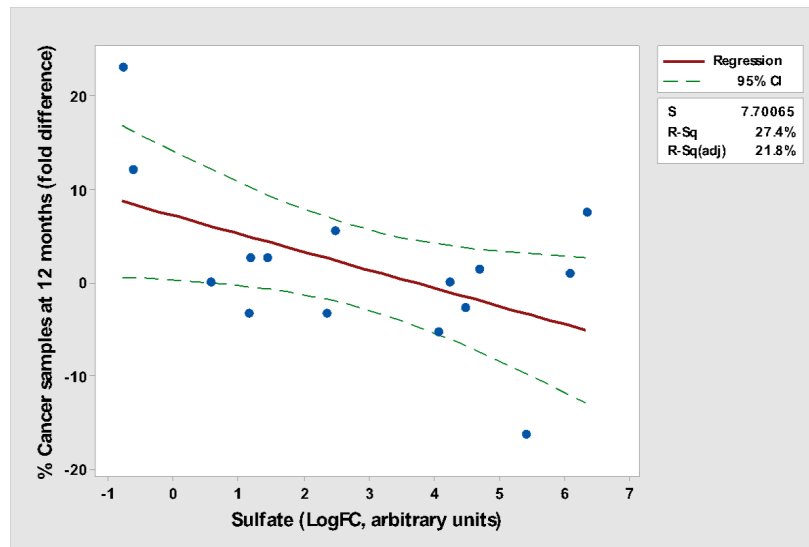


Figure 6.19 Linear regression analysis of sulfate levels in prostate tissue and the percentage of PCa samples found on repeat template prostate biopsy at 12 months post dietary intervention in a subgroup of ESCAPE study volunteers (n=15) (p=0.04).

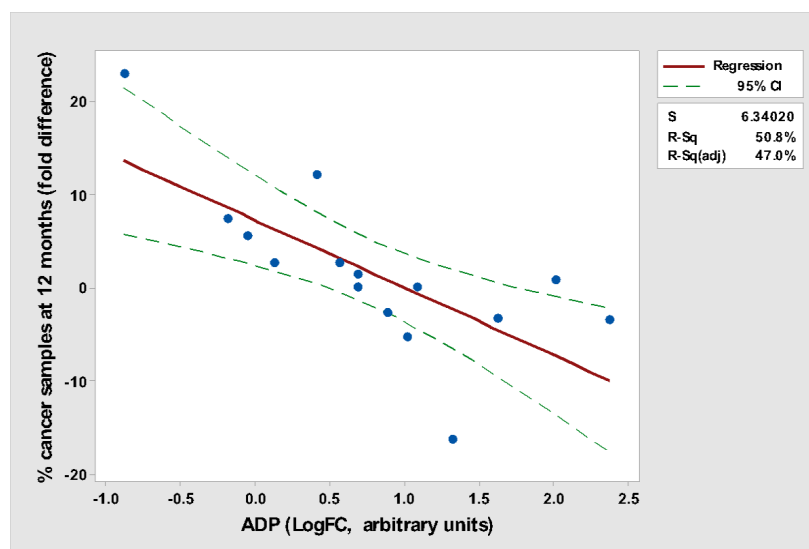


Figure 6.20 Linear regression analysis of adenosine diphosphate (ADP) levels in prostate tissue and the percentage of PCa samples found on repeat template prostate biopsy at 12 months post dietary intervention in a subgroup of ESCAPE study volunteers (n=15) (p=0.003).

6.4.5.3.2. *Glutathione metabolites*

Tissue metabolite profiling indicated a change in glutathione metabolism with a significant increase of reduced glutathione (GSH) (p=0.03), S-methylglutathione (p=0.02) and cysteine-glutathione disulfide (p=0.006). This corresponds to significant change in the glutathione metabolism pathway (p=0.009) (Table 6.2 and Table 6.3). GSH was inversely correlated with the amount of PCa found on repeat biopsy but this trend did not reach statistical significance (p=0.1) (Figure 6.21).

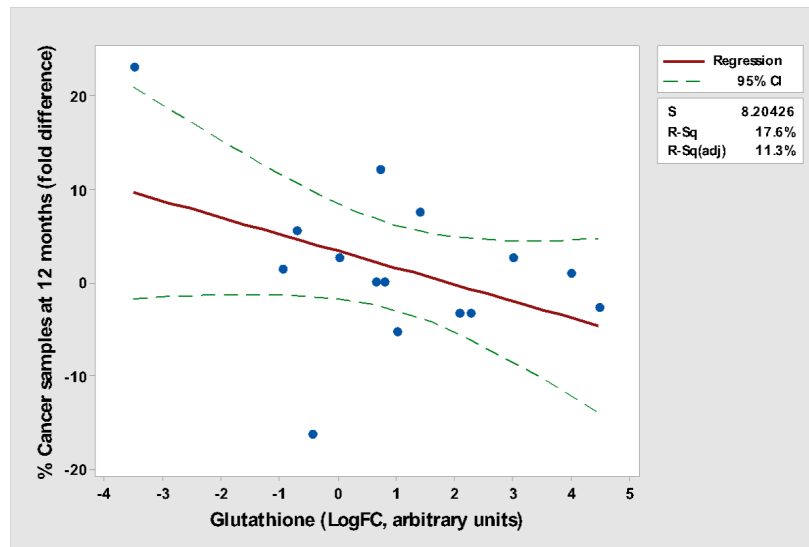


Figure 6.21 Linear regression analysis of glutathione levels in prostate tissue and the percentage of PCa samples found on repeat template prostate biopsy at 12 months post dietary intervention in a subgroup of ESCAPE study volunteers (n=15) (p=0.1).

6.4.5.3.3. *Uridine-related metabolites*

Levels of uridine diphosphate (UDP) and UDP glucouronic acid were both lower after 12 months of the study (Table 6.2). Both UDP and UDP glucouronic acid are utilised in the *N*-glycosylation reactions to produce glycosaminoglycans and glycolipids as part of the hexoseamin biosynthesis pathway (252). Higher levels of these metabolites have been found in several human cancers including the prostate (252). Although study participants showed lower levels of UDP related metabolites on both multivariate and univariate analyses, neither were significantly correlated to the amount of cancer cores found on repeat prostate biopsy at the end of the study period (Figure 6.22).

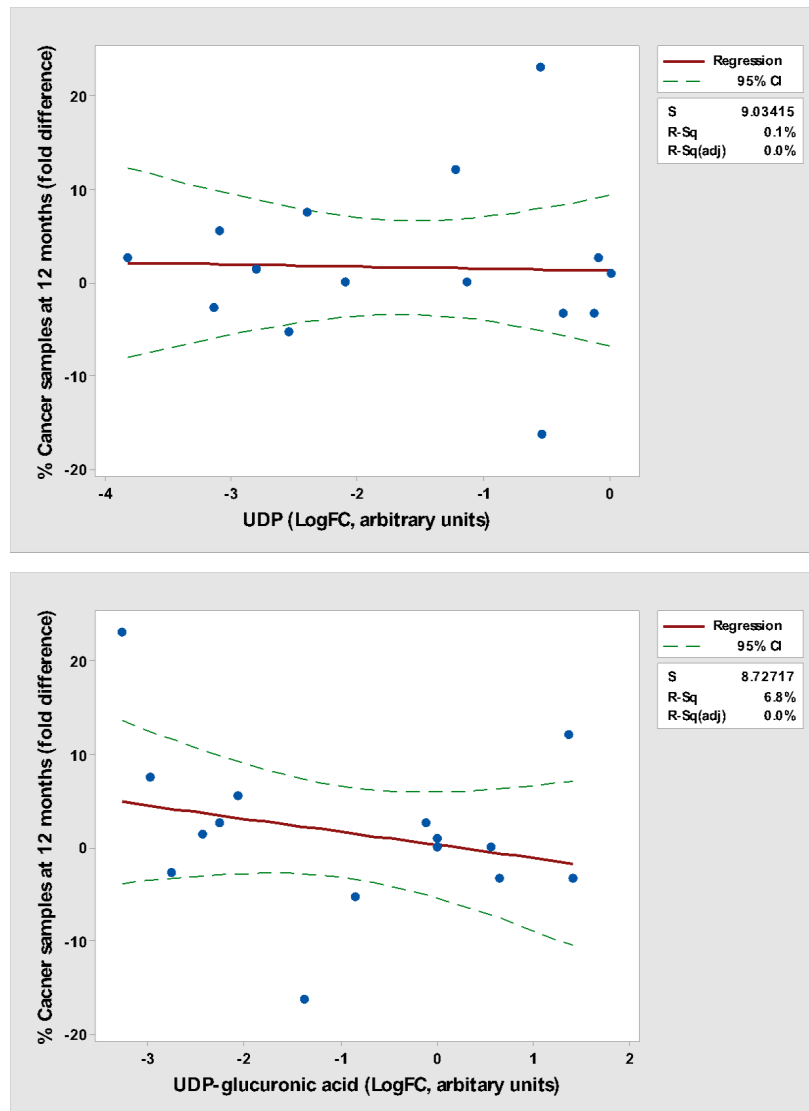


Figure 6.22 Linear regression analysis of Uridine diphosphate (UDP) (top graph) and UDP glucuronic acid (bottom graph) in prostate tissue and the percentage of Pca samples found on repeat template prostate biopsy at 12 months post dietary intervention in a subgroup of ESCAPE study volunteers (n=15) ($p > 0.05$).

6.5. Discussion

The ESCAPE study has now completed recruitment and sample analyses are currently in progress. For the purposes of the analysis presented in this chapter the study remained blinded. Trial arms were referred to as Diet A, B and C reflecting different levels of glucoraphanin content as previously described in Chapter 5 on page 134 (Figure 5.12). Despite the limitation of study blinding, the analysis of this subgroup of men has provided insights into the effects of the trial intervention and was important for method testing given the length of time between the start of the study and the predicted date for final sample analysis.

The subgroup of men (n=15) appeared homogenous with regards to baseline biochemical blood markers as well as BMI and physical activity levels. There were no reported toxicities with the study diet throughout the follow up period as indicated by normal liver and renal function and no significant changes in BMI. One notable difference was the change in consumption of cruciferous vegetables (Table 6.1). This is likely to be seasonal variation however, an observer effect which has been noted in other studies whereby participants alter their habits or behaviours as a result of awareness of being studied or observed could also be responsible for the difference (253).

Physical activity levels measured by calorie expenditure and type of activity were comparable between the study arms throughout the observed period (Figure 6.6). Although the number of participants was small in this subgroup and therefore limiting the statistical power, it was important to account for the effect of exercise on the observed results. Several studies have shown improved overall survival and PCa specific survival in men diagnosed with PCa who engage in regular physical activity such as brisk walking (speed ≥ 3 mph 3 times per week), cycling 20 minutes per day or exercising ≥ 1 hour per week (95, 254, 255). The ESCAPE study protocol did not include an exercise component but whether participating in a research study will change their activity levels as part of adopting a healthier lifestyle remains to be determined.

The AS cohort in the ESCAPE study is unique for a number of reasons; first, men were required to undergo a transperineal TPB biopsy at the beginning of the trial and a further biopsy at 12 months providing detailed histological data as well as clinical and biochemical follow up every 3 months. Second, the men who took part in the study reflect the true population of AS in the studied region (Norfolk) because in contrast to many institutions that restrict AS to men with low- or very low-risk PCa, the NNUH AS cohort also includes men with intermediate-risk PCa who are appropriately counselled regarding the risk of continued AS but still decline radical treatment.

Many healthcare regulators including NICE recommend annual prostate biopsies on men who choose AS but there is no guidance on the best type of biopsy procedure (222). TPB procedures offer several advantages over routine TRUS guided 12-core biopsies including better sampling of anterior parts of the prostate gland that could harbour high-grade disease and better mapping of tumour sites within the prostate (240, 241, 256). However despite these advantages, there is insufficient evidence in the literature regarding the continued use of TPBs to monitor PCa in men who choose AS. The ESCAPE trial to date has shown that repeat TPB is feasible and men choose it over TRUS guided biopsies when given the choice. With the limitation of the low number of participants it would appear that the

number of patients experiencing upgrade of PCa during surveillance is similar to published literature (257) Thirty- three percent of patients in the subgroup of ESCAPE presented in this Chapter had increased Gleason score on repeat biopsy (Figure 6.10). Cooperberg et al reported similar upgrade rates in men who were part of the University of California San Francisco (UCSF) AS programme (35% upgrade for low risk PCa and 30% for intermediate risk during 4 years of follow up, using UCSF Cancer of the Prostate Risk Assessment score which is very similar to D'amico risk groups) (257).

6.5.1 Changes in prostate tissue metabolites

The metabolite analysis indicated a significant alteration in several metabolic pathways especially sulfate, cysteine and glutathione regardless of study arm (Table 6.2, Figure 6.18). Sulfate levels measured from prostate tissue at baseline and then after 12 months of the study diet were significantly different (all three study arms grouped together). Sulfate content in food varies considerably with some vegetables being naturally rich in sulfate such as cruciferous vegetables, other sources are red meat, bread and food additives (238). Data on total sulfur intake from the ESCAPE volunteers was calculated from diet diaries (excluding the sulfur content of the study soup). Interestingly this did not show a significant difference between the three trial arms (Figure 6.7), therefore it would support the idea of higher sulfate levels in tissue as a direct result of the study soups. In the previous Chapter, the quantification of sulfate and SMCSO from the three types of study soups indicated a positive correlation between the level of glucoraphanin and these two compounds (Figure 5.12, Table 5.4). These findings are in keeping with those of Florin et al who measured sulfate content from several types of foods including brassica vegetables. Florin and colleagues found a positive linear correlation between glucosinolates content of brassicas and sulfate (239). The mechanism behind this accumulation needs further examination however, two main routes are likely, one of which is direct delivery of sulfate and sulfur-compounds through the serum, the other being urinary reflux into the prostate. A study looking at the bioavailability of such compounds in the sera of healthy volunteers after ingesting broccoli soup has detected several compounds that could act as sulfate donors in under two hours after consumption (unpublished data from BOBS study, ethics REC reference 14/EE/1121; ClinicalTrials.gov Identifier NCT02300324). A further study by Waring et al showed that radiolabelled sulfur in SMCSO was almost completely recoverable in healthy male volunteers up to 14 days from ingestion and that inorganic sulfate constituted a large proportion of sulfur containing molecules (258). This strengthens the argument that reflux of sulfur metabolites from urine into the prostate is a more likely route. Urinary reflux into the prostate has been previously put forward as a cause for non-

bacterial prostatitis. Kirby and colleagues showed that upon micturition almost 70% of men showed urine reflux into the prostate gland (259). In addition, the preliminary results of urinary metabolite profiling from ESCAPE participants indicated higher levels of sulforaphane-N-acetyl cysteine as well as a number of sulfate-containing compounds at 12 months in all participants compared to baseline that would support a theory of retrograde reflux of metabolites into the prostate (data not presented in this thesis). Regardless of the mechanism, sulfate accumulation in prostate tissue seems to inversely correlate with the amount of PCa found on repeat biopsy (Figure 6.19). This trend of sulfate accumulation is also mirrored by increased levels of ADP in prostate biopsy tissue (Figure 6.20). ADP to ATP interconversion is crucial to energy homeostasis through the transfer of hydrogen-phosphate ions (HPO_4^{2-}) (260). Therefore ADP and phosphate accumulation in prostate tissue may signify ATP shortage this coupled with the finding of low UDP-glucuronate may suggest increased phase 2 detoxification reactions through both increased sulfate and glucuronide conjugation (261). Sulfation (sulfate conjugation) requires the incorporation of sulfate with ATP to form adenosine phosphosulfate (APS) releasing phosphate, the resulting APS is then used to synthesise 3'-phosphoadenosine 5'-phosphosulfate (PAPS) consuming further molecules of ATP (262). Thus the high level of sulfate may enhance these reactions and ultimately starve cells from ATP limiting cancer growth (263). Furthermore, ATP is also utilised in glucuronide conjugation whereby UDP-glucuronate is used as a substrate, low levels of the latter may indicate upregulation of this reaction which would further deplete ATP stores.

6.6. Conclusion

The findings presented in this Chapter indicate a significant alteration in several metabolic pathways in prostate tissue with strong evidence to support a shift in sulfate mediated reactions that are likely to be induced by the dietary intervention with broccoli soups. The inverse correlation between sulfate accumulation in tissue and the percentage of PCa on final biopsy after 12 months may be related to ATP depletion with consequent accumulation of ADP and phosphate. This hypothesis is also supported by the observed decrease in UDP-glucuronate which also depletes ATP stores. Together these findings warrant further investigation into whether sulfate accumulation does indeed originate from a broccoli rich diet and if this leads to elimination of cancerous clones. This research question can be addressed by undertaking further human intervention trials specifically designed to investigate this hypothesis.

Chapter 7.

General Discussion

7.1. General discussion

PCa is a public health problem that claims the lives of over 10,000 men a year in the UK alone (2). Projections for cancer incidence in the UK indicate that PCa will represent 26% of all male cancers by 2030 (264). This, together with an ageing population, will no doubt place a significant burden on our already strained health system and affect the lives of many men.

The aetiology of PCa remains unknown, however, epidemiological and autopsy studies have identified that environmental factors and diet patterns play an important role in developing the disease with a long latent period (265-268). When examining modifiable environmental factors two main themes emerge as potential targets; first, dietary modification, and second, modifying physical activity levels; both of these areas have attracted extensive studies over the last 3 decades (94, 219, 269).

The effect of the dietary bioactive SF, which is derived from *Brassica* plants, on human health has been explored in cell, animal and human models of chronic diseases, including PCa (270). The mechanism behind the protective effect of healthy eating and physical activity against the development of PCa is likely to be multifactorial; however several authors agree that induction of phase II enzymes, and reduction of oxidative stress are key factors (103).

The experimental work presented in this thesis aimed to understand whether SF could affect the metabolism of the prostate in a way that would (i) reduce the transformation of normal cells to cancerous cells, and (ii) modify the environment in which existing cancerous cells would proliferate in order to retard the progression of the disease. A multidisciplinary approach was undertaken to investigate the role of SF on human prostate metabolism by using:

- *in vitro* models of human PCa;
- an *ex vivo* model based on the use of human tissue obtained from prostatectomy specimens;
- un-targeted metabolomic platforms for the analysis of prostate tissue collected from men with localised PCa recruited into an intervention trial.

It was envisaged that the interpretation of data obtained by applying this multidisciplinary approach would better inform on the effect of SF on the metabolism of the human prostate,

and furthermore, elucidate potential mechanisms of action by which SF intake could represent a successful cancer preventive strategy.

7.2. The limited translational value of experimental evidences obtained from *in vitro* models of prostate cancer

The effect of SF on cellular metabolism was investigated by using normal (PNT1A, RWPE-1), cancerous androgen-sensitive (LnCap), and androgen-independent (PC3, DU145) cell lines. These cell lines are commonly used for studying human prostate biology, and their genotypic and phenotypic features have been extensively characterised (271). RWPE-1 cells are less commonly used compared to the other prostate cell lines; however this cell line represents an alternative model to study the normal prostate epithelium (153).

Prostate cells are characterised by a different TCA cycle function compared to other mammalian cells. A long history of clinical and fundamental research has demonstrated the importance of studying the TCA cycle activity for developing new strategies against prostate carcinogenesis (159). A novel analytical method based on LC-MS/MS, which allows the simultaneous measurement of TCA cycle intermediates, even at low concentrations, from a variety of biological matrices including cultured prostate cells, was successfully established (Chapter 2). The application of this newly developed method has enabled (i) a full characterization of the chosen cell models in terms of their baseline levels of TCA cycle intermediates, and (ii) to explore the effects of exogenous compounds such as a ROS-inducer agent and dietary bioactives (SF), on TCA cycle function (Chapter 3). To our knowledge, there are no previous reports indicating the different levels of TCA intermediates in commonly used prostate cells, and how SF could affect their production by changing cellular redox status.

Interesting findings were obtained by measuring the concentration of citrate, and other TCA cycle intermediate compounds, from a variety of benign as well as cancerous prostate cell models using LC-MS/MS. Surprisingly, cancerous PC3 cells, which are regarded as highly aggressive, displayed the highest amounts of citrate amongst the cell lines tested. This is the opposite of what is reported in tissue, where it has been shown that citrate is persistently lower in PCa compared to benign prostate tissue (41, 114, 161). The high citrate content of PC3 cells compared to benign PNT1A cells was investigated by first unifying the culture growth medium (eliminating small traces of Zinc and pyruvate that were present in PC3 media) and measuring the activity of a key citrate regulating enzyme

(aconitase). The results demonstrated a persistent pattern of higher citrate content in PC3 cells compared to PNT1A. Moreover, the activity of the aconitase enzyme was more pronounced in PC3 cells. It is widely accepted that PC3 cells exist in high ROS environments (179), and previous cell and animal studies have shown that TCA cycle enzymes are inhibited by ROS (58, 59). Therefore, it was postulated that intracellular ROS were behind the observed high citrate level, due to the inactivation of aconitase *in vitro*. This was shown by challenging the cells with exogenous ROS in culture, which led to a statistically higher level of citrate. The addition of physiological levels of SF to cultured prostate cells prior to a hydrogen peroxide challenge protected PC3 cells against the dramatic increase in citrate observed in controls; these results indicated a protective effect of SF against oxidative stress-induced changes on the TCA cycle function. There is evidence that TCA cycle function is dramatically compromised by endogenous and exogenous compounds able to influence cellular oxidative status (58, 146, 180). Several chronic diseases have been associated with alteration of the TCA cycle function due to increased levels of ROS, mainly in diseases associated with neurodegeneration (182). The protective effect of SF, at physiologically achievable concentrations, in preventing H₂O₂-induced increase in citrate in prostate cells could suggest a potential mechanism by which SF may restore an ineffective TCA cycle function in pathological conditions; however, there is a strong need of further investigations in *in vivo* models.

These findings could also suggest a potential mechanism of action by which SF could prevent cancer cell proliferation *in vitro*. The higher citrate levels measured in cancer PC3 cells in response to oxidative stress may facilitate cell growth through the utilization of citrate as a substrate for the biosynthesis of cholesterol and steroids, which are known to drive proliferation (202, 272). A previous study carried out by Mycielska and colleagues has demonstrated a pro-metastatic effect of citrate in PC3 cells as a result of its increased metabolism by two enzymes (ACNTs and FAS) which are found to be up-regulated in PCa cells (Figure 7.1) (122). They reported an increased uptake of citrate from the PC3 extracellular space, which led to a reduction in cell adhesion, and enhanced cell motility, exacerbating their metastatic phenotype. Neither of these citrate-induced effects was observed in normal PNT1A cells under the same experimental conditions (122). It is important to stress that this study found higher levels of endogenous citrate in normal PNT1A cells, compared to PC3 cells, which have not been observed in our experimental conditions. However, Mycielska and colleagues have measured citrate concentrations by using spectrophotometric techniques that are considerably less specific, accurate, and sensitive, compared to the LC-MS/MS method developed for the purpose of this study.

Taking into consideration the pro-metastatic action of citrate in cultured PCa cells, future studies to determine whether SF could prevent the pro-metastatic effects of citrate *in vitro* are required.

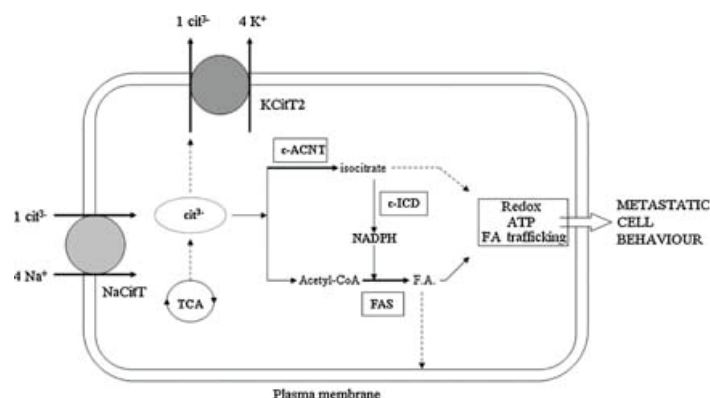


Figure 7.1 A model of citrate-enhanced metastatic cell behaviour described by Mycielska and colleagues (135).

In conclusion, based on the clinical relevance of reduced citrate levels found in prostatic fluids and tissue of cancer patients (273), these data mainly suggest that cultured PC3 cells, which are a model for aggressive PCa, do not share the same metabolic phenotype of cancer *in vivo*. Thus, a better understanding of their usefulness and limitations regarding the study of prostate metabolism is needed. These data also suggest a mechanism by which SF could influence the redox status in the prostate, and subsequently alter the metabolic environment through changes in the TCA cycle. How this translates in tissue, and indeed *in vivo*, has not been explored to date.

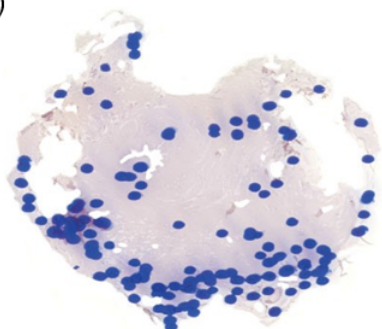
7.3. A prostatectomy-based *ex vivo* model as alternative tool for studying prostate metabolism

Cancer growth largely occurs in the PZ of the gland (~80%), and epithelial cells from this zone are considered metabolically different, mainly as a result of the higher levels of zinc, which affect TCA cycle activity (159, 161). To further understand the normal metabolome in the prostate gland, non-targeted metabolite profiles were obtained from non-cancerous prostate tissue in men undergoing surgery for PCa. Metabolomic analysis, using highly sensitive chromatography techniques, showed a unique metabolic phenotype in each of the two prostate zones. PZ tissue showed distinctly higher levels of lipid metabolites, neurotransmitters, and other classes of compounds that are known to be associated with

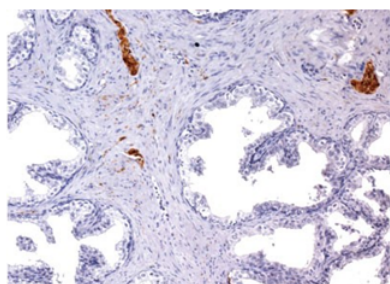
cancer phenotypes. However, multivariate and univariate analyses of TCA cycle metabolites in both zones did not show a significant difference.

The prostate gland is characterised by high innervation, and as with other mammalian organs, receives dual innervation by adrenergic and cholinergic nerves that regulate its growth and physiology (274). There is evidence that suggests a positive association between perineural innervation and PCa (215, 275-277). Most of these studies were carried out by using prostatectomy specimens where higher perineural space invasion was found in prostate adenocarcinoma (275, 276, 278). Furthermore, Powell and colleagues have established an *in vitro* model of perineural invasion that could be used to identify an effective strategy to reduce PCa metastasis (277). Metabolomic analysis, described in Chapter 4 of this thesis, revealed higher levels of neurotransmitter metabolites, such as NAAG and serotonin, in the PZ compared to the TZ. The neuroanatomy of the prostate gland has been previously described, and the PZ is known to have a significantly greater innervation than the TZ (Figure 7.2) (274); thus the significant difference in neurotransmitter levels between the two prostate zones that has been observed in this *ex vivo* model could be explained by anatomical reasons.

A)



B)



C)

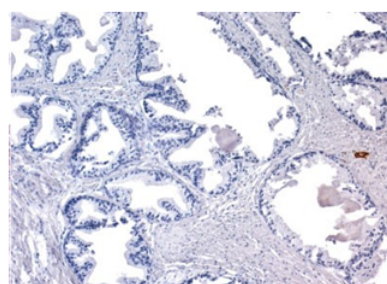


Figure 7.2 Images of prostate sections obtained by Powell and colleagues, showing the location of nerves (blue ink) across a wholemount slide (A), immunostained nerves from the PZ (B) and TZ (C). Statistical analysis indicated a significantly higher concentration of nerves in the PZ (21.45 units) compared to the TZ (8.50 units) ($p < 0.0006$).

Because of the strong link between neurotransmitters and cancer progression (211, 215), it is plausible to suggest that the high levels of NAAG and serotonin resulting from the neuroanatomical features of the PZ could contribute to create a tissue environment that favours cancer development in this region of the gland.

The two zones of the prostate were also characterised by a different profile in terms of lipid metabolites, with a total of 56 identified compounds belonging to different metabolic sub-pathways. It is well established that PCa, as with other cancer types, is closely linked with a metabolic dysregulation, which leads to a unique reprogramming of cellular metabolism (84). These metabolic alterations involve mainly glycolysis and lipogenesis processes that provide cancer cells with sufficient energy and membrane building blocks to support their abnormal proliferation (65, 202). Higher levels of lipid metabolites were found in the PZ, suggesting that this region of the gland is exposed to an environment rich in compounds, which are known to facilitate the emergence of cancer clones (Figure 7.3).

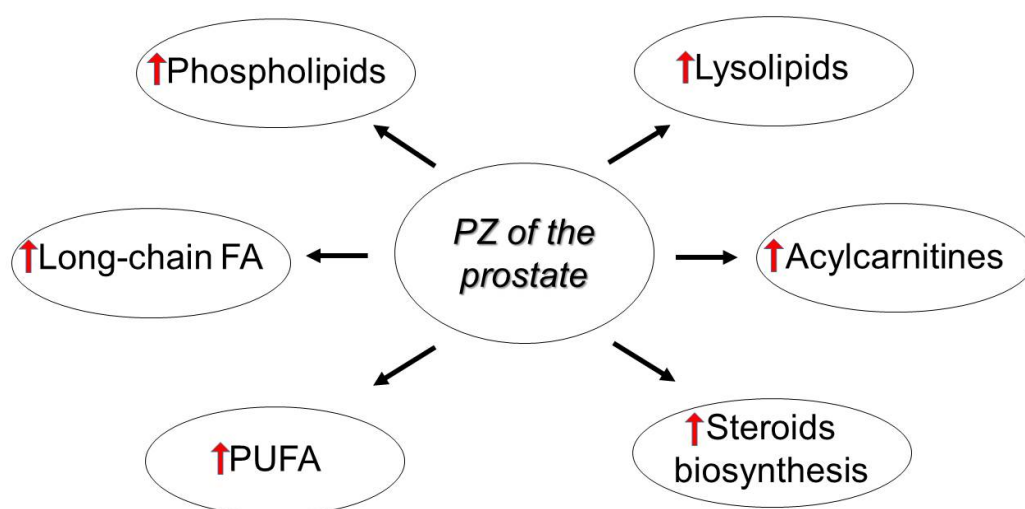


Figure 7.3 Metabolic sub-pathways found significantly higher in the PZ compared to the TZ.

These lipid signatures may represent potential targets for lifestyle interventions, including diet-based interventions designed to deliver dietary compounds potentially active on lipid metabolism. Armah and colleagues found reduced levels of plasma LDL-cholesterol following consumption of glucoraphanin-enriched broccoli in humans (279). This effect was explained by the modulatory action of broccoli-derived bioactives on cholesterol synthesis, which has also been demonstrated in animal studies (280, 281). This cholesterol lowering effect could be induced by their action on the Nrf2-antioxidant system, resulting

in the activation of AMPK and suppression of PI3K signalling pathways, which are both involved in cholesterol and steroid biosynthesis (282). Further evidence of the effect of broccoli consumption on lipid metabolism was provided by a randomised controlled trial recruiting subjects with a high risk of cardiovascular diseases (283). Diet-induced changes were observed in plasma mainly in terms of reduced levels of TCA cycle intermediates, acylcarnitines, and other lipid related compounds.

Undoubtedly, the applied *ex vivo* model has been a valuable experimental approach for the identification of pathways that are more likely to be responsible for the high susceptibility of the PZ to the emergence of cancerous clones. These metabolic pathways could be targeted by dietary bioactives, and further investigations are required for a better understanding of how diet-induced systemic changes may contribute to the changes of the unique metabolic profile of the prostate, and whether organ (prostate)-specific changes can be identified. Finally, it is plausible to suggest that the different metabolism of the prostatic zones should be taken into consideration when tissue sampling strategies are designed in future studies.

7.4. Changes of prostate metabolism induced by dietary bioactives: evidence from a randomised double-blinded trial

An *in vivo* approach was used to further understand the experimental findings obtained by performing the *in vitro* and *ex vivo* work discussed so far. The need of undertaking controlled randomised trials (CRTs) for exploring the effect of diet on PCa prevention is increasingly accepted by the research community. More often, observations emerging from *in vitro* and animal studies are not relevant in clinical settings, resulting in a significant loss of time and money. The cancer preventive properties of dietary ITCs from cruciferous vegetables have been extensively investigated in pre-clinical studies; however, how these experimental findings can translate to a clinical benefit remains unclear.

Epidemiological data have provided robust evidence of a reduced risk of PCa in men who regularly consume high levels of cruciferous vegetables (~ one portion/day) (86, 284). Cruciferous vegetables, such as broccoli, represent one of the major dietary sources of sulfur-containing compounds, including glucosinolates and their breakdown products (e.g. ITCs) (99, 285). The level of sulfate present in these vegetables is relatively high (>0.9 mg/g) compared to low-sulfate foods characterised by <0.1 mg/g (239). Among these sulfur compounds, SMCSO is present at high concentrations in cruciferous plants, and recent

work has confirmed its bioavailability following broccoli consumption (BOBS study, ClinicalTrials.gov Identifier NCT02300324, unpublished data). A previous study, carried out by administering an oral dose of radiolabelled SMCSO ($[^{35}\text{S}]$ -SMCSO) for 14 days to healthy subjects, found that it was mainly excreted in the urine as inorganic sulfate of which 20% was excreted during the first day (258). Until now, however, there has been very little research to explore how sulfur compounds, such as sulfate and SMCSO, contribute to the beneficial effect of cruciferous consumption against cancer (286-289).

The ESCAPE trial was designed to determine whether broccoli-derived compounds can influence the metabolism of the human prostate, resulting in changes to the tumour environment that would be unfavourable for cancer growth. The use of broccoli soups specifically developed for this trial has allowed a double-blinded trial to be undertaken. The advantage of a broccoli-based intervention, instead of a SF-rich supplement, was the simultaneous delivery of SF with other sulfur-containing compounds, including SMCSO and sulfate, that could potentially exert synergistic and/or additive effects. Metabolomic data, fully described in Chapter 6 of this thesis, revealed a significant increase of tissue sulfate levels in the prostate of men randomised to the ESCAPE trial after a 12-month broccoli intervention. These preliminary data were not informative on how the consumption of a different variety of broccoli (normal or glucoraphanin-enriched broccoli) influenced sulfate accumulation in the prostate, due to the blinded nature of the analyses described in this thesis. However, an increased level of sulfate in the prostate after a 12-month broccoli intervention, compared to baseline level, could have significant implications in explaining the key mechanisms underlying the beneficial effect of broccoli consumption which have been observed in epidemiological studies.

Sulfate can reach the systemic circulation from the gastrointestinal tract, where it is delivered as inorganic sulfate through the diet, and an intracellular pool generated by the metabolism of sulphur-containing compounds, such as amino acids (methionine and cysteine) and products of sulfonation reactions (i.e. xenobiotics detoxification, bile acids activation, steroids inactivation) (Figure 7.4) (238). Methionine is converted to cysteine through two reactions catalysed by cystathionine β - synthase (CBS) and cystathionine γ - lyase (CTH). Cysteine is metabolised by two different pathways; one pathway still requires CBS and CTH enzymes, whereas the other is regulated by cysteine dioxygenase (CDO), glutamic-oxaloacetic transaminase 1 (GOT1), and sulphide oxidase (SUOX). Intracellular sulfate is largely used for sulfonation of a wide range of endogenous and exogenous compounds, and as a result of the action of cytosolic sulfatases, more inorganic sulfate is

then released from sulfonated compounds. Sulfate is largely excreted in urine, and its faecal excretion is very poor (238).

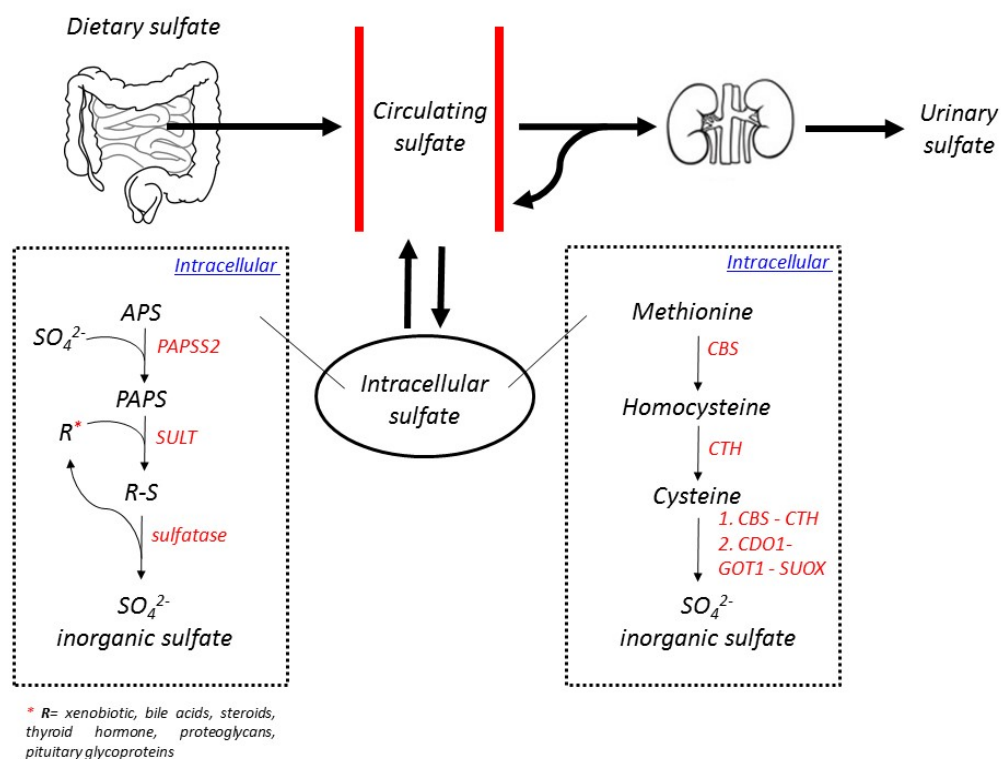


Figure 7.4 Physiological absorption and excretion of sulfate. Inorganic sulfate present in the diet is absorbed through the small intestine, and undergoes a reabsorption process in the kidneys before being excreted in urine. An intracellular pool of inorganic sulfate is generated by the metabolism of the sulfur-containing amino acids methionine and cysteine. Sulfate is used within the cells to form sulfonated metabolites of endogenous compounds and xenobiotics, which in turn generate more inorganic sulfate by the action of cytosolic sulfatases. Circulating sulfate is mainly excreted through the urine following a reabsorption process in the kidneys, and only a very small proportion is excreted with faeces. APS, adenosine 5'-phosphosulfate; PAPS, 3'-phosphoadenosine 5'-phosphosulfate; PAPS2, PAPS synthetase; SULT, sulfotransferases; CBS, cystathionine β - synthase; CTH, cystathionine γ - lyase; CDO1, cysteine dioxygenase; GOT1, glutamic-oxaloacetic transaminase 1; SUOX, sulphide oxidase;

The main biological role of sulfate is the regulation of phase II reactions which are part of the physiological system for xenobiotics detoxification (290), and as already mentioned, the products of these reactions (sulfonated compounds) contribute to sulfate homeostasis. The metabolism of xenobiotics occurs mainly in two phases through several enzymatic reactions based on the chemistry of the xenobiotic. Initially, the compound is converted to an intermediate metabolite containing nucleophilic groups by oxido-reduction and hydrolysis reactions (Phase 1 enzymes), and subsequently the nucleophilic moieties are conjugated with an endogenous molecule (glucuronic acid or glutathione) to be easily excreted in the urine (Figure 7.5). Diet can influence xenobiotic metabolism at different

levels (291); it is now well established that this modulatory action significantly contributes to the cancer preventative benefits of dietary bioactives through the elimination of carcinogens (291-293). However, the same mechanisms of action could represent a problem by interfering with drug metabolism (294).

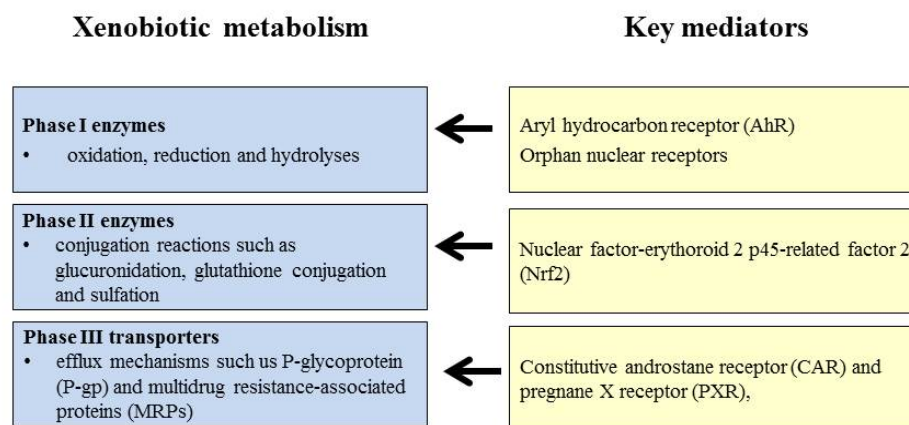


Figure 7.5 Schematic diagram of the physiological system for the metabolism of xenobiotics indicating the key mediators of phase I, II enzymes, and phase III transporters.

A large body of evidence suggest that food bioactives exert their beneficial effect on human health mainly by enhancing phase II metabolism through the activation of Nrf2 signalling pathway (295). SF is considered one of the most potent Nrf2 regulators, and its effects on phase 2 metabolism are well documented in *in vitro* and animal studies (296). To date, the significant inducing effect exerted by SF, and other brassica-derived ITCs, on phase II enzymes is considered the key mechanism responsible for the strong association between consuming diets rich in these vegetables and reduction of cancer risks (101). However, the accumulation of sulfate, observed in the ESCAPE cohort following a long term broccoli-based intervention, could suggest a new potential mechanism by which diets rich in these vegetables can enhance phase II metabolism in the prostate and prevent cancer progression. SMCSO could potentially be the key compound to explain the observed diet-induced metabolic changes in the prostate because the inorganic sulfate resulting from its metabolic fate within the cells, may enhance the synthesis of PAPS, known to be dependent on the availability of the intracellular sulfate pool. Increased PAPS synthesis may deplete intracellular ATP pools, with resulting production of ADP and phosphate. Accumulation of ADP and phosphate was found in the prostate tissue of men randomised to the ESCAPE intervention, and the significant association between ADP and reduced percentage of cancer at repeat biopsy could support the proposed hypothesis (Figure 7.6).

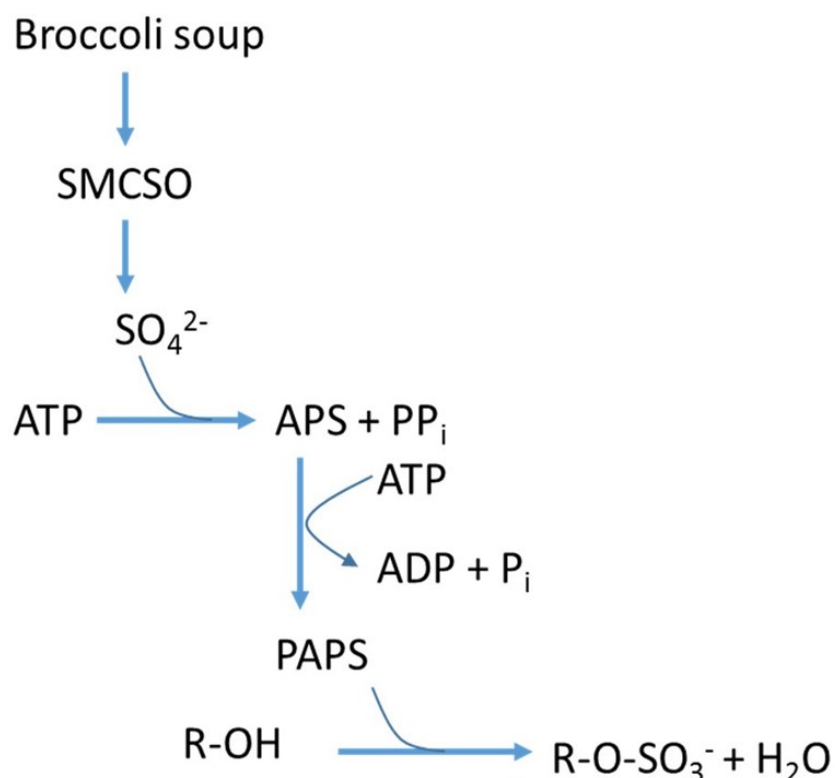


Figure 7.6 SMCSO is mainly metabolised to inorganic sulfate (~50% with urea) in humans. An increased availability of sulfate results in increasing synthesis of PAPS within the cells. PAPS is the universal sulfonate donor molecule for sulfonation reactions involved in the metabolism of xenobiotics.

The high urinary excretion of SMCSO and inorganic sulfate (produced from the intracellular metabolism of SMCSO and also delivered through the ESCAPE diet intervention) could support the role of the diet in inducing prostate sulfate levels, and therefore be potentially responsible for the ATP depletion and the reduced percentage of cancer found at repeat biopsy. The exposure of the prostate to high levels of SMCSO and sulfate could be caused by intraprostatic urinary reflux. There is evidence to support the theory of intraprostatic urinary reflux as an exposure route of the prostate to infectious agents and chemical compounds present in the systemic circulation (297, 298). Reflux of urine into intraprostatic ductuli and ejaculatory ducts may also influence cancer development and progression to advanced disease. The concept of intraprostatic reflux was introduced by Kirby and colleagues, who provided histological evidence of the presence of carbon particles in the prostate glands of men who had carbon particles injected into their bladders prior to a TURP procedure (298). The anatomy of the prostate facilitates the reflux of urine into the peripheral zone of the gland that, as a result is more exposed to bacterial agents, and this could explain the higher rate of prostatic infections in this zone of the

prostate (299, 300). It therefore seems plausible that urinary intraprostatic reflux could be a potential exposure route of the prostate epithelium to compounds delivered through diet.

Further investigations need to be carried out to gain additional evidence for the accumulation of sulfate in the prostate as a direct effect of consuming a broccoli-rich diet containing high levels of sulfur-containing compounds. Windows of opportunity trials could represent a valuable approach to test the proposed hypothesis in an independent patient cohort by investigating the specificity of sulfate accumulation in the prostate through the analyses of non-prostatic tissue. Furthermore, the use of a non-interventional arm will help in understanding whether tissue metabolic changes are specifically induced by sulfur-enriched diets.

7.5. Conclusions

The preliminary data obtained from the ESCAPE trial have provided valuable information to address some of the main challenges associated with cancer chemoprevention. First, the comprehensive characterization of the diets used in the trial in terms of concentrations of SF and other sulfur-containing compounds, along with bioavailability data obtained by parallel trials, has informed on (i) physiological achievable concentrations of these bioactives, (ii) their safety following long-term exposure, and (iii) advantages of using a food-based intervention instead of supplements. It is envisaged that this information will inform future preclinical studies on the use of sulfur-containing compounds at physiologically achievable concentrations. The design of future preclinical studies will also be improved through a more rigorous selection of cell culture models to study prostate biology, taking into consideration the points raised by the *in vitro* work described in this thesis.

Furthermore, the global approach applied to study the diet-induced changes in prostate metabolism, led to the identification of metabolites such as sulfate, ADP/phosphate pool, and glutathione that are affected by the broccoli intervention. Despite the fact that the ESCAPE trial has not been designed to assess clinical endpoints, the portfolio of clinical data gained from the extensive histological assessment of each prostate biopsy core has been valuable for the interpretation of metabolomic data. Linear regression analyses have shown an inverse correlation between tissue sulfate accumulation and cancer percentage at 12 months biopsy, which may be related to the ATP depletion with consequent accumulation of ADP and phosphate. The full body of obtained data on the composition of bioactives delivered by the trial intervention, their effect on prostate metabolite levels after

12-months exposure and percentage of cancer within the same tissue, suggests a new potential mechanism by which diet could prevent cancer progression. The proposed mechanism needs to be tested in an independent patient cohort and further explored in preclinical studies, including prostatectomy-based models, taking into consideration the unique metabolic signature of prostatic regions. A further understanding of the key mechanisms of action of sulfur bioactives as cancer preventive agents may also be important for the rational development of biomarkers.

Finally, the ESCAPE trial highlighted the advantages of undertaking interventional studies in cancer patients on AS. One of the major challenges of studying cancer preventive strategies is the selection of the patient population, and there is a strong need to better identify high-risk patient groups, in particular when testing lifestyle interventions. The AS protocol involves biopsy procedures at regular intervals and this represents a great advantage for collecting biological material together with extensive clinical information.

Appendix 1. Metabolites identified in the first batch of samples analysed through Metabolon® platforms (n=8 patients, n=32 tissue samples)

BIOCHEMICAL	SUPER_ PATHWAY	SUB_ PATHWAY	KEGG	HMDB _ID
1,2-propanediol	Xenobiotics	Chemical	C00583	HMDB01881
1,3-diaminopropane	Amino Acid	Polyamine Metabolism	C00986	HMDB00002
1,5-anhydroglucitol (1,5-AG)	Carbohydrate	Glycolysis, Gluconeogenesis, and Pyruvate Metabolism	C07326	HMDB02712
1,6-anhydroglucose	Xenobiotics	Food Component/Plant		HMDB00640
1-arachidonoylglycerophosphoethanolamine*	Lipid	Lysolipid		HMDB11517
1-arachidonoylglycerophosphoinositol*	Lipid	Lysolipid		
1-arachidonoylglycerol	Lipid	Monoacylglycerol	C13857	HMDB11572
1-docosahexaenoylglycerophosphoethanolamine*	Lipid	Lysolipid		
1-eicosatrienoylglycerophosphocholine (20:3)*	Lipid	Lysolipid		
1-eicosenoylglycerophosphocholine (20:1n9)*	Lipid	Lysolipid		
1-eicosenoylglycerophosphoethanolamine (20:1n9)*	Lipid	Lysolipid		
1-linoleoylglycerol (1-monolinolein)	Lipid	Monoacylglycerol		
1-linoleoylglycerophosphocholine (18:2n6)	Lipid	Lysolipid	C04100	
1-linoleoylglycerophosphoethanolamine*	Lipid	Lysolipid		HMDB11507
1-margaroylglycerophosphoethanolamine*	Lipid	Lysolipid		

BIOCHEMICAL	SUPER_ PATHWAY	SUB_ PATHWAY	KEGG	HMDB _ID
1-myristoylglycerophosphocholine (14:0)	Lipid	Lysolipid	C04230	HMDB10379
1-octadecanol	Lipid	Fatty Alcohol, Long Chain	D01924	HMDB02350
1-oleoylglycerophosphocholine (18:1)	Lipid	Lysolipid		
1-oleoylglycerophosphoethanolamine	Lipid	Lysolipid		HMDB11506
1-oleoylglycerophosphoinositol*	Lipid	Lysolipid		
1-oleoylglycerophosphoserine	Lipid	Lysolipid		
1-oleoylplasmeneylethanolamine*	Lipid	Lysolipid		
1-palmitoleoylglycerophosphocholine (16:1)*	Lipid	Lysolipid		
1-palmitoylglycerol (1-monopalmitin)	Lipid	Monoacylglycerol		HMDB31074
1-palmitoylglycerophosphocholine (16:0)	Lipid	Lysolipid		
1-palmitoylglycerophosphoethanolamine	Lipid	Lysolipid		HMDB11503
1-palmitoylglycerophosphoglycerol*	Lipid	Lysolipid		
1-palmitoylglycerophosphoinositol*	Lipid	Lysolipid		
1-palmitoylplasmeneylethanolamine*	Lipid	Lysolipid		
1-stearoylglycerol (1-monostearin)	Lipid	Monoacylglycerol	D01947	HMDB31075
1-stearoylglycerophosphocholine (18:0)	Lipid	Lysolipid		
1-stearoylglycerophosphoethanolamine	Lipid	Lysolipid		HMDB11130
1-stearoylglycerophosphoinositol	Lipid			
1-stearoylglycerophosphoserine*	Lipid	Lysolipid		
1-stearoylplasmeneylethanolamine*	Lipid	Lysolipid		
2-aminoadipate	Amino Acid	Lysine Metabolism	C00956	HMDB00510

BIOCHEMICAL	SUPER_ PATHWAY	SUB_ PATHWAY	KEGG	HMDB _ID
2-aminobutyrate	Amino Acid	Methionine, Cysteine, SAM and Taurine Metabolism	C0226 1	HMDB 00650
2-arachidonoyl glycerol	Lipid	Monoacylglycerol	C1385 6	HMDB 04666
2-arachidonoylglycerophosphocholine*	Lipid	Lysolipid		
2-arachidonoylglycerophosphoethanolamine*	Lipid	Lysolipid		
2-docosahexaenoylglycerophosphocholine*	Lipid	Lysolipid		
2-docosahexaenoylglycerophosphoethanolamine*	Lipid	Lysolipid		
2-docosapentaenoylglycerophosphoethanolamine*	Lipid	Lysolipid		
2-eicosapentaenoylglycerophosphoethanolamine*	Lipid	Lysolipid		
2-hydroxyacetaminophen sulfate*	Xenobiotics	Drug		
2-hydroxybutyrate (AHB)	Amino Acid	Methionine, Cysteine, SAM and Taurine Metabolism	C0598 4	HMDB 00008
2-hydroxyglutarate	Lipid	Fatty Acid, Dicarboxylate	C0263 0	HMDB 00606
2-linoleoylglycerophosphocholine*	Lipid	Lysolipid		
2-linoleoylglycerophosphoethanolamine*	Lipid	Lysolipid		
2-methylbutyrylcarnitine (C5)	Amino Acid	Leucine, Isoleucine and Valine Metabolism		HMDB 00378
2-myristoylglycerophosphocholine*	Lipid	Lysolipid		
2-oleoylglycerophosphocholine*	Lipid	Lysolipid		
2-oleoylglycerophosphoethanolamine*	Lipid	Lysolipid		

BIOCHEMICAL	SUPER_ PATHWAY	SUB_ PATHWAY	KEGG	HMDB _ID
2-palmitoylglycerol (2-monopalmitin)	Lipid	Monoacylglycerol		HMDB11533
2-palmitoylglycerophosphocholine*	Lipid	Lysolipid		
2-palmitoylglycerophosphoethanolamine*	Lipid	Lysolipid		
2-stearoylglycerophosphocholine*	Lipid	Lysolipid		
2-stearoylglycerophosphoinositol*	Lipid	Lysolipid		
3-(cystein-S-yl)acetaminophen*	Xenobiotics	Drug		
3-(N-acetyl-L-cystein-S-yl)acetaminophen*	Xenobiotics	Drug		
3-(N-morpholino)propanesulfonic acid	Xenobiotics	Chemical		
3-aminoisobutyrate	Nucleotide	Pyrimidine Metabolism, Thymine containing	C05145	HMDB03911
3-dehydrocarnitine*	Lipid	Carnitine Metabolism	C02636	HMDB12154
3-indoxyl sulfate	Amino Acid	Tryptophan Metabolism		HMDB00682
3-phosphoglycerate	Carbohydrate	Glycolysis, Gluconeogenesis, and Pyruvate Metabolism	C00597	HMDB00807
4-acetamidophenol	Xenobiotics	Drug	C06804	HMDB01859
4-acetaminophen sulfate	Xenobiotics	Drug	C06804	HMDB59911
4-androsten-3beta,17beta-diol disulfate (1)*	Lipid	Steroid	C04295	HMDB03818
4-hydroxybutyrate (GHB)	Lipid	Fatty Acid, Monohydroxy	C00989	HMDB00710
4-hydroxyhippurate	Xenobiotics	Benzoate Metabolism		HMDB13678
4-methylsulfinylbutyl glucosinolate	Xenobiotics	Food Component/Plant		
5-methylthioadenosine (MTA)	Amino Acid	Polyamine Metabolism	C00170	HMDB01173
5-oxoproline	Amino Acid	Glutathione Metabolism	C01879	HMDB00267

BIOCHEMICAL	SUPER_ PATHWAY	SUB_ PATHWAY	KEGG	HMDB _ID
6-phosphogluconate	Carbohydrate	Pentose Phosphate Pathway	C00345	HMDB01316
6-sialyl-N-acetylactosamine	Carbohydrate	Aminosugar Metabolism		HMDB06584
7-beta-hydroxycholesterol	Lipid	Sterol		HMDB06119
acetyl CoA	Lipid	Fatty Acid Metabolism	C00024	HMDB01206
acetylcarnitine	Lipid	Fatty Acid Metabolism (Acyl Carnitine)	C02571	HMDB00201
acetylcholine	Lipid	Neurotransmitter		
adenine	Nucleotide	Purine Metabolism, Adenine containing	C00147	HMDB00034
adenosine	Nucleotide	Purine Metabolism, Adenine containing	C00212	HMDB00050
adenosine 5'-diphosphate (ADP)	Nucleotide	Purine Metabolism, Adenine containing	C00008	HMDB01341
adenosine 5'-monophosphate (AMP)	Nucleotide	Purine Metabolism, Adenine containing	C00020	HMDB00045
adenosine 5'-triphosphate (ATP)	Nucleotide	Purine Metabolism, Adenine containing	C00002	HMDB00538
adenosine 5'diphosphoribose	Cofactors and Vitamins	Nicotinate and Nicotinamide Metabolism	C00301	HMDB01178
agmatine	Amino Acid	Polyamine Metabolism	C00179	HMDB01432
alanine	Amino Acid	Alanine and Aspartate Metabolism	C00041	HMDB00161
alpha-ketoglutarate	Energy	TCA Cycle	C00026	HMDB00208
alpha-tocopherol	Cofactors and Vitamins	Tocopherol Metabolism	C02477	HMDB01893
androsterone sulfate	Lipid	Steroid		HMDB02759

BIOCHEMICAL	SUPER_ PATHWAY	SUB_ PATHWAY	KEGG	HMDB _ID
arabitol	Carbohydrate	Pentose Metabolism	C0190 4	HMDB 01851
arachidate (20:0)	Lipid	Long Chain Fatty Acid	C0642 5	HMDB 02212
arachidonate (20:4n6)	Lipid	Polyunsaturated Fatty Acid (n3 and n6)	C0021 9	HMDB 01043
arginine	Amino Acid	Urea cycle; Arginine and Proline Metabolism	C0006 2	HMDB 00517
ascorbate (Vitamin C)	Cofactors and Vitamins	Ascorbate and Aldarate Metabolism	C0007 2	HMDB 00044
asparagine	Amino Acid	Alanine and Aspartate Metabolism	C0015 2	HMDB 00168
aspartate	Amino Acid	Alanine and Aspartate Metabolism	C0004 9	HMDB 00191
atenolol	Xenobiotics	Drug	D0023 5	HMDB 01924
beta-alanine	Nucleotide	Pyrimidine Metabolism, Uracil containing	C0009 9	HMDB 00056
beta-hydroxyisovaleroylcarnitine	Amino Acid			
butyrylcarnitine	Lipid	Fatty Acid Metabolism (also BCAA Metabolism)	C0286 2	HMDB 02013
C-glycosyltryptophan*	Amino Acid	Tryptophan Metabolism		
caffeine	Xenobiotics	Xanthine Metabolism	C0748 1	HMDB 01847
carboxyethyl-GABA	Amino Acid	Glutamate Metabolism		HMDB 02201
carnitine	Lipid	Carnitine Metabolism	C0031 8	HMDB 00062
chiro-inositol	Lipid	Inositol Metabolism	C1989 1	HMDB 34220
cholestanol	Lipid	Sterol	C1297 8	HMDB 00908
cholesterol	Lipid	Sterol	C0018 7	HMDB 00067

BIOCHEMICAL	SUPER_ PATHWAY	SUB_ PATHWAY	KEGG	HMDB _ID
choline	Lipid	Phospholipid Metabolism	C00114	HMDB00097
choline phosphate	Lipid	Phospholipid Metabolism	C00588	HMDB01565
cis-vaccenate (18:1n7)	Lipid	Long Chain Fatty Acid	C08367	HMDB03231
citrate	Energy	TCA Cycle	C00158	HMDB00094
coenzyme A	Cofactors and Vitamins	Pantothenate and CoA Metabolism	C00010	HMDB01423
creatine	Amino Acid	Creatine Metabolism	C00300	HMDB00064
creatinine	Amino Acid	Creatine Metabolism	C00791	HMDB00562
cysteine	Amino Acid	Methionine, Cysteine, SAM and Taurine Metabolism	C00097	HMDB00574
cysteine-glutathione disulfide	Amino Acid	Glutathione Metabolism		HMDB00656
cytidine	Nucleotide	Pyrimidine Metabolism, Cytidine containing	C00475	HMDB00089
cytidine 5'-diphosphocholine	Lipid	Phospholipid Metabolism	C00307	HMDB01413
cytidine 5'-monophosphate (5'-CMP)	Nucleotide	Pyrimidine Metabolism, Cytidine containing	C00055	HMDB00095
cytidine-5'-diphosphoethanolamine	Lipid	Phospholipid Metabolism	C00570	HMDB01564
dehydroascorbate	Cofactors and Vitamins	Ascorbate and Aldarate Metabolism	C05422	HMDB01264
dehydroisoandrosterone sulfate (DHEA-S)	Lipid	Steroid	C04555	HMDB01032
deoxycarnitine	Lipid	Carnitine Metabolism	C01181	HMDB01161
dihomo-linoleate (20:2n6)	Lipid	Polyunsaturated Fatty Acid (n3 and n6)	C16525	HMDB05060
dihomo-linolenate (20:3n3 or n6)	Lipid	Polyunsaturated Fatty Acid (n3 and n6)	C03242	HMDB02925

BIOCHEMICAL	SUPER_ PATHWAY	SUB_ PATHWAY	KEGG	HMDB _ID
docosahexaenoate (DHA; 22:6n3)	Lipid	Polyunsaturated Fatty Acid (n3 and n6)	C0642 9	HMDB 02183
docosapentaenoate (n3 DPA; 22:5n3)	Lipid	Polyunsaturated Fatty Acid (n3 and n6)	C1651 3	HMDB 01976
docosapentaenoate (n6 DPA; 22:5n6)	Lipid	Polyunsaturated Fatty Acid (n3 and n6)	C1651 3	HMDB 13123
eicosapentaenoate (EPA; 20:5n3)	Lipid	Polyunsaturated Fatty Acid (n3 and n6)	C0642 8	HMDB 01999
eicosenoate (20:1n9 or 11)	Lipid	Long Chain Fatty Acid		
erythritol	Xenobiotics	Food Component/Plant	C0050 3	HMDB 02994
erythronate*	Carbohydrate	Aminosugar Metabolism		HMDB 00613
ethanolamine	Lipid	Phospholipid Metabolism	C0018 9	HMDB 00149
flavin adenine dinucleotide (FAD)	Cofactors and Vitamins	Riboflavin Metabolism	C0001 6	HMDB 01248
fructose	Carbohydrate	Fructose, Mannose and Galactose Metabolism	C0009 5	HMDB 00660
fuco	Carbohydrate	Pentose Metabolism	C0101 8	HMDB 00174
fumarate	Energy	TCA Cycle	C0012 2	HMDB 00134
galactose	Carbohydrate	Fructose, Mannose and Galactose Metabolism	C0158 2	HMDB 00143
gamma-aminobutyrate (GABA)	Amino Acid	Glutamate Metabolism	C0033 4	HMDB 00112
gamma-glutamylcysteine	Peptide	Gamma-glutamyl Amino Acid	C0066 9	HMDB 01049
gamma-glutamylglutamate	Peptide	Gamma-glutamyl Amino Acid	C0528 2	HMDB 11737
gamma-glutamylglutamine	Peptide	Gamma-glutamyl Amino Acid	C0528 3	HMDB 11738
gluconate	Xenobiotics	Food Component/Plant	C0025 7	HMDB 00625
glucose	Carbohydrate	Glycolysis, Gluconeogenesis, and Pyruvate Metabolism	C0003 1	HMDB 00122

BIOCHEMICAL	SUPER_ PATHWAY	SUB_ PATHWAY	KEGG	HMDB _ID
glucose 1-phosphate	Carbohydrate	Glycolysis, Gluconeogenesis, and Pyruvate Metabolism	C0010 3	HMDB 01586
glucose-6-phosphate (G6P)	Carbohydrate	Glycolysis, Gluconeogenesis, and Pyruvate Metabolism	C0066 8	HMDB 01401
glutamate	Amino Acid	Glutamate Metabolism	C0002 5	HMDB 00148
glutamate, gamma-methyl ester	Amino Acid	Glutamate Metabolism		
glutamine	Amino Acid	Glutamate Metabolism	C0006 4	HMDB 00641
glutaryl carnitine (C5)	Amino Acid	Lysine Metabolism		HMDB 13130
glutathione, oxidized (GSSG)	Amino Acid	Glutathione Metabolism	C0012 7	HMDB 03337
glutathione, reduced (GSH)	Amino Acid	Glutathione Metabolism	C0005 1	HMDB 00125
glycerate	Carbohydrate	Glycolysis, Gluconeogenesis, and Pyruvate Metabolism	C0025 8	HMDB 00139
glycerol	Lipid	Glycerolipid Metabolism	C0011 6	HMDB 00131
glycerol 2-phosphate	Xenobiotics	Chemical	C0297 9	HMDB 02520
glycerol 3-phosphate (G3P)	Lipid	Glycerolipid Metabolism	C0009 3	HMDB 00126
glycerophosphoethanolamine	Lipid	Phospholipid Metabolism	C0123 3	HMDB 00114
glycerophosphorylcholine (GPC)	Lipid	Phospholipid Metabolism	C0067 0	HMDB 00086
glycine	Amino Acid	Glycine, Serine and Threonine Metabolism	C0003 7	HMDB 00123
glycylisoleucine	Peptide	Dipeptide		
glycylleucine	Peptide	Dipeptide	C0215 5	HMDB 00759
guanine	Nucleotide	Purine Metabolism, Guanine containing	C0024 2	HMDB 00132
guanosine	Nucleotide	Purine Metabolism,	C0038 7	HMDB 00133

BIOCHEMICAL	SUPER_ PATHWAY	SUB_ PATHWAY	KEGG	HMDB _ID
		Guanine containing		
guanosine 5'- monophosphate (5'-GMP)	Nucleotide	Purine Metabolism, Guanine containing	C00144	HMDB01397
heme	Cofactors and Vitamins	Hemoglobin and Porphyrin Metabolism		
hexanoylcarnitine	Lipid	Fatty Acid Metabolism(Acyl Carnitine)		HMDB00705
hippurate	Xenobiotics	Benzoate Metabolism	C01586	HMDB00714
histamine	Amino Acid	Histidine Metabolism	C00388	HMDB00870
histidine	Amino Acid	Histidine Metabolism	C00135	HMDB00177
hydroxybutyrylcarnitine*	Lipid	Fatty Acid Metabolism(Acyl Carnitine)		HMDB13127
hypotaurine	Amino Acid	Methionine, Cysteine, SAM and Taurine Metabolism	C00519	HMDB00965
hypoxanthine	Nucleotide	Purine Metabolism, (Hypo)Xanthine/I nosine containing	C00262	HMDB00157
inosine	Nucleotide	Purine Metabolism, (Hypo)Xanthine/I nosine containing	C00294	HMDB00195
inositol 1-phosphate (I1P)	Lipid	Inositol Metabolism	C04006	HMDB00213
Isobar: fructose 1,6-diphosphate, glucose 1,6-diphosphate, myo-inositol 1,4 or 1,3-diphosphate	Carbohydrate	Glycolysis, Gluconeogenesis, and Pyruvate Metabolism		
isobutyrylcarnitine	Amino Acid	Leucine, Isoleucine and Valine Metabolism		HMDB00736
isocitrate	Energy	TCA Cycle	C00311	HMDB00193
isoleucine	Amino Acid	Leucine, Isoleucine and	C00407	HMDB00172

BIOCHEMICAL	SUPER_ PATHWAY	SUB_ PATHWAY	KEGG	HMDB _ID
		Valine Metabolism		
isovalerylcarnitine	Amino Acid	Leucine, Isoleucine and Valine Metabolism		HMDB 00688
itaconate (methylenesuccinate)	Energy	TCA Cycle	C0049 0	HMDB 02092
kynurenine	Amino Acid	Tryptophan Metabolism	C0032 8	HMDB 00684
lactate	Carbohydrate	Glycolysis, Gluconeogenesis, and Pyruvate Metabolism	C0018 6	HMDB 00190
lactose	Carbohydrate	Disaccharides and Oligosaccharides	C0024 3	HMDB 00186
leucine	Amino Acid	Leucine, Isoleucine and Valine Metabolism	C0012 3	HMDB 00687
lidocaine	Xenobiotics	Drug	D0035 8	HMDB 14426
linoleate (18:2n6)	Lipid	Polyunsaturated Fatty Acid (n3 and n6)	C0159 5	HMDB 00673
lysine	Amino Acid	Lysine Metabolism	C0004 7	HMDB 00182
malate	Energy	TCA Cycle	C0014 9	HMDB 00156
maltose	Carbohydrate	Glycogen Metabolism	C0020 8	HMDB 00163
maltotriose	Carbohydrate	Glycogen Metabolism	C0183 5	HMDB 01262
mannitol	Carbohydrate	Fructose, Mannose and Galactose Metabolism	C0039 2	HMDB 00765
mannose	Carbohydrate	Fructose, Mannose and Galactose Metabolism	C0015 9	HMDB 00169
margarate (17:0)	Lipid	Long Chain Fatty Acid		HMDB 02259
methyl-alpha-glucopyranoside	Xenobiotics	Food Component/Plant	C0260 3	
methylphosphate	Nucleotide	Purine and Pyrimidine Metabolism		

BIOCHEMICAL	SUPER_ PATHWAY	SUB_ PATHWAY	KEGG	HMDB _ID
myo-inositol	Lipid	Inositol Metabolism	C00137	HMDB00211
N-acetyl-aspartyl-glutamate (NAAG)	Amino Acid	Glutamate Metabolism	C12270	HMDB01067
N-acetylaspartate (NAA)	Amino Acid	Alanine and Aspartate Metabolism	C01042	HMDB00812
N-acetylneuraminate	Carbohydrate	Aminosugar Metabolism	C00270	HMDB00230
N-acetylputrescine	Amino Acid	Polyamine Metabolism	C02714	HMDB02064
N1-methyladenosine	Nucleotide	Purine Metabolism, Adenine containing	C02494	HMDB03331
nicotinamide	Cofactors and Vitamins	Nicotinate and Nicotinamide metabolism	C00153	HMDB01406
nicotinamide adenine dinucleotide (NAD+)	Cofactors and Vitamins	Nicotinate and Nicotinamide Metabolism	C00003	HMDB00902
nicotinamide adenine dinucleotide reduced (NADH)	Cofactors and Vitamins	Nicotinate and Nicotinamide Metabolism	C00004	HMDB01487
octanoylcarnitine	Lipid	Fatty Acid Metabolism(Acyl Carnitine)	C02838	HMDB00791
oleamide	Lipid	Fatty Acid, Amide	C19670	HMDB02117
oleate (18:1n9)	Lipid	Long Chain Fatty Acid	C00712	HMDB00207
oleoylcarnitine	Lipid	Fatty Acid Metabolism(Acyl Carnitine)		HMDB05065
ophthalmate	Amino Acid	Glutathione Metabolism		HMDB05765
ornithine	Amino Acid	Urea cycle; Arginine and Proline Metabolism	C00077	HMDB03374
p-acetamidophenylglucuronide	Xenobiotics	Drug		HMDB10316
p-cresol sulfate	Amino Acid	Phenylalanine and Tyrosine Metabolism	C01468	HMDB11635
palmitate (16:0)	Lipid	Long Chain Fatty Acid	C00249	HMDB00220

BIOCHEMICAL	SUPER_ PATHWAY	SUB_ PATHWAY	KEGG	HMDB _ID
palmitoleate (16:1n7)	Lipid	Long Chain Fatty Acid	C0836 2	HMDB 03229
palmitoyl sphingomyelin	Lipid	Sphingolipid Metabolism		
palmitoylcarnitine	Lipid	Fatty Acid Metabolism(Acyl Carnitine)	C0299 0	HMDB 00222
pantothenate	Cofactors and Vitamins	Pantothenate and CoA Metabolism	C0086 4	HMDB 00210
phenol sulfate	Amino Acid	Phenylalanine and Tyrosine Metabolism	C0218 0	HMDB 60015
phenylacetylglutamine	Amino Acid	Phenylalanine and Tyrosine Metabolism	C0414 8	HMDB 06344
phenylalanine	Amino Acid	Phenylalanine and Tyrosine Metabolism	C0007 9	HMDB 00159
phosphate	Energy	Oxidative Phosphorylation	C0000 9	HMDB 01429
phosphoethanolamine	Lipid	Phospholipid Metabolism	C0034 6	HMDB 00224
proline	Amino Acid	Urea cycle; Arginine and Proline Metabolism	C0014 8	HMDB 00162
propionylcarnitine	Lipid	Fatty Acid Metabolism (also BCAA Metabolism)	C0301 7	HMDB 00824
pseudouridine	Nucleotide	Pyrimidine Metabolism, Uracil containing	C0206 7	HMDB 00767
putrescine	Amino Acid	Polyamine Metabolism	C0013 4	HMDB 01414
pyroglutamine*	Amino Acid	Glutamate Metabolism		
pyrophosphate (PPi)	Energy	Oxidative Phosphorylation	C0001 3	HMDB 00250
ribitol	Carbohydrate	Pentose Metabolism	C0047 4	HMDB 00508
ribose	Carbohydrate	Pentose Metabolism	C0012 1	HMDB 00283
S-adenosylhomocysteine (SAH)	Amino Acid	Methionine, Cysteine, SAM and Taurine Metabolism	C0002 1	HMDB 00939

BIOCHEMICAL	SUPER_ PATHWAY	SUB_ PATHWAY	KEGG	HMDB _ID
S-methylcysteine	Amino Acid	Methionine, Cysteine, SAM and Taurine Metabolism		HMDB02108
scyllo-inositol	Lipid	Inositol Metabolism	C06153	HMDB06088
serine	Amino Acid	Glycine, Serine and Threonine Metabolism	C00065	HMDB00187
serotonin (5HT)	Amino Acid	Tryptophan Metabolism	C00780	HMDB00259
sorbitol	Carbohydrate	Fructose, Mannose and Galactose Metabolism	C00794	HMDB00247
spermidine	Amino Acid	Polyamine Metabolism	C00315	HMDB01257
spermine	Amino Acid	Polyamine Metabolism	C00750	HMDB01256
sphingosine	Lipid	Sphingolipid Metabolism	C00319	HMDB00252
stearamide	Lipid	Fatty Acid, Amide	C13846	HMDB34146
stearate (18:0)	Lipid	Long Chain Fatty Acid	C01530	HMDB00827
stearoyl sphingomyelin	Lipid	Sphingolipid Metabolism	C00550	HMDB01348
stearoylcarnitine	Lipid	Fatty Acid Metabolism(Acyl Carnitine)		HMDB00848
succinate	Energy	TCA Cycle	C00042	HMDB00254
succinylcarnitine	Energy	TCA Cycle		
taurine	Amino Acid	Methionine, Cysteine, SAM and Taurine Metabolism	C00245	HMDB00251
theobromine	Xenobiotics	Xanthine Metabolism	C07480	HMDB02825
thiosulfate	Xenobiotics	Chemical	C05529	
threonate	Cofactors and Vitamins	Ascorbate and Aldarate Metabolism	C01620	HMDB00943
threonine	Amino Acid	Glycine, Serine and Threonine Metabolism	C00188	HMDB00167

BIOCHEMICAL	SUPER_ PATHWAY	SUB_ PATHWAY	KEGG	HMDB _ID
trans-4-hydroxyproline	Amino Acid	Urea cycle; Arginine and Proline Metabolism	C0115 7	HMDB 00725
trans-aconitate	Energy	TCA Cycle	C0234 1	HMDB 00958
trizma acetate	Xenobiotics	Chemical	C0718 2	
tryptophan	Amino Acid	Tryptophan Metabolism	C0007 8	HMDB 00929
tryptophan betaine	Amino Acid	Tryptophan Metabolism	C0921 3	HMDB 61115
tyrosine	Amino Acid	Phenylalanine and Tyrosine Metabolism	C0008 2	HMDB 00158
uracil	Nucleotide	Pyrimidine Metabolism, Uracil containing	C0010 6	HMDB 00300
urate	Nucleotide	Purine Metabolism, (Hypo)Xanthine/I nosine containing	C0036 6	HMDB 00289
urea	Amino Acid	Urea cycle; Arginine and Proline Metabolism	C0008 6	HMDB 00294
uridine	Nucleotide	Pyrimidine Metabolism, Uracil containing	C0029 9	HMDB 00296
uridine monophosphate (5' or 3')	Nucleotide	Pyrimidine Metabolism, Uracil containing	C0136 8 , C0010 5	HMDB 00288
valine	Amino Acid	Leucine, Isoleucine and Valine Metabolism	C0018 3	HMDB 00883
xanthine	Nucleotide	Purine Metabolism, (Hypo)Xanthine/I nosine containing	C0038 5	HMDB 00292
xanthosine	Nucleotide	Purine Metabolism, (Hypo)Xanthine/I nosine containing	C0176 2	HMDB 00299
xylitol	Carbohydrate	Pentose Metabolism	C0037 9	HMDB 02917

Appendix 2 Metabolites identified in the second batch of samples analysed through Metabolon® platforms (n=10 patients, n=40 tissue samples)

BIOCHEMICAL	SUPER_ PATHWAY	SUB_ PATHWAY	KEGG	HMDB _ID
1,2,3-benzenetriol sulfate (2)	Xenobiotics	Chemical		
1,2-dilinoleoyl-GPC (18:2/18:2)	Lipid	Phospholipid Metabolism		
1,2-dioleoyl-GPC (18:1/18:1)*	Lipid	Phospholipid Metabolism		
1,2-dioleoyl-GPE (18:1/18:1)	Lipid	Phospholipid Metabolism		
1,2-dipalmitoyl-GPC (16:0/16:0)	Lipid	Phospholipid Metabolism		HMDB 00564
1,3-dimethylurate	Xenobiotics	Xanthine Metabolism		HMDB 01857
1,5-anhydroglucitol (1,5-AG)	Carbohydrate	Glycolysis, Gluconeogenesis, and Pyruvate Metabolism	C0732 6	HMDB 02712
1,7-dimethylurate	Xenobiotics	Xanthine Metabolism	C1635 6	HMDB 11103
1-(1-enyl-oleoyl)-2-arachidonoyl-GPE (P-18:1/20:4)*	Lipid	Plasmalogen		
1-(1-enyl-oleoyl)-GPE (P-18:1)*	Lipid	Lysolipid		
1-(1-enyl-palmitoyl)-2-arachidonoyl-GPC (P-16:0/20:4)*	Lipid	Phospholipid Metabolism		
1-(1-enyl-palmitoyl)-2-arachidonoyl-GPE (P-16:0/20:4)*	Lipid	Plasmalogen		
1-(1-enyl-palmitoyl)-2-linoleoyl-GPC (P-16:0/18:2)*	Lipid	Phospholipid Metabolism		
1-(1-enyl-palmitoyl)-2-linoleoyl-GPE (P-16:0/18:2)*	Lipid	Plasmalogen		
1-(1-enyl-palmitoyl)-2-oleoyl-GPC (P-16:0/18:1)*	Lipid	Plasmalogen		
1-(1-enyl-palmitoyl)-2-oleoyl-GPE (P-16:0/18:1)*	Lipid	Plasmalogen		
1-(1-enyl-palmitoyl)-2-palmitoleoyl-GPC (P-16:0/16:1)*	Lipid	Plasmalogen		
1-(1-enyl-palmitoyl)-2-palmitoyl-GPC (P-16:0/16:0)*	Lipid	Plasmalogen		
1-(1-enyl-palmitoyl)-GPE (P-16:0)*	Lipid	Lysoplasmalogen		
1-(1-enyl-stearoyl)-2-arachidonoyl-GPE (P-18:0/20:4)*	Lipid	Phospholipid Metabolism		HMDB 05779

BIOCHEMICAL	SUPER_ PATHWAY	SUB_ PATHWAY	KEGG	HMDB _ID
1-(1-enyl-stearoyl)-2-linoleoyl-GPE (P-18:0/18:2)*	Lipid	Plasmalogen		
1-(1-enyl-stearoyl)-2-oleoyl-GPE (P-18:0/18:1)	Lipid	Plasmalogen		
1-(1-enyl-stearoyl)-GPE (P-18:0)*	Lipid	Lysolipid		
1-arachidonoyl-GPC (20:4)*	Lipid	Lysolipid	C05208	HMDB10395
1-arachidonoyl-GPE (20:4)*	Lipid	Lysolipid		HMDB11517
1-arachidonoyl-GPI (20:4)*	Lipid	Lysolipid		HMDB61690
1-dihomo-linolenylglycerol (20:3)	Lipid	Monoacylglycerol		
1-linoleoyl-2-arachidonoyl-GPC (18:2/20:4)*	Lipid	Phospholipid Metabolism		
1-linoleoyl-GPC (18:2)	Lipid	Lysolipid	C04100	HMDB10386
BIOCHEMICAL	SUPER_P ATHWAY	SUB_PATHWAY	KEGG	HMDB _ID
1-linoleoyl-GPE (18:2)*	Lipid	Lysolipid		HMDB11507
1-linoleoylglycerol (18:2)	Lipid	Monoacylglycerol		
1-methylguanidine	Amino Acid	Guanidino and Acetamido Metabolism	C02294	HMDB01522
1-methylhistamine	Amino Acid	Histidine Metabolism	C05127	HMDB00898
1-methylhistidine	Amino Acid	Histidine Metabolism	C01152	HMDB00001
1-methylimidazoleacetate	Amino Acid	Histidine Metabolism	C05828	HMDB02820
1-methylnicotinamide	Cofactors and Vitamins	Nicotinate and Nicotinamide Metabolism	C02918	HMDB00699
1-methylurate	Xenobiotics	Xanthine Metabolism	C16359	HMDB03099
1-oleoyl-2-linoleoyl-GPC (18:1/18:2)*	Lipid	Phospholipid Metabolism		
1-oleoyl-2-linoleoyl-GPE (18:1/18:2)*	Lipid	Phospholipid Metabolism		HMDB05349
1-oleoyl-GPC (18:1)	Lipid	Lysolipid		HMDB02815
1-oleoyl-GPE (18:1)	Lipid	Lysolipid		HMDB11506

BIOCHEMICAL	SUPER_ PATHWAY	SUB_ PATHWAY	KEGG	HMDB _ID
1-oleoyl-GPI (18:1)*	Lipid	Lysolipid		
1-oleoyl-GPS (18:1)	Lipid	Lysolipid		
1-palmitoleoyl-2-linoleoyl-GPC (16:1/18:2)*	Lipid	Phospholipid Metabolism		
1-palmitoleoyl-GPC (16:1)*	Lipid	Lysolipid		HMDB 10383
1-palmitoyl-2-arachidonoyl-GPC (16:0/20:4)	Lipid	Phospholipid Metabolism		
1-palmitoyl-2-arachidonoyl-GPE (16:0/20:4)*	Lipid	Phospholipid Metabolism		HMDB 05323
1-palmitoyl-2-linoleoyl-GPC (16:0/18:2)	Lipid	Phospholipid Metabolism		
1-palmitoyl-2-linoleoyl-GPE (16:0/18:2)	Lipid	Phospholipid Metabolism		HMDB 05322
1-palmitoyl-2-oleoyl-GPC (16:0/18:1)	Lipid	Phospholipid Metabolism		
1-palmitoyl-2-oleoyl-GPE (16:0/18:1)	Lipid	Phospholipid Metabolism		HMDB 05320
1-palmitoyl-2-oleoyl-GPI (16:0/18:1)*	Lipid	Phospholipid Metabolism		
1-palmitoyl-2-oleoyl-GPS (16:0/18:1)	Lipid	Phospholipid Metabolism	C13880	
1-palmitoyl-2-palmitoleoyl-GPC (16:0/16:1)*	Lipid	Phospholipid Metabolism		
1-palmitoyl-2-stearoyl-GPC (16:0/18:0)	Lipid	Phospholipid Metabolism		
1-palmitoyl-3-linoleoyl-glycerol (16:0/18:2)*	Lipid	Phospholipid Metabolism		
1-palmitoyl-GPC (16:0)	Lipid	Lysolipid		HMDB 10382
1-palmitoyl-GPE (16:0)	Lipid	Lysolipid		HMDB 11503
1-palmitoyl-GPG (16:0)*	Lipid	Lysolipid		
1-palmitoyl-GPI (16:0)*	Lipid	Lysolipid		HMDB 61695
1-stearoyl-2-arachidonoyl-GPC (18:0/20:4)	Lipid	Phospholipid Metabolism		
BIOCHEMICAL	SUPER_P ATHWAY	SUB_PATHWAY	KEGG	HMDB _ID
1-stearoyl-2-arachidonoyl-GPE (18:0/20:4)	Lipid	Phospholipid Metabolism		

BIOCHEMICAL	SUPER_ PATHWAY	SUB_ PATHWAY	KEGG	HMDB _ID
1-stearoyl-2-arachidonoyl-GPI (18:0/20:4)	Lipid	Phospholipid Metabolism		
1-stearoyl-2-arachidonoyl-GPS (18:0/20:4)	Lipid	Phosphatidylserine (PS)		
1-stearoyl-2-linoleoyl-GPC (18:0/18:2)*	Lipid	Phospholipid Metabolism		
1-stearoyl-2-linoleoyl-GPE (18:0/18:2)*	Lipid	Phospholipid Metabolism		
1-stearoyl-2-oleoyl-GPC (18:0/18:1)	Lipid	Phospholipid Metabolism		
1-stearoyl-2-oleoyl-GPE (18:0/18:1)	Lipid	Phospholipid Metabolism		
1-stearoyl-2-oleoyl-GPG (18:0/18:1)	Lipid	Phospholipid Metabolism		
1-stearoyl-2-oleoyl-GPS (18:0/18:1)	Lipid	Phosphatidylserine (PS)		
1-stearoyl-GPC (18:0)	Lipid	Lysolipid		HMDB 10384
1-stearoyl-GPE (18:0)	Lipid	Lysolipid		HMDB 11130
1-stearoyl-GPG (18:0)	Lipid	Lysolipid		
1-stearoyl-GPI (18:0)	Lipid	Lysolipid		HMDB 61696
1-stearoyl-GPS (18:0)*	Lipid	Lysolipid		
10-nonadecenoate (19:1n9)	Lipid	Long Chain Fatty Acid		HMDB 13622
2-aminoadipate	Amino Acid	Lysine Metabolism	C00956	HMDB 00510
2-aminophenol sulfate	Xenobiotics	Chemical		HMDB 61116
2-hydroxyacetaminophen sulfate*	Xenobiotics	Drug		
2-hydroxybutyrate/2-hydroxyisobutyrate	Amino Acid	Methionine, Cysteine, SAM and Taurine Metabolism		
2-hydroxydecanoate	Lipid	Fatty Acid, Monohydroxy		
2-hydroxyglutarate	Lipid	Fatty Acid, Dicarboxylate	C02630	HMDB 00606
2-hydroxyhippurate (salicylurate)	Xenobiotics	Benzoate Metabolism	C07588	HMDB 00840
2-methoxyacetaminophen glucuronide*	Xenobiotics	Drug		

BIOCHEMICAL	SUPER_ PATHWAY Y	SUB_ PATHWAY	KEGG	HMDB _ID
2-methoxyacetaminophen sulfate*	Xenobiotics	Drug		
2-methylbutyrylcarnitine (C5)	Amino Acid	Leucine, Isoleucine and Valine Metabolism		HMDB 00378
2-oleoylglycerol (18:1)	Lipid	Monoacylglycerol		
2-palmitoyl-GPC (16:0)*	Lipid	Lysolipid		HMDB 61702
2-stearoyl-GPE (18:0)*	Lipid	Lysolipid		
3-(3-hydroxyphenyl)propionate sulfate	Amino Acid	Phenylalanine and Tyrosine Metabolism		
3-(4-hydroxyphenyl)lactate	Amino Acid	Phenylalanine and Tyrosine Metabolism	C0367 2	HMDB 00755
3-(cystein-S-yl)acetaminophen*	Xenobiotics	Drug		
3-(N-acetyl-L-cystein-S-yl) acetaminophen	Xenobiotics	Drug		
3-aminoisobutyrate	Nucleotide	Pyrimidine Metabolism, Thymine containing	C0514 5	HMDB 03911
3-carboxy-4-methyl-5-propyl-2- furanpropanoate (CMPF)	Lipid	Fatty Acid, Dicarboxylate		HMDB 61112
3-hydroxy-3-methylglutarate	Lipid	Mevalonate Metabolism	C0376 1	HMDB 00355
3-hydroxybutyrate (BHBA)	Lipid	Ketone Bodies	C0108 2	HMDB 00357
3-hydroxybutyrylcarnitine (1)	Lipid	Fatty Acid Metabolism(Acyl Carnitine)		HMDB 13127
3-hydroxybutyrylcarnitine (2)	Lipid	Fatty Acid Metabolism(Acyl Carnitine)		
3-hydroxyhippurate	Xenobiotics	Benzoate Metabolism		HMDB 06116
3-hydroxypyridine sulfate	Xenobiotics	Chemical		
3-indoxyl sulfate	Amino Acid	Tryptophan Metabolism		HMDB 00682
3-methylhistidine	Amino Acid	Histidine Metabolism	C0115 2	HMDB 00479
3-phosphoglycerate	Carbohydra te	Glycolysis, Gluconeogenesis, and Pyruvate Metabolism	C0059 7	HMDB 00807

BIOCHEMICAL	SUPER_ PATHWAY Y	SUB_ PATHWAY	KEGG	HMDB _ID
4-acetamidophenol	Xenobiotics	Drug	C06804	HMDB01859
4-acetamidophenylglucuronide	Xenobiotics	Drug		HMDB10316
4-acetaminophen sulfate	Xenobiotics	Drug	C06804	HMDB59911
4-androsten-3beta,17beta-diol disulfate (1)	Lipid	Steroid	C04295	HMDB03818
4-guanidinobutanoate	Amino Acid	Guanidino and Acetamido Metabolism	C01035	HMDB03464
4-hydroxybutyrate (GHB)	Lipid	Fatty Acid, Monohydroxy	C00989	HMDB00710
4-hydroxyhippurate	Xenobiotics	Benzoate Metabolism		HMDB13678
4-methylbenzenesulfonate	Xenobiotics	Chemical	C06677	
4-methylcatechol sulfate	Xenobiotics	Benzoate Metabolism		
5-methylthioadenosine (MTA)	Amino Acid	Polyamine Metabolism	C00170	HMDB01173
5-oxoproline	Amino Acid	Glutathione Metabolism	C01879	HMDB00267
6-phosphogluconate	Carbohydrate	Pentose Phosphate Pathway	C00345	HMDB01316
6-sialyl-N-acetyllactosamine	Carbohydrate	Aminosugar Metabolism		HMDB06584
7-alpha-hydroxy-3-oxo-4-cholestenoate (7-Hoca)	Lipid	Sterol	C17337	HMDB12458
7-methylguanine	Nucleotide	Purine Metabolism, Guanine containing	C02242	HMDB00897
Acetylcarnitine	Lipid	Fatty Acid Metabolism(Acyl Carnitine)	C02571	HMDB00201
Acetylcholine	Lipid	Neurotransmitter		
Acisoga	Amino Acid	Polyamine Metabolism		
Adenine	Nucleotide	Purine Metabolism, Adenine containing	C00147	HMDB00034
Adenosine	Nucleotide	Purine Metabolism,	C00212	HMDB00050

BIOCHEMICAL	SUPER_ PATHWAY	SUB_ PATHWAY	KEGG	HMDB _ID
		Adenine containing		
Adenosine 3',5'-cyclic monophosphate (camp)	Nucleotide	Purine Metabolism, Adenine containing	C00575	HMDB00058
Adenosine 5'-diphosphate (ADP)	Nucleotide	Purine Metabolism, Adenine containing	C00008	HMDB01341
Adenosine 5'-diphosphoribose (ADP-ribose)	Cofactors and Vitamins	Nicotinate and Nicotinamide Metabolism	C00301	HMDB01178
Adenosine 5'-monophosphate (AMP)	Nucleotide	Purine Metabolism, Adenine containing	C00020	HMDB00045
Alanine	Amino Acid	Alanine and Aspartate Metabolism	C00041	HMDB00161
Allantoin	Nucleotide	Purine Metabolism, (Hypo)Xanthine/I nosine containing	C02350	HMDB00462
Alpha-ketoglutarate	Energy	TCA Cycle	C00026	HMDB00208
Alpha-tocopherol	Cofactors and Vitamins	Tocopherol Metabolism	C02477	HMDB01893
Androsterone sulfate	Lipid	Steroid		HMDB02759
Anserine	Peptide	Dipeptide Derivative	C01262	HMDB00194
Arabitol/xylitol	Carbohydrate	Pentose Metabolism		
Arabonate/xylonate	Carbohydrate	Pentose Phosphate Pathway		
Arachidate (20:0)	Lipid	Long Chain Fatty Acid	C06425	HMDB02212
Arginine	Amino Acid	Urea cycle; Arginine and Proline Metabolism	C00062	HMDB00517
Argininosuccinate	Amino Acid	Urea cycle; Arginine and Proline Metabolism	C03406	HMDB00052

BIOCHEMICAL	SUPER_ PATHWAY Y	SUB_ PATHWAY	KEGG	HMDB _ID
Ascorbate (Vitamin C)	Cofactors and Vitamins	Ascorbate and Aldarate Metabolism	C0007 2	HMDB 00044
Asparagine	Amino Acid	Alanine and Aspartate Metabolism	C0015 2	HMDB 00168
Aspartate	Amino Acid	Alanine and Aspartate Metabolism	C0004 9	HMDB 00191
Azelate (nonanedioate)	Lipid	Fatty Acid, Dicarboxylate	C0826 1	HMDB 00784
Behenoyl sphingomyelin (d18:1/22:0)*	Lipid	Sphingolipid Metabolism		
Beta-alanine	Nucleotide	Pyrimidine Metabolism, Uracil containing	C0009 9	HMDB 00056
Betaine	Amino Acid	Glycine, Serine and Threonine Metabolism	C0071 9	HMDB 00043
Betonicine	Xenobiotics	Food Component/Plant	C0826 9	HMDB 29412
Biliverdin	Cofactors and Vitamins	Hemoglobin and Porphyrin Metabolism	C0050 0	HMDB 01008
Butyrylcarnitine	Lipid	Fatty Acid Metabolism (also BCAA Metabolism)	C0286 2	HMDB 02013
C-glycosyltryptophan	Amino Acid	Tryptophan Metabolism		
Caffeine	Xenobiotics	Xanthine Metabolism	C0748 1	HMDB 01847
Carnitine	Lipid	Carnitine Metabolism	C0031 8	HMDB 00062
Carnosine	Peptide	Dipeptide Derivative	C0038 6	HMDB 00033
Catechol sulfate	Xenobiotics	Benzoate Metabolism	C0009 0	HMDB 59724
Cholesterol	Lipid	Sterol	C0018 7	HMDB 00067
Choline	Lipid	Phospholipid Metabolism	C0011 4	HMDB 00097
Choline phosphate	Lipid	Phospholipid Metabolism	C0058 8	HMDB 01565

BIOCHEMICAL	SUPER_ PATHWAY Y	SUB_ PATHWAY	KEGG	HMDB _ID
Cis-4-decenoyl carnitine	Lipid	Fatty Acid Metabolism(Acyl Carnitine)		
Cis-urocanate	Amino Acid	Histidine Metabolism		
Citrate	Energy	TCA Cycle	C00158	HMDB00094
Citrulline	Amino Acid	Urea cycle; Arginine and Proline Metabolism	C00327	HMDB00904
Creatine	Amino Acid	Creatine Metabolism	C00300	HMDB00064
Creatine phosphate	Amino Acid	Creatine Metabolism	C02305	HMDB01511
Creatinine	Amino Acid	Creatine Metabolism	C00791	HMDB00562
Cysteine	Amino Acid	Methionine, Cysteine, SAM and Taurine Metabolism	C00097	HMDB00574
Cysteine-glutathione disulfide	Amino Acid	Glutathione Metabolism		HMDB00656
Cysteinylglycine	Amino Acid	Glutathione Metabolism	C01419	HMDB00078
Cystine	Amino Acid	Methionine, Cysteine, SAM and Taurine Metabolism	C00491	HMDB00192
Cytidine	Nucleotide	Pyrimidine Metabolism, Cytidine containing	C00475	HMDB00089
Cytidine 5'-diphosphocholine	Lipid	Phospholipid Metabolism	C00307	HMDB01413
Cytidine 5'-monophosphate (5'-CMP)	Nucleotide	Pyrimidine Metabolism, Cytidine containing	C00055	HMDB00095
Cytidine-5'-diphosphoethanolamine	Lipid	Phospholipid Metabolism	C00570	HMDB01564
Decanoylcarnitine	Lipid	Fatty Acid Metabolism(Acyl Carnitine)		HMDB00651
Dehydroisoandrosterone sulfate (DHEA-S)	Lipid	Steroid	C04555	HMDB01032

BIOCHEMICAL	SUPER_ PATHWAY	SUB_ PATHWAY	KEGG	HMDB _ID
Deoxycarnitine	Lipid	Carnitine Metabolism	C0118 1	HMDB 01161
Dihomo-linoleate (20:2n6)	Lipid	Polyunsaturated Fatty Acid (n3 and n6)	C1652 5	HMDB 05060
Dihomo-linolenate (20:3n3 or n6)	Lipid	Polyunsaturated Fatty Acid (n3 and n6)	C0324 2	HMDB 02925
Diltiazem	Xenobiotics	Drug	C0695 8	HMDB 14487
Dimethylarginine (SDMA + ADMA)	Amino Acid	Urea cycle; Arginine and Proline Metabolism	C0362 6	HMDB 01539
Dimethylglycine	Amino Acid	Glycine, Serine and Threonine Metabolism	C0102 6	HMDB 00092
Docosadienoate (22:2n6)	Lipid	Polyunsaturated Fatty Acid (n3 and n6)	C1653 3	HMDB 61714
Docosapentaenoate (n3 DPA; 22:5n3)	Lipid	Polyunsaturated Fatty Acid (n3 and n6)	C1651 3	HMDB 01976
Docosapentaenoate (n6 DPA; 22:5n6)	Lipid	Polyunsaturated Fatty Acid (n3 and n6)	C1651 3	HMDB 01976
Eicosenoate (20:1)	Lipid	Long Chain Fatty Acid		HMDB 02231
Ergothioneine	Xenobiotics	Food Component/Plant	C0557 0	HMDB 03045
Erythronate*	Carbohydra te	Aminosugar Metabolism		HMDB 00613
Ethylmalonate	Amino Acid	Leucine, Isoleucine and Valine Metabolism		HMDB 00622
Flavin adenine dinucleotide (FAD)	Cofactors and Vitamins	Riboflavin Metabolism	C0001 6	HMDB 01248
Fructose	Carbohydra te	Fructose, Mannose and Galactose Metabolism	C0009 5	HMDB 00660
Fumarate	Energy	TCA Cycle	C0012 2	HMDB 00134
Gamma-aminobutyrate (GABA)	Amino Acid	Glutamate Metabolism	C0033 4	HMDB 00112

BIOCHEMICAL	SUPER_ PATHWAY Y	SUB_ PATHWAY	KEGG	HMDB _ID
Gamma-glutamyl-epsilon-lysine	Peptide	Gamma-glutamyl Amino Acid		HMDB 03869
Gamma-glutamylalanine	Peptide	Gamma-glutamyl Amino Acid		HMDB 29142
Gamma-glutamylcysteine	Peptide	Gamma-glutamyl Amino Acid	C0066 9	HMDB 01049
Gamma-glutamylglutamate	Peptide	Gamma-glutamyl Amino Acid	C0528 2	HMDB 11737
Gamma-glutamylglutamine	Peptide	Gamma-glutamyl Amino Acid	C0528 3	HMDB 11738
Gamma-glutamylleucine	Peptide	Gamma-glutamyl Amino Acid		HMDB 11171
Gamma-glutamylmethionine	Peptide	Gamma-glutamyl Amino Acid		HMDB 29155
Gamma-glutamylvaline	Peptide	Gamma-glutamyl Amino Acid		HMDB 11172
Gamma-tocopherol/beta-tocopherol	Cofactors and Vitamins	Tocopherol Metabolism		
Gluconate	Xenobiotics	Food Component/Plant	C0025 7	HMDB 00625
Glucose	Carbohydrate	Glycolysis, Gluconeogenesis, and Pyruvate Metabolism	C0003 1	HMDB 00122
Glucuronate	Carbohydrate	Aminosugar Metabolism	C0019 1	HMDB 00127
Glutamate	Amino Acid	Glutamate Metabolism	C0002 5	HMDB 00148
Glutamate, gamma-methyl ester	Amino Acid	Glutamate Metabolism		
Glutamine	Amino Acid	Glutamate Metabolism	C0006 4	HMDB 00641
Glutarate (pentanedioate)	Amino Acid	Lysine Metabolism	C0048 9	HMDB 00661
Glutathione, oxidized (GSSG)	Amino Acid	Glutathione Metabolism	C0012 7	HMDB 03337
Glutathione, reduced (GSH)	Amino Acid	Glutathione Metabolism	C0005 1	HMDB 00125
Glycerate	Carbohydrate	Glycolysis, Gluconeogenesis, and Pyruvate Metabolism	C0025 8	HMDB 00139
Glycerol	Lipid	Glycerolipid Metabolism	C0011 6	HMDB 00131

BIOCHEMICAL	SUPER_ PATHWAY	SUB_ PATHWAY	KEGG	HMDB _ID
Glycerol 3-phosphate	Lipid	Glycerolipid Metabolism	C00093	HMDB00126
Glycerophosphoethanolamine	Lipid	Phospholipid Metabolism	C01233	HMDB00114
Glycerophosphoglycerol	Lipid	Glycerolipid Metabolism	C03274	
Glycerophosphoinositol*	Lipid	Phospholipid Metabolism		
Glycerophosphorylcholine (GPC)	Lipid	Phospholipid Metabolism	C00670	HMDB00086
Glycine	Amino Acid	Glycine, Serine and Threonine Metabolism	C00037	HMDB00123
Glycosyl-N-palmitoyl-sphingosine	Lipid	Sphingolipid Metabolism		
Glycosyl-N-stearoyl-sphingosine	Lipid	Sphingolipid Metabolism		
Glycylleucine	Peptide	Dipeptide	C02155	HMDB00759
Glycylvaline	Peptide	Dipeptide		HMDB28854
Guanidinoacetate	Amino Acid	Creatine Metabolism	C00581	HMDB00128
Guanidinosuccinate	Amino Acid	Guanidino and Acetamido Metabolism	C03139	HMDB03157
Guanine	Nucleotide	Purine Metabolism, Guanine containing	C00242	HMDB00132
Guanosine	Nucleotide	Purine Metabolism, Guanine containing	C00387	HMDB00133
Guanosine 5'- monophosphate (5'-GMP)	Nucleotide	Purine Metabolism, Guanine containing	C00144	HMDB01397
Gulonic acid*	Cofactors and Vitamins	Ascorbate and Aldarate Metabolism		
Heme	Cofactors and Vitamins	Hemoglobin and Porphyrin Metabolism	C00032	HMDB03178

BIOCHEMICAL	SUPER_ PATHWAY	SUB_ PATHWAY	KEGG	HMDB _ID
Hexanoylcarnitine	Lipid	Fatty Acid Metabolism(Acyl Carnitine)		HMDB 00705
Hippurate	Xenobiotics	Benzoate Metabolism	C0158 6	HMDB 00714
Histamine	Amino Acid	Histidine Metabolism	C0038 8	HMDB 00870
Histidine	Amino Acid	Histidine Metabolism	C0013 5	HMDB 00177
Homoarginine	Amino Acid	Urea cycle; Arginine and Proline Metabolism	C0192 4	HMDB 00670
Homocitrulline	Amino Acid	Urea cycle; Arginine and Proline Metabolism	C0242 7	HMDB 00679
Hypotaurine	Amino Acid	Methionine, Cysteine, SAM and Taurine Metabolism	C0051 9	HMDB 00965
Hypoxanthine	Nucleotide	Purine Metabolism, (Hypo)Xanthine/I nosine containing	C0026 2	HMDB 00157
Imidazole lactate	Amino Acid	Histidine Metabolism	C0556 8	HMDB 02320
Imidazole propionate	Amino Acid	Histidine Metabolism		HMDB 02271
Indolelactate	Amino Acid	Tryptophan Metabolism	C0204 3	HMDB 00671
Inosine	Nucleotide	Purine Metabolism, (Hypo)Xanthine/I nosine containing	C0029 4	HMDB 00195
Isobar: fructose 1,6-diphosphate, glucose 1,6-diphosphate, myo- inositol 1,4 or 1,3-diphosphate	Carbohydra te	Glycolysis, Gluconeogenesis, and Pyruvate Metabolism		
Isobutyrylcarnitine	Amino Acid	Leucine, Isoleucine and Valine Metabolism		HMDB 00736
Isocitrate	Energy	TCA Cycle	C0031 1	HMDB 00193
Isoleucine	Amino Acid	Leucine, Isoleucine and	C0040 7	HMDB 00172

BIOCHEMICAL	SUPER_ PATHWAY Y	SUB_ PATHWAY	KEGG	HMDB _ID
		Valine Metabolism		
Isoleucylglycine	Peptide	Dipeptide		
Isovalerylcarnitine	Amino Acid	Leucine, Isoleucine and Valine Metabolism		HMDB 00688
Kynurenate	Amino Acid	Tryptophan Metabolism	C0171 7	HMDB 00715
Kynurenine	Amino Acid	Tryptophan Metabolism	C0032 8	HMDB 00684
Lactate	Carbohydra te	Glycolysis, Gluconeogenesis, and Pyruvate Metabolism	C0018 6	HMDB 00190
Lactosyl-N-palmitoyl-sphingosine	Lipid	Sphingolipid Metabolism		
Laurylcarnitine	Lipid	Fatty Acid Metabolism(Acyl Carnitine)		HMDB 02250
Leucine	Amino Acid	Leucine, Isoleucine and Valine Metabolism	C0012 3	HMDB 00687
Leucylglycine	Peptide	Dipeptide		
Lidocaine	Xenobiotics	Drug	D0035 8	HMDB 14426
Linoleoylcarnitine*	Lipid	Fatty Acid Metabolism(Acyl Carnitine)		HMDB 06469
Lysine	Amino Acid	Lysine Metabolism	C0004 7	HMDB 00182
Malate	Energy	TCA Cycle	C0014 9	HMDB 00156
Maleate	Lipid	Fatty Acid, Dicarboxylate	C0138 4	HMDB 00176
Malonate	Lipid	Fatty Acid Synthesis	C0038 3	HMDB 00691
Malonylcarnitine	Lipid	Fatty Acid Synthesis		HMDB 02095
Mannitol/sorbitol	Carbohydra te	Fructose, Mannose and Galactose Metabolism	C0150 7	HMDB 00247

BIOCHEMICAL	SUPER_ PATHWAY Y	SUB_ PATHWAY	KEGG	HMDB _ID
Mannose	Carbohydrate	Fructose, Mannose and Galactose Metabolism	C00159	HMDB00169
Margarate (17:0)	Lipid	Long Chain Fatty Acid		HMDB02259
Mead acid (20:3n9)	Lipid	Polyunsaturated Fatty Acid (n3 and n6)		HMDB10378
Metformin	Xenobiotics	Drug	C07151	HMDB01921
Methionine	Amino Acid	Methionine, Cysteine, SAM and Taurine Metabolism	C00073	HMDB00696
Methionine sulfone	Amino Acid	Methionine, Cysteine, SAM and Taurine Metabolism		
Methionine sulfoxide	Amino Acid	Methionine, Cysteine, SAM and Taurine Metabolism	C02989	HMDB02005
Methyl glucopyranoside (alpha + beta)	Xenobiotics	Food Component/Plant		
Methyl-4-hydroxybenzoate sulfate	Xenobiotics	Benzoate Metabolism		
Methylmalonate (MMA)	Lipid	Fatty Acid Metabolism (also BCAA Metabolism)	C02170	HMDB00202
Methylphosphate	Nucleotide	Purine and Pyrimidine Metabolism		HMDB61711
Methylsuccinate	Amino Acid	Leucine, Isoleucine and Valine Metabolism		HMDB01844
Myo-inositol	Lipid	Inositol Metabolism	C00137	HMDB00211
Myristoleoylcarnitine*	Lipid	Fatty Acid Metabolism(Acyl Carnitine)		
Myristoylcarnitine	Lipid	Fatty Acid Metabolism(Acyl Carnitine)		HMDB05066
N(1)-acetylspermine	Amino Acid	Polyamine Metabolism	C02567	HMDB01186

BIOCHEMICAL	SUPER_ PATHWAY Y	SUB_ PATHWAY	KEGG	HMDB _ID
N-(2-furoyl)glycine	Xenobiotics	Food Component/Plant		HMDB 00439
N-acetyl-aspartyl-glutamate (NAAG)	Amino Acid	Glutamate Metabolism	C1227 0	HMDB 01067
N-acetylalanine	Amino Acid	Alanine and Aspartate Metabolism	C0284 7	HMDB 00766
N-acetyllaiiin	Xenobiotics	Food Component/Plant		
N-acetylarginine	Amino Acid	Urea cycle; Arginine and Proline Metabolism	C0256 2	HMDB 04620
N-acetylaspartate (NAA)	Amino Acid	Alanine and Aspartate Metabolism	C0104 2	HMDB 00812
N-acetylcarnosine	Peptide	Dipeptide Derivative		HMDB 12881
N-acetylglucosaminylasparagine	Carbohydra te	Aminosugar Metabolism	C0454 0	HMDB 00489
N-acetylglutamate	Amino Acid	Glutamate Metabolism	C0062 4	HMDB 01138
N-acetylglutamine	Amino Acid	Glutamate Metabolism	C0271 6	HMDB 06029
N-acetylglycine	Amino Acid	Glycine, Serine and Threonine Metabolism		HMDB 00532
N-acetylhistidine	Amino Acid	Histidine Metabolism	C0299 7	HMDB 32055
N-acetylmethionine	Amino Acid	Methionine, Cysteine, SAM and Taurine Metabolism	C0271 2	HMDB 11745
N-acetylneuraminate	Carbohydra te	Aminosugar Metabolism	C0027 0	HMDB 00230
N-acetylputrescine	Amino Acid	Polyamine Metabolism	C0271 4	HMDB 02064
N-acetylserine	Amino Acid	Glycine, Serine and Threonine Metabolism		HMDB 02931
N-acetyltaurine	Amino Acid	Methionine, Cysteine, SAM and Taurine Metabolism		

BIOCHEMICAL	SUPER_ PATHWAY	SUB_ PATHWAY	KEGG	HMDB _ID
N-acetylthreonine	Amino Acid	Glycine, Serine and Threonine Metabolism		
N-delta-acetylornithine	Amino Acid	Urea cycle; Arginine and Proline Metabolism		
N-ethylglycinexylidide	Xenobiotics	Drug	C1656 1	HMDB 60656
N-formylmethionine	Amino Acid	Methionine, Cysteine, SAM and Taurine Metabolism	C0314 5	HMDB 01015
N-methylpipercolate	Xenobiotics	Chemical		
N-methylproline	Amino Acid	Urea cycle; Arginine and Proline Metabolism		
N-palmitoyl-sphinganine (d18:0/16:0)	Lipid	Sphingolipid Metabolism		HMDB 11760
N-palmitoyl-sphingosine (d18:1/16:0)	Lipid	Sphingolipid Metabolism		HMDB 04949
N1,N12-diacetylspermine	Amino Acid	Polyamine Metabolism	C0341 3	HMDB 02172
N1-Methyl-2-pyridone-5- carboxamide	Cofactors and Vitamins	Nicotinate and Nicotinamide Metabolism	C0584 2	HMDB 04193
N1-methyladenosine	Nucleotide	Purine Metabolism, Adenine containing	C0249 4	HMDB 03331
N2,N2-dimethylguanosine	Nucleotide	Purine Metabolism, Guanine containing		HMDB 04824
N2-acetyllysine/N6-acetyllysine	Amino Acid	Lysine Metabolism		
N6,N6,N6-trimethyllysine	Amino Acid	Lysine Metabolism	C0379 3	HMDB 01325
N6-succinyladenosine	Nucleotide	Purine Metabolism, Adenine containing	HMDB 00912	
Nicotinamide	Cofactors and Vitamins	Nicotinate and Nicotinamide Metabolism	C0015 3	HMDB 01406

BIOCHEMICAL	SUPER_	SUB_	KEGG	HMDB
	PATHWAY	PATHWAY		_ID
	Y			
Nicotinamide adenine dinucleotide (NAD⁺)	Cofactors and Vitamins	Nicotinate and Nicotinamide Metabolism	C00003	HMDB00902
Nicotinamide adenine dinucleotide reduced (NADH)	Cofactors and Vitamins	Nicotinate and Nicotinamide Metabolism	C00004	HMDB01487
Nonadecanoate (19:0)	Lipid	Long Chain Fatty Acid	C16535	HMDB00772
O-methylcatechol sulfate	Xenobiotics	Benzoate Metabolism		
BIOCHEMICAL	SUPER_	SUB_	KEGG	HMDB
	P	PATHWAY		_ID
	ATHWAY			
O-methyltyrosine	Amino Acid	Phenylalanine and Tyrosine Metabolism		
O-sulfo-L-tyrosine	Xenobiotics	Chemical		
Octanoylcarnitine	Lipid	Fatty Acid Metabolism(Acyl Carnitine)	C02838	HMDB00791
Oleamide	Lipid	Fatty Acid, Amide	C19670	HMDB02117
Oleoylcarnitine	Lipid	Fatty Acid Metabolism(Acyl Carnitine)		HMDB05065
Ophthalmate	Amino Acid	Glutathione Metabolism		HMDB05765
Ornithine	Amino Acid	Urea cycle; Arginine and Proline Metabolism	C00077	HMDB03374
Orotate	Nucleotide	Pyrimidine Metabolism, Orotate containing	C00295	HMDB00226
Orotidine	Nucleotide	Pyrimidine Metabolism, Orotate containing	C01103	HMDB00788
Oxalate (ethanedioate)	Cofactors and Vitamins	Ascorbate and Aldarate Metabolism	C00209	HMDB02329
Oxypurinol	Xenobiotics	Drug	D02365	HMDB00786
P-cresol sulfate	Amino Acid	Phenylalanine and Tyrosine Metabolism	C01468	HMDB11635

BIOCHEMICAL	SUPER_ PATHWAY Y	SUB_ PATHWAY	KEGG	HMDB _ID
P-cresol-glucuronide*	Amino Acid	Phenylalanine and Tyrosine Metabolism		HMDB 11686
Palmitate (16:0)	Lipid	Long Chain Fatty Acid	C0024 9	HMDB 00220
Palmitoyl dihydrosphingomyelin (d18:0/16:0)*	Lipid	Sphingolipid Metabolism		
Palmitoyl sphingomyelin (d18:1/16:0)	Lipid	Sphingolipid Metabolism		
Palmitoylcarnitine	Lipid	Fatty Acid Metabolism(Acyl Carnitine)	C0299 0	HMDB 00222
Pantothenate	Cofactors and Vitamins	Pantothenate and CoA Metabolism	C0086 4	HMDB 00210
Paraxanthine	Xenobiotics	Xanthine Metabolism	C1374 7	HMDB 01860
Phenol sulfate	Amino Acid	Phenylalanine and Tyrosine Metabolism	C0218 0	HMDB 60015
Phenylacetylglutamine	Amino Acid	Phenylalanine and Tyrosine Metabolism	C0414 8	HMDB 06344
Phenylalanine	Amino Acid	Phenylalanine and Tyrosine Metabolism	C0007 9	HMDB 00159
Phosphate	Energy	Oxidative Phosphorylation	C0000 9	HMDB 01429
Phosphoethanolamine	Lipid	Phospholipid Metabolism	C0034 6	HMDB 00224
Pipecolate	Amino Acid	Lysine Metabolism	C0040 8	HMDB 00070
Piperine	Xenobiotics	Food Component/Plant	C0388 2	HMDB 29377
Pro-hydroxy-pro	Amino Acid	Urea cycle; Arginine and Proline Metabolism		HMDB 06695
Proline	Amino Acid	Urea cycle; Arginine and Proline Metabolism	C0014 8	HMDB 00162
Propionylcarnitine	Lipid	Fatty Acid Metabolism (also	C0301 7	HMDB 00824

BIOCHEMICAL	SUPER_ PATHWAY Y	SUB_ PATHWAY	KEGG	HMDB _ID
		BCAA Metabolism)		
Propyl 4-hydroxybenzoate sulfate	Xenobiotics	Benzoate Metabolism		
Pseudoephedrine	Xenobiotics	Drug	C0276 5	HMDB 01943
Pseudouridine	Nucleotide	Pyrimidine Metabolism, Uracil containing	C0206 7	HMDB 00767
Putrescine	Amino Acid	Polyamine Metabolism	C0013 4	HMDB 01414
Pyridoxate	Cofactors and Vitamins	Vitamin B6 Metabolism	C0084 7	HMDB 00017
Pyroglutamine*	Amino Acid	Glutamate Metabolism		
Pyruvate	Carbohydra te	Glycolysis, Gluconeogenesis, and Pyruvate Metabolism	C0002 2	HMDB 00243
Quinate	Xenobiotics	Food Component/Plant	C0029 6	HMDB 03072
Quinolate	Cofactors and Vitamins	Nicotinate and Nicotinamide Metabolism	C0372 2	HMDB 00232
Ranitidine	Xenobiotics	Drug	D0042 2	HMDB 01930
Ribitol	Carbohydra te	Pentose Metabolism	C0047 4	HMDB 00508
Ribonate	Carbohydra te	Pentose Metabolism	C0168 5	HMDB 00867
S-adenosylhomocysteine (SAH)	Amino Acid	Methionine, Cysteine, SAM and Taurine Metabolism	C0002 1	HMDB 00939
S-adenosylmethionine (SAM)	Amino Acid	Methionine, Cysteine, SAM and Taurine Metabolism	C0001 9	HMDB 01185
S-methylcysteine	Amino Acid	Methionine, Cysteine, SAM and Taurine Metabolism		HMDB 02108
S-methylglutathione	Amino Acid	Glutathione Metabolism	C1134 7	

BIOCHEMICAL	SUPER_ PATHWAY	SUB_ PATHWAY	KEGG	HMDB _ID
S-nitrosoglutathione (GSNO)	Amino Acid	Glutathione Metabolism		HMDB 04645
Saccharin	Xenobiotics	Food Component/Plant	D0108 5	HMDB 29723
Sedoheptulose-7-phosphate	Carbohydrate	Pentose Phosphate Pathway	C0538 2	HMDB 01068
Serine	Amino Acid	Glycine, Serine and Threonine Metabolism	C0006 5	HMDB 00187
Serotonin	Amino Acid	Tryptophan Metabolism	C0078 0	HMDB 00259
Solanidine	Xenobiotics	Food Component/Plant	C0654 3	HMDB 03236
Spermidine	Amino Acid	Polyamine Metabolism	C0031 5	HMDB 01257
Spermine	Amino Acid	Polyamine Metabolism	C0075 0	HMDB 01256
Sphinganine	Lipid	Sphingolipid Metabolism	C0083 6	HMDB 00269
Sphingomyelin (d18:1/14:0, d16:1/16:0)*	Lipid	Sphingolipid Metabolism		
Sphingomyelin (d18:1/15:0, d16:1/17:0)*	Lipid	Sphingolipid Metabolism		
Sphingomyelin (d18:1/17:0, d17:1/18:0, d19:1/16:0)	Lipid	Sphingolipid Metabolism		
Sphingomyelin (d18:1/18:1, d18:2/18:0)	Lipid	Sphingolipid Metabolism		
Sphingomyelin (d18:1/20:0, d16:1/22:0)*	Lipid	Sphingolipid Metabolism		
Sphingomyelin (d18:1/20:1, d18:2/20:0)*	Lipid	Sphingolipid Metabolism		
Sphingomyelin (d18:1/21:0, d17:1/22:0, d16:1/23:0)*	Lipid	Sphingolipid Metabolism		
Sphingomyelin (d18:1/22:1, d18:2/22:0, d16:1/24:1)*	Lipid	Sphingolipid Metabolism		
Sphingomyelin (d18:1/24:1, d18:2/24:0)*	Lipid	Sphingolipid Metabolism		
Sphingomyelin (d18:2/16:0, d18:1/16:1)*	Lipid	Sphingolipid Metabolism		
Sphingomyelin (d18:2/23:0, d18:1/23:1, d17:1/24:1)*	Lipid	Sphingolipid Metabolism		
Sphingomyelin (d18:2/24:1, d18:1/24:2)*	Lipid	Sphingolipid Metabolism		

BIOCHEMICAL	SUPER_ PATHWAY	SUB_ PATHWAY	KEGG	HMDB _ID
Sphingosine	Lipid	Sphingolipid Metabolism	C00319	HMDB00252
Stachydrine	Xenobiotics	Food Component/Plant	C10172	HMDB04827
Stearate (18:0)	Lipid	Long Chain Fatty Acid	C01530	HMDB00827
Stearoyl sphingomyelin (d18:1/18:0)	Lipid	Sphingolipid Metabolism	C00550	HMDB01348
Stearoylcarnitine	Lipid	Fatty Acid Metabolism(Acyl Carnitine)		HMDB00848
Succinate	Energy	TCA Cycle	C00042	HMDB00254
Succinylcarnitine	Energy	TCA Cycle		
Sucrose	Carbohydrate	Disaccharides and Oligosaccharides	C00089	HMDB00258
Sulfate*	Xenobiotics	Chemical	C00059	HMDB01448
Taurine	Amino Acid	Methionine, Cysteine, SAM and Taurine Metabolism	C00245	HMDB00251
Theanine	Xenobiotics	Food Component/Plant	C01047	HMDB34365
Theobromine	Xenobiotics	Xanthine Metabolism	C07480	HMDB02825
Theophylline	Xenobiotics	Xanthine Metabolism	C07130	HMDB01889
Threonate	Cofactors and Vitamins	Ascorbate and Aldarate Metabolism	C01620	HMDB00943
Threonine	Amino Acid	Glycine, Serine and Threonine Metabolism	C00188	HMDB00167
Thymol sulfate	Xenobiotics	Food Component/Plant	C09908	HMDB01878
Tiglylcarnitine	Amino Acid	Leucine, Isoleucine and Valine Metabolism		HMDB02366
Trans-4-hydroxyproline	Amino Acid	Urea cycle; Arginine and Proline Metabolism	C01157	HMDB00725

BIOCHEMICAL	SUPER_ PATHWAY	SUB_ PATHWAY	KEGG	HMDB _ID
Trans-urocanate	Amino Acid	Histidine Metabolism	C00785	HMDB00301
Trigonelline (N'-methylnicotinate)	Cofactors and Vitamins	Nicotinate and Nicotinamide Metabolism	C01004	HMDB00875
Trimethylamine N-oxide	Lipid	Phospholipid Metabolism	C01104	HMDB00925
Tryptophan	Amino Acid	Tryptophan Metabolism	C00078	HMDB00929
Tryptophan betaine	Amino Acid	Tryptophan Metabolism	C09213	HMDB61115
Tyrosine	Amino Acid	Phenylalanine and Tyrosine Metabolism	C00082	HMDB00158
UDP-acetylglucosamine/galactosamine	Carbohydrate	Nucleotide Sugar		
Uracil	Nucleotide	Pyrimidine Metabolism, Uracil containing	C00106	HMDB00300
Urate	Nucleotide	Purine Metabolism, (Hypo)Xanthine/I nosine containing	C00366	HMDB00289
Urea	Amino Acid	Urea cycle; Arginine and Proline Metabolism	C00086	HMDB00294
Uridine	Nucleotide	Pyrimidine Metabolism, Uracil containing	C00299	HMDB00296
Uridine 5'-monophosphate (UMP)	Nucleotide	Pyrimidine Metabolism, Uracil containing	C00105	HMDB00288
Valine	Amino Acid	Leucine, Isoleucine and Valine Metabolism	C00183	HMDB00883
Valylleucine	Peptide	Dipeptide		
Xanthine	Nucleotide	Purine Metabolism, (Hypo)Xanthine/I nosine containing	C00385	HMDB00292

Appendix 3 Shared metabolites identified in the combined dataset of samples analysed through Metabolon® platforms (n=18 patients, n=72 tissue samples)

BIOCHEMICAL	SUPER_PATHWAY	SUB_PATHWAY	KEGG	HMDB_ID
Glutamine	Amino Acid	Glutamate Metabolism	C00064	HMDB00641
Tryptophan	Amino Acid	Tryptophan Metabolism	C00078	HMDB00929
Beta-alanine	Nucleotide	Pyrimidine Metabolism, Uracil containing	C00099	HMDB00056
Glutamate	Amino Acid	Glutamate Metabolism	C00025	HMDB00148
Histidine	Amino Acid	Histidine Metabolism	C00135	HMDB00177
Leucine	Amino Acid	Leucine, Isoleucine and Valine Metabolism	C00123	HMDB00687
Cholesterol	Lipid	Sterol	C00187	HMDB00067
Phenylalanine	Amino Acid	Phenylalanine and Tyrosine Metabolism	C00079	HMDB00159
Spermidine	Amino Acid	Polyamine Metabolism	C00315	HMDB01257
Creatinine	Amino Acid	Creatine Metabolism	C00791	HMDB00562
Cytidine	Nucleotide	Pyrimidine Metabolism, Cytidine containing	C00475	HMDB00089
Lactate	Carbohydrate	Glycolysis, Gluconeogenesis, and Pyruvate Metabolism	C00186	HMDB00190
Adenine	Nucleotide	Purine Metabolism, Adenine containing	C00147	HMDB00034
Adenosine	Nucleotide	Purine Metabolism, Adenine containing	C00212	HMDB00050
Adenosine 5'-diphosphoribose (ADP-ribose)	Cofactors and Vitamins	Nicotinate and Nicotinamide Metabolism	C00301	HMDB01178
Caffeine	Xenobiotics	Xanthine Metabolism	C07481	HMDB01847
Fructose	Carbohydrate	Fructose, Mannose and Galactose Metabolism	C00095	HMDB00660
Mannose	Carbohydrate	Fructose, Mannose and Galactose Metabolism	C00159	HMDB00169

BIOCHEMICAL	SUPER_PATHWAY	SUB_PATHWAY	KEGG	HMDB_ID
Gluconate	Xenobiotics	Food Component/Plant	C00257	HMDB00625
Hypotaurine	Amino Acid	Methionine, Cysteine, SAM and Taurine Metabolism	C00519	HMDB00965
Nicotinamide	Cofactors and Vitamins	Nicotinate and Nicotinamide Metabolism	C00153	HMDB01406
Spermine	Amino Acid	Polyamine Metabolism	C00750	HMDB01256
Uracil	Nucleotide	Pyrimidine Metabolism, Uracil containing	C00106	HMDB00300
Uridine	Nucleotide	Pyrimidine Metabolism, Uracil containing	C00299	HMDB00296
Margarate (17:0)	Lipid	Long Chain Fatty Acid		HMDB02259
Inosine	Nucleotide	Purine Metabolism, (Hypo)Xanthine/Inosine containing	C00294	HMDB00195
Isoleucine	Amino Acid	Leucine, Isoleucine and Valine Metabolism	C00407	HMDB00172
Alanine	Amino Acid	Alanine and Aspartate Metabolism	C00041	HMDB00161
Threonine	Amino Acid	Glycine, Serine and Threonine Metabolism	C00188	HMDB00167
Tyrosine	Amino Acid	Phenylalanine and Tyrosine Metabolism	C00082	HMDB00158
Lysine	Amino Acid	Lysine Metabolism	C00047	HMDB00182
Malate	Energy	TCA Cycle	C00149	HMDB00156
Palmitate (16:0)	Lipid	Long Chain Fatty Acid	C00249	HMDB00220
Stearate (18:0)	Lipid	Long Chain Fatty Acid	C01530	HMDB00827
Putrescine	Amino Acid	Polyamine Metabolism	C00134	HMDB01414
Gamma-aminobutyrate (GABA)	Amino Acid	Glutamate Metabolism	C00334	HMDB00112
5-methylthioadenosine (MTA)	Amino Acid	Polyamine Metabolism	C00170	HMDB01173
Succinate	Energy	TCA Cycle	C00042	HMDB00254

BIOCHEMICAL	SUPER_PATHWAY	SUB_PATHWAY	KEGG	HMDB_ID
Ornithine	Amino Acid	Urea cycle; Arginine and Proline Metabolism	C00077	HMDB03374
5-oxoproline	Amino Acid	Glutathione Metabolism	C01879	HMDB00267
Pantothenate	Cofactors and Vitamins	Pantothenate and CoA Metabolism	C00864	HMDB00210
Alpha-tocopherol	Cofactors and Vitamins	Tocopherol Metabolism	C02477	HMDB01893
Citrate	Energy	TCA Cycle	C00158	HMDB00094
3-aminoisobutyrate	Nucleotide	Pyrimidine Metabolism, Thymine containing	C05145	HMDB03911
Glycerate	Carbohydrate	Glycolysis, Gluconeogenesis, and Pyruvate Metabolism	C00258	HMDB00139
Guanosine	Nucleotide	Purine Metabolism, Guanine containing	C00387	HMDB00133
Phosphoethanolamine	Lipid	Phospholipid Metabolism	C00346	HMDB00224
Urate	Nucleotide	Purine Metabolism, (Hypo)Xanthine/Inosine containing	C00366	HMDB00289
Arginine	Amino Acid	Urea cycle; Arginine and Proline Metabolism	C00062	HMDB00517
Fumarate	Energy	TCA Cycle	C00122	HMDB00134
Serine	Amino Acid	Glycine, Serine and Threonine Metabolism	C00065	HMDB00187
Valine	Amino Acid	Leucine, Isoleucine and Valine Metabolism	C00183	HMDB00883
Urea	Amino Acid	Urea cycle; Arginine and Proline Metabolism	C00086	HMDB00294
Gamma-glutamylcysteine	Peptide	Gamma-glutamyl Amino Acid	C00669	HMDB01049
Proline	Amino Acid	Urea cycle; Arginine and Proline Metabolism	C00148	HMDB00162
Glutathione, reduced (GSH)	Amino Acid	Glutathione Metabolism	C00051	HMDB00125
Flavin adenine dinucleotide (FAD)	Cofactors and Vitamins	Riboflavin Metabolism	C00016	HMDB01248
Serotonin	Amino Acid	Tryptophan Metabolism	C00780	HMDB00259

BIOCHEMICAL	SUPER_PATHWAY	SUB_PATHWAY	KEGG	HMDB_ID
Cytidine 5'-monophosphate (5'-CMP)	Nucleotide	Pyrimidine Metabolism, Cytidine containing	C00055	HMDB00095
Gamma-glutamylglutamine	Peptide	Gamma-glutamyl Amino Acid	C05283	HMDB1738
Guanosine 5'-monophosphate (5'-GMP)	Nucleotide	Purine Metabolism, Guanine containing	C00144	HMDB01397
Adenosine 5'-diphosphate (ADP)	Nucleotide	Purine Metabolism, Adenine containing	C00008	HMDB01341
Hypoxanthine	Nucleotide	Purine Metabolism, (Hypo)Xanthine/Inosine containing	C00262	HMDB0157
Xanthine	Nucleotide	Purine Metabolism, (Hypo)Xanthine/Inosine containing	C00385	HMDB0292
2-aminoadipate	Amino Acid	Lysine Metabolism	C00956	HMDB0510
4-acetamidophenol	Xenobiotics	Drug	C06804	HMDB01859
Isocitrate	Energy	TCA Cycle	C00311	HMDB0193
Glycerol	Lipid	Glycerolipid Metabolism	C00116	HMDB0131
Kynurenine	Amino Acid	Tryptophan Metabolism	C00328	HMDB0684
6-phosphogluconate	Carbohydrate	Pentose Phosphate Pathway	C00345	HMDB01316
Carnitine	Lipid	Carnitine Metabolism	C00318	HMDB0062
Choline	Lipid	Phospholipid Metabolism	C00114	HMDB0097
N1-methyladenosine	Nucleotide	Purine Metabolism, Adenine containing	C02494	HMDB03331
Hippurate	Xenobiotics	Benzoate Metabolism	C01586	HMDB0714
Ribitol	Carbohydrate	Pentose Metabolism	C00474	HMDB0508
Glycerophosphoryl choline (GPC)	Lipid	Phospholipid Metabolism	C00670	HMDB0086
Sphingosine	Lipid	Sphingolipid Metabolism	C00319	HMDB0252
Dihomo-linoleate (20:2n6)	Lipid	Polyunsaturated Fatty Acid (n3 and n6)	C16525	HMDB05060

BIOCHEMICAL	SUPER_PATHWAY	SUB_PATHWAY	KEGG	HMDB_ID
Theobromine	Xenobiotics	Xanthine Metabolism	C07480	HMDB02825
Biochemical	SUPER_PATHWAY	SUB_PATHWAY	KEGG	HMDB_ID
Acetylcholine	Lipid	Neurotransmitter		
1-oleoyl-GPS (18:1)	Lipid	Lysolipid		
1-stearoyl-GPI (18:0)	Lipid	Lysolipid		HMDB61696
Stearoyl sphingomyelin (d18:1/18:0)	Lipid	Sphingolipid Metabolism	C00550	HMDB01348
Glucose	Carbohydrate	Glycolysis, Gluconeogenesis, and Pyruvate Metabolism	C00031	HMDB01122
1,5-anhydroglucitol (1,5-AG)	Carbohydrate	Glycolysis, Gluconeogenesis, and Pyruvate Metabolism	C07326	HMDB02712
N-acetylaspartate (NAA)	Amino Acid	Alanine and Aspartate Metabolism	C01042	HMDB00812
1-linoleoylglycerol (18:2)	Lipid	Monoacylglycerol		
3-indoxyl sulfate	Amino Acid	Tryptophan Metabolism		HMDB00682
Creatine	Amino Acid	Creatine Metabolism	C00300	HMDB00064
Glutathione, oxidized (GSSG)	Amino Acid	Glutathione Metabolism	C00127	HMDB03337
Threonate	Cofactors and Vitamins	Ascorbate and Aldarate Metabolism	C01620	HMDB00943
Nicotinamide adenine dinucleotide reduced (NADH)	Cofactors and Vitamins	Nicotinate and Nicotinamide Metabolism	C00004	HMDB01487
Androsterone sulfate	Lipid	Steroid		HMDB02759
Acetylcarnitine	Lipid	Fatty Acid Metabolism(Acyl Carnitine)	C02571	HMDB00201
Hexanoylcarnitine	Lipid	Fatty Acid Metabolism(Acyl Carnitine)		HMDB00705
Adenosine 5'-monophosphate (AMP)	Nucleotide	Purine Metabolism, Adenine containing	C00020	HMDB00045

BIOCHEMICAL	SUPER_PATHWAY	SUB_PATHWAY	KEGG	HMDB_ID
Guanine	Nucleotide	Purine Metabolism, Guanine containing	C0024 2	HMDB0132
N-acetylneuraminate	Carbohydrate	Aminosugar Metabolism	C0027 0	HMDB0230
Butyrylcarnitine	Lipid	Fatty Acid Metabolism (also BCAA Metabolism)	C0286 2	HMDB02013
Dehydroisoandrosterone sulfate (DHEA-S)	Lipid	Steroid	C0455 5	HMDB01032
Propionylcarnitine	Lipid	Fatty Acid Metabolism (also BCAA Metabolism)	C0301 7	HMDB00824
Docosapentaenoate (n3 DPA; 22:5n3)	Lipid	Polyunsaturated Fatty Acid (n3 and n6)	C1651 3	HMDB01976
Phenol sulfate	Amino Acid	Phenylalanine and Tyrosine Metabolism	C0218 0	HMDB60015
1-linoleoyl-GPE (18:2)*	Lipid	Lysolipid		HMDB11507
2-hydroxyacetaminophen sulfate*	Xenobiotics	Drug		
1-palmitoleoyl-GPC (16:1)*	Lipid	Lysolipid		HMDB10383
Isobutyrylcarnitine	Amino Acid	Leucine, Isoleucine and Valine Metabolism		HMDB00736
Pseudouridine	Nucleotide	Pyrimidine Metabolism, Uracil containing	C0206 7	HMDB00767
Glutamate, gamma-methyl ester	Amino Acid	Glutamate Metabolism		
Eicosenoate (20:1)	Lipid	Long Chain Fatty Acid		HMDB02231
Octanoylcarnitine	Lipid	Fatty Acid Metabolism(Acyl Carnitine)	C0283 8	HMDB00791
1-palmitoyl-GPC (16:0)	Lipid	Lysolipid		HMDB10382
1-stearoyl-GPC (18:0)	Lipid	Lysolipid		HMDB10384
1-arachidonoyl-GPI (20:4)*	Lipid	Lysolipid		HMDB61690
3-(cystein-S-yl)acetaminophen*	Xenobiotics	Drug		

BIOCHEMICAL	SUPER_PATHWAY	SUB_PATHWAY	KEGG	HMDB_ID
Choline phosphate	Lipid	Phospholipid Metabolism	C00588	HMDB01565
Glycylleucine	Peptide	Dipeptide	C02155	HMDB00759
Isovalerylcarnitine	Amino Acid	Leucine, Isoleucine and Valine Metabolism		HMDB00688
Stearoylcarnitine	Lipid	Fatty Acid Metabolism(Acyl Carnitine)		HMDB00848
Cytidine-5'-diphosphoethanolamine	Lipid	Phospholipid Metabolism	C00570	HMDB01564
Cytidine 5'-diphosphocholine	Lipid	Phospholipid Metabolism	C00307	HMDB01413
1-linoleoyl-GPC (18:2)	Lipid	Lysolipid	C04100	HMDB10386
4-hydroxybutyrate (GHB)	Lipid	Fatty Acid, Monohydroxy	C00989	HMDB00710
Ophthalmate	Amino Acid	Glutathione Metabolism		HMDB005765
Phenylacetylglutamine	Amino Acid	Phenylalanine and Tyrosine Metabolism	C04148	HMDB006344
Cysteine-glutathione disulfide	Amino Acid	Glutathione Metabolism		HMDB00656
Oleoylcarnitine	Lipid	Fatty Acid Metabolism(Acyl Carnitine)		HMDB005065
1-arachidonoyl-GPE (20:4)*	Lipid	Lysolipid		HMDB101517
2-palmitoyl-GPC (16:0)*	Lipid	Lysolipid		HMDB601702
1-palmitoyl-GPI (16:0)*	Lipid	Lysolipid		HMDB601695
4-hydroxyhippurate	Xenobiotics	Benzoate Metabolism		HMDB103678
1-oleoyl-GPE (18:1)	Lipid	Lysolipid		HMDB101506
1-palmitoyl-GPE (16:0)	Lipid	Lysolipid		HMDB101503
Lidocaine	Xenobiotics	Drug	D00358	HMDB104426
N-acetyl-aspartyl-glutamate (NAAG)	Amino Acid	Glutamate Metabolism	C12270	HMDB01067
Dihomo-linolenate (20:3n3 or n6)	Lipid	Polyunsaturated Fatty Acid (n3 and n6)	C03242	HMDB002925

BIOCHEMICAL	SUPER_PATHWAY	SUB_PATHWAY	KEGG	HMDB_ID
P-cresol sulfate	Amino Acid	Phenylalanine and Tyrosine Metabolism	C01468	HMDB1635
1-oleoyl-GPI (18:1)*	Lipid	Lysolipid		
Gamma-glutamylglutamate	Peptide	Gamma-glutamyl Amino Acid	C05282	HMDB1737
Deoxycarnitine	Lipid	Carnitine Metabolism	C01181	HMDB01161
Succinylcarnitine	Energy	TCA Cycle		
Methylphosphate	Nucleotide	Purine and Pyrimidine Metabolism		HMDB61711
Tryptophan betaine	Amino Acid	Tryptophan Metabolism	C09213	HMDB61115
4-androsten-3beta,17beta-diol disulfate (1)	Lipid	Steroid	C04295	HMDB03818
2-hydroxyglutarate	Lipid	Fatty Acid, Dicarboxylate	C02630	HMDB0606
Glycerophosphoethanolamine	Lipid	Phospholipid Metabolism	C01233	HMDB00114
4-acetaminophen sulfate	Xenobiotics	Drug	C06804	HMDB59911
Docosapentaenoate (n6 DPA; 22:5n6)	Lipid	Polyunsaturated Fatty Acid (n3 and n6)	C16513	HMDB01976
N-acetylputrescine	Amino Acid	Polyamine Metabolism	C02714	HMDB02064
Palmitoyl sphingomyelin (d18:1/16:0)	Lipid	Sphingolipid Metabolism		
1-(1-enyl-palmitoyl)-GPE (P-16:0)*	Lipid	Lysoplasmalogen		
1-(1-enyl-stearoyl)-GPE (P-18:0)*	Lipid	Lysolipid		
6-sialyl-N-acetyllactosamine	Carbohydrate	Aminosugar Metabolism		HMDB06584
Heme	Cofactors and Vitamins	Hemoglobin and Porphyrin Metabolism	C00032	HMDB03178
3-hydroxybutyrylcarnitine (1)	Lipid	Fatty Acid Metabolism(Acyl Carnitine)		HMDB13127
1-(1-enyl-oleoyl)-GPE (P-18:1)*	Lipid	Lysolipid		

BIOCHEMICAL	SUPER_PATHWAY	SUB_PATHWAY	KEGG	HMDB_ID
1-stearoyl-GPS (18:0)*	Lipid	Lysolipid		
1-palmitoyl-GPG (16:0)*	Lipid	Lysolipid		

Reference

1. Statistics OfN. Cancer Registration Statistics, England Statistical bulletins. 2015.
2. UK CR. Prostate cancer statistics [Available from: <http://www.cancerresearchuk.org/health-professional/prostate-cancer-statistics - heading-Zero>].
3. Uk CR. Prostate Cancer (C61), Average Number of New Cases per Year and Age-Specific Incidence Rates, Males, UK, 2011-2013 [Available from: <http://www.cancerresearchuk.org/health-professional/cancer-statistics/statistics-by-cancer-type/prostate-cancer/incidence - heading-One>].
4. [cited June 2013].
5. Waterhouse J, Muir, C.S.,Correa, P.,Powell, J. Cancer Incidence in Five Continents: IARC Scientific Publications; 1976.
6. Melia J, Moss S. Survey of the rate of PSA testing in general practice. *British journal of cancer*. 2001;85(5):656-7.
7. Brewster DH, Fraser LA, Harris V, Black RJ. Rising incidence of prostate cancer in Scotland: increased risk or increased detection? *BJU international*. 2000;85(4):463-72; discussion 72-3.
8. Pashayan N, Powles J, Brown C, Duffy SW. Incidence trends of prostate cancer in East Anglia, before and during the era of PSA diagnostic testing. *British journal of cancer*. 2006;95(3):398-400.
9. Lane JA, Hamdy FC, Martin RM, Turner EL, Neal DE, Donovan JL. Latest results from the UK trials evaluating prostate cancer screening and treatment: the CAP and ProtecT studies. *European journal of cancer (Oxford, England : 1990)*. 2010;46(17):3095-101.
10. Williams N, Hughes LJ, Turner EL, Donovan JL, Hamdy FC, Neal DE, et al. Prostate-specific antigen testing rates remain low in UK general practice: a cross-sectional study in six English cities. *BJU international*. 2011;108(9):1402-8.
11. Van Neste L, Hendriks RJ, Dijkstra S, Trooskens G, Cornel EB, Jannink SA, et al. Detection of High-grade Prostate Cancer Using a Urinary Molecular Biomarker-Based Risk Score. *European urology*. 2016.
12. Salido-Guadarrama AI, Morales-Montor JG, Rangel-Escareno C, Langley E, Peralta-Zaragoza O, Cruz Colin JL, et al. Urinary microRNA-based signature improves accuracy of detection of clinically relevant prostate cancer within the prostate-specific antigen grey zone. *Molecular medicine reports*. 2016.
13. Hendriks RJ, Dijkstra S, Jannink SA, Steffens MG, van Oort IM, Mulders PF, et al. Comparative analysis of prostate cancer specific biomarkers PCA3 and ERG in whole urine, urinary sediments and exosomes. *Clinical chemistry and laboratory medicine*. 2016;54(3):483-92.
14. McKiernan J, Donovan MJ, O'Neill V, Bentink S, Noerholm M, Belzer S, et al. A Novel Urine Exosome Gene Expression Assay to Predict High-grade Prostate Cancer at Initial Biopsy. *JAMA oncology*. 2016.
15. Rigau M, Oliván M, Garcia M, Sequeiros T, Montes M, Colas E, et al. The present and future of prostate cancer urine biomarkers. *International journal of molecular sciences*. 2013;14(6):12620-49.

16. Hodge KK, McNeal JE, Terris MK, Stamey TA. Random systematic versus directed ultrasound guided transrectal core biopsies of the prostate. *The Journal of urology*. 1989;142(1):71-4; discussion 4-5.
17. Takenaka A, Hara R, Ishimura T, Fujii T, Jo Y, Nagai A, et al. A prospective randomized comparison of diagnostic efficacy between transperineal and transrectal 12-core prostate biopsy. *Prostate cancer and prostatic diseases*. 2008;11(2):134-8.
18. Hara R, Jo Y, Fujii T, Kondo N, Yokoyama T, Miyaji Y, et al. Optimal approach for prostate cancer detection as initial biopsy: prospective randomized study comparing transperineal versus transrectal systematic 12-core biopsy. *Urology*. 2008;71(2):191-5.
19. Edge SB, Compton CC. The American Joint Committee on Cancer: the 7th edition of the AJCC cancer staging manual and the future of TNM. *Annals of surgical oncology*. 2010;17(6):1471-4.
20. Gleason DF, Mellinger GT. Prediction of prognosis for prostatic adenocarcinoma by combined histological grading and clinical staging. *The Journal of urology*. 1974;111(1):58-64.
21. Epstein JI, Allsbrook WC, Jr., Amin MB, Egevad LL. The 2005 International Society of Urological Pathology (ISUP) Consensus Conference on Gleason Grading of Prostatic Carcinoma. *Am J Surg Pathol*. 2005;29(9):1228-42.
22. Billis A, Guimaraes MS, Freitas LL, Meirelles L, Magna LA, Ferreira U. The impact of the 2005 international society of urological pathology consensus conference on standard Gleason grading of prostatic carcinoma in needle biopsies. *The Journal of urology*. 2008;180(2):548-52; discussion 52-3.
23. Humphrey PA, Moch H, Cubilla AL, Ulbright TM, Reuter VE. The 2016 WHO Classification of Tumours of the Urinary System and Male Genital Organs-Part B: Prostate and Bladder Tumours. *European urology*. 2016.
24. Chen N, Zhou Q. The evolving Gleason grading system. *Chinese journal of cancer research = Chung-kuo yen cheng yen chiu*. 2016;28(1):58-64.
25. Epstein JI, Egevad L, Amin MB, Delahunt B, Srigley JR, Humphrey PA. The 2014 International Society of Urological Pathology (ISUP) Consensus Conference on Gleason Grading of Prostatic Carcinoma: Definition of Grading Patterns and Proposal for a New Grading System. *Am J Surg Pathol*. 2016;40(2):244-52.
26. Johansson JE, Holmberg L, Johansson S, Bergstrom R, Adami HO. Fifteen-year survival in prostate cancer. A prospective, population-based study in Sweden. *JAMA : the journal of the American Medical Association*. 1997;277(6):467-71.
27. Klotz L. Active surveillance for prostate cancer: for whom? *Journal of clinical oncology : official journal of the American Society of Clinical Oncology*. 2005;23(32):8165-9.
28. Sanda MG, Dunn RL, Michalski J, Sandler HM, Northouse L, Hembroff L, et al. Quality of life and satisfaction with outcome among prostate-cancer survivors. *The New England journal of medicine*. 2008;358(12):1250-61.
29. Gleason DF, Mellinger GT. Prediction of prognosis for prostatic adenocarcinoma by combined histological grading and clinical staging. 1974. *The Journal of urology*. 2002;167(2 Pt 2):953-8; discussion 9.
30. Dall'Era MA, Cooperberg MR, Chan JM, Davies BJ, Albertsen PC, Klotz LH, et al. Active surveillance for early-stage prostate cancer: review of the current literature. *Cancer*. 2008;112(8):1650-9.

31. Kattan MW, Eastham JA, Wheeler TM, Maru N, Scardino PT, Erbersdobler A, et al. Counseling men with prostate cancer: a nomogram for predicting the presence of small, moderately differentiated, confined tumors. *The Journal of urology*. 2003;170(5):1792-7.
32. Bettencourt-Silva J, De La Iglesia B, Donell S, Rayward-Smith V. On creating a patient-centric database from multiple Hospital Information Systems. *Methods of information in medicine*. 2012;51(3):210-20.
33. Ohori M, Kattan M, Scardino PT, Wheeler TM. Radical prostatectomy for carcinoma of the prostate. *Modern pathology : an official journal of the United States and Canadian Academy of Pathology, Inc.* 2004;17(3):349-59.
34. Gandaglia G, Sammon JD, Chang SL, Choueiri TK, Hu JC, Karakiewicz PI, et al. Comparative effectiveness of robot-assisted and open radical prostatectomy in the postdissemination era. *Journal of clinical oncology : official journal of the American Society of Clinical Oncology*. 2014;32(14):1419-26.
35. Abdollah F, Sood A, Sammon JD, Hsu L, Beyer B, Moschini M, et al. Long-term cancer control outcomes in patients with clinically high-risk prostate cancer treated with robot-assisted radical prostatectomy: results from a multi-institutional study of 1100 patients. *European urology*. 2015;68(3):497-505.
36. Ramirez D, Zargar H, Caputo P, Kaouk JH. Robotic-assisted laparoscopic prostatectomy: An update on functional and oncologic outcomes, techniques, and advancements in technology. *Journal of Surgical Oncology*. 2015;112(7):746-52.
37. Hodson R. Small organ, big reach. *Nature*. 2015;528(7582):S118-9.
38. Warburg O PK, Negelein E. Über den Stoffwechsel von Tumoren. 1924; 152: 319-44. *Biochem Z* 1924;152:319-44.
39. Vander Heiden MG, Cantley LC, Thompson CB. Understanding the Warburg Effect: The Metabolic Requirements of Cell Proliferation. *Science*. 2009;324(5930):1029-33.
40. Costello LC, Franklin RB. A comprehensive review of the role of zinc in normal prostate function and metabolism; and its implications in prostate cancer. *Archives of Biochemistry and Biophysics*.
41. Costello LC, Franklin RB. Citrate metabolism of normal and malignant prostate epithelial cells. *Urology*. 1997;50(1):3-12.
42. Costello LC, Franklin RB, Narayan P. Citrate in the diagnosis of prostate cancer. *Prostate*. 1999;38(3):237-45.
43. Costello LC, Franklin RB. Novel role of zinc in the regulation of prostate citrate metabolism and its implications in prostate cancer. *Prostate*. 1998;35(4):285-96.
44. Costello LC, Franklin RB, Liu Y, Kennedy MC. Zinc causes a shift toward citrate at equilibrium of the m-aconitase reaction of prostate mitochondria. *Journal of inorganic biochemistry*. 2000;78(2):161-5.
45. Costello LC, Franklin RB. 'Why do tumour cells glycolyse?': from glycolysis through citrate to lipogenesis. *Molecular and cellular biochemistry*. 2005;280(1-2):1-8.
46. Singh KK, Desouki MM, Franklin RB, Costello LC. Mitochondrial aconitase and citrate metabolism in malignant and nonmalignant human prostate tissues. *Mol Cancer*. 2006;5:14.
47. Campbell PN. Principles of biochemistry second edition, by A L Lehninger, D L Nelson and M M Cox. Pp 1013. Worth, New York. 1993. £30 ISBN 0-87901-500-4. *Biochemical Education*. 1993;21(2):114-.

48. Martinez-Balibrea E, Plasencia C, Gines A, Martinez-Cardus A, Musulen E, Aguilera R, et al. A proteomic approach links decreased pyruvate kinase M2 expression to oxaliplatin resistance in patients with colorectal cancer and in human cell lines. *Molecular cancer therapeutics*. 2009;8(4):771-8.
49. Yamamoto T, Seino Y, Fukumoto H, Koh G, Yano H, Inagaki N, et al. Over-expression of facilitative glucose transporter genes in human cancer. *Biochemical and biophysical research communications*. 1990;170(1):223-30.
50. Joost HG, Thorens B. The extended GLUT-family of sugar/polyol transport facilitators: nomenclature, sequence characteristics, and potential function of its novel members (review). *Molecular membrane biology*. 2001;18(4):247-56.
51. Medina RA, Owen GI. Glucose transporters: expression, regulation and cancer. *Biological research*. 2002;35(1):9-26.
52. Haber RS, Rathana A, Weiser KR, Pritsker A, Itzkowitz SH, Bodian C, et al. GLUT1 glucose transporter expression in colorectal carcinoma: a marker for poor prognosis. *Cancer*. 1998;83(1):34-40.
53. Younes M, Brown RW, Stephenson M, Gondo M, Cagle PT. Overexpression of Glut1 and Glut3 in stage I nonsmall cell lung carcinoma is associated with poor survival. *Cancer*. 1997;80(6):1046-51.
54. Reinicke K, Sotomayor P, Cisterna P, Delgado C, Nualart F, Godoy A. Cellular distribution of Glut-1 and Glut-5 in benign and malignant human prostate tissue. *Journal of cellular biochemistry*. 2012;113(2):553-62.
55. Stewart GD, Gray K, Pennington CJ, Edwards DR, Riddick AC, Ross JA, et al. Analysis of hypoxia-associated gene expression in prostate cancer: lysyl oxidase and glucose transporter-1 expression correlate with Gleason score. *Oncology reports*. 2008;20(6):1561-7.
56. Liu Y. Fatty acid oxidation is a dominant bioenergetic pathway in prostate cancer. *Prostate cancer and prostatic diseases*. 2006;9(3):230-4.
57. Trock BJ. Application of metabolomics to prostate cancer. *Urologic oncology*. 2011;29(5):572-81.
58. Lushchak OV, Piroddi M, Galli F, Lushchak VI. Aconitase post-translational modification as a key in linkage between Krebs cycle, iron homeostasis, redox signaling, and metabolism of reactive oxygen species. *Redox Rep*. 2014;19(1):8-15.
59. Hurd TR, Collins Y, Abakumova I, Chouchani ET, Baranowski B, Fearnley IM, et al. Inactivation of pyruvate dehydrogenase kinase 2 by mitochondrial reactive oxygen species. *J Biol Chem*. 2012;287(42):35153-60.
60. Owen OE, Kalhan SC, Hanson RW. The key role of anaplerosis and cataplerosis for citric acid cycle function. *J Biol Chem*. 2002;277(34):30409-12.
61. Heath DF. The redistribution of carbon label by the reactions involved in glycolysis, gluconeogenesis and the tricarboxylic acid cycle in rat liver. *The Biochemical journal*. 1968;110(2):313-35.
62. Curi R, Newsholme P, Newsholme EA. Metabolism of pyruvate by isolated rat mesenteric lymphocytes, lymphocyte mitochondria and isolated mouse macrophages. *Biochemical Journal*. 1988;250(2):383-8.
63. Anastasiou D, Cantley LC. Breathless cancer cells get fat on glutamine. *Cell research*. 2012;22(3):443-6.
64. Chen JQ, Russo J. Dysregulation of glucose transport, glycolysis, TCA cycle and glutaminolysis by oncogenes and tumor suppressors in cancer cells. *Biochimica et biophysica acta*. 2012;1826(2):370-84.

65. Santos CR, Schulze A. Lipid metabolism in cancer. *FEBS J.* 2012;279(15):2610-23.
66. Rysman E, Brusselmans K, Scheys K, Timmermans L, Derua R, Munck S, et al. De novo lipogenesis protects cancer cells from free radicals and chemotherapeutics by promoting membrane lipid saturation. *Cancer research.* 2010;70(20):8117-26.
67. Ramirez de Molina A, Rodriguez-Gonzalez A, Gutierrez R, Martinez-Pineiro L, Sanchez J, Bonilla F, et al. Overexpression of choline kinase is a frequent feature in human tumor-derived cell lines and in lung, prostate, and colorectal human cancers. *Biochemical and biophysical research communications.* 2002;296(3):580-3.
68. Bertilsson H, Tessem MB, Flatberg A, Viset T, Gribbestad I, Angelsen A, et al. Changes in gene transcription underlying the aberrant citrate and choline metabolism in human prostate cancer samples. *Clinical cancer research : an official journal of the American Association for Cancer Research.* 2012;18(12):3261-9.
69. Hager MH, Solomon KR, Freeman MR. The role of cholesterol in prostate cancer. *Curr Opin Clin Nutr Metab Care.* 2006;9(4):379-85.
70. Gray-Bablin J, Rao S, Keyomarsi K. Lovastatin induction of cyclin-dependent kinase inhibitors in human breast cells occurs in a cell cycle-independent fashion. *Cancer research.* 1997;57(4):604-9.
71. Yokomizo A, Shiota M, Kashiwagi E, Kuroiwa K, Tatsugami K, Inokuchi J, et al. Statins reduce the androgen sensitivity and cell proliferation by decreasing the androgen receptor protein in prostate cancer cells. *Prostate.* 2011;71(3):298-304.
72. Wang T, Seah S, Loh X, Chan CW, Hartman M, Goh BC, et al. Simvastatin-induced breast cancer cell death and deactivation of PI3K/Akt and MAPK/ERK signalling are reversed by metabolic products of the mevalonate pathway. *Oncotarget.* 2016;7(3):2532-44.
73. Dale KM, Coleman CI, Henyan NN, Kluger J, White CM. Statins and cancer risk: a meta-analysis. *JAMA : the journal of the American Medical Association.* 2006;295(1):74-80.
74. Raval AD, Thakker D, Negi H, Vyas A, Salkini MW. Association between statins and clinical outcomes among men with prostate cancer: a systematic review and meta-analysis. *Prostate cancer and prostatic diseases.* 2016;19(2):151-62.
75. Weiss L, Hoffmann GE, Schreiber R, Andres H, Fuchs E, Korber E, et al. Fatty-acid biosynthesis in man, a pathway of minor importance. Purification, optimal assay conditions, and organ distribution of fatty-acid synthase. *Biological chemistry Hoppe-Seyler.* 1986;367(9):905-12.
76. Menendez JA, Lupu R. Fatty acid synthase and the lipogenic phenotype in cancer pathogenesis. *Nature reviews Cancer.* 2007;7(10):763-77.
77. Berg JM TJ, Stryer L. *Fatty Acids Are Key Constituents of Lipids.* 5th edition ed2002.
78. Menendez JA, Lupu R. Fatty acid synthase and the lipogenic phenotype in cancer pathogenesis. *Nature reviews Cancer.* 2007;7(10):763-77.
79. Hopperton KE, Duncan RE, Bazinet RP, Archer MC. Fatty acid synthase plays a role in cancer metabolism beyond providing fatty acids for phospholipid synthesis or sustaining elevations in glycolytic activity. *Experimental cell research.* 2014;320(2):302-10.

80. Swinnen JV, Vanderhoydonc F, Elgamal AA, Eelen M, Vercaeren I, Joniau S, et al. Selective activation of the fatty acid synthesis pathway in human prostate cancer. *Int J Cancer*. 2000;88(2):176-9.
81. Fritz V, Benfodda Z, Rodier G, Henriquet C, Iborra F, Avances C, et al. Abrogation of de novo lipogenesis by stearoyl-CoA desaturase 1 inhibition interferes with oncogenic signaling and blocks prostate cancer progression in mice. *Molecular cancer therapeutics*. 2010;9(6):1740-54.
82. Wu X, Daniels G, Lee P, Monaco ME. Lipid metabolism in prostate cancer. *Am J Clin Exp Urol*. 2014;2(2):111-20.
83. Dakubo GD, Parr RL, Costello LC, Franklin RB, Thayer RE. Altered metabolism and mitochondrial genome in prostate cancer. *Journal of clinical pathology*. 2006;59(1):10-6.
84. Schulze A, Harris AL. How cancer metabolism is tuned for proliferation and vulnerable to disruption. *Nature*. 2012;491(7424):364-73.
85. Trottier G, Bostrom PJ, Lawrentschuk N, Fleshner NE. Nutraceuticals and prostate cancer prevention: a current review. *Nature reviews Urology*. 2010;7(1):21-30.
86. Richman EL, Carroll PR, Chan JM. Vegetable and fruit intake after diagnosis and risk of prostate cancer progression. *Int J Cancer*. 2012;131(1):201-10.
87. Khan N, Adhami VM, Mukhtar H. Review: green tea polyphenols in chemoprevention of prostate cancer: preclinical and clinical studies. *Nutr Cancer*. 2009;61(6):836-41.
88. van Die MD, Bone KM, Williams SG, Pirotta MV. Soy and soy isoflavones in prostate cancer: a systematic review and meta-analysis of randomized controlled trials. *BJU international*. 2014;113(5b):E119-30.
89. Dalais FS, Meliala A, Wattanapenpaiboon N, Frydenberg M, Suter DA, Thomson WK, et al. Effects of a diet rich in phytoestrogens on prostate-specific antigen and sex hormones in men diagnosed with prostate cancer. *Urology*. 2004;64(3):510-5.
90. Haseen F, Cantwell MM, O'Sullivan JM, Murray LJ. Is there a benefit from lycopene supplementation in men with prostate cancer? A systematic review. *Prostate cancer and prostatic diseases*. 2009;12(4):325-32.
91. Schwartz GG. Vitamin D in blood and risk of prostate cancer: lessons from the Selenium and Vitamin E Cancer Prevention Trial and the Prostate Cancer Prevention Trial. *Cancer Epidemiol Biomarkers Prev*. 2014;23(8):1447-9.
92. Key TJ, Allen N, Appleby P, Overvad K, Tjonneland A, Miller A, et al. Fruits and vegetables and prostate cancer: no association among 1104 cases in a prospective study of 130544 men in the European Prospective Investigation into Cancer and Nutrition (EPIC). *Int J Cancer*. 2004;109(1):119-24.
93. Bradbury KE, Appleby PN, Key TJ. Fruit, vegetable, and fiber intake in relation to cancer risk: findings from the European Prospective Investigation into Cancer and Nutrition (EPIC). *Am J Clin Nutr*. 2014;100 Suppl 1:394s-8s.
94. Liu B, Mao Q, Cao M, Xie L. Cruciferous vegetables intake and risk of prostate cancer: a meta-analysis. *Int J Urol*. 2012;19(2):134-41.
95. Richman EL, Kenfield SA, Stampfer MJ, Pacionek A, Carroll PR, Chan JM. Physical activity after diagnosis and risk of prostate cancer progression: data from the cancer of the prostate strategic urologic research endeavor. *Cancer research*. 2011;71(11):3889-95.

96. Steinbrecher A, Nimptsch K, Husing A, Rohrmann S, Linseisen J. Dietary glucosinolate intake and risk of prostate cancer in the EPIC-Heidelberg cohort study. *Int J Cancer*. 2009;125(9):2179-86.
97. Juge N, Mithen RF, Traka M. Molecular basis for chemoprevention by sulforaphane: a comprehensive review. *Cell Mol Life Sci*. 2007;64(9):1105-27.
98. Sarikamis G, Marquez J, MacCormack R, Bennett RN, Roberts J, Mithen R. High glucosinolate broccoli: a delivery system for sulforaphane. *Mol Breed*. 2006;18(3):219-28.
99. Stoewsand GS. Bioactive organosulfur phytochemicals in Brassica oleracea vegetables—A review. *Food and Chemical Toxicology*. 1995;33(6):537-43.
100. Traka MH, Melchini A, Mithen RF. Sulforaphane and prostate cancer interception. *Drug discovery today*. 2014;19(9):1488-92.
101. Clarke JD, Dashwood RH, Ho E. Multi-targeted prevention of cancer by sulforaphane. *Cancer letters*. 2008;269(2):291-304.
102. Zhang C, Su ZY, Khor TO, Shu L, Kong AN. Sulforaphane enhances Nrf2 expression in prostate cancer TRAMP C1 cells through epigenetic regulation. *Biochemical pharmacology*. 2013;85(9):1398-404.
103. James D, Devaraj S, Bellur P, Lakkanna S, Vicini J, Boddupalli S. Novel concepts of broccoli sulforaphanes and disease: induction of phase II antioxidant and detoxification enzymes by enhanced-glucoraphanin broccoli. *Nutrition reviews*. 2012;70(11):654-65.
104. Brooks JD, Paton VG, Vidanes G. Potent induction of phase 2 enzymes in human prostate cells by sulforaphane. *Cancer Epidemiol Biomarkers Prev*. 2001;10(9):949-54.
105. Atwell LL, Hsu A, Wong CP, Stevens JF, Bella D, Yu TW, et al. Absorption and chemopreventive targets of sulforaphane in humans following consumption of broccoli sprouts or a myrosinase-treated broccoli sprout extract. *Molecular nutrition & food research*. 2015;59(3):424-33.
106. Oliviero T, Verkerk R, Vermeulen M, Dekker M. In vivo formation and bioavailability of isothiocyanates from glucosinolates in broccoli as affected by processing conditions. *Molecular nutrition & food research*. 2014;58(7):1447-56.
107. Saha S, Hollands W, Teucher B, Needs PW, Narbad A, Ortori CA, et al. Isothiocyanate concentrations and interconversion of sulforaphane to erucin in human subjects after consumption of commercial frozen broccoli compared to fresh broccoli. *Molecular nutrition & food research*. 2012;56(12):1906-16.
108. Clarke JD, Hsu A, Riedl K, Bella D, Schwartz SJ, Stevens JF, et al. Bioavailability and inter-conversion of sulforaphane and erucin in human subjects consuming broccoli sprouts or broccoli supplement in a cross-over study design. *Pharmacological research*. 2011;64(5):456-63.
109. Conaway CC, Getahun SM, Liebes LL, Pusateri DJ, Topham DK, Botero-Omary M, et al. Disposition of glucosinolates and sulforaphane in humans after ingestion of steamed and fresh broccoli. *Nutr Cancer*. 2000;38(2):168-78.
110. Fahey JW, Holtzclaw WD, Wehage SL, Wade KL, Stephenson KK, Talalay P. Sulforaphane Bioavailability from Glucoraphanin-Rich Broccoli: Control by Active Endogenous Myrosinase. *PloS one*. 2015;10(11):e0140963.
111. Gasper AV, Al-Janobi A, Smith JA, Bacon JR, Fortun P, Atherton C, et al. Glutathione S-transferase M1 polymorphism and metabolism of sulforaphane from standard and high-glucosinolate broccoli. *Am J Clin Nutr*. 2005;82(6):1283-91.

112. Devlin TM. The Tricarboxylic Acid Cycle. *Textbook of Biochemistry with Clinical Correlations*. 4th Edition ed. USA: Wiley-Liss, Inc; 1997. p. 231-66.
113. Kline EE, Treat EG, Aversa TA, Davis MS, Smith AY, Sillerud LO. Citrate concentrations in human seminal fluid and expressed prostatic fluid determined via ¹H nuclear magnetic resonance spectroscopy outperform prostate specific antigen in prostate cancer detection. *The Journal of urology*. 2006;176(5):2274-9.
114. Costello L. Intermediary metabolism of normal and malignant prostate: a neglected area of prostate research. *Prostate*. 1998;34(4):303-4.
115. McDunn JE, Li Z, Adam KP, Neri BP, Wolfert RL, Milburn MV, et al. Metabolomic signatures of aggressive prostate cancer. *Prostate*. 2013;73(14):1547-60.
116. Silva FR, Nabeshima CT, Bellini MH, Courrol LC. Early diagnosis of prostate cancer by citrate determination in urine with europium-oxytetracycline complex. *Appl Spectrosc*. 2012;66(8):958-61.
117. Mycielska ME, Djamgoz MBA. Citrate transport in the human prostate epithelial PNT2-C2 cell line: electrophysiological analyses. *J Physiol-London*. 2004;559(3):821-33.
118. Petrarulo M, Facchini P, Cerelli E, Marangella M, Linari F. Citrate in Urine Determined with a New Citrate Lyase Method. *Clin Chem*. 1995;41(10):1518-21.
119. Stenman K, Stattin P, Stenlund H, Riklund K, Grobner G, Bergh A. H HRMAS NMR Derived Bio-markers Related to Tumor Grade, Tumor Cell Fraction, and Cell Proliferation in Prostate Tissue Samples. *Biomark Insights*. 2011;6:39-47.
120. Cornel EB, Smits GA, de Ruijter JE, Oosterhof GO, Heerschap A, Debruyne FM, et al. In vitro proton magnetic resonance spectroscopy of four human prostate cancer cell lines. *Prostate*. 1995;26(5):275-80.
121. Matheson BK, Adams JL, Zou J, Patel R, Franklin RB. Effect of metabolic inhibitors on ATP and citrate content in PC3 prostate cancer cells. *Prostate*. 2007;67(11):1211-8.
122. Mycielska ME, Broke-Smith TP, Palmer CP, Beckerman R, Nastos T, Erguler K, et al. Citrate enhances in vitro metastatic behaviours of PC-3M human prostate cancer cells: Status of endogenous citrate and dependence on aconitase and fatty acid synthase. *The International Journal of Biochemistry & Cell Biology*. 2006;38(10):1766-77.
123. Pal R, Parker D, Costello LC. A europium luminescence assay of lactate and citrate in biological fluids. *Organic & biomolecular chemistry*. 2009;7(8):1525-8.
124. E. Uggerud SP, D. K. Bohme, F. Turecek, D. Schröder, H. Schwarz, D. Plattner, T. Wyttenbach, M. T. Bowers, P. B. Armentrout, S. A. Truger, T. Junker, G. Suizdak, Mark Brönstrup. *Modern Mass Spectroscopy. Topics in Current Chemistry 225*. Berlin: Springer-Verlag; 2003. p. 1-302.
125. contributors W. Citric acid cycle. *Wikipedia, The Free Encyclopedia*.
126. Al Kadhi O, Melchini A, Mithen R, Saha S. Development of a LC-MS/MS Method for the Simultaneous Detection of Tricarboxylic Acid Cycle Intermediates in a Range of Biological Matrices. *Journal of Analytical Methods in Chemistry*. 2017;2017:1-12.
127. Luo B, Groenke K, Takors R, Wandrey C, Oldiges M. Simultaneous determination of multiple intracellular metabolites in glycolysis, pentose phosphate

- pathway and tricarboxylic acid cycle by liquid chromatography-mass spectrometry. *J Chromatogr A*. 2007;1147(2):153-64.
128. Bylund D, Norstrom SH, Essen SA, Lundstrom US. Analysis of low molecular mass organic acids in natural waters by ion exclusion chromatography tandem mass spectrometry. *J Chromatogr A*. 2007;1176(1-2):89-93.
129. Nowatzke W, Woolf E. Best practices during bioanalytical method validation for the characterization of assay reagents and the evaluation of analyte stability in assay standards, quality controls, and study samples. *AAPS J*. 2007;9(2):E117-22.
130. Tan B, Lu Z, Dong S, Zhao G, Kuo MS. Derivatization of the tricarboxylic acid intermediates with O-benzylhydroxylamine for liquid chromatography-tandem mass spectrometry detection. *Anal Biochem*. 2014;465:134-47.
131. Arrabal-Polo MA, Arrabal-Martin M, Arias-Santiago S, Garrido-Gomez J, Poyatos-Andujar A, Zuluaga-Gomez A. Importance of citrate and the calcium : citrate ratio in patients with calcium renal lithiasis and severe lithogenesis. *BJU international*. 2013;111(4):622-7.
132. Akdeniz A, Caglayan MG, Anzenbacher P, Jr. A tri-serine tri-lactone scaffold for the quantification of citrate in urine. *Chemical communications (Cambridge, England)*. 2016;52(9):1827-30.
133. Hoppe B, Kemper MJ, Hvizd MG, Sailer DE, Langman CB. Simultaneous determination of oxalate, citrate and sulfate in children's plasma with ion chromatography. *Kidney Int*. 1998;53(5):1348-52.
134. Mariano F, Morselli M, Bergamo D, Hollo Z, Scella S, Maio M, et al. Blood and ultrafiltrate dosage of citrate as a useful and routine tool during continuous venovenous haemodiafiltration in septic shock patients. *Nephrology, dialysis, transplantation : official publication of the European Dialysis and Transplant Association - European Renal Association*. 2011;26(12):3882-8.
135. Mycielska ME, Patel A, Rizaner N, Mazurek MP, Keun H, Patel A, et al. Citrate transport and metabolism in mammalian cells: prostate epithelial cells and prostate cancer. *Bioessays*. 2009;31(1):10-20.
136. Kurhanewicz J, Vigneron DB, Nelson SJ, Hricak H, Macdonald JM, Konety B, et al. Citrate as an in-Vivo Marker to Discriminate Prostate-Cancer from Benign Prostatic Hyperplasia and Normal Prostate Peripheral Zone - Detection Via Localized Proton Spectroscopy. *Urology*. 1995;45(3):459-66.
137. Bingol K, Bruschiweiler-Li L, Li D, Zhang B, Xie M, Bruschiweiler R. Emerging new strategies for successful metabolite identification in metabolomics. *Bioanalysis*. 2016;8(6):557-73.
138. Becker S, Kortz L, Helmschrodt C, Thiery J, Ceglarek U. LC-MS-based metabolomics in the clinical laboratory. *J Chromatogr B*. 2012;883:68-75.
139. Grebe SK, Singh RJ. LC-MS/MS in the Clinical Laboratory - Where to From Here? *Clin Biochem Rev*. 2011;32(1):5-31.
140. Lu S, Sun X, Shi C, Zhang Y. Determination of tricarboxylic acid cycle acids and other related substances in cultured mammalian cells by gradient ion-exchange chromatography with suppressed conductivity detection. *J Chromatogr A*. 2003;1012(2):161-8.
141. Brugnara L, Vinaixa M, Murillo S, Samino S, Rodriguez MA, Beltran A, et al. Metabolomics approach for analyzing the effects of exercise in subjects with type 1 diabetes mellitus. *PloS one*. 2012;7(7):e40600.

142. Warburg E. Über Wärmeleitung und andere ausgleichende Vorgänge. Berlin,; J. Springer; 1924. x, 106 p. p.
143. Mailloux RJ, Beriault R, Lemire J, Singh R, Chenier DR, Hamel RD, et al. The Tricarboxylic Acid Cycle, an Ancient Metabolic Network with a Novel Twist. *PloS one*. 2007;2(8).
144. Costello LC, Franklin RB. Bioenergetic Theory of Prostate Malignancy. *Prostate*. 1994;25(3):162-6.
145. Costello LC, Liu YY, Franklin RB, Kennedy MC. Zinc inhibition of mitochondrial aconitase and its importance in citrate metabolism of prostate epithelial cells. *J Biol Chem*. 1997;272(46):28875-81.
146. Tretter L, Adam-Vizi V. Inhibition of Krebs cycle enzymes by hydrogen peroxide: A key role of [alpha]-ketoglutarate dehydrogenase in limiting NADH production under oxidative stress. *J Neurosci*. 2000;20(24):8972-9.
147. Keum YS, Khor TO, Lin W, Shen G, Kwon KH, Barve A, et al. Pharmacokinetics and pharmacodynamics of broccoli sprouts on the suppression of prostate cancer in transgenic adenocarcinoma of mouse prostate (TRAMP) mice: implication of induction of Nrf2, HO-1 and apoptosis and the suppression of Akt-dependent kinase pathway. *Pharmaceutical research*. 2009;26(10):2324-31.
148. Wattenberg LW. Inhibition of carcinogenic effects of polycyclic hydrocarbons by benzyl isothiocyanate and related compounds. *Journal of the National Cancer Institute*. 1977;58(2):395-8.
149. Singh SV, Warin R, Xiao D, Powolny AA, Stan SD, Arlotti JA, et al. Sulforaphane inhibits prostate carcinogenesis and pulmonary metastasis in TRAMP mice in association with increased cytotoxicity of natural killer cells. *Cancer research*. 2009;69(5):2117-25.
150. de Figueiredo SM, Filho SA, Nogueira-Machado JA, Caligiorne RB. The anti-oxidant properties of isothiocyanates: a review. *Recent Pat Endocr Metab Immune Drug Discov*. 2013;7(3):213-25.
151. Negrette-Guzman M, Huerta-Yepez S, Tapia E, Pedraza-Chaverri J. Modulation of mitochondrial functions by the indirect antioxidant sulforaphane: A seemingly contradictory dual role and an integrative hypothesis. *Free Radical Bio Med*. 2013;65:1078-89.
152. Cussenot O, Berthon P, Berger R, Mowszowicz I, Faille A, Hojman F, et al. Immortalization of human adult normal prostatic epithelial cells by liposomes containing large T-SV40 gene. *The Journal of urology*. 1991;146(3):881-6.
153. Bello D, Webber MM, Kleinman HK, Wartinger DD, Rhim JS. Androgen responsive adult human prostatic epithelial cell lines immortalized by human papillomavirus 18. *Carcinogenesis*. 1997;18(6):1215-23.
154. Stone KR, Mickey DD, Wunderli H, Mickey GH, Paulson DF. Isolation of a human prostate carcinoma cell line (DU 145). *Int J Cancer*. 1978;21(3):274-81.
155. Horoszewicz JS, Leong SS, Chu TM, Wajsman ZL, Friedman M, Papsidero L, et al. The LNCaP cell line--a new model for studies on human prostatic carcinoma. *Progress in clinical and biological research*. 1980;37:115-32.
156. Kaighn ME, Narayan KS, Ohnuki Y, Lechner JF, Jones LW. Establishment and characterization of a human prostatic carcinoma cell line (PC-3). *Investigative urology*. 1979;17(1):16-23.
157. Gasper AV, Al-Janobi A, Smith JA. Glutathione S-transferase M1 polymorphism and metabolism of sulforaphane from standard and high-glucosinolate broccoli (vol 82, pg 1283, 2005). *Am J Clin Nutr*. 2006;83(3):724-.

158. Wulaningsih W, Holmberg L, Garmo H, Malmstrom H, Lambe M, Hammar N, et al. Serum lactate dehydrogenase and survival following cancer diagnosis. *British journal of cancer*. 2015;113(9):1389-96.
159. Costello LC, Franklin RB. The intermediary metabolism of the prostate: a key to understanding the pathogenesis and progression of prostate malignancy. *Oncology*. 2000;59(4):269-82.
160. Swanson MG, Vigneron DB, Tabatabai ZL, Males RG, Schmitt L, Carroll PR, et al. Proton HR-MAS spectroscopy and quantitative pathologic analysis of MRI/3D-MRSI-targeted postsurgical prostate tissues. *Magnetic resonance in medicine : official journal of the Society of Magnetic Resonance in Medicine / Society of Magnetic Resonance in Medicine*. 2003;50(5):944-54.
161. Costello LC, Franklin RB, Feng P. Mitochondrial function, zinc, and intermediary metabolism relationships in normal prostate and prostate cancer. *Mitochondrion*. 2005;5(3):143-53.
162. McNeal JE. Normal histology of the prostate. *Am J Surg Pathol*. 1988;12(8):619-33.
163. McNeal JE. Normal anatomy of the prostate and changes in benign prostatic hypertrophy and carcinoma. *Seminars in ultrasound, CT, and MR*. 1988;9(5):329-34.
164. McNeal JE, Redwine EA, Freiha FS, Stamey TA. Zonal distribution of prostatic adenocarcinoma. Correlation with histologic pattern and direction of spread. *Am J Surg Pathol*. 1988;12(12):897-906.
165. Zu XY, Zhang QH, Liu JH, Cao RX, Zhong J, Yi GH, et al. ATP citrate lyase inhibitors as novel cancer therapeutic agents. *Recent Pat Anticancer Drug Discov*. 2012;7(2):154-67.
166. Swinnen JV, Brusselmans K, Verhoeven G. Increased lipogenesis in cancer cells: new players, novel targets. *Curr Opin Clin Nutr Metab Care*. 2006;9(4):358-65.
167. Jiang Z, Wu CL, Woda BA, Iczkowski KA, Chu PG, Tretiakova MS, et al. Alpha-methylacyl-CoA racemase: a multi-institutional study of a new prostate cancer marker. *Histopathology*. 2004;45(3):218-25.
168. Luo J, Zha S, Gage WR, Dunn TA, Hicks JL, Bennett CJ, et al. alpha-Methylacyl-CoA racemase: A new molecular marker for prostate cancer. *Cancer research*. 2002;62(8):2220-6.
169. Yoshii Y, Furukawa T, Oyama N, Hasegawa Y, Kiyono Y, Nishii R, et al. Fatty Acid Synthase Is a Key Target in Multiple Essential Tumor Functions of Prostate Cancer: Uptake of Radiolabeled Acetate as a Predictor of the Targeted Therapy Outcome. *PloS one*. 2013;8(5).
170. Shah US, Dhir R, Gollin SM, Chandran UR, Lewis D, Acquafondata M, et al. Fatty acid synthase gene overexpression and copy number gain in prostate adenocarcinoma. *Hum Pathol*. 2006;37(4):401-9.
171. Bright RK, Vocke CD, Emmert-Buck MR, Duray PH, Solomon D, Fetsch P, et al. Generation and genetic characterization of immortal human prostate epithelial cell lines derived from primary cancer specimens. *Cancer research*. 1997;57(5):995-1002.
172. Teahan O, Bevan CL, Waxman J, Keun HC. Metabolic signatures of malignant progression in prostate epithelial cells. *Int J Biochem Cell Biol*. 2011;43(7):1002-9.

173. Toghrol F, Franklin RB, Costello LC. Citrate synthesis from fatty acids and amino acids in rat ventral prostate. *Enzyme*. 1980;25(6):371-6.
174. Mycielska ME, Broke-Smith TP, Palmer CP, Beckerman R, Nastos T, Erguler K, et al. Citrate enhances in vitro metastatic behaviours of PC-3M human prostate cancer cells: status of endogenous citrate and dependence on aconitase and fatty acid synthase. *Int J Biochem Cell Biol*. 2006;38(10):1766-77.
175. Popovic Z, Templeton DM. Cell density-dependent shift in activity of iron regulatory protein 1 (IRP-1)/cytosolic (c-)aconitase. *Metallomics*. 2012;4(7):693-9.
176. Saraon P, Trudel D, Kron K, Dmitromanolakis A, Trachtenberg J, Bapat B, et al. Evaluation and prognostic significance of ACAT1 as a marker of prostate cancer progression. *Prostate*. 2014;74(4):372-80.
177. Jiang N, Zhu S, Chen J, Niu Y, Zhou L. A-methylacyl-CoA racemase (AMACR) and prostate-cancer risk: a meta-analysis of 4,385 participants. *PloS one*. 2013;8(10):e74386.
178. Eales KL, Hollinshead KE, Tennant DA. Hypoxia and metabolic adaptation of cancer cells. *Oncogenesis*. 2016;5:e190.
179. Kumar B, Koul S, Khandrika L, Meacham RB, Koul HK. Oxidative stress is inherent in prostate cancer cells and mediates aggressive phenotype. *J Urology*. 2008;179(4):192-3.
180. Starkov AA. An update on the role of mitochondrial alpha-ketoglutarate dehydrogenase in oxidative stress. *Mol Cell Neurosci*. 2013;55:13-6.
181. Gibson GE, Kingsbury AE, Xu H, Lindsay JG, Daniel S, Foster OJ, et al. Deficits in a tricarboxylic acid cycle enzyme in brains from patients with Parkinson's disease. *Neurochem Int*. 2003;43(2):129-35.
182. Gibson GE, Starkov A, Blass JP, Ratan RR, Beal MF. Cause and consequence: mitochondrial dysfunction initiates and propagates neuronal dysfunction, neuronal death and behavioral abnormalities in age-associated neurodegenerative diseases. *Biochimica et biophysica acta*. 2010;1802(1):122-34.
183. Gibson GE, Zhang H, Sheu KF, Bogdanovich N, Lindsay JG, Lannfelt L, et al. Alpha-ketoglutarate dehydrogenase in Alzheimer brains bearing the APP670/671 mutation. *Ann Neurol*. 1998;44(4):676-81.
184. Kumar MJ, Nicholls DG, Andersen JK. Oxidative alpha-ketoglutarate dehydrogenase inhibition via subtle elevations in monoamine oxidase B levels results in loss of spare respiratory capacity: implications for Parkinson's disease. *J Biol Chem*. 2003;278(47):46432-9.
185. Kalpana Deepa Priya D, Gayathri R, Gunassekaran GR, Sakthisekaran D. Protective role of sulforaphane against oxidative stress mediated mitochondrial dysfunction induced by benzo(a)pyrene in female Swiss albino mice. *Pulmonary Pharmacology & Therapeutics*. 2011;24(1):110-7.
186. DeFeo EM, Wu CL, McDougal WS, Cheng LL. A decade in prostate cancer: from NMR to metabolomics. *Nature reviews Urology*. 2011;8(6):301-11.
187. Maxeiner A, Adkins CB, Zhang Y, Taupitz M, Halpern EF, McDougal WS, et al. Retrospective analysis of prostate cancer recurrence potential with tissue metabolomic profiles. *Prostate*. 2010;70(7):710-7.
188. Costello LC, Lao L, Franklin R. Citrate modulation of high-affinity aspartate transport in prostate epithelial cells. *Cell Mol Biol (Noisy-le-grand)*. 1993;39(5):515-24.

189. Costello LC, Franklin RB. Zinc is decreased in prostate cancer: an established relationship of prostate cancer! *J Biol Inorg Chem*. 2011;16(1):3-8.
190. Warde N. Imaging: MRSI can potentially differentiate between aggressive and indolent prostate cancer. *Nature reviews Urology*. 2011;8(5):234.
191. Krycer JR, Brown AJ. Cholesterol accumulation in prostate cancer: a classic observation from a modern perspective. *Biochimica et biophysica acta*. 2013;1835(2):219-29.
192. van der Heul-Nieuwenhuijsen L, Hendriksen PJ, van der Kwast TH, Jenster G. Gene expression profiling of the human prostate zones. *BJU international*. 2006;98(4):886-97.
193. Sinnott JA, Rider JR, Carlsson J, Gerke T, Tyekucheva S, Penney KL, et al. Molecular differences in transition zone and peripheral zone prostate tumors. *Carcinogenesis*. 2015;36(6):632-8.
194. Xia JG, Mandal R, Sinelnikov IV, Broadhurst D, Wishart DS. MetaboAnalyst 2.0-a comprehensive server for metabolomic data analysis. *Nucleic Acids Res*. 2012;40(W1):W127-W33.
195. Xia JG, Wishart DS. Web-based inference of biological patterns, functions and pathways from metabolomic data using MetaboAnalyst. *Nat Protoc*. 2011;6(6):743-60.
196. Xia J, Sinelnikov IV, Han B, Wishart DS. MetaboAnalyst 3.0--making metabolomics more meaningful. *Nucleic Acids Res*. 2015;43(W1):W251-7.
197. Xia J, Wishart DS. Metabolomic data processing, analysis, and interpretation using MetaboAnalyst. *Curr Protoc Bioinformatics*. 2011;Chapter 14:Unit 14 0.
198. Xia J, Psychogios N, Young N, Wishart DS. MetaboAnalyst: a web server for metabolomic data analysis and interpretation. *Nucleic Acids Res*. 2009;37(Web Server issue):W652-60.
199. Andersson KE. Muscarinic acetylcholine receptors in the urinary tract. *Handbook of experimental pharmacology*. 2011(202):319-44.
200. Carter RE, Feldman AR, Coyle JT. Prostate-specific membrane antigen is a hydrolase with substrate and pharmacologic characteristics of a neuropeptidase. *P Natl Acad Sci USA*. 1996;93(2):749-53.
201. Siddiqui EJ, Shabbir M, Mikhailidis DP, Thompson CS, Mumtaz FH. The role of serotonin (5-hydroxytryptamine1A and 1B) receptors in prostate cancer cell proliferation. *The Journal of urology*. 2006;176(4 Pt 1):1648-53.
202. Zadra G, Photopoulos C, Loda M. The fat side of prostate cancer. *Biochimica et biophysica acta*. 2013;1831(10):1518-32.
203. Giskeodegard GF, Hansen AF, Bertilsson H, Gonzalez SV, Kristiansen KA, Bruheim P, et al. Metabolic markers in blood can separate prostate cancer from benign prostatic hyperplasia. *British journal of cancer*. 2015;113(12):1712-9.
204. Sreekumar A, Poisson LM, Rajendiran TM, Khan AP, Cao Q, Yu J, et al. Metabolomic profiles delineate potential role for sarcosine in prostate cancer progression. *Nature*. 2009;457(7231):910-4.
205. Kaushik AK, Vareed SK, Basu S, Putluri V, Putluri N, Panzitt K, et al. Metabolomic profiling identifies biochemical pathways associated with castration-resistant prostate cancer. *J Proteome Res*. 2014;13(2):1088-100.
206. Cao DL, Ye DW, Zhu Y, Zhang HL, Wang YX, Yao XD. Efforts to resolve the contradictions in early diagnosis of prostate cancer: a comparison of different

- algorithms of sarcosine in urine. Prostate cancer and prostatic diseases. 2011;14(2):166-72.
207. Jentzmik F, Stephan C, Lein M, Miller K, Kamlage B, Bethan B, et al. Sarcosine in Prostate Cancer Tissue is Not a Differential Metabolite for Prostate Cancer Aggressiveness and Biochemical Progression. *J Urology*. 2011;185(2):706-11.
208. Jentzmik F, Stephan C, Miller K, Schrader M, Erbersdobler A, Kristiansen G, et al. Sarcosine in Urine after Digital Rectal Examination Fails as a Marker in Prostate Cancer Detection and Identification of Aggressive Tumours. *European urology*. 2010;58(1):12-8.
209. Ross JS, Sheehan CE, Fisher HAG, Kaufman RP, Kaur P, Gray K, et al. Correlation of primary tumor prostate-specific membrane antigen expression with disease recurrence in prostate cancer. *Clinical Cancer Research*. 2003;9(17):6357-62.
210. She Y, Tang Z, Lapidus RG, Wozniak KM, Scher HI, Slusher BS. 2-MPPA, a selective inhibitor of PSMA, delays prostate cancer growth and attenuates taxol-induced neuropathy in mice. *Journal of Clinical Oncology*. 2005;23(16):742s-s.
211. Sonier B, Arseneault M, Lavigne C, Ouellette RJ, Vaillancourt C. The 5-HT_{2A} serotonergic receptor is expressed in the MCF-7 human breast cancer cell line and reveals a mitogenic effect of serotonin. *Biochemical and biophysical research communications*. 2006;343(4):1053-9.
212. Dizeyi N, Bjartell A, Hedlund P, Tasken KA, Gadaleanu V, Abrahamsson PA. Expression of serotonin receptors 2B and 4 in human prostate cancer tissue and effects of their antagonists on prostate cancer cell lines. *European urology*. 2005;47(6):895-900.
213. Cattaneo MG, Fesce R, Vicentini LM. Mitogenic effect of serotonin in human small cell lung carcinoma cells via both 5-HT_{1A} and 5-HT_{1D} receptors. *European journal of pharmacology*. 1995;291(2):209-11.
214. Heinrich E, Trojan L, Friedrich D, Voss M, Weiss C, Michel MS, et al. Neuroendocrine tumor cells in prostate cancer: evaluation of the neurosecretory products serotonin, bombesin, and gastrin - impact on angiogenesis and clinical follow-up. *Prostate*. 2011;71(16):1752-8.
215. Magnon C, Hall SJ, Lin J, Xue X, Gerber L, Freedland SJ, et al. Autonomic nerve development contributes to prostate cancer progression. *Science*. 2013;341(6142):1236361.
216. Fekete S, Kosa E, Szakall I. Nutritional role of carnitine. A review. *Magy Allatorvosok*. 2000;122(1):29-33.
217. Saylor PJ, Karoly ED, Smith MR. Prospective study of changes in the metabolomic profiles of men during their first three months of androgen deprivation therapy for prostate cancer. *Clinical cancer research : an official journal of the American Association for Cancer Research*. 2012;18(13):3677-85.
218. Aronson WJ, Glaspy JA, Reddy ST, Reese D, Heber D, Bagga D. Modulation of omega-3/omega-6 polyunsaturated ratios with dietary fish oils in men with prostate cancer. *Urology*. 2001;58(2):283-8.
219. Chua ME, Sio MC, Sorongon MC, Morales ML, Jr. The relevance of serum levels of long chain omega-3 polyunsaturated fatty acids and prostate cancer risk: A meta-analysis. *Canadian Urological Association journal = Journal de l'Association des urologues du Canada*. 2013;7(5-6):E333-43.

220. Traka MH, Spinks CA, Doleman JF, Melchini A, Ball RY, Mills RD, et al. The dietary isothiocyanate sulforaphane modulates gene expression and alternative gene splicing in a PTEN null preclinical murine model of prostate cancer. *Mol Cancer*. 2010;9:189.
221. Traka M, Gasper AV, Melchini A, Bacon JR, Needs PW, Frost V, et al. Broccoli consumption interacts with GSTM1 to perturb oncogenic signalling pathways in the prostate. *PloS one*. 2008;3(7):e2568.
222. NICE. Managing localised or locally advanced prostate cancer. 2016.
223. Onur R, Littrup PJ, Pontes JE, Bianco FJ, Jr. Contemporary impact of transrectal ultrasound lesions for prostate cancer detection. *The Journal of urology*. 2004;172(2):512-4.
224. Joseph MA, Moysich KB, Freudenheim JL, Shields PG, Bowman ED, Zhang Y, et al. Cruciferous vegetables, genetic polymorphisms in glutathione S-transferases M1 and T1, and prostate cancer risk. *Nutr Cancer*. 2004;50(2):206-13.
225. Traka MH, Saha S, Huseby S, Kopriva S, Walley PG, Barker GC, et al. Genetic regulation of glucoraphanin accumulation in Beneforte broccoli. *The New phytologist*. 2013;198(4):1085-95.
226. Bernaert N, Goetghebeur L, De Clercq H, De Loose M, Daeseleire E, Van Pamel E, et al. Influence of cultivar and harvest time on the amounts of isoalliin and methiin in leek (*Allium ampeloprasum* var. porrum). *J Agric Food Chem*. 2012;60(44):10910-9.
227. Stewart AL, Mills KM, King AC, Haskell WL, Gillis D, Ritter PL. CHAMPS physical activity questionnaire for older adults: outcomes for interventions. *Medicine and science in sports and exercise*. 2001;33(7):1126-41.
228. Cotton SC, Sharp L, Little J, Brockton N. Glutathione S-transferase polymorphisms and colorectal cancer: a HuGE review. *American journal of epidemiology*. 2000;151(1):7-32.
229. Gabbay KH, Hasty K, Breslow JL, Ellison RC, Bunn HF, Gallop PM. Glycosylated hemoglobins and long-term blood glucose control in diabetes mellitus. *J Clin Endocrinol Metab*. 1977;44(5):859-64.
230. Zander R, Lang W, Wolf HU. Alkaline haematin D-575, a new tool for the determination of haemoglobin as an alternative to the cyanhaemoglobin method. I. description of the method. *Clinica Chimica Acta*. 1984;136(1):83-93.
231. Miranda KC, Bond DT, McKee M, Skog J, Paunescu TG, Da Silva N, et al. Nucleic acids within urinary exosomes/microvesicles are potential biomarkers for renal disease. *Kidney Int*. 2010;78(2):191-9.
232. Anderson. M. D. [Bioinformatics]. *Sample Size for Microarray Experiments* [cited 2012 February]. Available from: <http://bioinformaticsmdandersonorg/MicroarraySampleSize/>.
233. Wei C, Li J, Bumgarner RE. Sample size for detecting differentially expressed genes in microarray experiments. *BMC genomics*. 2004;5:87.
234. Kirsh VA, Peters U, Mayne ST, Subar AF, Chatterjee N, Johnson CC, et al. Prospective study of fruit and vegetable intake and risk of prostate cancer. *Journal of the National Cancer Institute*. 2007;99(15):1200-9.
235. Kolonel LN, Hankin JH, Whittemore AS, Wu AH, Gallagher RP, Wilkens LR, et al. Vegetables, fruits, legumes and prostate cancer: A multiethnic case-control study. *Cancer Epidem Biomar*. 2000;9(8):795-804.

236. Schuurman AG, Goldbohm RA, Dorant E, van den Brandt PA. Vegetable and fruit consumption and prostate cancer risk: A cohort study in the Netherlands. *Cancer Epidem Biomar.* 1998;7(8):673-80.
237. Jain MG, Hislop GT, Howe GR, Ghadirian P. Plant foods, antioxidants, and prostate cancer risk: Findings from case-control studies in Canada. *Nutr Cancer.* 1999;34(2):173-84.
238. Florin T, Neale G, Gibson GR, Christl SU, Cummings JH. Metabolism of Dietary Sulfate - Absorption and Excretion in Humans. *Gut.* 1991;32(7):766-73.
239. Florin THJ, Neale G, Goretzki S, Cummings JH. The Sulfate Content of Foods and Beverages. *Journal of Food Composition and Analysis.* 1993;6(2):140-51.
240. Mabjeesh NJ, Lidawi G, Chen JZ, German L, Matzkin H. High detection rate of significant prostate tumours in anterior zones using transperineal ultrasound-guided template saturation biopsy. *BJU international.* 2012;110(7):993-7.
241. Dimmen M, Vlatkovic L, Hole KH, Nesland JM, Brennhovd B, Axcrona K. Transperineal prostate biopsy detects significant cancer in patients with elevated prostate-specific antigen (PSA) levels and previous negative transrectal biopsies. *BJU international.* 2012;110(2 Pt 2):E69-75.
242. Ehdai B, Poon BY, Sjoberg DD, Recabal P, Laudone V, Touijer K, et al. Variation in serum prostate-specific antigen levels in men with prostate cancer managed with active surveillance. *BJU international.* 2015.
243. Sharma I, Aaradhya M, Kodikonda M, Naik PR. Antihyperglycemic, antihyperlipidemic and antioxidant activity of phenolic rich extract of Brassica oleraceae var gongylodes on streptozotocin induced Wistar rats. *Springerplus.* 2015;4:212.
244. Cohen JH, Kristal AR, Stanford JL. Fruit and vegetable intakes and prostate cancer risk. *Journal of the National Cancer Institute.* 2000;92(1):61-8.
245. Giovannucci E, Rimm EB, Liu Y, Stampfer MJ, Willett WC. A prospective study of cruciferous vegetables and prostate cancer. *Cancer Epidem Biomar.* 2003;12(12):1403-9.
246. Villeneuve PJ, Johnson KC, Kreiger N, Mao Y. Risk factors for prostate cancer: Results from the Canadian National Enhanced Cancer Surveillance System. *Cancer Cause Control.* 1999;10(5):355-67.
247. Melchini A, Traka MH, Catania S, Miceli N, Taviano MF, Maimone P, et al. Antiproliferative activity of the dietary isothiocyanate erucin, a bioactive compound from cruciferous vegetables, on human prostate cancer cells. *Nutr Cancer.* 2013;65(1):132-8.
248. Vyas AR, Singh SV. Functional relevance of D,L-sulforaphane-mediated induction of vimentin and plasminogen activator inhibitor-1 in human prostate cancer cells. *Eur J Nutr.* 2014;53(3):843-52.
249. Chambers KF, Bacon JR, Kemsley EK, Mills RD, Ball RY, Mithen RF, et al. Gene expression profile of primary prostate epithelial and stromal cells in response to sulforaphane or iberin exposure. *Prostate.* 2009;69(13):1411-21.
250. Valgimigli L, Iori R. Antioxidant and pro-oxidant capacities of ITCs. *Environmental and molecular mutagenesis.* 2009;50(3):222-37.
251. Roe M, Pinchen H, Church S, Finglas P. McCance and Widdowson's The Composition of Foods Seventh Summary Edition and updated Composition of Foods Integrated Dataset. *Nutrition Bulletin.* 2015;40(1):36-9.

-
252. Hanover JA, Krause MW, Love DC. Bittersweet memories: linking metabolism to epigenetics through O-GlcNAcylation. *Nat Rev Mol Cell Biol*. 2012;13(5):312-21.
253. McCambridge J, Witton J, Elbourne DR. Systematic review of the Hawthorne effect: new concepts are needed to study research participation effects. *J Clin Epidemiol*. 2014;67(3):267-77.
254. Kenfield SA, Stampfer MJ, Giovannucci E, Chan JM. Physical activity and survival after prostate cancer diagnosis in the health professionals follow-up study. *Journal of clinical oncology : official journal of the American Society of Clinical Oncology*. 2011;29(6):726-32.
255. Bonn SE, Sjolander A, Lagerros YT, Wiklund F, Stattin P, Holmberg E, et al. Physical Activity and Survival among Men Diagnosed with Prostate Cancer. *Cancer Epidem Biomar*. 2015;24(1):57-64.
256. Ukimura O, Coleman JA, de la Taille A, Emberton M, Epstein JI, Freedland SJ, et al. Contemporary Role of Systematic Prostate Biopsies: Indications, Techniques, and Implications for Patient Care. *European urology*. 2013;63(2):214-30.
257. Cooperberg MR, Cowan JE, Hilton JF, Reese AC, Zaid HB, Porten SP, et al. Outcomes of active surveillance for men with intermediate-risk prostate cancer. *Journal of clinical oncology : official journal of the American Society of Clinical Oncology*. 2011;29(2):228-34.
258. Waring RH, Harris RM, Steventon GB, Mitchell SC. Degradation to sulphate of S-methyl-L-cysteine sulphoxide and S-carboxymethyl-L-cysteine sulphoxide in man. *Drug metabolism and drug interactions*. 2003;19(4):241-55.
259. Kirby RS, Lowe D, Bultitude MI, Shuttleworth KE. Intra-prostatic urinary reflux: an aetiological factor in abacterial prostatitis. *Br J Urol*. 1982;54(6):729-31.
260. McMurry JEF, Robert C. *Chemistry: Pearson New International Edition* 2013:973-.
261. Hollinger MA. *Introduction to Pharmacology*. Third ed: Taylor & Francis; 2007.
262. Klaassen CD, Boles JW. Sulfation and sulfotransferases .5. The importance of 3'-phosphoadenosine 5'-phosphosulfate (PAPS) in the regulation of sulfation. *Faseb J*. 1997;11(6):404-18.
263. Martin DS, Bertino JR, Koutcher JA. ATP Depletion + Pyrimidine Depletion Can Markedly Enhance Cancer Therapy: Fresh Insight for a New Approach. *Cancer research*. 2000;60(24):6776-83.
264. Mistry M, Parkin DM, Ahmad AS, Sasieni P. Cancer incidence in the United Kingdom: projections to the year 2030. *British journal of cancer*. 2011;105(11):1795-803.
265. Brawley OW, Knopf K, Merrill R. The epidemiology of prostate cancer part I: descriptive epidemiology. *Semin Urol Oncol*. 1998;16(4):187-92.
266. Singh GK, Miller BA. Health, life expectancy, and mortality patterns among immigrant populations in the United States. *Can J Public Health*. 2004;95(3):I14-I21.
267. Jacobsen SJ, Katusic SK, Bergstralh EJ, Oesterling JE, Ohrt D, Klee GG, et al. Incidence of prostate cancer diagnosis in the eras before and after serum prostate-specific antigen testing. *JAMA : the journal of the American Medical Association*. 1995;274(18):1445-9.

268. Haenszel W, Kurihara M. Studies of Japanese migrants. I. Mortality from cancer and other diseases among Japanese in the United States. *Journal of the National Cancer Institute*. 1968;40(1):43-68.
269. Liu Y, Hu F, Li D, Wang F, Zhu L, Chen W, et al. Does physical activity reduce the risk of prostate cancer? A systematic review and meta-analysis. *European urology*. 2011;60(5):1029-44.
270. Houghton CA, Fassett RG, Coombes JS. Sulforaphane: translational research from laboratory bench to clinic. *Nutrition reviews*. 2013;71(11):709-26.
271. Mitchell S, Abel P, Ware M, Stamp G, Lalani E. Phenotypic and genotypic characterization of commonly used human prostatic cell lines. *BJU international*. 2000;85(7):932-44.
272. Fritz V, Benfodda Z, Henriquet C, Hure S, Cristol JP, Michel F, et al. Metabolic intervention on lipid synthesis converging pathways abrogates prostate cancer growth. *Oncogene*. 2013;32(42):5101-10.
273. Kumar D, Gupta A, Mandhani A, Sankhwar SN. NMR spectroscopy of filtered serum of prostate cancer: A new frontier in metabolomics. *Prostate*. 2016.
274. Powell MS, Li R, Dai H, Sayeeduddin M, Wheeler TM, Ayala GE. Neuroanatomy of the normal prostate. *Prostate*. 2005;65(1):52-7.
275. Villers A, McNeal JE, Redwine EA, Freiha FS, Stamey TA. The role of perineural space invasion in the local spread of prostatic adenocarcinoma. *The Journal of urology*. 1989;142(3):763-8.
276. Bastacky SI, Walsh PC, Epstein JI. Relationship between perineural tumor invasion on needle biopsy and radical prostatectomy capsular penetration in clinical stage B adenocarcinoma of the prostate. *Am J Surg Pathol*. 1993;17(4):336-41.
277. Ayala GE, Wheeler TM, Shine HD, Schmelz M, Frolov A, Chakraborty S, et al. In vitro dorsal root ganglia and human prostate cell line interaction: Redefining perineural invasion in prostate cancer. *Prostate*. 2001;49(3):213-23.
278. Anderson PR, Hanlon AL, Patchefsky A, Al-Saleem T, Hanks GE. Perineural invasion and Gleason 7-10 tumors predict increased failure in prostate cancer patients with pretreatment PSA <10 ng/ml treated with conformal external beam radiation therapy. *International journal of radiation oncology, biology, physics*. 1998;41(5):1087-92.
279. Armah CN, Derdemezis C, Traka MH, Dainty JR, Doleman JF, Saha S, et al. Diet rich in high glucoraphanin broccoli reduces plasma LDL cholesterol: Evidence from randomised controlled trials. *Molecular nutrition & food research*. 2015;59(5):918-26.
280. Choi KM, Lee YS, Kim W, Kim SJ, Shin KO, Yu JY, et al. Sulforaphane attenuates obesity by inhibiting adipogenesis and activating the AMPK pathway in obese mice. *The Journal of nutritional biochemistry*. 2014;25(2):201-7.
281. Rodriguez-Cantu LN, Gutierrez-Urbe JA, Arriola-Vucovich J, Diaz-De La Garza RI, Fahey JW, Serna-Saldivar SO. Broccoli (*Brassica oleracea* var. *italica*) sprouts and extracts rich in glucosinolates and isothiocyanates affect cholesterol metabolism and genes involved in lipid homeostasis in hamsters. *J Agric Food Chem*. 2011;59(4):1095-103.
282. Hayes JD, Dinkova-Kostova AT. The Nrf2 regulatory network provides an interface between redox and intermediary metabolism. *Trends in biochemical sciences*. 2014;39(4):199-218.
283. Armah CN, Traka MH, Dainty JR, Defernez M, Janssens A, Leung W, et al. A diet rich in high-glucoraphanin broccoli interacts with genotype to reduce

- discordance in plasma metabolite profiles by modulating mitochondrial function. *Am J Clin Nutr.* 2013;98(3):712-22.
284. Kristal AR, Lampe JW. Brassica vegetables and prostate cancer risk: a review of the epidemiological evidence. *Nutr Cancer.* 2002;42(1):1-9.
285. Bednarek P. Sulfur-containing secondary metabolites from *Arabidopsis thaliana* and other Brassicaceae with function in plant immunity. *Chembiochem : a European journal of chemical biology.* 2012;13(13):1846-59.
286. Vasanthi HR, Mukherjee S, Das DK. Potential health benefits of broccoli-a chemico-biological overview. *Mini reviews in medicinal chemistry.* 2009;9(6):749-59.
287. Edmands WM, Beckonert OP, Stella C, Campbell A, Lake BG, Lindon JC, et al. Identification of human urinary biomarkers of cruciferous vegetable consumption by metabolomic profiling. *J Proteome Res.* 2011;10(10):4513-21.
288. Edmands WMB, Gooderham NJ, Holmes E, Mitchell SC. S-Methyl-l-cysteine sulphoxide: the Cinderella phytochemical? *Toxicology Research.* 2013;2(1):11-22.
289. De Gianni E, Fimognari C. Anticancer Mechanism of Sulfur-Containing Compounds. *The Enzymes.* 2015;37:167-92.
290. Strott CA. Sulfonation and molecular action. *Endocrine reviews.* 2002;23(5):703-32.
291. Yu S, Kong AN. Targeting carcinogen metabolism by dietary cancer preventive compounds. *Current cancer drug targets.* 2007;7(5):416-24.
292. Li Y, Revalde JL, Reid G, Paxton JW. Interactions of dietary phytochemicals with ABC transporters: possible implications for drug disposition and multidrug resistance in cancer. *Drug metabolism reviews.* 2010;42(4):590-611.
293. Stefanson AL, Bakovic M. Dietary regulation of Keap1/Nrf2/ARE pathway: focus on plant-derived compounds and trace minerals. *Nutrients.* 2014;6(9):3777-801.
294. Murray M. Altered CYP expression and function in response to dietary factors: potential roles in disease pathogenesis. *Current drug metabolism.* 2006;7(1):67-81.
295. Huang Y, Li W, Su ZY, Kong AN. The complexity of the Nrf2 pathway: beyond the antioxidant response. *The Journal of nutritional biochemistry.* 2015;26(12):1401-13.
296. Houghton CA, Fassett RG, Coombes JS. Sulforaphane and Other Nutrigenomic Nrf2 Activators: Can the Clinician's Expectation Be Matched by the Reality? *Oxidative medicine and cellular longevity.* 2016;2016:7857186.
297. Doble A, Walker MM, Harris JR, Taylor-Robinson D, Witherow RO. Intraprostatic antibody deposition in chronic abacterial prostatitis. *Br J Urol.* 1990;65(6):598-605.
298. Kirby RS, Lowe D, Bultitude MI, Shuttleworth KED. Intra-prostatic Urinary Reflux: an Aetiological Factor in Abacterial Prostatitis. *British Journal of Urology.* 1982;54(6):729-31.
299. Blacklock NJ. Anatomical factors in prostatitis. *Br J Urol.* 1974;46(1):47-54.
300. Nickel JC. *Textbook of Prostatitis: Taylor & Francis; 1999.*